MIGRATION OF ANTIOXIDANTS FROM POLY(LACTIC ACID), PLA, FILMS INTO FOOD SIMULANTS: A PARAMETER ESTIMATION APPROACH

By

Hayati Samsudin

A DISSERTATION

Submitted to
Michigan State University
in partial fulfillment of the requirements
for the degree of

Packaging-Doctor of Philosophy

2015

ABSTRACT

MIGRATION OF ANTIOXIDANTS FROM POLY(LACTIC ACID), PLA, FILMS INTO FOOD SIMULANTS: A PARAMETER ESTIMATION APPROACH

By

Hayati Samsudin

Development of antioxidant active packaging has vastly increased over the years with more focus on biodegradable polymeric films and natural antioxidants. However, few studies investigated the migration of antioxidants from films into food simulants/products by fully considering the kinetic migration parameters. To the best of the author's knowledge, a selective number of studies have simultaneously determined other migration parameters besides the diffusion coefficient (D), such as the convective mass transfer coefficient (h) and the partition coefficient ($K_{p,f}$). Thus, this dissertation explored experimental and theoretical approaches to gain insight on the migration kinetics of antioxidants from polymer films by using parameter estimation approaches (*e.g.*, ordinary least square (OLS), sequential, bootstrap *etc*).

A poly(lactic acid), PLA, functional film incorporated with marigold flower extract containing carotenoid-based antioxidant (*i.e.*, astaxanthin) was developed and the kinetic release of astaxanthin from this film into 95% ethanol was investigated. The mass migrated at equilibrium (M_∞) was estimated for the first time, in addition to the D. Further investigation was conducted on different migration case studies to compare the estimation of one parameter, 1P (*i.e.*, the D) versus 2P (*i.e.*, the D and the M_∞) and 3P (*i.e.*, the D, the M_∞ and the ratio of the mass of antioxidant migrated into the simulant to the mass of the antioxidant left in the film at equilibrium (α)) using general mass transfer solutions. The 3P estimation based on the corrected Akaike information criterion (AICc) was found to better describe the migration experiment without compromising the

estimation accuracy. The α parameter, experimentally determined at the end of the experiment and related to $K_{p,f}$ by $\alpha = \frac{V_f}{K_{p,f}V_p}$, was better estimated at early times without the need to reach equilibrium; however, these migration cases did not account for the convective mass transfer coefficient.

Hence, a two-step solution was developed to simultaneously assess the *D*, $K_{p,f}$, and *h* from migration experiments. The first step of the solution was to identify the right local minima region for minimizing sums of squared errors (SSE) and to provide a robust magnitude approximation for the initial guesses used in the second step of the OLS estimation. The $K_{p,f}$ parameter was directly used in this solution due to the ease of physical interpretation. *h*, the parameter that might be of importance in a non-stirring condition, viscous food product/simulant, *etc.* was also estimated and related to the overall migration resistance ($Bi = \frac{hL}{D}$). Commonly, *h* is not estimated. Neglecting *h* might lead to underestimation of *D*, thus compromising the accuracy of the parameter estimation. Different migration case studies were used as examples and the parameters were assessed using the two-step solution. The OLS results were found comparable with the sequential estimation. Residual bootstrap was conducted to improve the residual distribution in a large population. A comparative study between the two-step solution and the general mass transfer solutions available in the literature was also performed, and model selection was performed using the AICc. A decision tree analysis consisting of the newly proposed model with the general mass transfer solutions was proposed as a tool for analyzing migration data.

Finally, the estimation of the activation energy (E_a) of a non-isothermal migration study was conducted using the reparameterized Arrhenius equation to identify the optimum T_{ref} to obtain near zero correlation between the D_{ref} and the E_a, in turn, decreasing relative error of D_{ref}.

Copyright by
HAYATI SAMSUDIN
2015

This dissertation is dedicated to my beloved parents and sisters

ACKNOWLEDGEMENTS

"In the end, it's not the years in your life that count. It's the life in your years"-Abraham Lincoln.

My precious appreciation to Allah S.W.T for the strength he granted me during these years. It has been a very long journey. Having lived far away from my homeland is never easy. But, I am blessed with supportive family and surrounded with beautiful friendships. I am sincerely grateful for having Dr. Rafael Antonio Auras as my advisor. His kindness to accept me as his student despite his awareness of my health condition at the time is something that I can't ever forget. He has provided me with endless opportunity to grow as a person and has kept me grounded. He will always be my mentor, and I can't express and thank him enough for his endless supports. I would like to extend my gratitude to Dr. Dolan for introducing and patiently teaching me 'the inverse problem'. It is the topic I have tried to avoid, which eventually became part of my dissertation title. Something that I learnt..never say 'never'! Another person that I owe to for 'the inverse problem' is Dr. James Beck for his unlimited thoughtful inputs. I would like to thank Dra. Maria Rubino for giving me a chance to be her TA and for her continuous support. She always encouraged me with her kind words of support. My sincere gratitude to Dr. Herlinda Soto-Valdez for her continuous helps and for taking a great care of me when I was in Hermosillo. I really appreciate her kindness and supports at all time despite being geographically apart. My deepest appreciation to Dr. Selke for her timeless support. She was the first one to welcome me to this school and I am glad to have her as part as my committee member. I am thankful to Dr. Gary Burgess for giving me a chance to learn a bit about 'the math world' from him. He never hesitates to spend his time in answering all my doubts. Also, I want to extend my appreciation to Drs. Bruce Harte and Janice

Harte for their care and supports. To Dr. Clarke, thank you for teaching me a whole new world of packaging processes… a chance that I would have never thought to have.

For all my friends (not in any particular order); Faby, Pumpkin, P'Torn, Citlali, Kikyung, Pom, Javi, Edgar, Johana, Eli 'P', Panchita, thank you for all the great time we have shared together, and I will always cherish our friendship. A special thanks to both Mishra and Patna for sharing 'my upside down' world and for our timeless friendship. I also want to thank my friend, Rabiha for her continuous support. Also, I am thankful to Turk and Ploy for never fails at visiting and for being in contact with me. Special thanks to Masyitah for her friendship.

My appreciation for the RAA research group from 2007 until now. Many have come and gone, but every chance we had, we did share lots of fun and pain together. We have learnt a lot from each other and more importantly have supported each other. I think we all owe it to Dr. Auras for being a great 'academic daddy'.

Not to forget, my appreciation to the Ministry of Education Malaysia and University Sains Malaysia for the opportunity to study abroad and for their financial supports. My gratitude also goes to the School of Packaging, the College of Agricultural and Natural Resources for their financial supports and for giving me the educational opportunities on and off-campus.

Enormous love and thank you to my beloved parents; Samsudin Mohd. Ali and Fatimah Jamil for their unconditional supports and love. To both my sisters; Suhaily and Nur Radzimah and my grandma, Hjh. Aisha, thank you for never giving up on me. To my late grandma, Hjh. Habibah, thank you for raising me and for your love.

Hayati Samsudin

TABLE OF CONTENTS

LIST OF TABLES ..... **xiii**

LIST OF FIGURES ..... **xv**

KEY TO SYMBOLS AND ABBREVIATIONS ..... **xx**

Chapter 1 ..... **1**
Background and Motivation **1**
1.0 Introduction **1**
1.1 Research Importance and Motivation **2**
1.2 Objectives **6**
1.3 Dissertation Overview **7**
REFERENCES **10**

Chapter 2 ..... **15**
Literature Review **15**
2.0 Introduction **15**
2.1 Lipid Oxidation: Brief Introduction **15**
2.2 Lipid Oxidation: Classification **15**
2.2.1 Autoxidation 15
2.2.1.1 Step 1: Initiation 16
2.2.1.2 Step 2: Propagation 16
2.2.1.3 Step 3: Chain branching 16
2.2.1.4 Step 4: Chain termination 17
2.2.2 Photooxidation or Photosensitized Oxidation 18
2.2.2.1 Type I: photooxidation by excitation of lipids 19
2.2.2.2 Type II: photooxidation by excitation of O_2 19
2.2.3 Enzyme-Catalyzed Lipid Oxidation 19
2.3 Factors Affecting Lipid Oxidation **20**
2.3.1 Chemical Structure of Fatty Acids 20
2.3.2 Temperature 21
2.3.3 Light 21
2.3.4 Oxygen, O_2 22
2.3.4.1 Type of O_2 22
2.3.4.2 Concentration of O_2 22
2.3.5 Presence of Minor Compounds 23
2.3.5.1 Water and Water Activity, a_w 23
2.3.5.2 Metals 24
2.3.5.3 Free Fatty Acids 25
2.3.5.4 Phospholipids 25
2.3.5.5 Chlorophylls 26

2.4 Antioxidants **27**
2.4.1 Classification of Antioxidants 29
2.4.1.1 Primary Antioxidants (Chain-Breaking) 30
2.4.1.2 Secondary Antioxidants (Preventative Antioxidants) 31
2.4.1.3 An Example of an Antioxidant Reaction 33
2.5 Approaches to Extend the Shelf Life of Fatty Food Products **35**
2.5.1 Antioxidant Based Packaging System: Individual and Independent Antioxidant Devices 36
2.5.2 Antioxidant Functional Films 37
2.6 Migration **55**
2.6.1 Thermodynamic Equilibrium 56
2.6.2 Partition Coefficient, $K_{p,f}$ 57
2.6.3 Diffusion Coefficient, D 58
2.6.4 Migration Models 61
2.7 Parameter Estimation **68**
2.7.1 Parameters of Interest 68
2.7.2 Sensitivity Coefficient, X, and Scaled Sensitivity Coefficient, X' 69
2.7.3 Parameter Estimation using Ordinary Least Squares (OLS) 70
2.7.3.1 Standard Errors and Correlation Coefficient of the Parameters 71
2.7.4 Sequential Estimation 72
2.7.5 Corrected Akaike Information Criterion (AICc) 72
2.7.6 Bootstrap 73
2.7.7 Optimal Experimental Design 74
2.7.8 Activation Energy 74
REFERENCES **77**

Chapter 3 ..... **92**
Poly(lactic acid) membrane incorporated with marigold flower extract (*Tagetes erecta*) intended for fatty-food application **92**
3.0 Introduction **92**
3.1 Materials and Methods **95**
3.1.1 Materials 95
3.1.2 Fabrication of Antioxidant Functional Membrane 96
3.1.3 Quantification of Astaxanthin in the Fabricated Functional Membrane after Processing 97
3.1.4 Migration of Astaxanthin into A Food Simulant 97
3.1.4.1 Mathematical Models for Migration Study 98
3.1.5 Thermal Properties 99
3.1.6 Number Average Molecular Weight (M_n) and Weight Average Molecular Weight (M_w) 100
3.1.7 Scanning Electron Microscopy (SEM) 101
3.1.8 Oxygen (O_2), Water Vapor, and Carbon Dioxide (CO_2) Barrier Properties 101
3.1.9 Optical Properties 102
3.1.10 Fourier Transform Infrared Spectrophotometer (FTIR) 102
3.1.11 Oxidative Stability of Soybean Oil 103
3.2 Statistical Analysis **104**

3.3 Results and Discussions **104**
3.3.1 Quantification of astaxanthin in the fabricated membrane after processing 104
3.3.2 Migration of Astaxanthin into A Food Simulant (95% ETOH) 106
3.3.3 Thermal Properties 111
3.3.4 Number Average Molecular Weight (M_n), and Weight Average Molecular Weight (M_w) 114
3.3.5 Scanning Electron Microscopy (SEM) 120
3.3.6 Barrier properties 122
3.3.6.1 Oxygen (O_2) 122
3.3.6.2 Water Vapor (WV) 122
3.3.6.3 Carbon dioxide (CO_2) 124
3.3.7 Optical Properties 124
3.3.8 Fourier Transform Infrared Spectrophotometer (FTIR) 125
3.3.9 Oxidative Stability of Soybean Oil 128
3.4 Conclusion **130**
REFERENCES **132**

Chapter 4 ..... **139**
Parameter Estimation for Migration Studies of Antioxidant-Polymer Films **139**
4.0 Introduction **139**
4.1 Theoretical Background **141**
4.1.1 Part A: Migration 141
4.1.1.1 Partition Coefficient, $K_{p,f}$ 141
4.1.1.2 Biot number, Bi 142
4.1.1.3 Diffusion coefficient, D 143
4.1.2 Part B: Parameter Estimation 147
4.1.2.1 Sensitivity Coefficient and Scaled Sensitivity Coefficient 148
4.1.2.2 Ordinary Least Squares (OLS) Estimation 148
4.1.2.3 Corrected Akaike Information Criterion (AICc) 148
4.1.2.4 Optimal Experimental Design 149
4.2 Case Study **149**
4.2.1 A Selected Case Study: Poly(Lactic Acid), PLA-α-Tocopherol Functional Film in Contact With 100% Ethanol At 23 °C 150
4.2.1.1 Initial Scaled Sensitivity Coefficient, X' 150
4.2.1.2 Ordinary Least Square (OLS) Estimation and the Corrected Akaike Information Criterion (AICc) 151
4.2.1.3 Optimal Experimental Design 157
4.2.2 Other Case Studies 158
4.3 Conclusion **217**
REFERENCES **218**

Chapter 5 ..... **224**
A Two-Step Solution to Estimate Mass Transfer Parameters of Migration Experiments Controlled by Diffusion, Partition and Convective Mass Transfer Coefficients **224**
5.0 Introduction **224**
5.1 Theoretical Development **227**

5.1.1 Assumptions and Boundary Conditions 227
5.1.2.1 Step 1 228
5.1.2.2 Step 2 232
5.2 A Case Study Analysis 237
5.3 Assessment of the Two-Step Solutions Model 238
5.3.1 Step 1 238
5.3.2 Scaled Sensitivity Coefficient, *X'* 238
5.3.3 Step 2 238
5.3.3.1 Ordinary Least Square (OLS) Estimation 238
5.3.3.2 Sequential Estimation 239
5.4 Kinetic Phase Diagram (KPD) 239
5.5 Bootstrap Method 241
5.6 Results and Discussions 242
5.6.1 Step 1 242
5.6.2 Scaled Sensitivity Coefficient, *X'* 243
5.6.3 Step 2 245
5.6.3.1 Ordinary Least Square (OLS) Estimation 245
5.7 Sequential Estimation 249
5.8 Kinetic Phase Diagram (KPD) 251
5.9 Residual Bootstrap 253
5.10 Conclusion 255
APPENDICES 257
APPENDIX 5A: Migration of poly(lactic acid), PLA incorporated with 2.6 wt.% α-tocopherol into ethanol at 23 °C. 258
APPENDIX 5B: Migration of poly(lactic acid), PLA incorporated with 1.28 wt.% catechin into 95% ethanol at 40 °C. 270
APPENDIX 5C: Example of MATLAB coding 282
REFERENCES 303

Chapter 6 306
Assessment of Mass Transfer Models used in Migration Experiments to Determine Diffusion, Partition and Convective Mass Transfer Coefficients 306
6.0 Introduction 306
6.1 Materials and Methods 308
6.1.1 Migration Case Studies 308
6.1.2 Mathematical Models 309
6.1.2.1 Assumptions 309
6.1.2.2 Model 1: A Two-Step Solution (A detailed discussion of the model's development can be found in Chapter 5) 309
6.1.2.2.1 Step 1 309
6.1.2.2.2 Step 2 310
6.1.2.3 Model 2: Crank's solution with partition coefficient, $K_{p,f}$ and diffusion coefficient (D) as the governing factors (Carslaw & Jaeger, 1959; Crank, 1979) 310
6.1.2.4 Model 3: Crank's solution with diffusion coefficient (D) as the only governing factor (Crank, 1979) 311
6.1.3 Kinetic Parameter Estimation 315

6.1.3.1 Scaled Sensitivity Coefficient, *X'* ... 315
6.1.3.2 Ordinary Least Square (OLS) Estimation ... 315
6.1.3.3 Corrected Akaike Information Criterion (AICc) ... 316
6.2 Results and Discussions ... 317
6.2.1 Scaled Sensitivity Coefficient, *X'* ... 317
6.2.2 Ordinary Least Square (OLS) Estimation ... 319
6.2.3 Model Selection Using the Corrected Akaike Information Criterion (AICc) ... 322
6.3 Conclusion ... 326
APPENDICES ... 327
APPENDIX 6A: Migration of poly(lactic acid), PLA incorporated with 2.6 wt.% α-tocopherol into ethanol at 23 °C. ... 328
APPENDIX 6B: Migration of poly(lactic acid), PLA incorporated with 1.28 wt.% catechin into 95% ethanol at 40 °C. ... 334
REFERENCES ... 339

Chapter 7 ... 343
Estimation of the Activation Energy in Migration Studies ... 343
7.0 Introduction ... 343
7.1 Materials and Methods ... 345
7.1.1 A Case Study ... 345
7.1.2 Kinetic Parameter Estimation Procedure ... 345
7.1.3.1 Step 1: ... 346
7.1.3.1.1 Scaled Sensitivity Coefficient, *X'* ... 346
7.1.3.1.2 Temperature Simulation (T_{sim}) Approach ... 347
7.1.3.1.3 Non-Linear Regression Estimation ... 347
7.1.3.2 Step 2: ... 347
7.2 Results and Discussions ... 348
7.2.1 Initial Scaled Sensitivity Coefficient, *X'* and Reference Temperature, T_{ref} ... 348
7.2.1 Non-Linear Regression Estimation ... 354
7.3 Additional Observations ... 357
7.4 Conclusions ... 358
APPENDICES ... 360
APPENDIX 7A: Additional results of the randomly chosen T_{ref} within the experimental temperature range. ... 361
APPENDIX 7B: MATLAB coding for the estimation of activation energy ... 363
REFERENCES ... 371

Chapter 8 ... 374
Overall Conclusion and Recommended Future Work ... 374
8.0 Overall Conclusion ... 374
8.1 Recommended Future Work ... 379
APPENDIX ... 382
REFERENCES ... 385

LIST OF TABLES

Table 2-1 Compilation of studies reporting kinetic migration parameters for petroleum based functional films incorporated with natural antioxidants and the models used to determine these parameters. 40

Table 2-2 Compilation of studies reporting kinetic migration parameters for bio-based functional films incorporated with natural antioxidants and the models used to determine these parameters. 49

Table 3-1 Migration data of produced functional membranes. 108

Table 3-2 Characterization of the fabricated functional membranes. 118

Table 4-1 Summarized of estimated parameters for different migration studies of antioxidant-PLA film systems. 160

Table 5-1 Number of terms with its corresponding percent accuracy……237

Table 5-2 Additional information of OLS estimation. 248

Table 5-3 Comparison between OLS and sequential results..... 251

Table 5-4 Comparison between 95% asymptotic and 95% bootstrap confidence intervals of each parameter..... 254

Table 5A- 1 Additional information of OLS estimation for migration of 2.6 wt.% α-tocopherol into ethanol at 23 °C. 264

Table 5A- 2 Comparison between OLS and sequential results..... 265

Table 5A- 3 Comparison between 95% asymptotic and 95% bootstrap confidence intervals of each parameter..... 269

Table 5B- 1 Additional information of OLS estimation for migration of 1.28 wt.% catechin into 95% ethanol at 40 °C. 275

Table 5B- 2 Comparison between OLS and sequential results. 276

Table 5B- 3 Comparison between 95% asymptotic and 95% bootstrap confidence intervals of each parameter..... 280

Table 6-1 Comparison of the number of terms needed to achieve a given accuracy among model 1, 2, and 3…….315

Table 6-2 OLS results for the migration study of 3 wt.% resveratrol from PLA film into ethanol at 9 °C for model 1, 2, and 3. 320

Table 6-3 AICc analysis for selecting model for the migration of 3 wt. % resveratrol from PLA film into ethanol at 9 °C. 323

Table 6A- 1 OLS results for the migration study of 2.6 wt.% α-tocopherol from PLA film into ethanol at 23 °C for model 1 and 2. 331

Table 6A- 2 AICc analysis for selecting model for the migration study of 2.6 wt.% α-tocopherol from PLA film into ethanol at 23 °C. 333

Table 6B- 1 OLS results for the migration of 1.28 wt.% catechin from PLA film into 95% ethanol at 40 °C for model 1 and 3. 336

Table 6B- 2 AICc analysis for selecting model for the migration of 1.28 wt.% catechin from PLA film into 95% ethanol at 40 °C. 338

Table 7-1 Correlation matrix of the estimated parameters at the average T_{ref}=35 °C. 352

Table 7-2 Correlation matrix of the estimated parameters at the T_{ref}=45 °C. 353

Table 7-3 Correlation matrix of the estimated parameters at the optimum T_{ref}=44.94 °C. 355

Table 7-4 The parameters' estimates at the optimum T_{ref}=44.94 °C. 356

Table 7A- 1 Correlation matrix of the estimated parameters at the T_{ref}=40 °C. 361

Table 7A- 2 Correlation matrix of the estimated parameters at the T_{ref}=50 °C. 362

LIST OF FIGURES

Figure 2-1 Mechanism of oxidation of linoleic acid. Figure adapted from Gordon (2001) (Gordon, 2001). 18

Figure 2-2 Example of natural antioxidants. Figure was reproduced from Colín-Chávez et al. (2013), Gordon (2001), Mortensen & Skibsted (1997), Rice-Evans et al. (1996), and Soto-Valdez et al. (2010) (C. Colín-Chávez, H. Soto-Valdez, E. Peralta, J. Lizardi-Mendoza, & R.R. Balandrán-Quintana, 2013; Gordon, 2001; Mortensen & Skibsted, 1997; Rice-Evans, Miller, & Paganga, 1996; Soto-Valdez, Auras, & Peralta, 2010). 28

Figure 2-3 Examples of synthetic antioxidants. Figure was reproduced from Gordon (2001) (Gordon, 2001)..... 29

Figure 2-4 Resonance of an antioxidant radical in the phenol structure. Figure was adapted and reproduced from Choe & Min (2006) (Choe & Min, 2006). 31

Figure 2-5 Mechanism of an antioxidant (a-tocopherol) in inhibiting lipid oxidation (linoleic acid). Figure adapted from Gordon (2001) (Gordon, 2001). 34

Figure 2-6 3D rectangular elements to represent diffusion in a plane sheet. 59

Figure 2-7 Migration phenonema that are controlled by the diffusion in the film. Figure was adapted from Poças et al. (2008) (Poças et al., 2008)..... 63

Figure 2-8 Migration phenomena that are controlled by the diffusion in the film with boundary layer resistance in the food/simulant. Figure was adapted from Poças et al. (2008) (Poças et al., 2008). 64

Figure 2-9 Illustration of boundary layer resistance at the interface of film/simulant. Region 1-2: Overall resistance of diffusion within film; region 2-3: resistance at the partition between film-food/simulant; region 3-4: mass transfer resistance at interface of film-food/simulant. Figure was adapted from Vitrac et al. (2007) (Vitrac et al., 2007). 65

Figure 2-10 Migration phenomena that are controlled by diffusion in the film and in the food/simulant. Figure was adapted from Poças et al. (2008) (Poças et al., 2008). 67

Figure 3-1 Poly(lactic acid), PLA chemical structure..... 94

Figure 3-2 Astaxanthin chemical structure. 95

Figure 3-3 The concentration of astaxanthin migrated into 95% ETOH at 30 to 40 °C..... 109

Figure 3-4 (a) Migration of astaxanthin into 95% ETOH at 30 °C and (b) 40 °C during storage. 110

Figure 3-5 DSC thermogram of (a) PLA2M in contact with 95% ETOH at 40°C for 3 d; (b) PLA in contact with 95% ETOH at 40°C for 3 d; (c) PLA2M in contact with 95% ETOH at 30°C for 24 d; (d) PLA in contact with 95% ETOH at 30°C for 24 d; (e) PLA2M; and (f) PLA. 114

Figure 3-6 Molecular weight distributions of fabricated functional membranes PLA and PLA2M without and in contact with 95% ETOH at 30 and 40 °C for 24 and 3 d, respectively. 117

Figure 3-7 Top SEM surface section micrograph (a) PLA; (b) PLA2M; (c) PLA in contact with 95% ETOH at 30 °C for 24 d; (d) PLA2M in contact with 95% ETOH at 30 °C for 24 d; (e) PLA in contact with 95% ETOH at 40 °C for 3 d; (f) PLA2M in contact with 95% ETOH at 40 °C for 3 d. Bar=10 μm. 121

Figure 3-8 (a) FTIR spectrum of the fabricated functional membranes and (b) focused FTIR spectrum of the fabricated functional membranes. 127

Figure 3-9 Oxidative stability of soybean oil packaged in the glass bottles, pouches made of PLA and pouches made of PLA2M at 30 °C during 25 d. Straight green line indicated the cut off point for Codex Alimentarius..... 130

Figure 4-1 Summary of migration cases A, B, and C. Figure adapted from Poças et. al (2008) (Poças et al., 2008). 146

Figure 4-2 (a) Scaled sensitivity coefficients for 2P, and (b) for 3P of migration study of PLA-α-tocopherol system at 23 °C using forward difference approximation. Initial guesses used were: D= 0.06×10^{-9} cm^2/s, M_{inf}=3.95×10^{-5} g α-tocopherol/g ethanol, and α=0.35. 154

Figure 4-3 Migration of α-tocopherol into 100% ethanol at 23 °C during storage for (a) 1P, (b) 2P, and (c) 3P using OLS estimation and their corresponding residuals plot (d), (e), and (f), respectively. 155

Figure 4-4 (a) Final scaled sensitivity coefficients for 2P, and (b) for 3P of migration study of PLA-α-tocopherol system at 23 °C using forward difference approximation. Estimated values used for 2P were: D= 4.05×10^{-10} cm^2/s, M_{inf}=0.36×10^{-4} g α-tocopherol/g ethanol. Estimated values used for 3P were: D= 0.79×10^{-10} cm^2/s, M_{inf}=0.37×10^{-4} g α-tocopherol/g ethanol, and α=0.30. ……156

Figure 4-5 Optimal experimental designs for 2P of migration study of PLA-α-tocopherol system at 23 °C……158

Figure 5-1 Example of multiple local minima for SSE in the non-linear estimation. (a) Surface plot with default view, (b) surface plot view set at azimuth and elevation of 28, and 28, respectively, and (c) contour plot for minimum region of SSE. 226

Figure 5-2 Graphical representation of the kinetics of migration. 228

Figure 5-3 Experimental data fitting by using the simplified model of step 1. Initial approximation values obtained from this step were: D=5.88 × 10^{-12} cm^2/min, $K_{p,f}$=605.63 cm^3 PLA/cm^3 ethanol, and h=2.80 × 10^{-6} cm/min. 243

Figure 5-4 Scaled sensitivity coefficient of the kinetics migration parameters using initial guesses obtained from step 1. Initial guesses were: D=6.50 × 10^{-12} cm^2/min, $K_{p,f}$=605.00 cm^3 PLA/cm^3 ethanol, and h=5.90 × 10^{-6} cm/min. 244

Figure 5-5 Migration of 3 wt.% of resveratrol into ethanol at 9 °C. 246

Figure 5-6 Desorption kinetics of PLA-3 wt.% resveratrol at 9 °C in the dimensionless time space (Fourier number=$\frac{Dt}{L^2}$). 247

Figure 5-7 Residual plot for migration of 3 wt.% of resveratrol into ethanol at 9 °C. 248

Figure 5-8 Normalized sequential parameters as a function of time for migration of 3 wt.% of resveratrol into ethanol at 9 °C. 250

Figure 5-9 (a) Sorption kinetic of 3 wt.% resveratrol into ethanol, and (b) KPD. The blue line indicates the equilibrium state. 252

Figure 5-10 Histogram of the bootstrap residuals. 254

Figure 5-11 Migration of 3 wt.% of resveratrol into ethanol at 9 °C with added bootstrap results. 255

Figure 5A- 1 Experimental data fitting by using the simplified model of step 1. Initial approximation values obtained from this step were: D=1.88× 10^{-9} cm^2/min, $K_{p,f}$=608.11 cm^3 PLA/cm^3 ethanol, and h=4.19× 10^{-4} cm/min. 258

Figure 5A- 2 Scaled sensitivity coefficient of the kinetics migration parameters using initial guesses obtained from step 1. Initial guesses were: D=1.90 × 10^{-9} cm^2/min, $K_{p,f}$=608.11 cm^3 PLA/cm^3 ethanol, and h=8.00× 10^{-4} cm/min. 259

Figure 5A- 3 Scaled sensitivity coefficient of the kinetics migration parameters (D and $K_{p,f}$) using initial guesses obtained from step 1. Initial guesses were: D=2.00 × 10^{-9} cm^2/min, $K_{p,f}$=609.00 cm^3 PLA/cm^3 ethanol. 260

Figure 5A- 4 Migration of 2.6 wt.% α-tocopherol into ethanol at 23 °C. 261

Figure 5A- 5 Desorption kinetics of PLA-2.6 wt.% α-tocopherol at 23 °C in the dimensionless time space (Fourier number=$\frac{Dt}{L^2}$).. 262

Figure 5A- 6 Residual plot for migration of 2.6 wt.% α-tocopherol into ethanol at 23 °C for two parameters estimation. 263

Figure 5A- 7 Normalized sequential parameters as a function of time for migration of 2.6 wt.% of α-tocopherol into ethanol at 23 °C. 266

Figure 5A- 8 (a) Sorption kinetic of 2.6 wt.% α-tocopherol into ethanol, and (b) KPD. The blue line indicates the equilibrium state. 267

Figure 5A- 9 Histogram of the bootstrap residuals. 268

Figure 5A- 10 Migration of 2.6 wt.% α-tocopherol into ethanol at 23 °C with added bootstrap results. 269

Figure 5B- 1 Experimental data fitting by using a simplified model of step 1. Initial approximation values obtained from this step were: D=1.39 × 10^{-8} cm^2/min, $K_{p,f}$=318.97 cm^3 PLA/cm^3 ethanol, and h=0.0024 cm/min. 270

Figure 5B- 2 Scaled sensitivity coefficient of the kinetics migration parameters using initial guesses obtained from step 1. Initial guesses were: D=3.00 × 10^{-8} cm^2/min, $K_{p,f}$=318.97 cm^3 PLA/cm^3 ethanol, and h=0.0040 cm/min. 271

Figure 5B- 3 Migration of 1.28 wt.% catechin into 95% ethanol at 40 °C. 272

Figure 5B- 4 Desorption kinetics of PLA-1.28 wt.% catechin at 40 °C in the dimensionless time space (Fourier number=$\frac{Dt}{L^2}$) 273

Figure 5B- 5 Residual plot for migration of 1.28 wt.% catechin into 95% ethanol at 40 °C. ... 274

Figure 5B- 6 Normalized sequential parameters as a function of time for migration of 1.28 wt.% of catechin into 95% ethanol at 40 °C. 277

Figure 5B- 7 (a) Sorption kinetic of 1.28 wt.% catechin into 95% ethanol, and (b) KPD. The blue line indicates the equilibrium state. 278

Figure 5B- 8 Histogram of the bootstrap residuals. 279

Figure 5B- 9 Migration 1.28 wt.% catechin into ethanol at 40 °C with added bootstrap results. 281

Figure 6-1 Scaled sensitivity coefficient of migration of 3 wt. % resveratrol from PLA film into ethanol at 9 °C of (a) model 1 (initial guesses were: D=6.50 × 10^{-12} cm^2/min, $K_{p,f}$=605.00 cm^3 PLA/cm^3 ethanol, and h=5.9 × 10^{-6} cm/min), and (b) model 2 (initial guesses were: D=5.19 × 10^{-12} cm^2/min and $K_{p,f}$=430.00 cm^3 PLA/cm^3 ethanol). 318

Figure 6-2 Migration of 3 wt. % resveratrol from PLA film into ethanol at 9 °C of (a) model 1, (b) model 2 and (c) model 3 and their corresponding residuals (d), (e), and (f), respectively. .. 321

Figure 6-3 Decision tree analysis for determining the kinetic mass transfer parameters (*i.e.*, D, $K_{p,f}$, h) of a migration study. 325

Figure 6A- 1 Scaled sensitivity coefficient of migration of 2.6 wt.% α-tocopherol from PLA film into ethanol at 23 °C of (a) model 1 (initial guesses were: D=2.00 × 10^{-9} cm^2/min, $K_{p,f}$=609 cm^3 PLA/cm^3 ethanol), and (b) model 2 (initial guesses were: D=10.00 × 10^{-9} cm^2/min and $K_{p,f}$=500 cm^3 PLA/cm^3 ethanol). Note: the h was not estimated for model 1 due to high correlation issue with the D..... 329

Figure 6A- 2 Migration of 2.6 wt.% α-tocopherol from PLA film into ethanol at 23 °C of (a) model 1 and (b) model 2 and their corresponding residuals (c), and (d), respectively..... 332

Figure 6B- 1 Scaled sensitivity coefficient of the migration of 1.28 wt.% catechin from PLA film into 95% ethanol at 40 °C of model 1 (initial guesses were: D=3.00 × 10^{-8} cm^2/min, $K_{p,f}$=318.97 cm^3 PLA/cm^3 ethanol). 334

Figure 6B- 2 Migration of 1.28 wt.% catechin from PLA film into 95% ethanol at 40 °C of (a) model 1 and (b) model 3 and their corresponding residuals (c), and (d), respectively..... 337

Figure 7-1 Scaled sensitivity coefficient of the activation energy estimation of the migration of 1.28 wt.% catechin from PLA film into 95% ethanol ranging from 20, 30, 40, and 50 °C at T_{ref}=35 °C.. Initial guesses were: D_{ref}=1.00 × 10^{-9} cm^2/min, $K_{p,f}$=800 cm^3 PLA/cm^3 ethanol, h=10.00 × 10^{-4} cm/min, and E_a=150000 J/mol)..... 350

Figure 7-2 Scaled sensitivity coefficient of the activation energy estimation at T_{ref}=35 °C of the migration of 1.28 wt.% catechin from PLA film into 95% ethanol ranging from 20, 30, 40, and 50 °C. Initial guesses were: D_{ref}=2.00× 10^{-9} cm^2/min, $K_{p,f}$=800 cm^3 PLA/cm^3 ethanol, and E_a=150000 J/mol). 351

Figure 7-3 Plot of correlation coefficient of the D_{ref} and the E_a as a function of possible T_{ref}.. 354

Figure 7-4 Final scaled sensitivity coefficient of the activation energy estimation of the migration of 1.28 wt.% catechin from PLA film into 95% ethanol ranging from 20, 30, 40, and 50 °C. Final estimates were: D_{ref}=3.70× 10^{-9} cm^2/min, $K_{p,f}$=436.62 cm^3 PLA/cm^3 ethanol, and E_a=153000 J/mol). 357

Figure 8-1 Scaled sensitivity coefficient of (a) the case with *Biot* number < 200 (Initial guesses were: D_{ref}=3.00 × 10^{-9} cm^2/min, $K_{p,f}$=608 cm^3 PLA/cm^3 ethanol, and h=8 × 10^{-5} cm/min), (b) the case with *Biot* number > 200 (Initial guesses were: D_{ref}=3.00 × 10^{-9} cm^2/min, $K_{p,f}$=608 cm^3 PLA/cm^3 ethanol, and h=1.60 × 10^{-3} cm/min)..... 381

KEY TO SYMBOLS AND ABBREVIATIONS

α	the ratio of the mass of migrant migrated into food/simulant to the mass of migrant left in the film at equilibrium
a_i	chemical activity
a_w	water activity
A	surface area
A*	antioxidant radical
Bi	Biot number
C	concentration
C_0	initial concentration
$C_{p,\infty}$	the concentration of the migrant in the film at equilibrium
$C_{f,\infty}$	the concentration of migrant in the food simulant at equilibrium
CO_2	carbon dioxide
D	diffusion coefficient
D_{ref}	diffusivity rate of the additives at T_{ref}
E_a	activation energy
$\hat{\varepsilon}_i$	residual
F	Flow rate
F_o	Fourier number
h	convective mass transfer coefficient
k	rate constant
k_0	frequency or pre-exponential factor

k_{ref}	specific reaction rate at T_{ref}
$K_{p,f}$	partition coefficient
L	film thickness
M_f	mass of the migrant in the food or simulant
M_n	number average molecular weight
M_p	the mass of the migrant in the film
M_w	weight average molecular weight
M_z	z-average molecular weight
M_∞	the mass of the migrant in the food or simulant at equilibrium
μ_i	chemical potential of migrant
μ_i^o	chemical potential of migrant at a standard state
O_2	oxygen
$^1O_2$	singlet oxygen
$^3O_2$	atmospheric triplet oxygen
p	number of parameter
P	concentration of food at steady state
ρ	correlation coefficient
q_n	the non-zero positive roots of eigenvalues
R	universal gas constant
R	rate constant
R*	alkyl radicals
RH	lipid molecule
ROO*	peroxy radicals

ROOH	lipid hydroperoxides
T	temperature
T_{cc}	cold-crystallization-temperature
T_d	decomposition temperature
T_g	glass transition temperature
T_m	melting temperature
T_{ref}	reference temperature
t	time
$\bar{u}$	residual concentration
V_f	volume of food/simulant
V_p	volume of film
X	sensitivity coefficient
X'	scaled sensitivity coefficient
X_c	degree of crystallinity
y_i	response variable
$\hat{y}_i$	predicted value
$y^*_{i=1,2,3\ldots n}$	synthetic data
$\lvert X^T X \rvert$	determinant
Δ^n	determinant
ΔH_{cc}	enthalpies of cold crystallization
ΔH_m	enthalpies of melting
ΔH_f *	heat of fusion of 100% crystalline sample
AICc	corrected Akaike information criterion

BHA	butylated hydroxyanisole
BHT	butylated hydroxytoluene
CMC	carboxymethylcellulose
DSC	differential scanning calorimeter
EDTA	ethylenediaminetetraacetic acid
ETOH	ethanol
EVA	ethylene(vinyl acetate)
EVOH	ethylene(vinyl alcohol)
FDA	Food and Drug Administration
FTIR	Fourier transform infrared spectrophotometer
GPC	gel permeation chromatography
HDPE	high density poly(ethylene)
HPLC	high performance liquid chromatography
IP	induction period
KPD	kinetic phase diagram
LDPE	low density poly(ethylene)
LLDPE	linear low density poly(ethylene)
LOQ	limit of quantification
MMT	montmorillonite
OLS	ordinary least squares
PA	poly(amide)
PBAT	poly(butylene adipate *co*-terephthalate)
PCL	poly(caprolacton)

PE	poly(ethylene)
PEG	polyethylene glycol
PET	poly(ethylene terephthalate)
PHBV	poly(hydroxybutyrate-*co*-valerate)
PI	polydispersity index
PLA	poly(lactic acid)
PLGA	poly(lactide-*co*-glycolide)
PP	poly(propylene)
PS	polystyrene
PTFE	polytetrafluoroethylene
PV	peroxide value
PVA	poly(vinyl acetate)
RH	relative humidity
RMSE	root means square errors
SEM	scanning electron microscope
SDS	sodium dodecyl sulphate
SSE	sums of squared errors
TBHQ	tert-butylhydroquinone
TGA	thermogravimetric analyzer
THF	tetrahydrofuran
UV	ultraviolet
UV-DAD	ultraviolet-diode array detector
WVP	water vapor permeability

Chapter 1

Background and Motivation

1.0 Introduction

Preservation of food is a very crucial step to maintain food quality, safety, and wholesomeness from the moment the food is produced until it is consumed. There are many technologies available and applicable for food preservation. These include traditional preservation technologies (*e.g.*, the control of pH and water activity, heat treatment, and temperature control), and emerging preservation technologies (*e.g.*, high intensity light, irradiation, modified atmosphere packaging, and active packaging) (Zeuthen & Bøgh-Sørensen, 2003). Among these technologies, preservation through packaging in general is more practical and economical since the product is not modified and extra treatments are not needed. Packaging is already needed for marketing and distribution purposes; thus, the use of packaging as a preservation technique adds extra benefits to a product. One of those aforementioned examples is active packaging.

Active packaging can be defined as a packaging system that provides continuous active protection to a food product/system during its shelf life by the incorporation of active substances (*e.g* food additives) within the material or into the packaging system itself. Some examples of active packaging are oxygen scavengers and ethylene absorbers, which are commonly included into the food system as a separate component. Meanwhile, antimicrobial and/or antioxidant packaging are examples of active packaging that involve the incorporation of active substances into the material itself.

To the best of author's knowledge, among the previously mentioned examples of incorporating the active substances directly into the packaging material, the development of antioxidant packaging systems have been extensively investigated (Gómez-Estaca, López-de-

Dicastillo, Hernández-Muñoz, Catalá, & Gavara, 2014; Sanches-Silva et al., 2014). This type of active system is developed to control lipid oxidation in fatty food products (Wessling, Nielsen, Leufvén, & Jägerstad, 1998) since lipid oxidation is among the main causes contributing to food deterioration (Gómez-Estaca et al., 2014; Sanches-Silva et al., 2014).

1.1 Research Importance and Motivation

The development of antioxidant functional films has been seen as an effective tool in preserving the quality of food containing fats as it provides protection beyond the function of just being an inert barrier. This type of active packaging system helps to retard lipid oxidation by gradually releasing the active substances into food for an extended period of time to ensure prolonged shelf life. This technique is believed to be more efficient than that of one-time direct addition of antioxidants into food during processing (Balasubramanian, 2009). Antioxidants are subjected to degradation and loss during processing. For an intended long shelf life product, antioxidant will be completely consumed after a short period of time, thus leaving the product unprotected from lipid oxidation. In adddition, the amount of antioxidants permitted for use in food products, singly or in combination, is limited to 0.02% by weight based on fat content of the food (Miková, 2001). This amount, sometimes, may not be sufficient, due to possible loss of antioxidants during processing and might be fully diminished before the product (food) even reaches market shelves. The addition of relatively high concentrations of certain antioxidants (*e.g.*, tocopherol and ascorbic acid) into food systems could also result in pro-oxidation reactions in lipids (Balasubramanian, 2009). Consequently, products may have a short shelf life.

Even though there is other existing technology, like oxygen scavengers, that can help to retard oxidation, there are some concerns about their application. Oxygen scavengers are

commonly incorporated into a packaging system in the form of sachets. Their absorbing capacity for oxygen is typically limited to 100 mL (Smith, Hoshino, & Abe, 1995), requiring multiple sachets for use with a product designed for a long shelf life, which is not practical or acceptable commercially (Robertson, 2006). Besides, it requires additional materials, which consumers do not perceive as good management of resources. In addition, possible accidental ingestion of these compounds could happen, although their ingestion does not cause adverse health impacts (Floros, Dock, & Han, 1997), which further deters consumer from buying the products.

An antioxidant functional film could be a feasible alternative technology for such applications. This technology is beneficial for both the packaging and the packaged food because it stabilizes the polymer during processing and inhibits the product's oxidation, respectively, through a 3-step mechanism: 1) antioxidant diffusion through the polymer bulk-phase to the polymer surface; 2) antioxidant volatilization from the packaging surface to the packaging headspace or desorption of antioxidant from the packaging surface into the surroundings; and 3) sequential migration or sorption of the antioxidant onto the product's surface (Bailey, 1995). This technology prevents lipid oxidation by a controlled constant release of antioxidants from the polymer matrix to the product, thus constantly protecting products when it is most needed, during storage.

Despite the promising benefits of incorporating antioxidants into the polymeric structures over direct addition into the food products, some research has shown the effectiveness, and limitations of this technology. Oregano functional film was found to be efficient in improving lamb steak oxidative stability (Camo et al., 2008). Nerín et al. (2006) reported promising outcomes from the use of antioxidant functional films for beef products (Nerín et al., 2006). Wessling et al. (2000) reported that the addition of α-tocopherol (above 360 ppm) in low density poly(ethylene),

(LDPE) delayed the oxidation of linoleic acid at 6 °C, but not at higher temperatures (20 and 40 °C). There were also some concerns reported on the potential changes in the mechanical properties, color, and the oxygen permeability of LDPE film incorporated with α-tocopherol (Wessling, Nielsen, & Leufven, 2000). In antioxidant functional film applications, synthetic antioxidants, like BHT and BHA, are exploited widely. Although these antioxidants are effective and provide economic value, the safe use of these antioxidants in food products has been questioned (Day, 2003; Gómez-Estaca et al., 2014); hence, there is intensive research carry out on new potential natural antioxidants (Barbosa-Pereira et al., 2013; Calatayud et al., 2013; Chen, Lee, Zhu, & Yam, 2012; Contini et al., 2012; Hwang et al., 2012; Lopez de Dicastillo et al., 2011; Pereira de Abreu, Losada, Maroto, & Cruz, 2010; Sonkaew, Sane, & Suppakul, 2012; Zhu, Lee, & Yam, 2012; Zhu, Schaich, Chen, & Yam, 2013). Some natural antioxidants could be more potent, efficient, and safer than synthetic ones. Natural α-tocopherol, for instance, has higher antioxidant capability than synthetic racemic α-tocopherol because it is selectively recognized by the α-tocopherol transfer protein (HongLian et al., 2001). Natural antioxidants are also generally recognized as safe (GRAS), and their use is not limited when used in accordance with good manufacturing practice (GMP) (Rajalakshmi & Marasimhan, 1995).

Most of the research conducted in the area of antioxidant packaging systems focuses on non-renewable materials. Mainly, the developed antioxidant functional films are made of polyolefins such as low density poly(ethylene), (LDPE) and poly(propylene), (PP) (Gavara, Lagarón, & Catalá, 2004; Wessling et al., 1998). In recent years, there is a growing trend to use biodegradable materials to develop antioxidant functional films. This tendency may be associated with increasing concerns about municipal solid waste and growing environmental awareness among consumers (Endres, Siebert, & Kaneva, 2007).

Some biodegradable materials that have gained increasing interest are poly(lactic acid) (PLA), thermoplastic starch, and poly(butylene adipate *co*-terephthalate) (PBAT), to name a few. PLA is a biopolymer produced from polymerization of lactic acid (Endres et al., 2007), and it can be obtained from renewable resources, like corn (Auras, Harte, Selke, & Hernandez, 2003), sugar beet and sugarcane residues (Endres et al., 2007). PLA is a transparent material, so it is good for food packaging applications. It can be formed into a variety of containers, trays, films, and other type of packaging structures. PLA is biodegradable, compostable and recyclable, and it has been approved by the US Food Drug Administration (FDA) as suitable for food-contact packaging applications (Auras, Harte, & Selke, 2004). PLA is comparable to poly(ethylene terephthalate), (PET), and polystyrene, (PS) in terms of its physical and mechanical properties, and it has low barrier to gases such as carbon dioxide (CO_2) and oxygen (O_2) (Auras, Harte, & Selke, 2003). Therefore, its application in food packaging, for instance, might be limited to certain types of food. For example, fatty food products packaged in PLA would experience lipid oxidation as a result of its low barrier to oxygen. For this reason, the incorporation of antioxidants into a PLA polymeric structure could be a potential enhancement for this polymer's properties and a preservation tool for targeted food systems.

Research involving characterization of PLA with incorporated antioxidants is increasing rapidly. Both natural and synthetic antioxidants were investigated for their potential with PLA polymeric structures as antioxidant functional films. Butylated hydroxyanisole (BHA), butylated hydroxytoluene (BHT), propyl gallate, and tert-butylhydroquinone (TBHQ) are among common synthetic antioxidants that have been incorporated into a PLA matrix (Byun, Kim, & Whiteside, 2010; M. Jamshidian et al., 2012; Jamshidian, Tehrany, & Desobry, 2012; Ortiz-Vazquez, Shin, Soto-Valdez, & Auras, 2011). Catechin, epicatechin, tocopherol, and resveratrol are examples of

natural antioxidants that have been incorporated into PLA (Byun et al., 2010; Hwang et al., 2013; Hwang et al., 2012; Iñiguez-Franco et al., 2012; Manzanarez-López, Soto-Valdez, Auras, & Peralta, 2011; Soto-Valdez, Auras, & Peralta, 2010).

Even though antioxidant-PLA functional films have been widely investigated, most of the studied antioxidants are phenolic in nature, and to the author's best knowledge, there is scarce information about PLA incorporated with carotenoid-based antioxidants. Therefore, functionalization of PLA with carotenoid-based antioxidants is needed to fill this gap. Carotenoid-based antioxidants act by a different mechanism as antioxidants than the phenolic ones; thus different outcomes on the basis of polymer-antioxidant interactions and their corresponding properties are anticipated.

Most of the research on antioxidant functional films being researched focuses on migration studies and/or characterization of the film properties. To the extent of the author's knowledge, very limited research has emphasized mathematical modeling of the kinetic release of antioxidants from functional films, by means of parameter and sequential estimations. Numerous advantages can be gained by using mathematical modeling to understand the kinetic release of antioxidant functional films such as the physical interpretation of parameters with respect to experimental study, time and cost-saving, *etc.* Thus, the importance of mathematical modeling as a food safety tool and quality assurance needs to be considered.

1.2 Objectives

The main objectives of this dissertation were:

1. To produce a biodegradable bilayer functional film incorporated with a carotenoid-based natural antioxidant (astaxanthin), to characterize the produced film's properties,

to perform an oxidative stability study and to investigate the kinetic release of the incorporated antioxidant into a fatty food simulant at two different temperatures.

2. To introduce a parameter estimation approach to assess the kinetic migration parameters of antioxidant functional films.
3. To develop a new mathematical solution consisting of the three main kinetic migration parameters (*i.e.*, the diffusion coefficient (D), the partition coefficient ($K_{p,f}$), and the convective mass transfer coefficient (h)) that govern most of the migration experiments, and to compare this developed solution with the general mass transfer solutions provided by Carslaw & Jaeger (1959) and Crank (1979).
4. To estimate the activation energy (E_a) of non-isothermal migration experiments using a non-linear reparameterization approach to the Arrhenius equation.

1.3 Dissertation Overview

This dissertation is organized as follows.

Chapter 2 provides a literature review of three main sections; *i*) lipid oxidation, its mechanism with respect to different factors (*i.e.*, environmental conditions, presence of metal, *etc.*) and approaches to prevent lipid oxidation, *ii*) migration phenomena and general mathematical models used for migration studies, and *iii*) parameter estimation approach (*i.e.*, ordinary least square (OLS), sequential, bootstrap, *etc.*) to assess the kinetic migration parameters.

Chapter 3 explores the development of PLA-functional film incorporated with a natural carotenoid-based antioxidant (astaxanthin). The developed film was subjected to various testing, which included thermal analyses, barrier and molecular weight properties, morphological study,

oxidative stability and the kinetic release of astaxanthin from PLA-functional film into 95% ethanol at 30 and 40 °C.

Chapter 4 investigates the kinetic release for different migration case studies employing the general mass transfer solutions by Carslaw & Jaeger (1959) and Crank (1979) by means of the parameter estimation approach (*i.e.*, scaled sensitivity coefficient, *X'*, OLS estimation, optimal experimental design). Comparison of estimating 1 parameter, 1P (*i.e.*, *D*) versus 2P (*i.e.*, *D* and the mass of the migrant in the food or simulant at equilibrium, M_∞) and 3P (*i.e.*, *D*, M_∞, and the ratio of the mass of antioxidant migrated into the simulant to the mass of the antioxidant left in the film, at equilibrium (α), was also done by using the corrected Akaike information criterion (AICc) and root means square errors (RMSE).

Chapter 5 proposes a new two-step mathematical solution to estimate the three kinetic migration parameters (*i.e.*, *D*, $K_{p,f}$, *h*). This solution was developed based on the boundary conditions provided by Carslaw & Jaeger (1959) and Crank (1979). Three selected migration case studies were used to demonstrate the application of this solution by means of the parameter estimation approach (*i.e.*, *X'*, OLS estimation, sequential estimation, kinetic phase diagram (KPD), and bootstrap method).

Chapter 6 provides a comparative study between the two-step mathematical solution proposed in chapter 5 with the general mass transfer solutions by Carslaw & Jaeger (1959) and Crank (1979) using three different migration case studies. The *X'* and OLS estimation were performed. The model discrimination was evaluated using the AICc approach.

Chapter 7 explores the estimation of E_a of non-isothermal migration studies using the reparameterized Arrhenius equation. The simulation temperature (T_{sim}) was introduced for visual observation of E_a for *X'* plot.

Chapter 8 summarizes all the works in this dissertation and concludes with future work recommendations.

REFERENCES

REFERENCES

Auras, R., Harte, B., & Selke, S. (2003). Effect of water on the oxygen barrier properties of poly (ethylene terephthalate) and polylactide films. *Journal of Applied Polymer Science, 92*, 1790-1803.

Auras, R., Harte, B., & Selke, S. (2004). An overview of polylactides as packaging materials. *Macromolecular Bioscience, 4*(9), 835-864. doi: Doi 10.1002/Mabi.200400043

Auras, R., Harte, B., Selke, S., & Hernandez, R. J. (2003). Mechanical, Physical, and Barrier Properties of Poly(lactide) Films. *Journal of plastic film and sheeting, 19*, 123-134.

Bailey, L. A. (1995). Mass Transfer of 3, 5-di-tertiary-butyl-4-hydroxytoluene (BHT) from a Multi-layer Lamination. Michigan State University. School of Packaging.

Balasubramanian, A. (2009, March 1, 2009). Antioxidant Packaging. *Packaging World Magazine*.

Barbosa-Pereira, L., Cruz, J. M., Sendón, R., Rodríguez Bernaldo de Quirós, A., Ares, A., Castro-López, M., . . . Paseiro-Losada, P. (2013). Development of antioxidant active films containing tocopherols to extend the shelf life of fish. *Food Control, 31*(1), 236-243.

Byun, Y., Kim, Y. T., & Whiteside, S. (2010). Characterization of an antioxidant polylactic acid (PLA) film prepared with α-tocopherol, BHT and polyethylene glycol using film cast extruder. *Journal of Food Engineering, 100*(2), 239-244.

Calatayud, M., López-de-Dicastillo, C., López-Carballo, G., Vélez, D., Muñoz, P. H., & Gavara, R. (2013). Active films based on cocoa extract with antioxidant, antimicrobial and biological applications. *Food Chemistry*.

Camo, J., Beltrán, J. A., & Roncalés, P. (2008). Extension of the display life of lamb with an antioxidant active packaging. *Meat Science, 80*(4), 1086-1091.

Carslaw, H. S., & Jaeger, J. C. (1959). Conduction of heat in solids. *Oxford: Clarendon Press, 1959, 2nd ed., 1*.

Chen, X., Lee, D. S., Zhu, X., & Yam, K. L. (2012). Release kinetics of tocopherol and quercetin from binary antioxidant controlled-release packaging films. *Journal of Agricultural and Food Chemistry, 60*(13), 3492-3497.

Contini, C., Katsikogianni, M. G., O'Neill, F. T., O'Sullivan, M., Dowling, D. P., & Monahan, F. J. (2012). PET trays coated with Citrus extract exhibit antioxidant activity with cooked turkey meat. *LWT-Food Science and Technology, 47*(2), 471-477.

Crank, J. (1979). *The Mathematics of Diffusion* (2nd ed.). Bristol: Oxford University Press.

Day, B. P. F. (2003). Active packaging *Food packaging technology* (Vol. 6, pp. 282): Blackwell.

Endres, H.-J., Siebert, A., & Kaneva, Y. (2007). Overview of the current biopolymers market situation. *Bioplastic magazine, 2*, 3.

Floros, J. D., Dock, L. L., & Han, J. H. (1997). Active packaging technologies and applications. *Food Cosmetics and Drug Packaging, 20*(1), 10-17.

Gavara, R., Lagarón, J. M., & Catalá, R. (2004). *Materiales poliméricos para en diseñyo de envases actives.* Paper presented at the Seminario Cyted-Technológico de Monterrey, Monterrey, México.

Gómez-Estaca, J., López-de-Dicastillo, C., Hernández-Muñoz, P., Catalá, R., & Gavara, R. (2014). Advances in antioxidant active food packaging. *Trends in Food Science & Technology, 35*(1), 42-51.

HongLian, S., Noguchi, N., Niki, E., Pokorny, J., Yanishlieva, N., & Gordon, M. (2001). Introducing natural antioxidants *Antioxidants in Food: Practical Applications* (pp. 147-158): Woodhead Publishing Ltd.

Hwang, S. W., Shim, J. K., Selke, S., Soto-Valdez, H., Matuana, L., Rubino, M., & Auras, R. (2013). Migration of α-Tocopherol and Resveratrol from Poly (L-lactic acid)/Starch Blends Films into Ethanol. *Journal of Food Engineering*.

Hwang, S. W., Shim, J. K., Selke, S. E. M., Soto‐Valdez, H., Matuana, L., Rubino, M., & Auras, R. (2012). Poly (L‐lactic acid) with added α‐tocopherol and resveratrol: optical, physical, thermal and mechanical properties. *Polymer International, 61*(3), 418-425.

Iñiguez-Franco, F., Soto-Valdez, H., Peralta, E., Ayala-Zavala, J. F., Auras, R., & Gámez-Meza, N. (2012). Antioxidant Activity and Diffusion of Catechin and Epicatechin from Antioxidant Active Films Made of Poly (l-lactic acid). *Journal of Agricultural and Food Chemistry, 60*(26), 6515-6523.

Jamshidian, M., Tehrany, E. A., Cleymand, F., Leconte, S., Falher, T., & Desobry, S. (2012). Effects of synthetic phenolic antioxidants on physical, structural, mechanical and barrier properties of poly lactic acid film. *Carbohydrate polymers, 87*(2), 1763-1773.

Jamshidian, M., Tehrany, E. A., & Desobry, S. (2012). Release of synthetic phenolic antioxidants from extruded poly lactic acid (PLA) film. *Food Control*.

Lopez de Dicastillo, C., Nerin, C., Alfaro, P., Catalá, R., Gavara, R., & Hernandez-Muñoz, P. (2011). Development of new antioxidant active packaging films based on ethylene vinyl alcohol copolymer (EVOH) and green tea extract. *Journal of Agricultural and Food Chemistry, 59*(14), 7832-7840.

Manzanarez-López, F., Soto-Valdez, H., Auras, R., & Peralta, E. (2011). Release of α-Tocopherol from Poly (lactic acid) films, and its effect on the oxidative stability of soybean oil. *Journal of Food Engineering, 104*(4), 508-517.

Miková, K. (2001). The regulation of antioxidants in food. In J. Pokorny, N. Yanishlieva & M. Gordon (Eds.), *Antioxidants in Food* (pp. 284-287). Cambridge, U.K.: Woodhead Publishing Limited.

Nerín, C., Tovar, L., Djenane, D., Camo, J., Salafranca, J., Beltrán, J. A., & Roncalés, P. (2006). Stabilization of beef meat by a new active packaging containing natural antioxidants. *Journal of Agricultural and Food Chemistry, 54*(20), 7840-7846.

Ortiz-Vazquez, H., Shin, J. M., Soto-Valdez, H., & Auras, R. (2011). Release of butylated hydroxytoluene (BHT) from Poly (lactic acid) films. *Polymer Testing, 30*(5), 463-471.

Pereira de Abreu, D. A., Losada, P. P., Maroto, J., & Cruz, J. M. (2010). Evaluation of the effectiveness of a new active packaging film containing natural antioxidants (from barley husks) that retard lipid damage in frozen Atlantic salmon (Salmo salar). *Food Research International, 43*(5), 1277-1282.

Rajalakshmi, D., & Marasimhan, S. (1995). Food Antioxidants: Sources and Methods of Evaluation *Food Antioxidants: Technological: Toxicological and Health Perspectives* (Vol. 71, pp. 65): CRC.

Robertson, G. L. (2006). Active and intelligent packaging. In G. L. Robertson (Ed.), *Food Packaging: Principles and Practice* (2nd ed., pp. 292-294). Boca Raton: CRC Press.

Sanches-Silva, A., Costa, D., Albuquerque, T. G., Buonocore, G., Ramos, F., Castilho, M. C., . . . Costa, H. S. (2014). Trends in the use of natural antioxidants in active food packaging: a review. *Food Additives & Contaminants: Part A*(just-accepted).

Smith, J. P., Hoshino, J., & Abe, Y. (1995). Active packaging in polymer films. In M. Rooney (Ed.), *Active Food Packaging* (pp. 143-172). Glasgow: Blackie Academic & Professional.

Sonkaew, P., Sane, A., & Suppakul, P. (2012). Antioxidant activities of curcumin and ascorbyl dipalmitate nanoparticles and their activities after incorporation into cellulose-based packaging films. *Journal of Agricultural and Food Chemistry, 60*(21), 5388-5399.

Soto-Valdez, H., Auras, R., & Peralta, E. (2010). Fabrication of Poly(lactic acid) Films with Resveratrol and the Diffusion of Resveratrol into Ethanol. *Journal of Applied Polymer Science*. doi: 10.1002/app.33687

Wessling, C., Nielsen, T., & Leufven, A. (2000). The influence of alpha-tocopherol concentration on the stability of linoleic acid and the properties of low-density polyethylene. *Packaging Technology and Science, 13*(1), 19-28.

Wessling, C., Nielsen, T., Leufvén, A., & Jägerstad, M. (1998). Mobility of α-tocopherol and BHT in LDPE in contact with fatty food simulants. *Food additives and contaminants, 15*(6), 709-715. doi: 10.1080/02652039809374701

Zeuthen, P., & Bøgh-Sørensen, L. (2003). *Food preservation techniques*: CRC Press.

Zhu, X., Lee, D. S., & Yam, K. L. (2012). Release property and antioxidant effectiveness of tocopherol-incorporated LDPE/PP blend films. *Food Additives and Contaminants: Part A, 29*(3), 461-468.

Zhu, X., Schaich, K. M., Chen, X., & Yam, K. L. (2013). Antioxidant Effects of Sesamol Released from Polymeric Films on Lipid Oxidation in Linoleic Acid and Oat Cereal. *Packaging Technology and Science, 26*(1), 31-38. doi: 10.1002/pts.1964

Chapter 2

Literature Review

2.0 Introduction

The first part of this chapter focuses on lipid oxidation and its classification, factors influencing lipid oxidation, and approaches used to inhibit lipid oxidation. The second part covers the migration process and commonly encountered migration systems. The last part of this chapter describes the parameter estimation technique for modeling different migration systems.

2.1 Lipid Oxidation: Brief Introduction

Foods containing fats, such as meats, milk, and butter, to name a few, are subject to reduced shelf life as a result of lipid degradation. Understanding the pathway of lipid oxidation is crucial to prevent this deterioration process from causing undesirable organoleptic modification of fatty-based foods (*i.e.,* off-flavors and aromas, detrimental effect on nutrition, and carcinogenic by-products).

2.2 Lipid Oxidation: Classification

Deterioration of lipids can be classified into three main types: autoxidation, photooxidation or photosensitized oxidation, and lipoxygenase-catalyzed oxidation.

2.2.1 Autoxidation

Autoxidation is the most common process contributing to oxidative deterioration (Gordon, 2001). This reaction often shows an induction period (IP). During the IP, the deterioration of lipids occurs at a very slow rate, while at the end of this period, noticeable and rapid deterioration takes

place. The autoxidation mechanism consists of four mechanism steps; i) initiation, ii) propagation, iii) chain branching, and iv) chain termination (Figure 2-1) (Gordon, 1990).

2.2.1.1 Step 1: Initiation

This process is called initiation because for it to occur, initiators are required. Initiators are compounds containing double bonds that are in singlet spin states. Lipid needs molecules (RH) that have similar spin states to be able to produce a lipid free radical (Schaich, Shahidi, Zhong, & Eskin, 2013). Therefore, at this early stage, an RH is ruptured to a lipid free radical by a metal catalyst, exposure to light, by hydroperoxide decomposition or by reaction with singlet oxygen molecules or an enzyme-catalyzed reaction (Gordon, 2001).

$$RH \longrightarrow R^* + H^*$$

2.2.1.2 Step 2: Propagation

The chain reaction is propagated by the abstraction of H at a position α to double bonds. The reaction of lipid free radicals with atmospheric triplet oxygen ($^3O_2$) then results in the formation of peroxy radicals (ROO*). Lipid hydroperoxides (ROOH) and alkyl radicals (R*) are formed later after peroxy radicals react with more lipid molecules (Gordon, 2001; Schaich et al., 2013). This process is continuous as long as the source of H is still available or no interception of the chains occurs (Schaich et al., 2013).

$$R^* + {}^3O_2 \longrightarrow ROO^*$$

$$ROO^* + RH \longrightarrow ROOH + R^*$$

2.2.1.3 Step 3: Chain branching

This step involves the decomposition of hydroperoxides to generate more free radicals

$$ROOH \longrightarrow RO^* + {}^*OH$$

2.2.1.4 Step 4: Chain termination

Free radicals are combined to form peroxide compounds. Since these compounds are unstable, they decompose to release hydrocarbons, alcohols or aldehydes (Gordon, 2001; Schaich et al., 2013). The by-products produced depend on the type of chain scission reactions (α or β), the composition and concentration of hydroperoxides, temperature, and/or O_2, to name a few (Laguerre, Lecomte, & Villeneuve, 2007; Schaich et al., 2013).

$$2R^* \longrightarrow R\text{-}R$$

$$R^* + ROO^* \longrightarrow ROOR$$

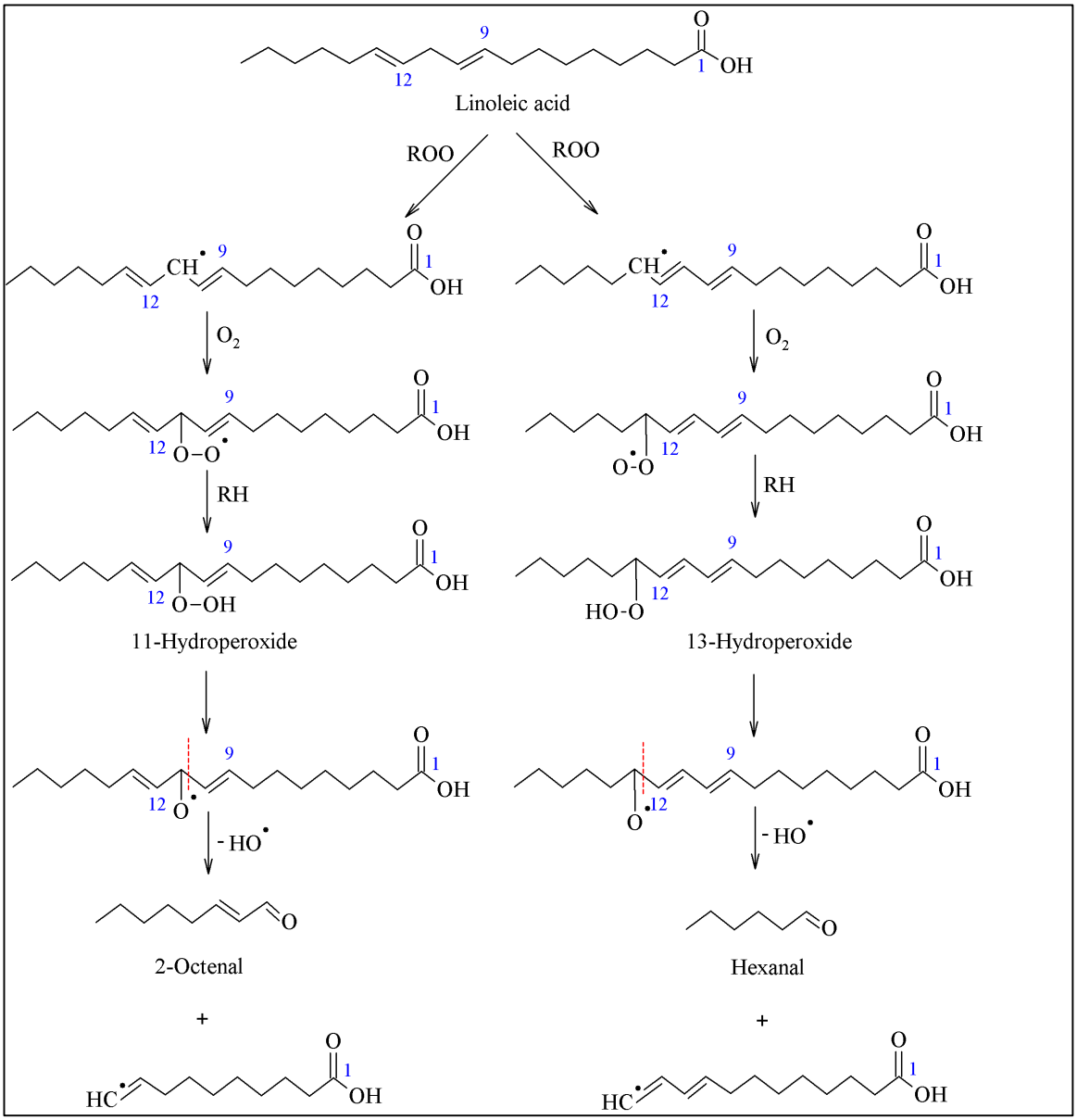

Figure 2-1 Mechanism of oxidation of linoleic acid. Figure adapted from Gordon (2001) (Gordon, 2001).

2.2.2 Photooxidation or Photosensitized Oxidation

There are two types of photooxidation: Type I results from excitation of lipids, and Type II is associated with excitation of O_2 which may occur in the presence of light and a sensitizer

(Gordon, 2001). Photooxidation has no induction period; thus the level of hydroperoxides formed steadily increases. This type of oxidation highly depends on the concentration of sensitizers, is independent of O_2 concentration unless it is limited, and the rate of oxidation increases accordingly with the number of double bonds of the fatty acids (Schaich et al., 2013; Terao & Matsushita, 1977).

2.2.2.1 Type I: photooxidation by excitation of lipids

This type of oxidation is characterized by hydrogen atom transfer or electron transfer between a substrate and an excited triplet sensitizer, which later forms free radical ions. This type of oxidation require a certain or specific wavelength for initiation (Gordon, 2001). Some of the most common photosensitizers type I are chlorophyll, hemes (*e.g.*, myoglobin, hemoglobin), xanthenes, anthroquinones, and food dyes (Schaich et al., 2013).

2.2.2.2 Type II: photooxidation by excitation of O_2

In the presence of light and a sensitizer, a triplet oxygen ($^3O_2$) will become excited to a singlet oxygen ($^1O_2$). This state of oxygen ($^1O_2$) reacts more than 1500 times faster with a polyunsaturated fatty acid to form a hydroperoxide than triplet oxygen (Gordon, 2001). Some examples of sensitizers that fall into this category are chlorophyll, erythrosine, flavins, and eosin (Schaich et al., 2013).

2.2.3 Enzyme-Catalyzed Lipid Oxidation

Lipoxygenase is an enzyme found in both plant and animal tissues. This enzyme functions by catalyzing the incorporation of oxygen into polyunsaturated fatty acids and/or their esters, and acylglycerols containing the *cis*, *cis*-1,4-pentadiene system. This process later leads to the formation of conjugated *cis*, *trans* hydroperoxide (Gordon, 2001).

2.3 Factors Affecting Lipid Oxidation

There are many factors that may contribute towards oxidation in fatty food products. Identifying these factors may benefit food manufacturers in protecting their products from oxidation and also aid packaging engineers in designing packaging for oxygen-sensitized products that complies with regulations as well as optimizes function and extends shelf life. The factors that affect the oxidation rate of a fatty food product are discussed in the following section.

2.3.1 Chemical Structure of Fatty Acids

Fatty food products are generally susceptible to lipid oxidation. The tendency of these products to undergo oxidation can be predicted by knowing the chemical composition of their respective fatty acids. Fatty acids that contain more conjugated double bonds are more likely to oxidize since the alkene groups reduce the bond dissociation energy of neighboring C-H bonds. Consequently, the tendency of hydrogen abstraction that leads to the formation of alkyl radicals that are readily available for interaction with oxygen increases (Gordon, 2001). In addition, the amount and the rate of formation of primary oxidation compounds at the final stage of the induction period also increases with increased degree of unsaturation (Choe & Min, 2006; Martin-Polvillo, Márquez-Ruiz, & Dobarganes, 2004). It is also crucial to highlight that the isomeric form of the fatty acids influences the rate of the oxidation process. The *cis* isomer of fatty acids will likely oxidize faster than the *trans* isomer due to the unsaturated site that is ready for H abstraction (Schaich et al., 2013).

2.3.2 Temperature

In general, an increase of 10 °C in temperature increases the rate of biological reactions by 2 to 3 fold, as stated by van't Hoff's Rule (Cohen Stuart, 1912). Increased temperature has been reported to accelerate lipid oxidation due to the increase in the rate of hydroperoxide decomposition (Labuza & Dugan Jr, 1971; Schaich et al., 2013). In addition, at temperatures greater than 150 °C, the chances for lipid oxidation to take place are higher due to molecular degradation and autoxidation in the presence of initiators and air that results from thermally-induced chain scission (Nawar, 1969; Schaich et al., 2013). In contrast, some literature reports that temperature has little effect on lipid oxidation as a result of its low activation energy (0 to 6 kcal/mole) (Choe & Min, 2006; Rahmani & Csallany, 1998; Yang & Min, 1994).

2.3.3 Light

The effect of light on lipid oxidation has been reported to be more pronounced than the effect of temperature. Shorter wavelengths are reported to be more damaging than longer ones (Sattar, DeMan, & Alexander, 1976), and the effect of light on lipid oxidation lessens as temperature increases (Choe & Min, 2006; Velasco & Dobarganes, 2002). Lipid oxidation of a mayonnaise product was greater at wavelengths lower than 470 nm, where a significant detrimental effect was observed with decreasing wavelengths of light (i.e., 365>405>435 nm) (Lennersten & Lingnert, 2000), due to the higher energy.

Fatty acids contain chromaphores, which consist of carbonyl groups, unsaturated sites (double bonds), and peroxide (O-O) bonds. Among those, peroxide bonds possess bond energies that are in the appropriate range to interact with UV light. Moreover, UV light was reported to have more damaging effect on fatty acids than visible light because of its capability to produce

strong oxidizing hydroxyl radicals rather than hydroxyl ions (Schaich et al., 2013). Visible light, on the other hand, requires photosensitizers (*e.g.*, chlorophyll, xanthenes) to be able to absorb low energy light that later excites the atoms from the ground state to a high energy state before forming free radicals or singlet oxygen by shifting the excitation energy to fatty acids or to oxygen, respectively (Murray, 1979; Schaich et al., 2013).

2.3.4 Oxygen, O_2

One of the key factors that significantly influences lipid oxidation is oxygen (O_2). Both the type and the concentration of O_2 may directly or indirectly affect the kinetics of lipid oxidation.

2.3.4.1 Type of O_2

There are two types of oxygen that affect lipid oxidation: i) atmospheric triplet oxygen, $^3O_2$, and ii) singlet oxygen, $^1O_2$. The former is responsible for autoxidation by reacting with lipid radicals and the latter is a product of photosensitized oxidation of edible oils, an oxidation mechanism that takes place in the presence of light, sensitizers and atmospheric oxygen. $^1O_2$ was reported to be able to directly react with lipids while $^3O_2$ reacts with lipid radicals (Choe & Min, 2006).

2.3.4.2 Concentration of O_2

The kinetics of lipid oxidation not only depend on the types of O_2, but also on the concentration of O_2. At high temperature and in the presence of light and sensitizers, the oxidation rate increases proportionally with increasing concentration of O_2. High temperature increases the diffusivity of O_2 into oil; meanwhile the light and sensitizers transfer sufficient excitation energy

to allow the O_2 to react readily with unsaturated sites of fatty acids, thus increasing the oxidation rate in the presence of higher O_2 concentrations (Choe & Min, 2006). Under limited O_2 concentrations, the oxidation rate increases with increasing O_2 pressure (Schaich et al., 2013). However, in the presence of excessively high concentrations of O_2 in comparison with the amount of fatty acids, the rate of lipid oxidation is not affected due to insufficient unsaturated sites for oxidation to occur (i.e., controlling mechanism for oxidation). It is also worth mentioning that the rate of lipid oxidation increases with increasing surface area for food products (liquid or solid) since the reaction between O_2 in the atmosphere with fatty acids on the product's surface is faster than that with O_2 that diffuses into the product (Schaich et al., 2013).

2.3.5 Presence of Minor Compounds

Lipid oxidation is a complex process that can take place by various mechanisms with different pathways. This process may end up with similar or different by-products such as hexanal, nonanal, decanal, 1-pentene-3-one, 2-pentylfuran, etc., regardless whether the mechanisms and pathways are similar or different. Therefore, any single or combination of different minor chemical compounds present in the food system may have an effect on the oxidation of lipids and needs to be understood to foresee the best approach to improve the quality and the shelf life of the food system.

2.3.5.1 Water and Water Activity, a_w

Water and water activity, a_w play an important role in lipid oxidation. Both can demonstrate either antioxidant or pro-oxidant effects on lipid oxidation of food. a_w refers to the water that is present in the food product and is available, but it is not bound through chemical reactions. a_w

ranges from 0 to 1.0 with the former being a completely dry system and the latter being a highly moist system. In the case of lipid oxidation in dry systems within a_w ranges of 0 to 0.2, the rate of lipid oxidation increases with decreasing a_w. A dry system allows more accessibility towards molecular sites of oxidation because of the system's matrix porosity, thus increasing chances for the unsaturated chain site to chemically interact with O_2 (Karel, 1980; Labuza & Dugan Jr, 1971; Schaich et al., 2013). The rate of lipid oxidation is typically lowest in a food system that has a_w 0.2 to 0.5 (monolayer region for food system) as a result of limited mobility of O_2 and catalysts. For a system that has a_w between 0.5 and 0.7, lipid oxidation of a particular food system increases with increasing a_w due to the increased mobility of catalysts and O_2 with reactive sites, also due to higher catalyst and O_2 diffusivities in the system. On the other hand, at $a_w > 0.7$, the occurrence of lipid oxidation is at its highest and then decreases with increasing a_w because of the dilution of catalysts and reactants. In addition, the non-enzymatic browning reaction that produces some antioxidants is also higher at a high a_w level (Karel, 1980; Labuza & Dugan Jr, 1971; Schaich et al., 2013).

2.3.5.2 Metals

Metals enhance lipid oxidation by directly/indirectly interacting with fatty acids, thus forming some compounds that increase the rate of oxidation, including peroxy radicals, $^1O_2$ that are highly reactive, and hydrogen peroxides, to name a few (Andersson, 1998; Choe & Min, 2006). Oxidized metals are documented as more powerful than reduced metals since they can directly produce initial radicals. Some examples of metals that exist naturally in products like crude oil are copper and ferrous ions (Schaich et al., 2013).

2.3.5.3 Free Fatty Acids

Lipids contain various free fatty acids, esters, and triacylglycerols. The nature and quantity of these groups determines the mechanism of lipid oxidation. Therefore, it is vital to understand the composition of lipids because of their huge impact on the kinetics of lipid oxidation. Free fatty acids are naturally existing compounds in crude oils (Choe & Min, 2006). They can demonstrate either pro-oxidant or antioxidant effects depending on the food system and the presence of other minor components in the particular system. Free fatty acids are reported to oxidize more slowly than esters and triacylglycerols due to the involvement of acid groups in the non-radical decomposition of hydroperoxides (Schaich et al., 2013). This mechanism later initiates nucleophilic rearrangements that slow down the rate of oxidation by preventing chain branching reactions (Schaich et al., 2013). It was reported that free fatty acids increased the O_2 diffusivity into edible oil, thus increasing the oxidation rate. The reason was due to the chemical structure of free fatty acids that contain both hydrophilic and hydrophobic groups that help in reducing the surface tension of edible oils (Choe & Min, 2006; Mistry & Min, 1987). Having mentioned about some of the free fatty acids mechanisms as a pro-oxidant, to the contrary, the presence of carboxylic groups in the free fatty acids' structure can also demonstrate their antioxidant mechanism. The carboxylic groups in free fatty acids may act as excellent metal complexers that help in blocking the electron transfer in metals, resulting in a decrease in the rate of oxidation due to the reduction of the redox potential (Schaich et al., 2013).

2.3.5.4 Phospholipids

Similar to free fatty acids, phospholipids may also act as antioxidants or as pro-oxidants. The ability of phospholipids to bind water enhances the mobilization of catalysts that results in an

increase of oxidation rate (Nwosu, Boyd, & Sheldon, 1997; Schaich et al., 2013). In addition, the presence of hydrophilic and hydrophobic groups in their structure causes a reduction in the surface tension of their respective systems and increases the O_2 diffusivity, which results in an acceleration of the system's oxidation rate (Choe & Min, 2006; Yoon & Min, 1987). The non-radical decomposition of hydroperoxides of phospholipids was reported to show an antioxidant effect since it intercepts the radical chain reactions (Corliss & Dugan Jr, 1970; O'brien, 1969; Schaich et al., 2013), in turns reducing the rate of oxidation. However, this mechanism does not hinder other possible pathways for lipid oxidation. In a food system containing metals, phospholipids were reported to bind the metals from further reacting with the unsaturated sites of the system, thus slowing down the oxidation process (Choe & Min, 2006; Yoon & Min, 1987).

2.3.5.5 Chlorophylls

Chlorophyll is a photosensitizer that accelerates the rate of oxidation by transferring the excitation energy of electrons in the form of either free radicals or $^1O_2$, in the presence of light and $^3O_2$ (Fakourelis, Lee, & Min, 1987; Gutiérrez-Rosales, Garrido-Fernández, Gallardo-Guerrero, Gandul-Rojas, & Minguez-Mosquera, 1992; Whang & Peng, 1988). The by-products (*i.e.,* pheophytins, pheophorbides) of chlorophyll degradation can also act as sensitizers. It was reported that pheophytin is a stronger sensitizer than chlorophyll (Endo, Usuki, & Kaneda, 1984; Rahmani & Csallany, 1998). Although chlorophyll is most known for its pro-oxidant effect, it may act as an antioxidant under certain circumstances. Some studies have reported that chlorophyll stabilizes free radicals in the absence of light by possibly the donation of hydrogen (Choe & Min, 2006; Endo, Usuki, & Kaneda, 1985; Gutiérrez-Rosales et al., 1992). In highly unsaturated fatty

acid systems, the effect of chlorophyll as an antioxidant was reported to be greater than in a system low in unsaturated fatty acids (Endo et al., 1985).

2.4 Antioxidants

Lipid oxidation contributes to undesirable changes in fatty food products, which in turn reduces the product's shelf life. This problem could be delayed with the use of antioxidants. Antioxidants are naturally occurring compounds that can be found in plants (Wang & Lin, 2000). Some of the examples of natural antioxidants are astaxanthin (algae, shrimp), lycopene (tomato, autumnberry), catechin (green tea), resveratrol (grapes), and others (Figure 2-2). Antioxidants can also be produced synthetically. Synthetic antioxidants include gallates, butylated hydroxytoluene (BHT), butylated hydroxyanisole (BHA), and others (Figure 2-3). In some cases, natural antioxidants can also be produced synthetically and considered as antioxidants of natural origin (but not as a natural antioxidant), like tocopherol (Figure 2-2).

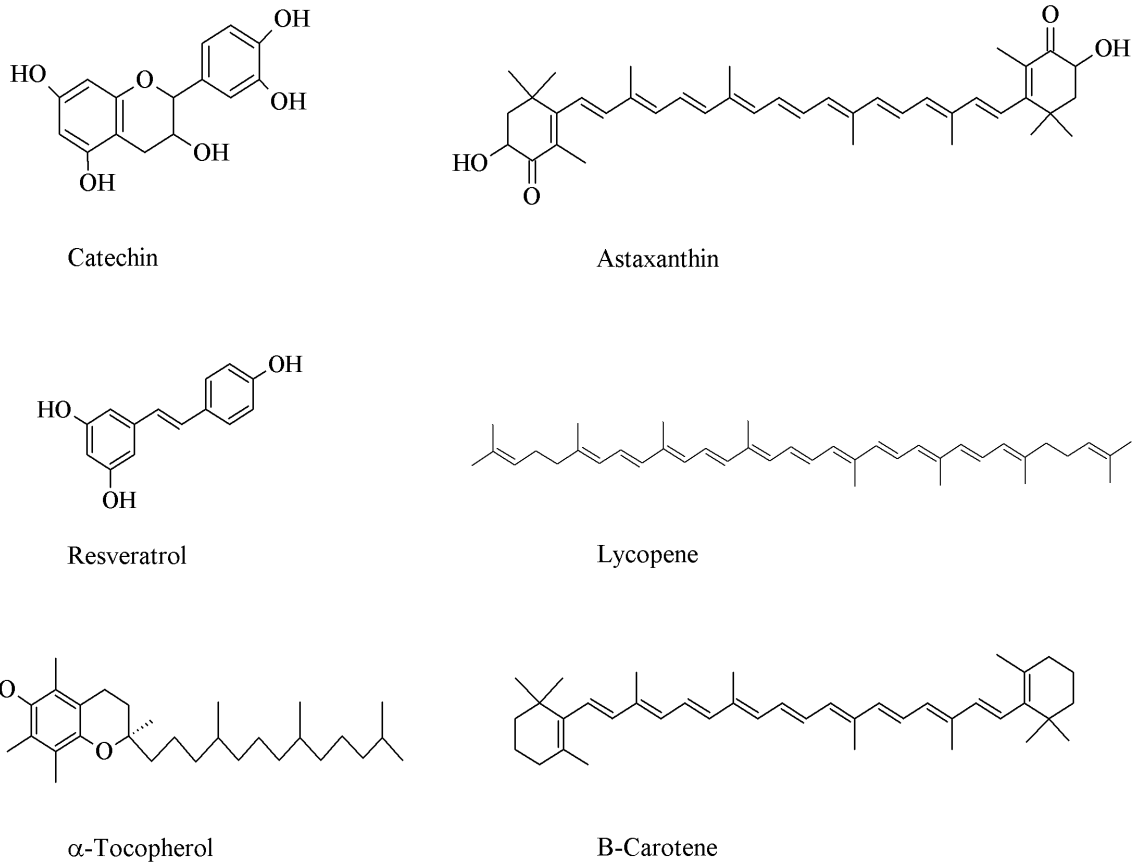

Figure 2-2 Example of natural antioxidants. Figure was reproduced from Colín-Chávez et al. (2013), Gordon (2001), Mortensen & Skibsted (1997), Rice-Evans et al. (1996), and Soto-Valdez et al. (2010) (C. Colín-Chávez, H. Soto-Valdez, E. Peralta, J. Lizardi-Mendoza, & R.R. Balandrán-Quintana, 2013; Gordon, 2001; Mortensen & Skibsted, 1997; Rice-Evans, Miller, & Paganga, 1996; Soto-Valdez, Auras, & Peralta, 2010).

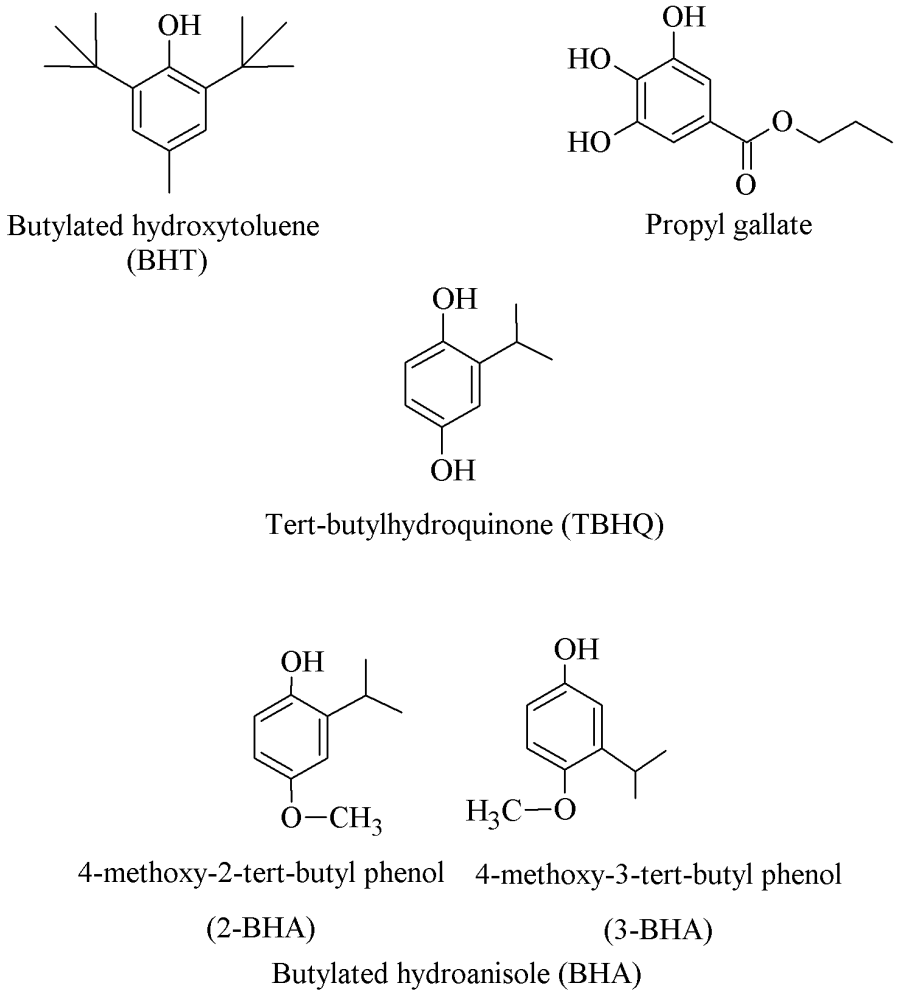

Figure 2-3 Examples of synthetic antioxidants. Figure was reproduced from Gordon (2001) (Gordon, 2001).

2.4.1 Classification of Antioxidants

In general, antioxidants can be classified into two groups based on their mechanisms, which are primary antioxidants (chain-breaking), and secondary antioxidants (preventive antioxidants) (Gordon, 2001; Laguerre et al., 2007; McClements & Decker, 2000). Primary antioxidants work by scavenging free radicals (Gordon, 2001). These compounds are mainly phenolic substances and act as electron donors (Kochhar & Rossell, 1990). They are also consumed during the induction

period. Secondary antioxidants function by binding metal ions, scavenging oxygen, transforming hydroperoxides into non-radical species, absorbing UV radiation or deactivating singlet oxygen. These compounds are normally effective in the presence of a second minor compound (Gordon, 2001).

2.4.1.1 Primary Antioxidants (Chain-Breaking)

The mechanism of chain-breaking antioxidants is based on hydrogen atom donation (Laguerre et al., 2007; Schaich et al., 2013). Once lipid oxidation has started, this process forms non-stable by-products, namely, peroxyl radicals. Since peroxyl radicals are non-stable, they are highly reactive and continuously react with more lipid molecules to form more hydroperoxides and alkyl radicals. Then, the hydroperoxides decompose to generate more free radicals and alkyl radicals continuously react with atmospheric triplet oxygen ($^3O_2$) to produce other peroxyl radicals (Choe & Min, 2006; Gordon, 2001; Schaich et al., 2013). Based on the nature of this continuous reaction, chain-breaking antioxidants function by donating their hydrogen atoms to those aforementioned non-stable by-products, thus transforming these by-products into more stable radicals or non-radical products (McClements & Decker, 2000). The efficacy of chain-breaking antioxidants relies on their higher affinity toward free radicals than that of lipids and also their ability to produce less reactive antioxidant radicals than those of lipids and peroxyl radicals (McClements & Decker, 2000). In addition, chain-breaking antioxidants should pose lower reduction potentials in comparison to free radicals to be able to donate their hydrogen atoms (Buettner, 1993; Choe & Min, 2006). Free radicals of polyunsaturated fatty acids such as alkoxy, peroxy, and alkyl radicals were reported to have standard 1-electron reduction potential of 1600, 1000, and 600 mV, respectively, while antioxidants generally have standard reduction potentials

of 500 mV or lower (e.g., α-tocopherol (500 mV) and ascorbic acid (282 mV)) (Buettner, 1993; Choe & Min, 2006).

Most of the chain-breaking antioxidants are phenolic compounds. The capability of these compounds to donate their hydrogen atoms is measured by their bond dissociation energy. The lower the bond dissociation energy of these compounds, the greater is their ability to donate hydrogen atoms (Laguerre et al., 2007). Moreover, the presence of phenolic groups in the chain-breaking antioxidant molecules not only helps to stabilize the free radicals, but also helps to decelerate the oxidation process by the resonance stabilization of antioxidant radicals (Choe & Min, 2006; Laguerre et al., 2007; Schaich et al., 2013) (Figure 2-4). Therefore, in general, the higher the number of phenolic groups, the greater antioxidant activity is anticipated. However, the location of this phenolic group in the antioxidant structure may also determine the antioxidant activity (Schaich et al., 2013).

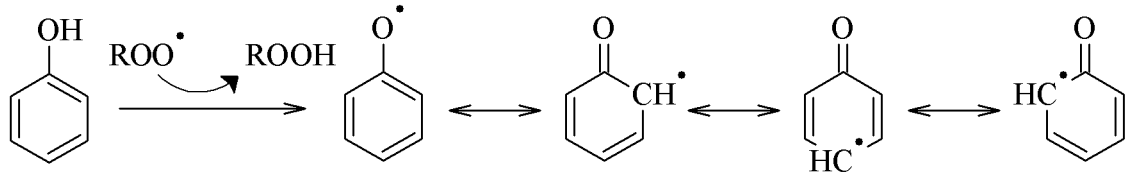

Figure 2-4 Resonance of an antioxidant radical in the phenol structure. Figure was adapted and reproduced from Choe & Min (2006) (Choe & Min, 2006).

2.4.1.2 Secondary Antioxidants (Preventative Antioxidants)

Preventative antioxidants work even before the oxidation starts as a preventative measure. This type of antioxidant typically inhibits lipid oxidation by either chelating the metals or scavenging the $^1O_2$ (Schaich et al., 2013).

Chelation of metals may involve metal chelators or metal complexers. Commonly used metal chelators are ethylenediaminetetraacetic acid (EDTA) and phytate. Metal complexers include citric acid, ascorbic acid, and diamines. Both metal chelators and complexers can perform efficiently as preventative antioxidants by having a structure that inhibits electron transfers by surrounding the metals present in the food system (Schaich et al., 2013). The reason behind this mechanism is to be able to hinder the metals from reacting with lipids, thus inhibiting the formation of alkyl radicals and some other reactive species like $^1O_2$ and hydroperoxides (Andersson, 1998; Choe & Min, 2006). In addition, they must have sufficiently high concentration to retard lipid oxidation (Schaich et al., 2013). Some metal chelators and metal complexers may alter the redox potential or may increase the diffusivity of the metals present in the food system, which in turn, enhances pro-oxidant effects of these metals (Decker, 1998; McClements & Decker, 2000).

There are two quenching mechanisms: physical quenching and chemical quenching. Physical quenching involves transformation of $^1O_2$ into $^3O_2$ by transferring the energy or the charge without antioxidant oxidation. Chemical quenching occurs when antioxidants chemically react with $^1O_2$, thus forming oxidized products (Min & Boff, 2002).

Singlet oxygen quenchers are generally carotenoid-based antioxidants. These compounds contain conjugated double bonds in their structure. In $^1O_2$ oxidation, the type of double bond is not as important as the number of double bonds in the lipid structure (Min & Boff, 2002). Since $^1O_2$ is electrophilic in nature, it is always in need of filling the vacancy of its molecular orbital, which targets electron-riched conjugated double bonds (Adam, 1975; Min & Boff, 2002; Stahl & Sies, 2005). Therefore, in the presence of singlet oxygen quenchers (*i.e.*, carotenoid-based antioxidants), its tendency to react with the extended conjugated double bonds of carotenoid-based antioxidants is higher than that of the unsaturated sites of the lipid (Schaich et al., 2013; Stahl & Sies, 2005).

2.4.1.3 An Example of an Antioxidant Reaction

The alkyl peroxy radical (ROO*) is readily reduced to the related anion, and converted to a hydroperoxide by an electron donor.

$$ROO^* \xrightarrow{+e} ROO^- \xrightarrow{H+} ROOH$$

The presence of an antioxidant (AH) acts to interrupt the propagation step, and form an antioxidant radical (A*). This radical has a low reactivity, thus inhibiting further oxidation steps (Yanishlieva-Maslarova, Pokorny, Yanishlieva, & Gordon, 2001).

$$ROO^* + AH \rightarrow ROOH + A^*$$

$$RO^* + AH \leftrightarrow ROH + A^*$$

Figure 2-5 shows visual comparison of an antioxidant mechanism to inhibit lipid oxidation.

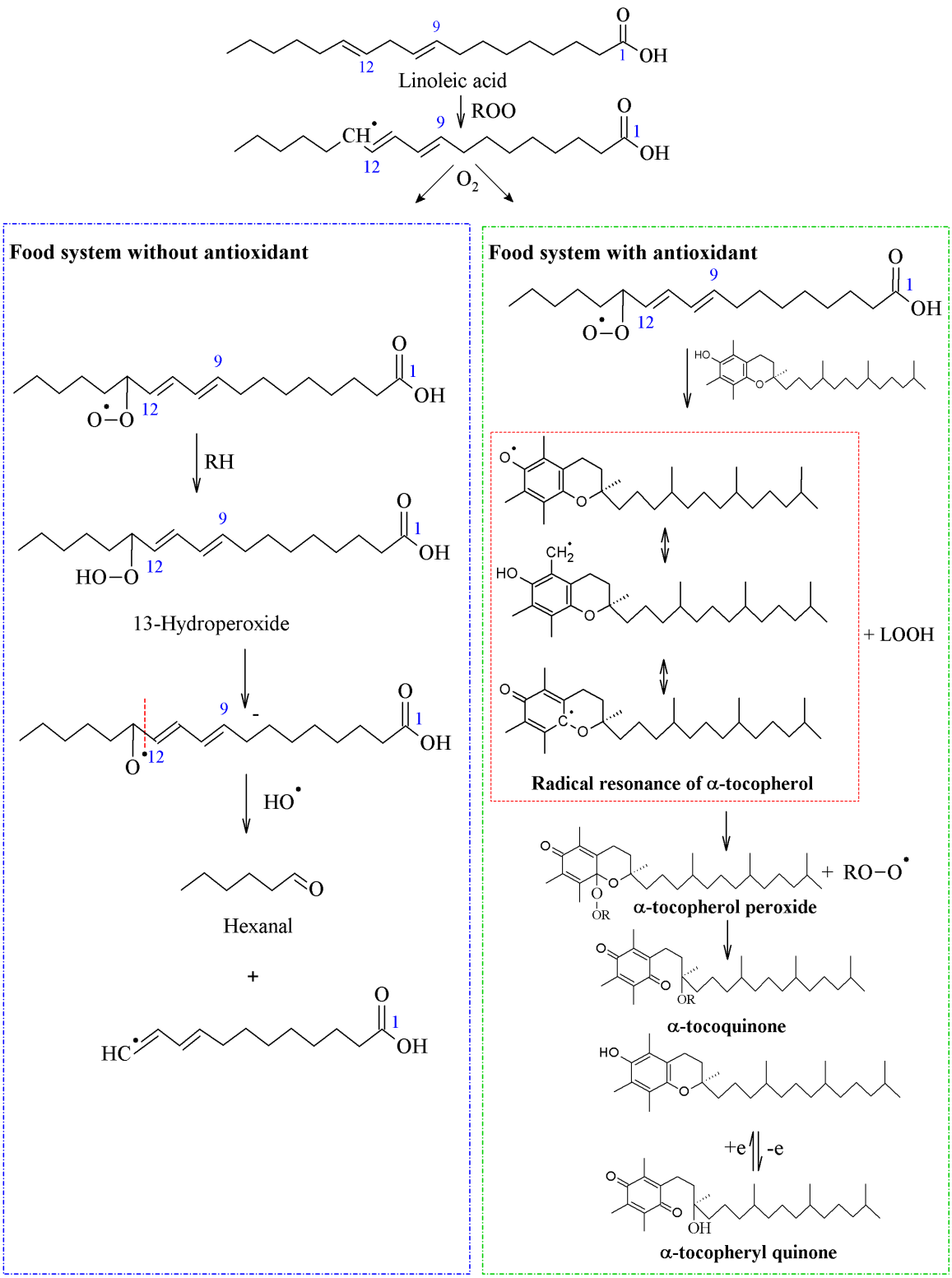

Figure 2-5 Mechanism of an antioxidant (a-tocopherol) in inhibiting lipid oxidation (linoleic acid). Figure adapted from Gordon (2001) (Gordon, 2001).

2.5 Approaches to Extend the Shelf Life of Fatty Food Products

Lipid oxidation is the most critical issue when dealing with fatty food products. This type of food deterioration is mainly caused by the high content of unsaturated fatty acids in the fatty food products. As has been described in the previous sections, the chances for oxidation to occur are very high because of the nature of the product itself and the environmental conditions. Therefore, it is crucial to find the right approach to protect this type of food system in order to be able to provide acceptable organoleptic properties with maximum quality and safety assurance for the product.

Many approaches are available to help in inhibiting lipid oxidation. However, it is quite challenging to find a single approach that can resolve this issue due to the wide variety of fatty food products and the complexity of the food systems themselves. Nevertheless, the efforts to control such a critical issue have been extensively investigated and some are commercially available. Among the typical approaches used to inhibit lipid oxidation of fatty food products are direct addition of antioxidants into the systems, controlled environments (exclusion of O_2, dark and chilled storage), and antioxidant packaging systems.

The common practice in the food industry involves direct addition of antioxidants into the food system. Nevertheless, some concerns about this approach are the loss of antioxidants during processing due to the thermal conditions required in most food practices, the limits on use of antioxidants to comply with regulations (whenever applicable), the pro-oxidant issue that may happen due to the presence of minor components in the food, and others. Even though a certain amount of added antioxidant might still be left in the food system, the question is how much antioxidant is sufficient, and can it maintain the quality of the product during distribution and storage before reaching consumers?

For those reasons, it seems feasible to approach this issue by manipulating the product's packaging system. Not only does the product from the beginning need a package to carry and contain it, but also the package may beneficially enhance the nutritional value of the product while prolonging the product's shelf stability. Antioxidant-based packaging systems can be divided into two categories: i) individual and independent antioxidant devices, ii) antioxidant incorporated polymeric films by means of blending, functional layers via multilayer structures or chemically/ enzymatically-modified structures, and coatings.

2.5.1 Antioxidant Based Packaging System: Individual and Independent Antioxidant Devices

For this category, the antioxidant is kept separately in another extra packaging material like a sachet/pouch. This individual and independent device will then be incorporated into the primary package of the product. The most common application for this category is O_2 scavenger, a type of device that is capable of removing O_2 from the package headspace. To a certain extent this device can also be tailored to be able to reduce the amount of O_2 significantly. However, the obstacles for such packaging systems to be implemented rely on the type of the intended product, the practicality of usage, possible interaction with other reactants or compounds in the food product and the consumer's perception. This type of device may only be used for solid products, and it seems impractical to use this device for an extended shelf life due to its limited absorbing capacity. It was reported that the capacity of this device to absorb O_2 is limited to 100 mL (Smith, Hoshino, & Abe, 1995). In addition, Lee (2014) estimated that iron-based O_2 scavenger could absorb approximately 300 mL of O_2 in the presence of 0.43 g of water (D. S. Lee, 2014). Moreover, additional packaging material is also required apart from the primary and secondary packaging that are normally used for packaging food products, thus generating more waste. The presence of other reactants such as

CO_2 is also known to reduce the efficiency of iron-based scavengers in absorbing O_2 (D. S. Lee, 2014). Extra efforts need to be taken to educate consumers not to mistake these devices for part of the food product, as that might lead to a food safety hazard.

Many issues have been associated with metal-based individual and independent devices such as the danger of microwave arcing in certain applications, detection by metal detectors, etc. (Cruz, Camilloto, & dos Santos Pires, 2012). Therefore, some initiatives have been made to use organic substrates like ascorbic acid and catechol. These new alternative substrates may contain a small amount of metal to control their self-oxidation mechanisms (Cruz et al., 2012; D. S. Lee, 2014).

2.5.2 Antioxidant Functional Films

In recent years, focus on modification of polymer films has intensified to gain positive perception from the public and to fulfill the needs of the industry. Commonly used compounds for individual and independent antioxidant devices (*i.e.,* metal-based scavengers, organic substrates) and antioxidants (*i.e.,* natural-based compounds) have been incorporated into polymer films to create a functional film with single or multiple layers. The incorporation of antioxidants into polymer films is beneficial not only to retard lipid oxidation of intended food systems but also to stabilize the polymer during processing.

Direct incorporation of antioxidant compounds into polymer films has a long history worldwide. Incorporation of iron compounds into polymer films has resulted in products such as Oxyguard® of Toyo Seikan (Japan), Shelfplus O_2® of Ciba Specialty Chemicals (Switzerland), Oxycap® of Standa Industrie (France), and ActiTUF® of M&G (Italy) (D. S. Lee, 2011, 2014). Chemically modified unsaturated hydrocarbons were also introduced as part of polymeric films to

scavenge O_2 in package-product systems (Cruz et al., 2012; Ferrari et al., 2009). Immobilized-yeast was incorporated into the liner of beer bottle caps to consume O_2 and to release CO_2 from/into the headspace, respectively, without changing the organoleptic properties of the product (Cruz et al., 2012; Edens, Farin, Ligtvoet, & Van Der Plaat, 1992). Nanocrystalline titania was also added into polymeric films for scavenging O_2 to inhibit oxidation by activating it via UV light (Azeredo, 2009; D. S. Lee, 2014; Mills, Doyle, Peiro, & Durrant, 2006; Xiao-e, Green, Haque, Mills, & Durrant, 2004).

BHT and α-tocopherol are among the antioxidants that have been widely investigated as part of the packaging system (Bailey, 1995; Byun, Kim, & Whiteside, 2010; Galindo-Arcega, 2004; Granda-Restrepo et al., 2009; Hwang et al., 2013; Jurina, Azizah, Siah, & Ngadiman, 2011; Manzanarez-López, Soto-Valdez, Auras, & Peralta, 2011; Ortiz-Vazquez, Shin, Soto-Valdez, & Auras, 2011; Wessling, Nielsen, & Giacin, 2001; Wessling, Nielsen, & Leufven, 2000; Wessling, Nielsen, Leufvén, & Jägerstad, 1998; Yanidis, 1989). Currently, the tendency of using natural antioxidants (*e.g.*, α-tocopherol, catechin, plant extract) is increasing due to the abundance and availability of these compounds, positive perception by consumers, non-limited use by regulation, and others. However, the majority of the developed antioxidant functional films are made of petroleum-based polymers such as low density poly(ethylene) (LDPE), and poly(propylene) (PP) (Gavara, Lagarón, & Catalá, 2004; Wessling et al., 1998). Table 2-1 shows examples of these systems.

Nevertheless, the growth in the development of bio-based functional films with natural antioxidants added has increased (Table 2-2). The driving factors behind this evolution are mainly the rising environmental awareness and continuous oil price volatility (Jiang & Zhang, 2013; Siracusa, Rocculi, Romani, & Rosa, 2008). Fabricated bio-based functional films include polymers

that are extracted directly from biomass, particularly polysaccharides, synthesized from bio-derived monomers, and/or produced from natural or genetically modified organisms (Siracusa et al., 2008; Tuil, Fowler, Lawther, & Weber, 2000), with the majority being made of polyester that is synthesized from bio-derived monomers (*i.e.*, poly(lactic acid), PLA).

Table 2-1 Compilation of studies reporting kinetic migration parameters for petroleum based functional films incorporated with natural antioxidants and the models used to determine these parameters.

Petroleum-based functional films	**Natural antioxidant compounds**	**Parameters estimated**	**Mathematical equations applied for estimating the kinetic migration parameters**	**References**
PE and PA laminate with PS tray	-Oregano extract -Rosemary extract	NE**		(Camo, Beltrán, & Roncalés, 2008)
EVOH LDPE EVA EVA and LDPE PP	-Quercetin -Tocopherol	D and $K_{p,f}$	$\frac{M_{f,t}}{M_{f,\infty}} = 1 - \frac{8}{\pi^2}\sum_{n=1}^{\infty}\frac{1}{(2n+1)^2}exp\left[-\frac{(2n+1)^2}{L^2}D\pi^2 t\right]$ $\frac{M_{f,t}}{M_{f,\infty}} = \frac{4}{L}\sqrt{\frac{Dt}{\pi}}$	(Chen, Lee, Zhu, & Yam, 2012)
PET	-DFC Amosorb 4020 (containing cobalt salt)	NE		(Galdi, Nicolais, Di Maio, & Incarnato, 2008)

Table 2-1 (Cont'd)

Petroleum-based functional films	Natural antioxidant compounds	Parameters estimated	Mathematical equations applied for estimating the kinetic migration parameters	References
LDPE: EVOH: HDPE+7% Titanium dioxide	-α-Tocopherol	D and $K_{p,f}$	$\frac{M_{f,t}}{M_{f,\infty}} = 1 - \frac{8}{\pi^2}\sum_{n=1}^{\infty}\frac{1}{(2n+1)^2}exp\left[-\frac{(2n+1)^2}{L^2}D\pi^2 t\right]$	(Granda-Restrepo et al., 2009)
LDPE LDPE adsorbed on Syloblock LDPE adsorbed on SBA-15 EVA	-α-Tocopherol	D	$\frac{M_{f,t}}{M_{f,\infty}} = 1 - \frac{8}{\pi^2}\sum_{n=1}^{\infty}\frac{1}{(2n+1)^2}exp\left[-\frac{(2n+1)^2}{L^2}D\pi^2 t\right]$	(Heirlings et al., 2004)
PVA-Chitosan	-Mint extract -Pomegranate extract	NE		(Kanatt, Rao, Chawla, & Sharma, 2012)

Table 2-1 (Cont'd)

Petroleum-based functional films	Natural antioxidant compounds	Parameters estimated	Mathematical equations applied for estimating the kinetic migration parameters	References
Ziegler-Natta LLDPE Metallocene LLDPE	-α-Tocopherol -β-Cyclodextrin + α-tocopherol -Quercetin -γ-Cyclodextrin + quercetin	NE		(Koontz et al., 2010)
HDPE+ Surlyn/EVA®	-α-Tocopherol	NE		(Y. S. Lee, Shin, Han, Lee, & Giacin, 2004)

Table 2-1 (Cont'd)

Petroleum-based functional films	Natural antioxidant compounds	Parameters estimated	Mathematical equations applied for estimating the kinetic migration parameters	References
EVOH	-Quercetin -Catechin	D and $K_{p,f}$	$\frac{A_{f,t}}{A_{f,\infty}} = \frac{M_{f,t}}{M_{f,\infty}} = 1 - \frac{8}{\pi^2}\sum_{n=1}^{\infty}\frac{1}{(2n+1)^2}exp\left[-\frac{(2n+1)^2}{L^2}D\pi^2 t\right]$	(López-de-Dicastillo, Alonso, Catalá, Gavara, & Hernández-Muñoz, 2010)
EVOH	-Green tea extract	D and $K_{p,f}$	$\frac{M_{f,t}}{M_{f,\infty}} = 1 - \frac{8}{\pi^2}\sum_{n=1}^{\infty}\frac{1}{(2n+1)^2}exp\left[-\frac{(2n+1)^2}{L^2}D\pi^2 t\right]$ $\frac{M_{f,t}}{M_{f,\infty}} = 1 - \sum_{n=1}^{\infty}\frac{2\alpha(1+\alpha)}{1+\alpha+\alpha^2 q_n^2}exp\left[-\frac{Dq_n^2 t}{L^2}\right]$	(Lopez de Dicastillo et al., 2011)

Table 2-1 (Cont'd)

Petroleum-based functional films	Natural antioxidant compounds	Parameters estimated	Mathematical equations applied for estimating the kinetic migration parameters	References
EVOH	-Green tea extract -Ascorbic acid -Ferulic acid -Quercetin	D and $K_{p,f}$	$\frac{M_{f,t}}{M_{f,\infty}} = 1 - \sum_{n=1}^{\infty} \frac{2\alpha(1+\alpha)}{1+\alpha+\alpha^2 q_n^2} exp\left[-\frac{Dq_n^2 t}{L^2}\right]$	(López-de-Dicastillo, Gómez-Estaca, Catalá, Gavara, & Hernández-Muñoz, 2012)
PP photografted HEMA	-Caffeic acid	NE		(Arrua, Strumia, & Nazareno, 2010)
Grafted PP	-Poly(acrylic acid) (metal chelator)	NE		(Tian, Decker, & Goddard, 2012)

Table 2-1 (Cont'd)

Petroleum-based functional films	Natural antioxidant compounds	Parameters estimated	Mathematical equations applied for estimating the kinetic migration parameters	References
HDPE	-Carvacrol	*D*	$\frac{M_{f,t}}{M_{f,\infty}} = \frac{2}{L}\sqrt{\frac{Dt}{\pi}}$ $D = 10^4 exp(A_p^{'} - 0.1351 M_r^{\frac{2}{3}} + 0.003 M_r - \frac{\tau - 10454}{T})$	(Peltzer, Wagner, & Jiménez, 2009)
LDPE	-Barley husks derived antioxidant	NE		(Pereira de Abreu, Losada, Maroto, & Cruz, 2010)
PET	-Green tea extract -Green coffee extract -Grapefruit extract	NE		(Colon & Nerin, 2012)

Table 2-1 (Cont'd)

Petroleum-based functional films	Natural antioxidant compounds	Parameters estimated	Mathematical equations applied for estimating the kinetic migration parameters	References
PP	-Rosemary extract	NE		(Nerín, Tovar, & Salafranca, 2008)
EVOH	-Cocoa extract	D and $K_{p,f}$	$\frac{A_{f,t}}{A_{f,\infty}} = \frac{M_{f,t}}{M_{f,\infty}} = 1 - \frac{8}{\pi^2}\sum_{n=1}^{\infty}\frac{1}{(2n+1)^2}exp\left[-\frac{(2n+1)^2}{L^2}D\pi^2 t\right]$	(Calatayud et al., 2013)
LDPE	-TOCOBIOL -TOCOBIOL® GL -NUTRABIOL® T90 -TOCOBIOL® PV -NUTRABIOL® T50 PV	NE		(Barbosa-Pereira et al., 2012)

Table 2-1 (Cont'd)

Petroleum-based functional films	Natural antioxidant compounds	Parameters estimated	Mathematical equations applied for estimating the kinetic migration parameters	References
LDPE	-α-tocopherol -β-cyclodextrin + α-tocopherol	D and $K_{p,f}$	$\frac{M_{f,t}}{M_{f,\infty}} = 1 - \frac{8}{\pi^2}\sum_{n=1}^{\infty}\frac{1}{(2n+1)^2}exp\left[-\frac{(2n+1)^2}{L^2}D\pi^2 t\right]$	(Siró et al., 2006)
LDPE/PP blend	-Tocopherol	D	$\frac{M_{f,t}}{M_{f,\infty}} = \frac{4}{L}\sqrt{\frac{Dt}{\pi}}$	(Zhu, Lee, & Yam, 2012)
LLDPE:HDPE + A*:HDPE HDPE:HDPE+A* :EVA	-Sesamol	NE		(Zhu, Schaich, Chen, & Yam, 2013)

Table 2-1 (Cont'd)

Petroleum-based functional films	Natural antioxidant compounds	Parameters estimated	Mathematical equations applied for estimating the kinetic migration parameters	References
PP	-Catechin -Green tea extract (gallic acid, quercetin, caffeine)	*D*	$\frac{M_{f,t}}{M_{f,\infty}} = \frac{4}{L}\sqrt{\frac{Dt}{\pi}}$ $D = \left(\frac{(slope\ of\ \frac{M_{f,t}}{M_{f,\infty}}\ vs.\ t_{1/2})L}{2}\right)^2$	(Castro López, López de Dicastillo, López Vilariño, & González Rodríguez, 2013)
Recycled PET	-Citrus extract	NE		(Contini et al., 2012)

*PE-Poly(ethylene); PA-Poly(amide); PS-Poly(styrene); EVOH-Ethylene(vinyl alcohol); LDPE-Low density poly(ethylene); HDPE-High density poly(ethylene); EVA-Ethylene(vinyl acetate); PP-Poly(propylene); PET-Poly(ethylene terephthalate); PVA-Poly(vinyl acetate); LLDPE-Linear low density poly(ethylene).**A*-Antioxidant.***NE-Not estimated.

Table 2-2 Compilation of studies reporting kinetic migration parameters for bio-based functional films incorporated with natural antioxidants and the models used to determine these parameters.

Bio-based functional films	Natural antioxidant compounds	Parameters estimated	Mathematical equations applied for estimating the kinetic migration parameters	References
Chitosan	-α-Tocopherol	NE		(Martins, Cerqueira, & Vicente, 2012)
Chitosan-MMT	-Rosemary essential oil	NE		(Abdollahi, Rezaei, & Farzi, 2012)
Grafted chitosan	-Gallic acid	NE		(Schreiber, Bozell, Hayes, & Zivanovic, 2013)
Sodium caseinate Calcium caseinate	-Carvacrol	NE		(Arrieta, Peltzer, Garrigós, & Jiménez, 2013)

Table 2-2 (Cont'd)

Bio-based functional films	Natural antioxidant compounds	Parameters estimated	Mathematical equations applied for estimating the kinetic migration parameters	References
CMC-MMT	-Murta leaves extract	NE		(Quilaqueo-Gutiérrez, Echeverría, Ihl, Bifani, & Mauri, 2012)
Chitosan	-Green tea extract	NE		(Siripatrawan & Noipha, 2012)
Cellulose	-Curcumin nanoparticles -Ascorbyl dipalmitate nanoparticles	NE		(Sonkaew, Sane, & Suppakul, 2012)

Table 2-2 (Cont'd)

Bio-based functional films	Natural antioxidant compounds	Parameters estimated	Mathematical equations applied for estimating the kinetic migration parameters	References
PLA	-Resveratrol	D and $K_{p,f}$	$\frac{M_{f,t}}{M_{f,\infty}} = 1 - \frac{8}{\pi^2}\sum_{n=1}^{\infty}\frac{1}{(2n+1)^2}exp\left[-\frac{(2n+1)^2}{L^2}D\pi^2 t\right]$	(Soto-Valdez et al., 2010; Soto-Valdez , Peralta, & Auras, 2008)
PLA	-α-Tocopherol	NE; D, $K_{p,f}$ and α	$\frac{M_{f,t}}{M_{f,\infty}} = 1 - \frac{8}{\pi^2}\sum_{n=1}^{\infty}\frac{1}{(2n+1)^2}exp\left[-\frac{(2n+1)^2}{L^2}D\pi^2 t\right]$ $\frac{M_{f,t}}{M_{f,\infty}} = 1 - \sum_{n=1}^{\infty}\frac{2\alpha(1+\alpha)}{1+\alpha+\alpha^2 q_n^2}exp\left[-\frac{Dq_n^2 t}{L^2}\right]$	(Goncalves et al., 2012; Manzanarez-López et al., 2011)

Table 2-2 (Cont'd)

Bio-based functional films	Natural antioxidant compounds	Parameters estimated	Mathematical equations applied for estimating the kinetic migration parameters	References
PLA	-α-Tocopherol -Ascorbyl palmitate	D and $K_{p,f}$	$\frac{M_{f,t}}{M_{f,\infty}} = 1 - \frac{8}{\pi^2}\sum_{n=1}^{\infty}\frac{1}{(2n+1)^2}exp\left[-\frac{(2n+1)^2}{L^2}D\pi^2 t\right]$ $\frac{M_{f,t}}{M_{f,\infty}} = \frac{4}{L}\sqrt{\frac{Dt}{\pi}}$ $D = \left(\frac{(slope\ of\ \frac{M_{f,t}}{M_{f,\infty}}\ vs.\ t_{1/2})L}{2}\right)^2$	(Jamshidian, Tehrany, & Desobry, 2012)

Table 2-2 (Cont'd)

Bio-based functional films	Natural antioxidant compounds	Parameters estimated	Mathematical equations applied for estimating the kinetic migration parameters	References
PLA	-Catechin -Epicatechin	D, $K_{p,f}$, α, and $M\infty$	$\frac{M_{f,t}}{M_{f,\infty}} = 1 - \frac{8}{\pi^2}\sum_{n=1}^{\infty}\frac{1}{(2n+1)^2}exp\left[-\frac{(2n+1)^2}{L^2}D\pi^2 t\right]$ $\frac{M_{f,t}}{M_{f,\infty}} = 1 - \sum_{n=1}^{\infty}\frac{2\alpha(1+\alpha)}{1+\alpha+\alpha^2 q_n^2}exp\left[-\frac{Dq_n^2 t}{L^2}\right]$	(Iñiguez-Franco et al., 2012)
PLA/Starch blend	-α-Tocopherol -Resveratrol	D, $K_{p,f}$, α, and $M\infty$	$\frac{M_{f,t}}{M_{f,\infty}} = 1 - \frac{8}{\pi^2}\sum_{n=1}^{\infty}\frac{1}{(2n+1)^2}exp\left[-\frac{(2n+1)^2}{L^2}D\pi^2 t\right]$	(Hwang et al., 2013)

Table 2-2 (Cont'd)

Bio-based functional films	Natural antioxidant compounds	Parameters estimated	Mathematical equations applied for estimating the kinetic migration parameters	References
PLGA	-α-Tocopherol	NE		(Van Aardt et al., 2007)
PLA PCL PHBV	-β-Carotene	NE		(López-Rubio & Lagaron, 2010)

*MMT-Montmorillonite; CMC-Carboxymethylcellulose; PLA-Poly(lactic acid); PLGA-Poly(lactide-*co*-glycolide); PCL-Poly(caprolacton); PBHV-Poly(hydroxybutyrate-*co*-valerate).

**NE-Not estimated.

Even though the fabrication of antioxidant functional film systems is continuously growing with more trends toward the use of bio-based polymers with natural antioxidants, issues related to migration of the incorporated antioxidants into food systems are still not fully addressed. It is very important to understand the migration phenomena in order to ensure optimized release of the incorporated antioxidants into the intended food system so that an extended shelf life may be achieved.

2.6 Migration

Migration is a phenomenon involving the transfer of substances originating from the packaging material into a packaged product. These substances could be monomers, solvents, additives (*e.g.*, antioxidants), etc., and are known as migrants. Migration could be a desirable or undesirable event that occurs in a packaged product. Residual solvents (*e.g.*, toluene and hexane), for instance, when they migrate into food product will result in unwanted odor and taste. However, migration is desired when it is intentionally designed in order to protect a polymer and packaged product, as in the case of antioxidant packaging systems. The initial concentration of migrants in the packaging systems and the partition coefficient between the package and the packaged food determine the extent of migration (Selke, Culter, & Hernandez, 2004). The better the understanding of the migration phenomena, the more efficient the prediction of the shelf life of a product and the better the assessment of specific migration limits in accordance with regulation can be achieved (Poças, Oliveira, Oliveira, & Hogg, 2008).

Migration phenomena can be described through established mathematical models with the following assumptions: i) initial concentration of the migrants is uniformly distributed in the film, ii) migration happens on the side of the film that is in contact with food/simulant, iii) the food/simulant is well mixed and has a large surface mass transfer coefficient, h (Biot no. >100),

iv) Fickian diffusion controls the migration in the film, v) migration depends only on temperature and the diffusion coefficient, D, and the partition coefficient, $K_{p,f}$, are constants, vi) the film interface and the food are always at equilibrium, and vii) no interaction exists between the film and the food/simulant and the edge effect is negligible (Chung, Papadakis, & Yam, 2001, 2002; Crank, 1979; Poças et al., 2008).

2.6.1 Thermodynamic Equilibrium

The chemical potential is the driving force that causes a molecule to diffuse within a film or to transfer between a film and a surrounding phase, and it is described as follows:

$$\mu_i = \mu_i^o + RT \ln a_i \qquad \text{(Eq. 2-1)}$$

μ_i = chemical potential of migrant I

μ_i^o = chemical potential of migrant I at a standard state

R = universal gas constant

T = temperature, K

a_i = chemical activity

Substances like migrants naturally tend to move from a high chemical potential to a low chemical potential. The drive of migrants' movement is equivalent to the tendency to equilibrate the migrants' chemical potential in a phase, which means the migrants tend to reach thermodynamic equilibrium.

In addition, the general mass balance equation can be used to describe the migration model of a product-package system, assuming no chemical reaction or evaporation process is involved (Poças et al., 2008).

$$M_p(0) = M_p(t) + M_f(t) \quad \text{or} \qquad \text{(Eq. 2-2)}$$

$$M_p(0) = M_p(\infty) + M_f(\infty) \quad \text{(Eq. 2-3)}$$

$M_p(0)$= Initial mass of the migrant in the film

$M_p(t)$= Mass of the migrant in the film at time, t

$M_f(t)$= Mass of the migrant in the food or simulant at time, t

$M_p(\infty)$= Mass of the migrant in the film at time, ∞

$M_f(\infty)$= Mass of the migrant in the food or simulant at time, ∞

2.6.2 Partition Coefficient, $K_{p,f}$

The partition coefficient, $K_{p,f}$, can be described as the equilibrium concentration and distribution of migrants in a film and in a food/simulant (De Meulenaer, 2009; Franz & Störmer, 2008; Selke et al., 2004).

$$K_{p,f} = \frac{C_{p,\infty}}{C_{f,\infty}} \quad \text{(Eq. 2-4)}$$

$C_{p,\infty}$= the concentration of the migrant in the film at equilibrium.

$C_{f,\infty}$= the concentration of migrant in the food simulant at equilibrium.

The value of $K_{p,f}$ is always a good indication of the behavior of the migrant in correlation with the type of food/simulant used. For example, when the migrant is hydrophobic and the food/simulant nature is non-polar like oil, a $K_{p,f} < 1$ is anticipated due to the 'like dissolves like' nature, meaning that most or all of the migrant will migrate from the film into the food/simulant. However, if the food/simulant is polar in nature, a $K_{p,f} > 1$ is expected, in which most of the migrant stays in the film instead of migrating into the food/simulant (Poças et al., 2008). The extent of $K_{p,f}$ will also be influenced by factors like temperature and the nature of the film.

2.6.3 Diffusion Coefficient, *D*

The diffusion coefficient, *D* is used to describe the migration of a migrant from a film into a food/simulant. *D* is a function of temperature, and it may increase when the concentration of the migrant is relatively high in the film (Baner, Franz, & Piringer, 1994). Fick's first and second law of diffusion are used to explain the diffusion process. Fick's first law describes the steady state flow of diffusion by the equation below (for a one-dimensional diffusion process) (Selke et al., 2004):

$$F = -D\frac{\partial C}{\partial x} \qquad \text{(Eq. 2.5)}$$

F= flow rate

D= diffusion coefficient

c= migrant concentration in the film

x= the distance (in the direction of the diffusion)

Fick's Second Law refers to the unsteady state flow or transient state of the diffusion process. The following equation is used when diffusion occurs in one dimension (Selke et al., 2004):

$$\frac{\partial C}{\partial t} = D\frac{\partial^2 C}{\partial x^2} \qquad \text{(Eq. 2-6)}$$

Both equations can be visualized further by considering a 3D rectangular element with the parallel sides to the axes coordinates represented with length 2 dx, 2 dy, 2dz. The center of this 3D element is set at P (x,y,z) with the concentration of diffusing migrant C (Figure 2-6).

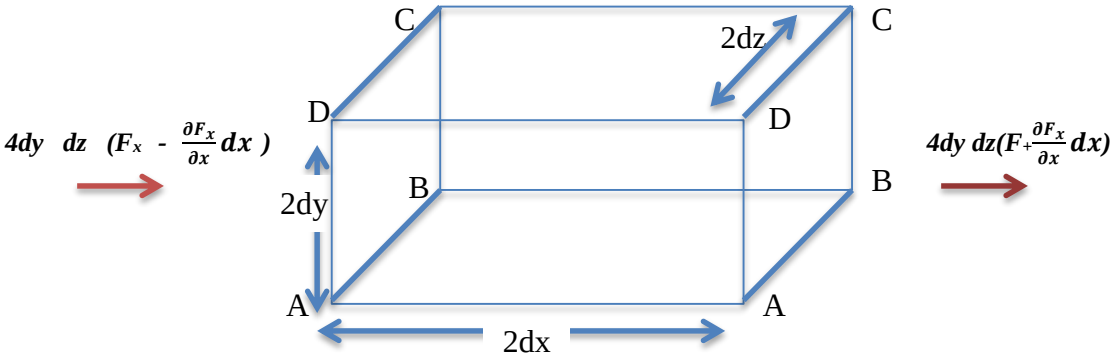

Figure 2-6 3D rectangular elements to represent diffusion in a plane sheet.

$$4dy\ dz\ (F_x - \frac{\partial F_x}{\partial x} dx) \quad \text{(Eq. 2-7)}$$

$$4dy\ dz\ (F_+ \frac{\partial F_x}{\partial x} dx) \quad \text{(Eq. 2-8)}$$

$$-8\ dx\ dy\ dz\ (\frac{\partial F_x}{\partial x}) \quad \text{(Eq. 2-9)}$$

From the other two faces of axes:

$$-8\ dx\ dy\ dz\ (\frac{\partial F_y}{\partial y}) \text{ and } -8\ dx\ dy\ dz\ (\frac{\partial F_z}{\partial z})$$

The rate that the concentration of diffusing migrant increases:

$$8\ dx\ dy\ dz\ (\frac{\partial F}{\partial t}) \quad \text{(Eq. 2-10)}$$

$$\frac{\partial C}{\partial t} + \frac{\partial F_x}{\partial x} + \frac{\partial F_y}{\partial y} + \frac{\partial F_z}{\partial z} = 0 \quad \text{(Eq. 2-11)}$$

If the diffusion coefficient is constant, F_x, F_y, F_z, substituting Eq. 2-5 into Eq. 2-11,

$$\frac{\partial C}{\partial t} + \frac{\partial(-D\frac{\partial C}{\partial x})}{\partial x} + \frac{\partial(-D\frac{\partial C}{\partial y})}{\partial y} + \frac{\partial(-D\frac{\partial C}{\partial z})}{\partial z} = 0$$

Fick's second law is obtained:

$$\frac{\partial C}{\partial t} = D\frac{\partial^2 C}{\partial x^2} + \frac{\partial^2 C}{\partial y^2} + \frac{\partial^2 C}{\partial z^2} \quad \text{(Eq. 2-12)}$$

If the diffusion is one-dimensional where the gradient concentration is only in the direction of the x-axis, then this is simplified to:

$$\frac{\partial C}{\partial t} = D\frac{\partial^2 C}{\partial x^2} \quad \text{(Eq. 2-13)}$$

Moreover, the diffusion process is affected by: *i)* the film's nature and its processing approach that can be directly/indirectly linked to the molecular weight and molecular weight distribution, solubility parameters (polarity, dispersion forces, and hydrogen bonding), crystallinity, orientation and density; *ii)* the nature of the migrant such as its hydrophilicity or hydrophobicity and molecular weight; *iii)* the nature of the food/simulant that is in contact with the film in terms of its aggressiveness, solvency (polar vs. non-polar); *iv)* film-migrant-food/simulant interaction effects such as plasticization; and *v)* experimental/ environmental temperature that affects the relaxation rate of the film depending on the film's glass transition temperature and/or melting temperature (De Meulenaer, 2009; Limm & Hollifield, 1996; Poças et al., 2008).

Generally, the behavior of the film based on relaxation rate and its correlation to Fickian diffusion can be classified into three main cases (De Meulenaer, 2009; Schlotter & Furlan, 1992): **Case 1:** Fickian diffusion takes place in a situation where the rate of diffusion is lower than the relaxation rate of the film. This type of diffusion commonly occurs for polymers like LDPE and HDPE with their glass transition temperatures well below room temperature so both exhibit a rubbery nature in their amorphous regions.

Case 2: When the rate of diffusion is faster than the relaxation rate of the film, then so called apparent Fickian diffusion occurs. In this case, the mass sorption is proportional to time. This case may occur due to the aggressive nature of food/simulant to penetrate the film at a constant velocity, thus resulted in rapid diffusivity of the migrant. This situation could happen in the case of a glassy

polymer such as PLA, due to solvent-induced phenomena that are time-dependent, which influence the diffusion rate of the migrant.

Case 3: Non-Fickian or anomalous diffusion takes place if the rate of diffusion and the relaxation rate of the film are similar.

2.6.4 Migration Models

In general, there are three migration models that are used to describe migration of a migrant from a film into a liquid food/simulant:

Model A: Film in contact with a finite volume of food/simulant and negligible external mass transfer coefficient (Figure 2-7).

This model is normally in conjunction with $K_{p,f}$>1 which occurs when most of the migrant stays in the film instead of migrating into the food/simulant. Normally, the solution for this model (Eq. 2-14) is applied in the case of migration at a relatively low temperature. The final solution for this model is as follows:

$$\frac{M_{f,t}}{M_{f,\infty}} = 1 - \sum_{n=1}^{\infty} \frac{2\alpha(1+\alpha)}{1+\alpha+\alpha^2 q_n^2} exp\left[-\frac{D q_n^2 t}{L^2}\right] \qquad \text{(Eq. 2-14)}$$

where $M_{f,t}$ is the mass of migrant release at time t, and $M_{f,\infty}$ is the mass of migrant at $t = \infty$, $\alpha = V_F / K_{p,f} V_P$, q_n are the non-zero positive roots of $\tan q_n = \alpha \times q_n$, and L is the thickness of the sample, D is the diffusion coefficient.

Model B: Film in contact with an infinite volume of food/simulant and negligible external mass transfer coefficient (Figure 2-7).

This model is often used in the case where $\alpha \gg 1$ as a result of a larger volume of food/simulant (20-50 times) than the volume of the film (Hamdani, Feigenbaum, & Vergnaud,

1997), that denotes most of the migrant, if not all, migrates into the food/simulant. The final solution for this model is as follows:

$$\frac{M_{f,t}}{M_{f,\infty}} = 1 - \frac{8}{\pi^2}\sum_{n=1}^{\infty}\frac{1}{(2n+1)^2}exp\left[-\frac{(2n+1)^2}{L^2}D\pi^2 t\right] \quad \text{(Eq. 2-15)}$$

Both model A and B are often known as Piringer models. These models are controlled by diffusion in the film. For short migration times, the U.S Food and Drug Administration (FDA) model is applied (Poças et al., 2008). The final solution for short migration times is shown in Figure 2-7.

Model C: Film in contact with an infinite volume of food/simulant and non-negligible external mass transfer coefficient (Figure 2-8).

This model involves a convection process, in which resistance exists at the interface between the film and the food/simulant. In this case, a dimensionless Biot number (Bi) is calculated by taking into consideration the thickness of the film, the convective mass transfer coefficient, and diffusion that takes place in the film (Vitrac, Mougharbel, & Feigenbaum, 2007). Commonly, in the case of Bi <200 which suggests high resistance at the film-food/simulant interface (Figure 2-8 and Figure 2-9), the following solution is used:

$$\frac{M_{f,t}}{M_{f,\infty}} = 1 - \sum_{n=1}^{\infty}\frac{2\mathrm{Bi}}{(q_n^2+Bi+Bi^2)q_n^2}exp\left[-\frac{Dq_n^2 t}{L^2}\right] \quad \text{(Eq. 2-16)}$$

In a situation where the food/liquid is strongly stirred (Bi>200) (Mascheroni, Guillard, Nalin, Mora, & Piergiovanni, 2010), Eq. 2-15 is then used as a solution.

Initial conditions

$$C_p(x,0) = C_0 \qquad C_f(x,0) = 0$$

Boundary condition

$$\left.\frac{\partial C_p}{\partial x}\right|_{x=0} = 0 \qquad -D\left.\frac{\partial C_p}{\partial x}\right|_{x=L} = \frac{V_f}{A}\left.\frac{\partial C_f}{\partial t}\right|_{x=L}$$

Balance equation

$$\frac{\partial C_p}{\partial t} = D\frac{\partial^2 C_p}{\partial x^2}$$

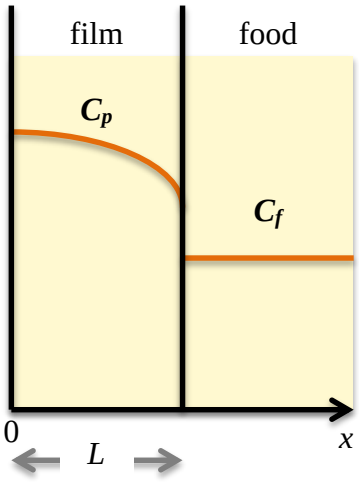

Solutions

$$\frac{M_{f,t}}{M_{f,\infty}} = 1 - \sum_{n=1}^{\infty} \frac{2\alpha(1+\alpha)}{1+\alpha+\alpha^2 q_n^2} exp\left[-\frac{Dq_n^2 t}{L^2}\right]$$

q_n= the non-zero positive roots of tan $q_n = -\alpha q_n$

If $\alpha \gg 1$ because $V_f \gg V_p$ and/ or $K_{p,f} < 1$, a simplified solution:

$$\frac{M_{f,t}}{M_{f,\infty}} = 1 - \frac{8}{\pi^2}\sum_{n=1}^{\infty} \frac{1}{(2n+1)^2} exp\left[-\frac{(2n+1)^2}{L^2} D\pi^2 t\right]$$

$$K_{p,f} = \frac{C_{p,\infty}}{C_{f,\infty}}$$

$$\alpha = \frac{V_f}{K_{p,f} V_p}$$

FDA model:

For short migration time:

$$\frac{M_{f,t}}{M_{p,0}} = \frac{2}{L\sqrt{\pi}}\sqrt{Dt}$$

If $\alpha \ll 1$ because $V_f \approx V_p$ and/ or $K_{p,f} \gg 1$, a simplified solution:

$$\frac{M_{f,t}}{M_{f,\infty}} = 1 - \exp(Z^2)\, erfc(Z)$$

$$Z = \frac{K_{p,f}}{a}\sqrt{Dt}$$

$$a = \frac{V_f}{A}$$

Figure 2-7 Migration phenomena that are controlled by the diffusion in the film. Figure was adapted from Poças et al. (2008) (Poças et al., 2008).

Initial conditions

$$C_p(x,0) = C_0 \qquad C_f(x,0) = 0$$

Boundary condition

$$\left.\frac{\partial C_p}{\partial x}\right|_{x=0} = 0 \qquad -D\left.\frac{\partial C_p}{\partial x}\right|_{x=L} = h(C_p - C_{p,\infty})$$

Balance equation

$$\frac{\partial C_p}{\partial t} = D\frac{\partial^2 C_p}{\partial x^2}$$

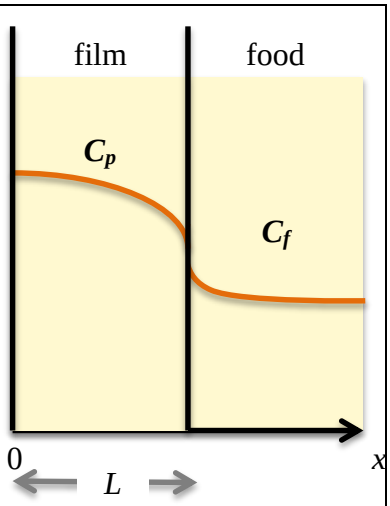

Solutions

$$\frac{M_{f,t}}{M_{f,\infty}} = 1 - \sum_{n=1}^{\infty} \frac{2\text{Bi}}{(q_n^2 + Bi + Bi^2)q_n^2} exp\left[-\frac{Dq_n^2 t}{L^2}\right]$$

Biot number (Bi)= $q_n \tan q_n$

q_n= the non-zero positive roots or eigenvalues

If Bi is very high (>200):

$$\frac{M_{f,t}}{M_{f,\infty}} = 1 - \frac{8}{\pi^2}\sum_{n=1}^{\infty} \frac{1}{(2n+1)^2} exp\left[-\frac{(2n+1)^2}{L^2} D\pi^2 t\right]$$

$$Bi = \frac{Lh}{D}$$

h= convective mass transfer coefficient

L= thickness of film

Figure 2-8 Migration phenomena that are controlled by the diffusion in the film with boundary layer resistance in the food/simulant. Figure was adapted from Poças et al. (2008) (Poças et al., 2008).

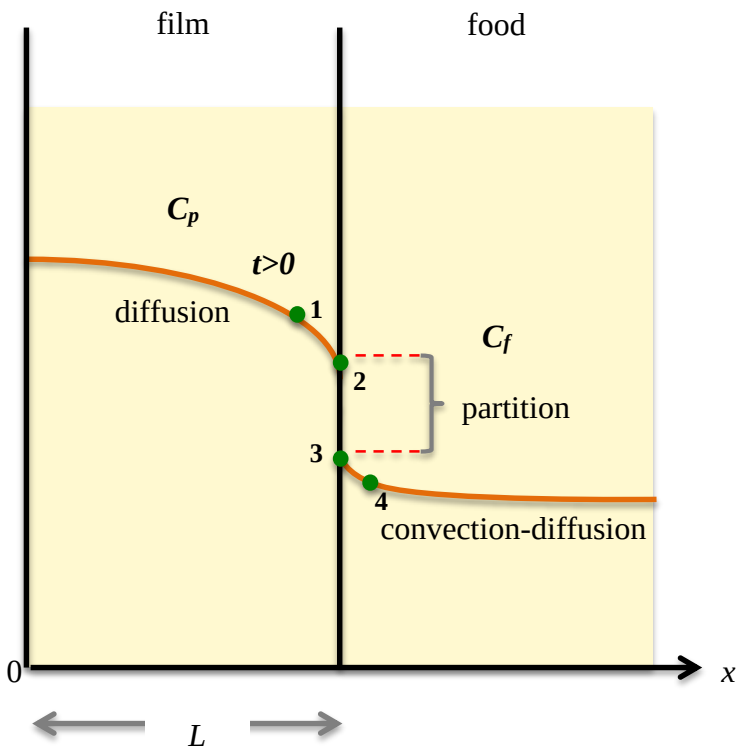

Figure 2-9 Illustration of boundary layer resistance at the interface of film/simulant. Region 1-2: Overall resistance of diffusion within film; region 2-3: resistance at the partition between film-food/simulant; region 3-4: mass transfer resistance at interface of film-food/simulant. Figure was adapted from Vitrac et al. (2007) (Vitrac et al., 2007).

Meanwhile, in the case of migration phenomena involving solid or semi solid food, a numerical solution using the finite difference method can be applied (Figure 2-10). The solution to this case can be approached based on discretization of time and/or discretization of space (Piringer & Beu, 2000; Poças et al., 2008). The accuracy of the solution is dependent on the degree of implicitness: fully explicit, fully implicit or Crank-Nicholson. The fully explicit solution uses forward finite differences, and it is not a stable solution. Often, this approach results in algorithm oscillations that grow exponentially as a function of time. The fully implicit solution applies

backward finite differences, and it is quite an accurate solution. Even though it is not as accurate as Crank-Nicholson, it does not produce the algorithm oscillations. The Crank-Nicholson method takes an average of both fully explicit and fully implicit and provides highly accurate and stable solutions (Piringer & Beu, 2000).

By having all migration models portrayed, it is very important to further estimate the parameters of interest, and thus be able to predict their behavior as well as to assist the experimental design of a variety of migration study.

Initial conditions

$$C_p(x,0) = C_0 \qquad C_f(x,0) = 0$$

Boundary condition

$$\left.\frac{\partial C_p}{\partial x}\right|_{x=0} = 0 \qquad -D_p \left.\frac{\partial C_p}{\partial x}\right|_{x=L} = -D_f \left.\frac{\partial C_f}{\partial x}\right|_{x=L}$$

Balance equation

$$\frac{\partial C_p}{\partial t} = D_p \frac{\partial^2 C_p}{\partial x^2} \qquad \frac{\partial C_f}{\partial t} = D_f \frac{\partial^2 C_f}{\partial x^2}$$

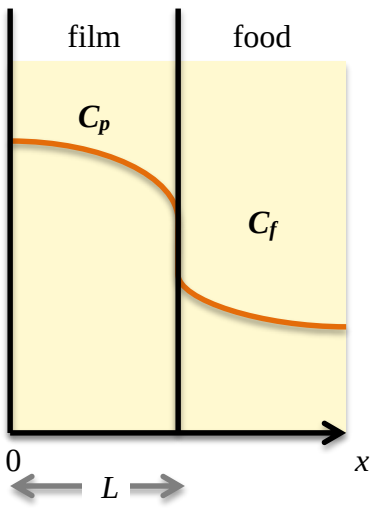

Solutions

Numerical solution using finite differences method:

Discretization of time:

$$\frac{C_i^{n+1} - C_i^n}{\partial t} = D\left[\theta \frac{C_{i-1}^{n+1} - 2C_i^{n+1} + C_{i+1}^{n+1}}{(\partial x)^2} + (1-\theta)\frac{C_{i-1}^{n} - 2C_i^{n} + C_{i+1}^{n}}{(\partial x)^2}\right]$$

Discretization of space:

$$\frac{\partial^2 C_i}{\partial x^2} = \frac{\varepsilon C_{i-1} - (1+\varepsilon)C_i + C_{i+1}}{(\partial x)^2}$$

θ= degree of implicitness:

Fully implicit, $\theta = 0$

Fully explicit, $\theta = 1$

Crank-Nicolson, $\theta = 0.5$

Figure 2-10 Migration phenomena that are controlled by diffusion in the film and in the food/simulant. Figure was adapted from Poças et al. (2008) (Poças et al., 2008).

2.7 Parameter Estimation

The use of the modeling approach aids data simulation and prediction; thus time and cost needed for performing an experiment can be reduced to a certain extent. The modeling approach can be classified into two parts, which are the forward problem and the inverse problem.

The forward problem is a direct approach using an explicit or differential solution where the parameters are known. The observational data are not required for a forward problem operation. The inverse problem requires data to be able to determine parameters or functions of the model (Dolan & Mishra, 2013). Experimental studies are often designed to collect observational data (dependent variable) with unknown functions or parameters. This approach is an inverse problem and also is known as parameter estimation.

Parameter estimation helps to estimate the parameters/constants of interest involved in mathematical models and to a certain extent it may provide some physical meaning for parameters relevant to the experiment. Beck and Arnold (1977) defined parameter estimation as "a discipline that provides tools for the efficient use of data in the estimation of constants appearing in mathematical models and for aiding in modeling of phenomena" (Beck & Arnold, 1977).

2.7.1 Parameters of Interest

Generally, in a migration study, one is very interested in determining the parameter *D*, that is the diffusion coefficient. This parameter helps to explain the kinetic release of a migrant from/to film to/from food/simulant, respectively. When the experiment is set up for a range of temperatures, with the parameter values obtained, the activation energy may be assessed.

Recently, some researchers have started the quest of estimating the mass transfer coefficient, h in the case of a resistance boundary layer (Mascheroni et al., 2010; Vitrac et al., 2007). Other parameters that are worth estimating are the $M_{f,\infty}$ and the α, that may provide extra

information for the migration study. Although some researchers have estimated the former, none has taken a step further to either report or explain it (C. Colín-Chávez et al., 2013; Citlali Colín-Chávez, Herlinda Soto-Valdez, Elizabeth Peralta, Jaime Lizardi-Mendoza, & René Renato Balandrán-Quintana, 2013; Hwang et al., 2013; Iñiguez-Franco et al., 2012; Manzanarez-López et al., 2011; Ortiz-Vazquez et al., 2011).

2.7.2 Sensitivity Coefficient, *X*, and Scaled Sensitivity Coefficient, *X'*

Depending on the particular research, parameter estimation may involve one particular parameter or more. As stated earlier, in a migration study, estimation of *D* is a necessity. However, by taking a more upfront approach, estimating some other parameters (*i.e.*, $h, M_{f,\infty}$ and α) that are importance in the research could result in more fruitful findings. When there are more parameters involved, it is vital to investigate whether those parameters can be estimated simultaneously, easily and accurately; thus, more interpretable results can be anticipated.

By taking the first derivative of the dependent variable (response variable) with respect to the parameter of interest, a sensitivity coefficient can be obtained (Eq. 2-17). The sensitivity coefficient is an important tool to determine the correlation among parameters estimated, the ease of accurately estimating each of the parameters involved, and in turn, to find the parameter that results in the smallest relative error (Dolan & Mishra, 2013). The sensitivity coefficient also provides insight about the magnitude of change with respect to response as a result of perturbations in the parameters (Beck & Arnold, 1977; Dolan & Mishra, 2013). In MATLAB®, a sensitivity coefficient matrix is constructed and known as the Jacobian matrix (Eq. 2-18).

$$X_D = \frac{\partial \eta}{\partial D} \qquad \text{(Eq. 2-17)}$$

$$X = \begin{pmatrix} \left(\frac{\partial \eta_1}{\partial D}\right) \dots \dots \dots \dots \left(\frac{\partial \eta_1}{\partial M_\infty}\right) \\ \left(\frac{\partial \eta_n}{\partial D}\right) \dots \dots \dots \dots \left(\frac{\partial \eta_n}{\partial M_\infty}\right) \end{pmatrix} \quad \text{(Eq. 2-18)}$$

However, for the purpose of comparing the parameters involved on the same scale, a scaled sensitivity coefficient figure is often plotted. By using the finite forward difference method (Eq. 2-19), the scaled sensitivity coefficient can be numerically approximated (Eq. 2-20) (Beck & Arnold, 1977). The scaled sensitivity coefficient is obtained by multiplying the sensitivity coefficient with its respective parameter (Eq. 2-21) (Dolan & Mishra, 2013).

$$[f](x) = \frac{f(x+h)-f(x)}{\Delta h} \quad \text{(Eq. 2-19)}$$

$$X'_{lj} = D_j \left(\frac{\partial \eta_{l(i)}}{\partial D_j}\right) = b_j \frac{\eta_l(b_i..,b_j+\partial b_j,..b_p)-\eta_l(b_i..,b_j,..b_p)}{\partial b_j} \quad \text{(Eq. 2-20)}$$

$$X'_D = D \frac{\partial \eta}{\partial D} \quad \text{(Eq. 2-21)}$$

2.7.3 Parameter Estimation using Ordinary Least Squares (OLS)

Parameter estimation can be performed by OLS using the non-linear regression (nlinfit) command in MATLAB®. Statistical assumptions need to be analyzed before data fitting. Statistical assumptions that need to be taken into account include (but are not limited to) (Beck & Arnold, 1977):

1. Errors are additive in the measurement
2. Errors in the measurement contain zero mean
3. The measurement errors have constant variance

4. The measurement errors are uncorrelated
5. Errors are normally, independently, identically distributed
6. Statistical parameters describing errors are known
7. Independent variables are errorless
8. The nature of the parameters (constant vs. random vector parameter; prior information vs. unknown statistics of the parameter)

Regardless of the outcome, the results of how the model fits and meets the aforementioned statistical assumptions should be reported, and based on that, further changes can be considered whenever necessary and applicable (Dolan & Mishra, 2013).

2.7.3.1 Standard Errors and Correlation Coefficient of the Parameters

Standard errors of the parameters can be obtained by using OLS through a variance-covariance matrix (Eq. 2-22). In this context, the sensitivity coefficient or Jacobian matrix, *X*, is also directly correlated with the determination of standard errors of the parameters. The standard error of an individual parameter, σ, can be further divided by the parameter vector itself to obtain its relative standard error (Mishra, Dolan, & Yang, 2008).

$$cov(a) = (X^T X)^{-1}\sigma^2 = \begin{pmatrix} \sigma_D^2 & \sigma_{D,M_\infty} \\ \sigma_{D,M_\infty} & \sigma_{M_\infty}^2 \end{pmatrix} \quad \text{(Eq. 2-22)}$$

The correlation coefficient is an important tool to determine the correlation among the estimated parameters (Eq. 2-23). The value obtained is absolute, ranges from 0 to 1, and the closer the value is to 1, the more highly correlated the parameters are. As a result, the parameters may be difficult to estimate accurately. The correlation coefficient matrix is also shown as follows (Eq. 2-24).

$$\rho_{D,M_\infty} = \frac{\sigma_{D,M_\infty}}{\sigma_D \sigma_{M_\infty}} \quad \text{(Eq. 2-23)}$$

$$\begin{pmatrix} 1.0 & \rho_{D,M_\infty} \\ \rho_{D,M_\infty} & 1.0 \end{pmatrix} \quad \text{(Eq. 2-24)}$$

2.7.4 Sequential Estimation

In addition to the OLS method, sequential estimation can be used to estimate parameters of interest. This method was developed based on the Gauss minimization method by using the matrix inversion lemma (Beck & Arnold, 1977). This method requires iteration steps in the case of a non-linear model like in most migration models. It is more powerful than OLS in the sense that it may provide the duration required for an experimental study, and it is still able to estimate the parameters accurately. This method also updates the parameter whenever new responses are added. However, prior information is always required (Beck & Arnold, 1977; Dolan & Mishra, 2013). It is always good practice to compare the outcomes between OLS and sequential estimation.

2.7.5 Corrected Akaike Information Criterion (AICc)

Mathematical models used for migration phenomena contain parameters such as *D* and the *h*. Some researchers, as discussed earlier, have started to focus on other relevant parameters for migration such as the $M_{f,\infty}$. Therefore, the idea of investigating more parameters is very crucial to correlate the physical meanings behind these parameters with respect to the migration experiment. However, the more parameters are estimated, the more uncertainty will be introduced, in turn, decreasing the accuracy of the estimation. Therefore, it is important to be able to select the right model containing a sufficient number of parameters to justify the estimation process.

Often, the sums of squared errors (SSE) or the root mean square error (RMSE) is used to get an indication of a better model by selecting the model with the lowest corresponding SSE or

RMSE. This approach may be useful for comparing different models with a similar number of parameters. However, for comparing models (nested or non-nested) with different numbers of parameters, the use of SSE or RMSE will introduce bias since generally the more parameters estimated, the better the SSE or RMSE will be. Thus, in such cases, the corrected Akaike information criterion (AICc) can be used.

The AICc is the second order of the AIC. This approach penalizes additional parameters, thus eliminating the bias introduced by having more parameters. The AICc is recommended for cases involving small sample sizes (*n*). However, it is applicable for all cases since with larger *n*, the correction term ($\frac{2K(K+1)}{n-K-1}$) becomes trivial; thus the AICc is reduced to the AIC expression (Motulsky & Christopoulos, 2004a).

$$AICc = n\ ln\left(\frac{SSE}{n}\right) + 2K + \frac{2K(K+1)}{n-K-1} \qquad \text{(Eq. 2-25)}$$

where *n*=number of data; *p*=number of parameters; *K=p+1*

2.7.6 Bootstrap

The bootstrap method is a resampling approach to draw relevant information that represents the population. Bootstrap is beneficial when the error distribution is unknown (Mishra, Dolan, & Yang, 2011). This method can provide accurate statistical inferences in cases when the number of data points is insufficient or the data are ill-posed (Fox, 2015). There are three main types of bootstraps; i) parametric, ii) residuals, and iii) data. The parametric bootstrap is the strict one since it relies on how better is the model for some parameters. For this type of bootstrap, the model is first estimated and the simulation is done from the estimated model. The residuals bootstrap does not rely on the model and does not assume the residuals distribution (Fox, 2015). This method in particular is beneficial for a small data set and when the magnitude response of the parameter is

large at a certain data interval. Once the model is estimated, the residuals of the estimates are then simulated. The resampled residuals are then added to the fitted values, thus producing synthetic data. The data bootstrap ignores the model and the data is then resampled from the data range, thus making this type of bootstrap the safest choice (Anonymous, 2013) and produces widened confidence and prediction bandwidths.

2.7.7 Optimal Experimental Design

By maximizing the determinant Δ^n (Eq. 2-25), the optimal time to perform an experimental study can be determined. Optimal experimental design helps in finding the optimal point at which the parameters can be estimated and have lower errors. The C matrix is needed in order to achieve a desirable maximum determinant (Eq. 2-26). This approach is beneficial in terms of optimizing not only the resources used, but also the time spent for a given experiment (Beck & Arnold, 1977; Dolan & Mishra, 2013).

$$\Delta^n = |X^T X| \qquad \text{(Eq. 2-26)}$$

$$C_{ij} = \frac{1}{t_n}\int_0^{t_n} X_i'(t) X_j'(t) dt \qquad \text{(Eq. 2-27)}$$

2.7.8 Activation Energy

All of the kinetic reactions are temperature dependent. A well-recognized mathematical expression used to describe the dependency of kinetic reactions on temperature is the Arrhenius equation (Eq. 2-28).

$$k = k_0 exp\left(-\frac{E_a}{RT}\right) \qquad \text{(Eq. 2-28)}$$

where k= rate constant; k_0=frequency or pre-exponential factor; E_a=activation energy; R=gas constant; T=temperature.

The Arrhenius equation is used to obtain information about the activation energy, E_a. The E_a is the rate of migration changes with temperature. The mathematical expression of the Arrhenius equation is known to complicate the estimation process due to the high correlation that is commonly found between the k_0 and the E_a. As a result, the linearized form of this equation is commonly applied to obtain the estimation of the E_a. For such approach, the error structure of the k_0 is not known since it is not attained experimentally. Since this equation is a non-linear model, its error structure is more complex than the error structure of a linear model, which the latter can be obtained from observational data (Schwaab & Pinto, 2007; Watts, 1994). Thus, to avoid the correlation issue between parameters and the risk of introducing more error to the estimation process, a reparameterization approach is recommended (Agarwal & Brisk, 1985a, 1985b; Schwaab, Lemos, & Pinto, 2008; Schwaab & Pinto, 2007). This approach was first introduced by Box, 1960 and later Himmelblau, 1970. The reparameterized form of the Arrhenius equation is as follows;

$$k = k_{ref} exp\left[-\frac{E_a}{R}\left(\frac{1}{T} - \frac{1}{T_{ref}}\right)\right] \quad \text{(Eq. 2-29)}$$

where k_{ref}=specific reaction rate at T_{ref} ; T_{ref}=reference temperature.

Numerous advantages can be gained from using the reparameterized Arrhenius equation. Among them are; i) the ease of the simultaneous estimation of parameters following the optimum T_{ref} resulted in a lower correlation, thus minimized errors of the parameters (Schwaab et al., 2008; Schwaab & Pinto, 2007); ii) the need for heavy computational work to achieve the minimization of the objective function is eliminated (Espie & Macchietto, 1988) and iii) the improvement of the elliptical confidence region can be obtained (Schwaab et al., 2008; Schwaab & Pinto, 2007; Watts, 1994).

The reparameterized form of the Arrhenius equation has been used in various applications such as microbial inactivation, starch gelatinization, *in situ* vibrational spectroscopy *etc*.(Dolan, Valdramidis, & Mishra, 2013; Furusjö, Svensson, & Danielsson, 2003; Sulaiman, Dolan, & Mishra, 2013).

To apply this approach to mass transfer (*i.e.*, migration), the following equation can be used (Eq. 2-30);

$$D = D_{ref} exp\left[-\frac{E_a}{R}\left(\frac{1}{T} - \frac{1}{T_{ref}}\right)\right] \quad \text{(Eq. 2-30)}$$

where D_{ref}=the diffusivity rate of the additives at T_{ref}.

REFERENCES

REFERENCES

Abdollahi, M., Rezaei, M., & Farzi, G. (2012). A novel active bionanocomposite film incorporating rosemary essential oil and nanoclay into chitosan. *Journal of Food Engineering, 111*(2), 343-350.

Adam, W. (1975). Singlet molecular oxygen and its role in organic peroxide chemistry. *Chemiker Zeitung, 99*, 142-155.

Agarwal, A. K., & Brisk, M. L. (1985a). Sequential experimental design for precise parameter estimation. 1. Use of reparameterization. *Industrial & Engineering Chemistry Process Design and Development, 24*(1), 203-207.

Agarwal, A. K., & Brisk, M. L. (1985b). Sequential experimental design for precise parameter estimation. 2. Design criteria. *Industrial & Engineering Chemistry Process Design and Development, 24*(1), 207-210.

Andersson, K. (1998). *Influence of reduced oxygen concentrations on lipid oxidation in food during storage* (PhD thesis), Chalmers University of Technology and the Swedish Institute for Food and Biotechnology, Sweden.

Anonymous. (2013). Which Bootstrap When. Carnegies Mellon University.

Arrieta, M. P., Peltzer, M. A., Garrigós, M. C., & Jiménez, A. (2013). Structure and mechanical properties of sodium and calcium caseinate edible active films with carvacrol. *Journal of Food Engineering*.

Arrua, D., Strumia, M. C., & Nazareno, M. A. (2010). Immobilization of caffeic acid on a polypropylene film: Synthesis and antioxidant properties. *Journal of Agricultural and Food Chemistry, 58*(16), 9228-9234.

Azeredo, H. (2009). Nanocomposites for food packaging applications. *Food Research International, 42*(9), 1240-1253.

Bailey, L. A. (1995). *Mass Transfer of 3, 5-di-tertiary-butyl-4-hydroxytoluene (BHT) from a Multi-layer Lamination.* Michigan State University. School of Packaging.

Baner, A. L., Franz, R., & Piringer, O. (1994). Alternative fatty food simulants for polymer migration testing. In M. Mathlouthi (Ed.), *Food Packaging and Preservation* (pp. 24-31). Glasgow: Blackie Academic and Professional

Barbosa-Pereira, L., Cruz, J. M., Sendón, R., Ana Ares, A. R. B. d. Q., Castro-López, M., Abad, M. J., . . . Paseiro-Losada, P. (2012). Development of antioxidant active films containing tocopherols to extend the shelf life of fish. *Food Control*.

Beck, J. V., & Arnold, K. J. (1977). *Parameter Estimation in Engineering and Science* (Vol. 8): Wiley New York.

Box, G. E. (1960). Fitting empirical data. *Annals of the New York Academy of Sciences, 86*(3), 792-816.

Buettner, G. R. (1993). The pecking order of free radicals and antioxidants: lipid peroxidation, α-tocopherol, and ascorbate. *Archives of Biochemistry and Biophysics, 300*(2), 535-543.

Byun, Y., Kim, Y. T., & Whiteside, S. (2010). Characterization of an antioxidant polylactic acid (PLA) film prepared with α-tocopherol, BHT and polyethylene glycol using film cast extruder. *Journal of Food Engineering, 100*(2), 239-244.

Calatayud, M., López-de-Dicastillo, C., López-Carballo, G., Vélez, D., Muñoz, P. H., & Gavara, R. (2013). Active films based on cocoa extract with antioxidant, antimicrobial and biological applications. *Food Chemistry*.

Camo, J., Beltrán, J. A., & Roncalés, P. (2008). Extension of the display life of lamb with an antioxidant active packaging. *Meat Science, 80*(4), 1086-1091.

Castro López, M. M., López de Dicastillo, C., López Vilariño, J. M., & González Rodríguez, M. V. (2013). Improving the Capacity of Polypropylene To Be Used in Antioxidant Active Films: Incorporation of Plasticizer and Natural Antioxidants. *Journal of Agricultural and Food Chemistry, 61*(35), 8462-8470.

Chen, X., Lee, D. S., Zhu, X., & Yam, K. L. (2012). Release kinetics of tocopherol and quercetin from binary antioxidant controlled-release packaging films. *Journal of Agricultural and Food Chemistry, 60*(13), 3492-3497.

Choe, E., & Min, D. B. (2006). Mechanisms and factors for edible oil oxidation. *Comprehensive Reviews in Food Science and Food Safety, 5*(4), 169-186.

Chung, D., Papadakis, S. E., & Yam, K. L. (2001). Release of propyl paraben from a polymer coating into water and food simulating solvents for antimicrobial packaging applications. *Journal of Food Processing and Preservation, 25*(1), 71-87.

Chung, D., Papadakis, S. E., & Yam, K. L. (2002). Simple models for assessing migration from food-packaging films. *Food Additives and Contaminants, 19*(6), 611-617.

Cohen Stuart, C. (1912). *A study of temperature-coefficients and van't Hoff's rule.* Paper presented at the KNAW, Proceedings.

Colín-Chávez, C., Soto-Valdez, H., Peralta, E., Lizardi-Mendoza, J., & Balandrán-Quintana, R. R. (2013). Diffusion of natural astaxanthin from polyethylene active packaging films into a fatty food simulant. *Food Research International, 54*(1), 873-880.

Colín-Chávez, C., Soto-Valdez, H., Peralta, E., Lizardi-Mendoza, J., & Balandrán-Quintana, R. R. (2013). Fabrication and Properties of Antioxidant Polyethylene-based Films Containing Marigold (Tagetes erecta) Extract and Application on Soybean Oil Stability. *Packaging Technology and Science, 26*(5), 267-280. doi: 10.1002/pts.1982

Colon, M., & Nerin, C. (2012). Role of catechins in the antioxidant capacity of an active film containing green tea, green coffee, and grapefruit extracts. *Journal of Agricultural and Food Chemistry, 60*(39), 9842-9849.

Contini, C., Katsikogianni, M. G., O'Neill, F. T., O'Sullivan, M., Dowling, D. P., & Monahan, F. J. (2012). PET trays coated with Citrus extract exhibit antioxidant activity with cooked turkey meat. *LWT-Food Science and Technology, 47*(2), 471-477.

Corliss, G. A., & Dugan Jr, L. (1970). Phospholipid oxidation in emulsions. *Lipids, 5*(10), 846-853.

Crank, J. (1979). *The Mathematics of Diffusion* (2nd ed.). Bristol: Oxford University Press.

Cruz, R. S., Camilloto, G. P., & dos Santos Pires, A. C. (2012). Oxygen scavengers: an approach on food preservation. In A. A. Eissa (Ed.), *Structure and Function of Food Engineering* (pp. 21-42). New York: InTech

De Meulenaer, B. (2009). Migration from Packaging Materials. In R. Cósta & K. Kristbergsson (Eds.), *Predictive Modeling and Risk Assessment*. New york: Springer Science

Decker, E. (1998). Strategies for manipulating the prooxidative/antioxidative balance of foods to maximize oxidative stability. *Trends in Food Science and Technology, 9*(6), 241-248.

Dolan, K. D., & Mishra, D. K. (2013). Parameter estimation in food science. *The Annual Review of Food Science and Technology, 4*, 401-422.

Dolan, K. D., Valdramidis, V. P., & Mishra, D. K. (2013). Parameter estimation for dynamic microbial inactivation: which model, which precision? *Food Control, 29*(2), 401-408.

Edens, L., Farin, F., Ligtvoet, A. F., & Van Der Plaat, J. B. (1992). U.S. Patent No.: D. C. U. S. P. a. T. O. Washington.

Endo, Y., Usuki, R., & Kaneda, T. (1984). Prooxidant activities of chlorophylls and their decomposition products on the photooxidation of methyl linoleate. *Journal of the American Oil Chemists' Society, 61*(4), 781-784.

Endo, Y., Usuki, R., & Kaneda, T. (1985). Antioxidant effects of chlorophyll and pheophytin on the autoxidation of oils in the dark. I. Comparison of the inhibitory effects. *Journal of the American Oil Chemists' Society, 62*(9), 1375-1378.

Espie, D. M., & Macchietto, S. (1988). Nonlinear transformations for parameter estimation. *Industrial & engineering chemistry research, 27*(11), 2175-2179.

Fakourelis, N., Lee, E., & Min, D. (1987). Effects of Chlorophyll and β-Carotene on the Oxidation Stability of Olive Oil. *Journal of Food Science, 52*(1), 234-235.

Ferrari, M., Carranza, S., Bonnecaze, R., Tung, K., Freeman, B., & Paul, D. (2009). Modeling of oxygen scavenging for improved barrier behavior: Blend films. *Journal of Membrane Science, 329*(1), 183-192.

Fox, J. (2015). Bootstrapping Regression Models. In J. Fox (Ed.), *Applied regression analysis and generalized linear models* (3 ed., pp. 587-606). Thousand Oaks, CA: Sage Publications

Franz, R., & Störmer, A. (2008). Migration of plastic constituents *Plastic Packaging: Interactions with Food and Pharmaceuticals* (pp. 349-415)

Furusjö, E., Svensson, O., & Danielsson, L.-G. (2003). Estimation of kinetic parameters from non-isothermal batch experiments monitored by in situ vibrational spectroscopy. *Chemometrics and intelligent laboratory systems, 66*(1), 1-14.

Galdi, M., Nicolais, V., Di Maio, L., & Incarnato, L. (2008). Production of active PET films: evaluation of scavenging activity. *Packaging Technology and Science, 21*(5), 257-268.

Galindo-Arcega, C. E. (2004). *Migración del BHT de películas de PEBD y su efecto en la estabilidad del aceite de soya.* (MSc), Centro de Investigación en Alimentación y Desarrollo Hermosillo.

Gavara, R., Lagarón, J. M., & Catalá, R. (2004). *Materiales poliméricos para en diseñyo de envases actives.* Paper presented at the Seminario Cyted-Technológico de Monterrey, Monterrey, México.

Goncalves, C., Tomé, L. C., Garcia, H., Brandão, L., Mendes, A. M., & Marrucho, I. M. (2012). Effect of natural and synthetic antioxidants incorporation on the gas permeation properties of poly (lactic acid) films. *Journal of Food Engineering*.

Gordon, M. H. (1990). The mechanism of antioxidant action in vitro. *Food Antioxidants, 1*, 1-18.

Gordon, M. H. (2001). The development of oxidative rancidity in foods *Antioxidants in Food: Practical Applications* (pp. 7-21): Woodhead Publishing Limited, Cambridge

Granda-Restrepo, D. M., Soto-Valdez, H., Peralta, E., Troncoso-Rojas, R., Vallejo-Córdoba, B., Gámez-Meza, N., & Graciano-Verdugo, A. Z. (2009). Migration of α-tocopherol from an active multilayer film into whole milk powder. *Food Research International, 42*(10), 1396-1402.

Gutiérrez-Rosales, F., Garrido-Fernández, J., Gallardo-Guerrero, L., Gandul-Rojas, B., & Minguez-Mosquera, M. I. (1992). Action of chlorophylls on the stability of virgin olive oil. *Journal of the American Oil Chemists Society*, *69*(9), 866-871.

Hamdani, M., Feigenbaum, A., & Vergnaud, J. M. (1997). Prediction of worst case migration from packaging to food using mathematical models. *Food Additives and Contaminants*, *14*(5), 499-506.

Heirlings, L., Siró, I., Devlieghere, F., Van Bavel, E., Cool, P., De Meulenaer, B., . . . Debevere, J. (2004). Influence of polymer matrix and adsorption onto silica materials on the migration of α-tocopherol into 95% ethanol from active packaging. *Food Additives and Contaminants*, *21*(11), 1125-1136.

Himmelblau, D. M. (1970). *Process analysis by statistical methods*. New York: Wiley&Sons.

Hwang, S. W., Shim, J. K., Selke, S., Soto-Valdez, H., Matuana, L., Rubino, M., & Auras, R. (2013). Migration of α-Tocopherol and Resveratrol from Poly (L-lactic acid)/Starch Blends Films into Ethanol. *Journal of Food Engineering*.

Iñiguez-Franco, F., Soto-Valdez, H., Peralta, E., Ayala-Zavala, J. F., Auras, R., & Gámez-Meza, N. (2012). Antioxidant Activity and Diffusion of Catechin and Epicatechin from Antioxidant Active Films Made of Poly (l-lactic acid). *Journal of Agricultural and Food Chemistry*, *60*(26), 6515-6523.

Jamshidian, M., Tehrany, E. A., & Desobry, S. (2012). Antioxidants release from solvent-cast pla film: investigation of pla antioxidant-active packaging. *Food and Bioprocess Technology*, 1-14.

Jiang, L., & Zhang, J. (2013). Biodegradable polymers and polymer blends. In S. Ebnesajjad (Ed.), *Handbook of Biopolymers and Biodegradable Plastics: Properties, Processing, and Applications* (pp. 109-128). Oxford, UK: William Andrew

Jurina, J., Azizah, A. N., Siah, W., & Ngadiman, K. (2011). Effects of butylated hydroxytoluene (BHT) impregnated film on storage of vegetable crackers. *Journal of Tropical Agriculture and Food Science*, *39*(1), 37-43.

Kanatt, S. R., Rao, M., Chawla, S., & Sharma, A. (2012). Active chitosan–polyvinyl alcohol films with natural extracts. *Food Hydrocolloids*, *29*(2), 290-297.

Karel, M. (1980). Lipid oxidation, secondary reactions, and water activity of foods.

Kochhar, S., & Rossell, J. (1990). Detection, estimation and evaluation of antioxidants in food systems (Vol. 19): Elsevier, Amsterdam.

Koontz, J. L., Marcy, J. E., O'Keefe, S. F., Duncan, S. E., Long, T. E., & Moffitt, R. D. (2010). Polymer processing and characterization of LLDPE films loaded with α-tocopherol, quercetin, and their cyclodextrin inclusion complexes. *Journal of Applied Polymer Science, 117*(4), 2299-2309.

Labuza, T. P., & Dugan Jr, L. R. (1971). Kinetics of lipid oxidation in foods. *Critical Reviews in Food Science and Nutrition, 2*(3), 355-405.

Laguerre, M., Lecomte, J., & Villeneuve, P. (2007). Evaluation of the ability of antioxidants to counteract lipid oxidation: Existing methods, new trends and challenges. *Progress in Lipid Research, 46*(5), 244-282.

Lee, D. S. (2011). Active Packaging. In D. W. Sun (Ed.), *Handbook of Frozen Food Processing and Packaging* (2nd ed., Vol. 18, pp. 819-836). London, GBR: CRC Press

Lee, D. S. (2014). Antioxidative Packaging System. In J. H. Han (Ed.), *Innovation in Food Packaging* (2nd ed., pp. 111-131). Waltham, MA: Academic Press

Lee, Y. S., Shin, H.-S., Han, J.-K., Lee, M., & Giacin, J. R. (2004). Effectiveness of antioxidant-impregnated film in retarding lipid oxidation. *Journal of the Science of Food and Agriculture, 84*(9), 993-1000.

Lennersten, M., & Lingnert, H. (2000). Influence of wavelength and packaging material on lipid oxidation and colour changes in low-fat mayonnaise. *LWT-Food Science and Technology, 33*(4), 253-260.

Limm, W., & Hollifield, H. C. (1996). Modelling of additive diffusion in polyolefins. *Food Additives and Contaminants, 13*(8), 949-967.

Lopez de Dicastillo, C., Nerin, C., Alfaro, P., Catalá, R., Gavara, R., & Hernandez-Muñoz, P. (2011). Development of new antioxidant active packaging films based on ethylene vinyl alcohol

copolymer (EVOH) and green tea extract. *Journal of Agricultural and Food Chemistry, 59*(14), 7832-7840.

López-de-Dicastillo, C., Alonso, J. M., Catalá, R., Gavara, R., & Hernández-Muñoz, P. (2010). Improving the Antioxidant Protection of Packaged Food by Incorporating Natural Flavonoids into Ethylene− Vinyl Alcohol Copolymer (EVOH) Films. *Journal of Agricultural and Food Chemistry*.

López-de-Dicastillo, C., Gómez-Estaca, J., Catalá, R., Gavara, R., & Hernández-Muñoz, P. (2012). Active antioxidant packaging films: Development and effect on lipid stability of brined sardines. *Food Chemistry, 131*(4), 1376-1384.

López-Rubio, A., & Lagaron, J. M. (2010). Improvement of UV stability and mechanical properties of biopolyesters through the addition of β-carotene. *Polymer Degradation and Stability, 95*(11), 2162-2168.

Manzanarez-López, F., Soto-Valdez, H., Auras, R., & Peralta, E. (2011). Release of α-Tocopherol from Poly (lactic acid) films, and its effect on the oxidative stability of soybean oil. *Journal of Food Engineering, 104*(4), 508-517.

Martin-Polvillo, M., Márquez-Ruiz, G., & Dobarganes, M. (2004). Oxidative stability of sunflower oils differing in unsaturation degree during long-term storage at room temperature. *Journal of the American Oil Chemists' Society, 81*(6), 577-583.

Martins, J. T., Cerqueira, M. A., & Vicente, A. A. (2012). Influence of α-tocopherol on physicochemical properties of chitosan-based films. *Food Hydrocolloids, 27*(1), 220-227.

Mascheroni, E., Guillard, V., Nalin, F., Mora, L., & Piergiovanni, L. (2010). Diffusivity of propolis compounds in Polylactic acid polymer for the development of anti-microbial packaging films. *Journal of Food Engineering, 98*(3), 294-301.

McClements, D., & Decker, E. (2000). Lipid Oxidation in Oil‐in‐Water Emulsions: Impact of Molecular Environment on Chemical Reactions in Heterogeneous Food Systems. *Journal of Food Science, 65*(8), 1270-1282.

Mills, A., Doyle, G., Peiro, A. M., & Durrant, J. (2006). Demonstration of a novel, flexible, photocatalytic oxygen-scavenging polymer film. *Journal of Photochemistry and Photobiology A: Chemistry, 177*(2), 328-331.

Min, D., & Boff, J. (2002). Chemistry and reaction of singlet oxygen in foods. *Comprehensive Reviews in Food Science and Food Safety, 1*(2), 58-72.

Mishra, D. K., Dolan, K. D., & Yang, L. (2008). Confidence intervals for modeling anthocyanin retention in grape pomace during nonisothermal heating. *Journal of Food Science, 73*(1), E9-E15.

Mishra, D. K., Dolan, K. D., & Yang, L. (2011). Bootstrap confidence intervals for the kinetic parameters of degradation of anthocyanins in grape pomace. *Journal of Food Process Engineering, 34*(4), 1220-1233.

Mistry, B. S., & Min, D. B. (1987). Effects of fatty acids on the oxidative stability of soybean oil. *Journal of Food Science, 52*(3), 831-832.

Mortensen, A., & Skibsted, L. H. (1997). Importance of carotenoid structure in radical-scavenging reactions. *Journal of Agricultural and Food Chemistry, 45*(8), 2970-2977.

Murray, R. (1979). Chemical sources of singlet oxygen. *Singlet Oxygen, 40*.

Nawar, W. W. (1969). Thermal degradation of lipids. *Journal of Agricultural and Food Chemistry, 17*(1), 18-21.

Nerín, C., Tovar, L., & Salafranca, J. (2008). Behaviour of a new antioxidant active film versus oxidizable model compounds. *Journal of Food Engineering, 84*(2), 313-320.

Nwosu, C. V., Boyd, L. C., & Sheldon, B. (1997). Effect of fatty acid composition of phospholipids on their antioxidant properties and activity index. *Journal of the American Oil Chemists' Society, 74*(3), 293-297.

O'brien, P. J. (1969). Intracellular mechanisms for the decomposition of a lipid peroxide. I. Decomposition of a lipid peroxide by metal ions, heme compounds, and nucleophiles. *Canadian Journal of Biochemistry, 47*(5), 485-492.

Ortiz-Vazquez, H., Shin, J. M., Soto-Valdez, H., & Auras, R. (2011). Release of butylated hydroxytoluene (BHT) from Poly (lactic acid) films. *Polymer Testing, 30*(5), 463-471.

Peltzer, M. A., Wagner, J., & Jiménez, A. (2009). Migration study of carvacrol as a natural antioxidant in high-density polyethylene for active packaging. *Food Additives and Contaminants, 26*(6), 938-946.

Pereira de Abreu, D. A., Losada, P. P., Maroto, J., & Cruz, J. M. (2010). Evaluation of the effectiveness of a new active packaging film containing natural antioxidants (from barley husks) that retard lipid damage in frozen Atlantic salmon (Salmo salar). *Food Research International, 43*(5), 1277-1282.

Piringer, O. G., & Beu, T. (2000). Transport equations and their solutions. In A. L. Baner & O.-G. Piringer (Eds.), *Plastic Packaging Materials for Food, Barrier Function,Mass Transport, Quality Assurance and Legislation* (pp. 195-246). Weinheim: Wiley-VCH

Poças, M. F., Oliveira, J. C., Oliveira, F. A. R., & Hogg, T. (2008). A critical survey of predictive mathematical models for migration from packaging. *Critical Reviews in Food Science and Nutrition, 48*(10), 913-928.

Quilaqueo-Gutiérrez, M., Echeverría, I., Ihl, M., Bifani, V., & Mauri, A. N. (2012). Carboxymethylcellulose–montmorillonite nanocomposite films activated with murta (< i> Ugni molinae</i> Turcz) leaves extract. *Carbohydrate Polymers, 87*(2), 1495-1502.

Rahmani, M., & Csallany, A. S. (1998). Role of minor constituents in the photooxidation of virgin olive oil. *Journal of the American Oil Chemists' Society, 75*(7), 837-843.

Rice-Evans, C. A., Miller, N. J., & Paganga, G. (1996). Structure-antioxidant activity relationships of flavonoids and phenolic acids. *Free Radical Biology and Medicine, 20*(7), 933-956.

Sattar, A., DeMan, J., & Alexander, J. (1976). Effect of wavelength on light induced quality deterioration of edible oils and fats. *Canadian Institute of Food Science and Technology Journal, 9*(3), 108-113.

Schaich, K. M., Shahidi, F., Zhong, Y., & Eskin, N. A. M. (2013). Lipid Oxidation. In N. M. Eskin & F. Shahidi (Eds.), *Biochemistry of Foods*: Academic Press

Schlotter, N. E., & Furlan, P. Y. (1992). A review of small molecule diffusion in polyolefins. *Polymer, 33*(16), 3323-3342.

Schreiber, S. B., Bozell, J. J., Hayes, D. G., & Zivanovic, S. (2013). Introduction of primary antioxidant activity to chitosan for application as a multifunctional food packaging material. *Food Hydrocolloids*.

Schwaab, M., Lemos, L. P., & Pinto, J. C. (2008). Optimum reference temperature for reparameterization of the Arrhenius equation. Part 2: Problems involving multiple reparameterizations. *Chemical Engineering Science, 63*(11), 2895-2906.

Schwaab, M., & Pinto, J. C. (2007). Optimum reference temperature for reparameterization of the Arrhenius equation. Part 1: Problems involving one kinetic constant. *Chemical Engineering Science, 62*(10), 2750-2764.

Selke, S. E. M., Culter, J. D., & Hernandez, R. J. (2004). *Plastics Packaging- Properties, Processing, Applications and Regulations* (2nd ed.). Cincinnati: Hanser Gardner Publications Inc.

Siracusa, V., Rocculi, P., Romani, S., & Rosa, M. D. (2008). Biodegradable polymers for food packaging: a review. *Trends in Food Science and Technology, 19*(12), 634-643.

Siripatrawan, U., & Noipha, S. (2012). Active film from chitosan incorporating green tea extract for shelf life extension of pork sausages. *Food Hydrocolloids, 27*(1), 102-108.

Siró, I., Fenyvesi, É., Szente, L., De Meulenaer, B., Devlieghere, F., Orgoványi, J., . . . Barta, J. (2006). Release of alpha-tocopherol from antioxidative low-density polyethylene film into fatty food simulant: influence of complexation in beta-cyclodextrin. *Food Additives and Contaminants, 23*(8), 845-853.

Smith, J. P., Hoshino, J., & Abe, Y. (1995). Active packaging in polymer films. In M. Rooney (Ed.), *Active Food Packaging* (pp. 143-172). Glasgow: Blackie Academic & Professional

Sonkaew, P., Sane, A., & Suppakul, P. (2012). Antioxidant activities of curcumin and ascorbyl dipalmitate nanoparticles and their activities after incorporation into cellulose-based packaging films. *Journal of Agricultural and Food Chemistry, 60*(21), 5388-5399.

Soto-Valdez, H., Auras, R., & Peralta, E. (2010). Fabrication of Poly(lactic acid) Films with Resveratrol and the Diffusion of Resveratrol into Ethanol. *Journal of Applied Polymer Science*. doi: 10.1002/app.33687

Soto-Valdez , H., Peralta, E., & Auras, R. (2008). *Poly(lactic acid) films added with resveratrol as active packaging with potential application in the food industry.* Paper presented at the 16th IAPRI World Conference on Packaging Bangkok, Thailand.

Stahl, W., & Sies, H. (2005). Bioactivity and protective effects of natural carotenoids. *Biochimica et Biophysica Acta (BBA)-Molecular Basis of Disease, 1740*(2), 101-107.

Sulaiman, R., Dolan, K. D., & Mishra, D. K. (2013). Simultaneous and sequential estimation of kinetic parameters in a starch viscosity model. *Journal of Food Engineering, 114*(3), 313-322.

Terao, J., & Matsushita, S. (1977). Products formed by photosensitized oxidation of unsaturated fatty acid esters. *Journal of the American Oil Chemists Society, 54*(6), 234-238.

Tian, F., Decker, E. A., & Goddard, J. M. (2012). Control of Lipid Oxidation by Nonmigratory Active Packaging Films Prepared by Photoinitiated Graft Polymerization. *Journal of Agricultural and Food Chemistry, 60*(31), 7710-7718.

Tuil, V. R., Fowler, P., Lawther, M., & Weber, C. J. (2000). Properties of bio-based packaging materials. In C. J. Weber (Ed.), *Bio-based Packaging Material for the Food Industry-Status and Perspectives* (pp. 13-44). Copenhagen: The Royal Veterinary and Agricultural University

Van Aardt, M., Duncan, S. E., Marcy, J. E., Long, T. E., O'Keefe, S. F., & Sims, S. R. (2007). Release of antioxidants from poly(lactide-co-glycolide) films into dry milk products and food simulating liquids. *International Journal of Food Science and Technology, 42*(11), 1327-1337. doi: 10.1111/j.1365-2621.2006.01329.x

Velasco, J., & Dobarganes, C. (2002). Oxidative stability of virgin olive oil. *European Journal of Lipid Science and Technology, 104*(9‐10), 661-676.

Vitrac, O., Mougharbel, A., & Feigenbaum, A. (2007). Interfacial mass transport properties which control the migration of packaging constituents into foodstuffs. *Journal of Food Engineering, 79*(3), 1048-1064.

Wang, S. Y., & Lin, H. S. (2000). Antioxidant activity in fruits and leaves of blackberry, raspberry, and strawberry varies with cultivar and developmental stage. *Journal of Agricultural and Food Chemistry, 48*(2), 140-146.

Watts, D. G. (1994). Estimating parameters in nonlinear rate equations. *The Canadian Journal of Chemical Engineering, 72*(4), 701-710.

Wessling, C., Nielsen, T., & Giacin, J. R. (2001). Antioxidant ability of BHT‐and α‐tocopherol‐impregnated LDPE film in packaging of oatmeal. *Journal of the Science of Food and Agriculture, 81*(2), 194-201.

Wessling, C., Nielsen, T., & Leufven, A. (2000). The influence of alpha-tocopherol concentration on the stability of linoleic acid and the properties of low-density polyethylene. *Packaging Technology and Science, 13*(1), 19-28.

Wessling, C., Nielsen, T., Leufvén, A., & Jägerstad, M. (1998). Mobility of α‐tocopherol and BHT in LDPE in contact with fatty food simulants. *Food Additives and Contaminants, 15*(6), 709-715. doi: 10.1080/02652039809374701

Whang, K., & Peng, I. (1988). Electron paramagnetic resonance studies of the effectiveness of myoglobin and its derivatives as photosensitizers in singlet oxygen generation. *Journal of Food Science, 53*(6), 1863-1865.

Xiao-e, L., Green, A. N., Haque, S. A., Mills, A., & Durrant, J. R. (2004). Light-driven oxygen scavenging by titania/polymer nanocomposite films. *Journal of Photochemistry and Photobiology A: Chemistry, 162*(2), 253-259.

Yang, W. T., & Min, D. B. (1994). *Chemistry of singlet oxygen oxidation of foods.* Paper presented at the ACS Symposium Series.

Yanidis, A. (1989). U.S. Patent No.: D. C. U. S. P. a. T. O. Washington.

Yanishlieva-Maslarova, N. V., Pokorny, J., Yanishlieva, N., & Gordon, M. (2001). Inhibiting oxidation *Antioxidants in Food: Practical Applications* (pp. 22-70): Woodhead Publishing Limited

Yoon, S., & Min, D. (1987). Roles of phospholipids in flavor stability of soybean oil. *Korean Journal of Food Science and Technology, 19*.

Zhu, X., Lee, D. S., & Yam, K. L. (2012). Release property and antioxidant effectiveness of tocopherol-incorporated LDPE/PP blend films. *Food Additives and Contaminants: Part A, 29*(3), 461-468.

Zhu, X., Schaich, K. M., Chen, X., & Yam, K. L. (2013). Antioxidant Effects of Sesamol Released from Polymeric Films on Lipid Oxidation in Linoleic Acid and Oat Cereal. *Packaging Technology and Science, 26*(1), 31-38. doi: 10.1002/pts.1964

Chapter 3

Poly(lactic acid) membrane incorporated with marigold flower extract (*Tagetes erecta*) intended for fatty-food application

3.0 Introduction

A functional membrane used in food packaging can be described as a membrane or packaging system that provides a continuous active protection to a food product during its shelf life by the incorporation of active substances (food additives) within the membrane. Some examples of active functional membranes are oxygen scavenger, ethylene absorber, and antimicrobial and antioxidant packaging (Rooney, 1995). Among those, the information and research related to antioxidant packaging are considerably limited (Camo, Beltrán, & Roncalés, 2008) in comparison with antimicrobial packaging, and include compounds such as α-tocopherol, ascorbic acid, butylated hyroxyanisole (BHA), and butylated hydroxytoluene (BHT), to name a few. Antioxidant packaging is the active system developed to control, for example, lipid oxidation in fatty food products (Wessling, Nielsen, Leufvén, & Jägerstad, 1998). Even though there is other existing technology like oxygen scavenger, that can help to retard oxidation, there are some concerns regarding their application. Oxygen scavenger is commonly incorporated into a packaging system in the form of a sachet. Its capacity to absorb oxygen is limited to 100 mL (Smith, Hoshino, & Abe, 1995), requiring multiple sachets for use with a product that is designed for a long shelf life, which is not practical and commercially acceptable (Robertson, 2006). It also requires additional materials, which consumers do not perceive as good management of resources, besides the accidental ingestion of these compounds could happen. Although their ingestion does not cause adverse health impacts (Floros, Dock, & Han, 1997), it can further deter consumer from buying these products.

The addition of antioxidants into food during processing seems to provide another solution for lipid oxidation. However, generally, the amount of antioxidants permitted for use in food products, singly or in combination, is limited to 0.02% by weight based on fat content of the food (Miková, 2001). This antioxidant amount may not be sufficient to protect the food due to possible loss of antioxidants during processing and may gradually diminish before the product (food) even reaches market shelves. The addition of relatively high concentration of certain antioxidants (*e.g.,* tocopherol and ascorbic acid) into food systems could also result in pro-oxidation reactions in lipids, subjecting products to a short shelf life (Balasubramanian, 2009).

Antioxidant functional membrane systems are a feasible alternative technology for such applications. This technology is beneficial for both the packaging and the packaged food because the incorporated antioxidants stabilize the polymer during processing and inhibit product's oxidation. However, most of the research conducted in this area focuses on non-renewable materials mainly made of polyolefins (Gavara, Lagarón, & Catalá, 2004; Wessling et al., 1998). Current consumer and environmental trends are increasing pressure to develop antioxidant functional membranes from bio-based polymers such as poly(lactic acid), PLA, poly (hydroxybutyrate-*co*-valerate), PHBV, soy-protein, starch-based polymers, to name a few, mainly due to driving factors such as price volatility of petroleum resources, replacement of non-renewable resources that may lead to the reduction of environmental burden and contribution towards a sustainable packaging industry with positive perceptions from consumers (Robertson, 2006).

Among those bio-based materials, PLA (Figure 3-1), a bioplastic produced from the ring-opening polymerization of lactide (Endres, Siebert, & Kaneva, 2007) has increasingly gained interest. PLA can be obtained from renewable resources, like corn (R. Auras, B. Harte, & S. Selke,

2004a), sugar beet and biomass residues. It is a transparent polymer, which is good for food packaging applications. It can be formed into a variety of containers, trays, membranes, and other types of packaging structures. PLA is biodegradable, compostable and recyclable (Auras et al., 2004a), and it has been approved by the Food Drug Administration (FDA) for intended use in fabricated materials for food-contact applications (Conn et al., 1995; Mutsuga, Kawamura, & Tanamoto, 2008; Ortiz-Vazquez, Shin, Soto-Valdez, & Auras, 2011; Soto-Valdez, 2011). PLA is comparable to poly(ethylene terepthalate), PET, and polystyrene, PS, in terms of its physical and mechanical properties. However, its lower barrier property to gases such as carbon dioxide (CO_2) and oxygen (O_2) than PET imposes limited function for food packaging application. For example, fatty food products packaged in PLA material would experience lipid oxidation as a result of its low oxygen barrier property. For this reason, the incorporation of antioxidants from natural sources like astaxanthin into the PLA membrane could be a potential enhancement for PLA's properties and a preservation tool for targeted food systems.

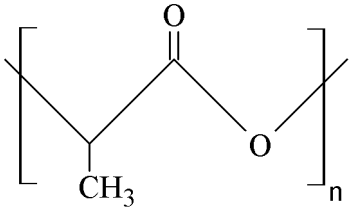

Figure 3-1 Poly(lactic acid), PLA chemical structure.

Astaxanthin is a keto-carotenoid that can be found naturally ranging from crustacean products and by-products, plants, and yeast (Figure 3-2). Astaxanthin is commonly fed to crustacean, salmonids, and farmed fish to enhance their color appearance as well as to provide healthy growth and reproduction systems (Higuera-Ciapara, Félix-Valenzuela, & Goycoolea, 2006). Astaxanthin has been reported to have more antioxidant capacity in comparison to lutein, β-carotene, and lycopene (Naguib, 2000). Quenching of singlet O_2 and inhibition of lipid oxidation

are the most noticeable antioxidant activities of astaxanthin. In this study, marigold flower extract was used directly as the astaxanthin source. The utilization of this extract was preferred due to its accessibility (abundance in nature) and economical value (cheaper than the commercial astaxanthin in the market). Besides, to the authors' best knowledge, there is scarce information about PLA membranes incorporated with carotenoid-based antioxidants preferably from natural sources. Thus, the objectives of this study were: *1)* to fabricate a bilayer bio-based membrane made of PLA and incorporated with marigold flower extract, *2)* to study the migration of astaxanthin from the fabricated membrane towards a fatty food simulant, *3)* to determine the thermal, molecular, surface, and barrier properties of the produced functional membrane, and *4)* to assess the effectiveness of the fabricated membrane in the oxidative stability of soybean oil during storage under accelerated condition.

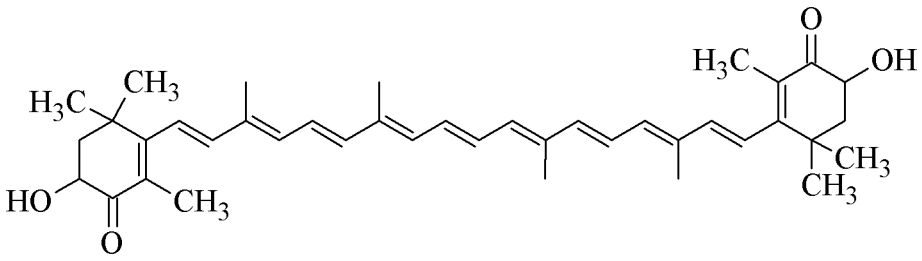

Figure 3-2 Astaxanthin chemical structure.

3.1 Materials and Methods

3.1.1 Materials

PLA 4043D (94% L-lactic acid content) was bought from PromaPlast (Monterrey, México) with a weight average molecular weight (M_w) of 120,980 ± 2,425 Da and number average molecular weight (M_n) of 81,375 ± 955 Da. Marigold flower extract (Florafil 93^{TM}) with an oil-

based consistency of fatty acid esters containing 0.7 wt.% astaxanthin in a water emulsion was donated by Vepinsa (Industrias Vepinsa, S.A. de C.V., Los Mochis, México). The amount of astaxanthin in the marigold flower extract was quantified by using a High Performance Liquid Chromatography (HPLC) equipment equipped with a UV-DAD detector at 474 nm. Astaxanthin standard was obtained from Alexis Biochemicals with a purity of 97 wt.% (San Diego, CA, USA). Additive-free soybean oil was provided by Industrializadora Oleofinos S.A. de C.V. (Zapopan, Jalisco, México). Glacial acetic acid A.C.S reagent grade, isooctane HPLC grade, sodium lauryl sulfate (SDS) and potato starch were purchased from J.T. Baker (New Jersey, USA). Sodium thiosulfate solution (0.1 N) was provided by Golden Bell (México City, México), and potassium iodide A.C.S reagent was obtained from Fermont (Monterrey, México). Ethanol 99.9% (HPLC grade), methanol (HPLC grade), and tert-methyl butyl ether (HPLC grade), water (HPLC grade), and formic acid (A.C.S reagent grade) were obtained from Sigma-Aldrich (MO, USA).

3.1.2 Fabrication of Antioxidant Functional Membrane

PLA resins were dried at 40 °C for 8 h in a vacuum oven and was extruded to produce bilayer membranes without (PLA), and with 2 nominal wt.% (PLA2M) marigold flower extract in the inner layer by using a pilot plant size blow-extrusion machine (Beutelespacher, México) at the Centro de Investigación en Alimentación y Desarrollo, A.C. campus, Hermosillo, México. The L/D ratio of both extruders is 26:1 with a screw diameter of 2 cm. Marigold flower extract in a form of liquid was mixed directly with the PLA resin on the weight basis and this mixture was then introduced into the hopper of the extruder 1 for membrane processing. The temperatures of extruder 1 for zone 1, 2, 3 and 4 were 140, 150, 150, and 150 °C, respectively, with an extruder velocity of 23 rpm. Meanwhile the temperatures set for extruder 2 were the same in all zones but

3, of which was 155 °C, with an extruder velocity of 35 rpm. The total thickness of the produced membrane was 4.1 ± 0.35 mil (104.1 ± 8.89 μm).

3.1.3 Quantification of Astaxanthin in the Fabricated Functional Membrane after Processing

Pieces of the membranes weighing approximately 0.5 g (0.25×0.25 cm) were extracted with methanol with constant stirring in the darkness at 40 °C for a designated period of time (24, 48, 72 h). A fourth extraction after 96 h was performed to ensure a complete extraction. The extracted aliquot (100 μL) was injected into a High Performance Liquid Chromatography (HPLC) equipment equipped with a UV-DAD detector at 474 nm. The antioxidants quantification was performed by using an YMC Carotenoid 3 μm 2.0x250 mm column (Waters Corporation, Milford, Massachusetts, US) with a gradient mode mobile phase of methanol (81%): tert-butyl methyl ether (15%): acidified water (4%), and a standard flow of 0.3 mL/min. An external calibration curve was prepared by using astaxanthin standard (97%) diluted with methanol in the range of 0.01 to 1 μg/mL with a $R^2 \geq 0.9905$. Limit of quantification (LOQ) was determined and was found to be <0.01 μg/mL.

3.1.4 Migration of Astaxanthin into A Food Simulant

Migration of astaxanthin was studied in an accordance with ASTM 4754-98 with some modification (ASTM, 2003a). The produced membranes were used to make a 4 x 4 cm pouch with the active layer outside. The pouch was then inserted into a 40 mL screw cap amber glass vial containing 30 mL of 95% ethanol (ETOH) (volume-area ratio of 0.9375 mL/cm^2) as fatty food simulant, and then was kept at 30 ± 2 °C, and 40 ± 0.5 °C for a designated period of time until the equilibrium was reached. The quantification of astaxanthin in the simulants was periodically

determined as previously described.

3.1.4.1 Mathematical Models for Migration Study

The migration process involves the transfer of substances (*e.g.*, antioxidant, monomer, etc.) originated from the packaging membrane into a packaged product, and the diffusion coefficient is used to describe this process based on the Fick's second law. The following assumptions were taken into account to describe the migration process of this study: 1) the antioxidant (astaxanthin) was distributed well and uniformly in the PLA antioxidant membrane layer; 2) the migration only occurs from one side of membrane layer that was in contact with the simulant; 3) the simulant was well-mixed; 4) the migration process was only affected by the temperature where the partition coefficient ($K_{p,f}$) and diffusion coefficient (D) were constants during experimental period; and 5) the interaction between the PLA membrane and the simulant was negligible. The analytical solution for a finite volume of food simulant and negligible mass transfer coefficient for the membrane thickness of 2L can be described as follow:

$$\frac{M_t}{M_\infty} = 1 - \sum_{n=1}^{\infty} \frac{2\alpha(1+\alpha)}{1+\alpha+\alpha^2 q_n^2} exp\left[-\frac{Dq_n^2 t}{L^2}\right] \quad \text{(Eq.3-1)}$$

where M_t is the concentration of migrant migrating into the food simulant at time t; M_∞ is the concentration of the migrant migrating into food simulant at equilibrium; q_n^2 is the non-zero positive roots of tan $q_n = -\alpha q_n$ where $\alpha = \frac{V_f}{K_{p,f} V_p}$; V_f is the volume of food; V_p is the volume of membrane; $K_{p,f}$ is the partition coefficient where $K_{p,f} = \frac{C_{p,\infty}}{C_{f,\infty}}$ where $C_{p,\infty}$ is the concentration of the migrant in the membrane at equilibrium; and $C_{f,\infty}$ is the concentration of migrant in the food simulant at equilibrium. D is the diffusion coefficient of the migrant; L is the thickness of the

membrane containing the antioxidant (Baner, 2000; Crank, 1979; De Meulenaer, 2009; Hamdani, Feigenbaum, & Vergnaud, 1997).

In a case where the food simulant is considered to have a larger volume than the polymer resulting in negligible mass transfer coefficient for the polymer thickness of 2L, and $\alpha \gg 1$ (when $V_f >> V_p$ and/or $K_{p,f} <1$), the following simplified solution can be applied to determine the diffusion coefficient of the Fick's second law (D):

$$\frac{M_t}{M_\infty} = 1 - \frac{8}{\pi^2}\sum_{n=1}^{\infty}\frac{1}{(2n+1)^2} exp\left[-\frac{(2n+1)^2}{4L^2} D\pi^2 t\right] \quad \text{(Eq. 3-2)}$$

MATLAB R2011b (MathWorks, Natick, MA, USA) was utilized to solve for equations 1 & 2 for the two parameters, D and M_∞, by using the non-linear regression function (Colín-Chávez, Soto-Valdez, Peralta, Lizardi-Mendoza, & Balandrán-Quintana, 2012; Dhoot, Auras, Rubino, Dolan, & Soto-Valdez, 2009; Iñiguez-Franco et al., 2012).

3.1.5 Thermal Properties

The glass transition temperature (T_g), cold-crystallization-temperature (T_{cc}), melting temperature (T_m), enthalpies of cold crystallization (ΔH_{cc}) and melting (ΔH_m), and the degree of crystallinity (X_c) of the produced functional membranes were characterized in accordance with ASTM 3418-03 (ASTM, 2003b) by using a differential scanning calorimeter (DSC) Q100 (New Castle, DE). Samples of about 6 – 8 mg were heated up from -10 to 200 °C at 10 °C/min with a N_2 flow of 50 mL/min with heat-cool-heat cycle. The data obtained was then analyzed by using the Thermal Analysis Universal 2000 version 4.5A software. The degree of crystallinity (X_c) of PLA and PLA2M was calculated as follow:

$$\%\ \text{Crystallinity},\ X_c = \frac{\Delta H_m - \Delta H_{cc}}{\Delta H_f\,(1-x)} \times\ 100 \quad \text{(Eq. 3-3)}$$

where ΔH_f *= heat of fusion of 100% crystalline sample (PLA= 93.7 J/g); x is the amount of antioxidant in the membrane.

The decomposition temperature (T_d) of the fabricated samples (approximately 6 - 10 mg) was determined by using a thermogravimetric analyzer (TGA Q50, TA Instruments, New Castle, DE). Temperature was set to start at 0 °C and heated up to 700 °C with a rate of 10 °C/min in a presence of air of a 60 mL/min flow rate to simulate oxidation condition. The analysis was carried out in accordance with ASTM E 1131-08 (ASTM, 2008).

3.1.6 Number Average Molecular Weight (M_n) and Weight Average Molecular Weight (M_w)

Fabricated samples of about 20 mg were weighted and transferred into a 10 mL volumetric flask. These samples were then dissolved with tetrahydrofuran (THF). The solvent containing the dissolved sample was then filtered through polytetrafluoroethylene (PTFE) filter membrane, and the filtrate was then transferred into a 2 mL glass vial with a PTFE septum. Then, M_n, M_w and the polydispersity index (PI) were determined by using a Water Gel Permeation Chromatography (GPC) (Waters 1515, Waters, Milford MA, USA) equipped with a Refractive Index detector (Waters 2414) with a flow rate of 1 mL/min. The columns used were HR Styragel® HR4, HR3, HR2 (300 mm x 7.8 mm (I.D)) with a temperature of 35 °C. The universal calibration curve (R^2=0.9983) was prepared by using a polystyrene standard with a range of molecular weights of 1.20 x 10^3 to 3.64 x 10^6 Da. The Mark-Houwink-Sakurada equation ($[\eta] = KM^{\alpha}$) was employed with α=0.704, and K=0.00164 mL/g to find the correlation between eluted volume of intrinsic viscosity of polymer and the absolute M_w with THF as a particular solvent.

3.1.7 Scanning Electron Microscopy (SEM)

PLA and PLA2M were investigated for their corresponding surface changes before and after being in contact with 95% ETOH at 30 and 40 °C for 24 and 3 d, respectively by using a Scanning Electron Microscope (SEM), model JEOL JSM 6610LV (JEOL Inc., MA, USA) with an accelerating voltage of 10keV. Samples were dried prior to analysis, and were coated with gold sputter coater by an EMSCOPE SC500 Sputter Coater (Kent, Britain).

3.1.8 Oxygen (O_2), Water Vapor, and Carbon Dioxide (CO_2) Barrier Properties

The sample for each barrier test was prepared with a masking aluminum to obtain the exposure area of 3.14 cm^2. *O_2 permeability* was determined using an Illinois Oxygen Permeation Analyzer 8001 (Illinois Instruments Inc., Johnsburg, IL) in accordance with ASTM D3985-05 (ASTM, 2005a). The testing temperature was 23 °C, 0% relative humidity (RH), and 21% permeant concentration with a carrier gas of 2% H_2: 98% N_2. *Water vapor permeability* (WVP) of the sample was performed in accordance with ASTM F1249-06 by using a MoCON Permatran W3/33 (MOCON Inc., Minneapolis, MN) (ASTM, 2006). The temperature and RH applied during this test were 38.7 °C and 100%, respectively, with N_2 as a carrier gas. *Carbon dioxide (CO_2) permeability* was done in accordance to ASTM F2476-05 by using a MOCON Permatran 4/41 Module C (MOCON Inc., Minneapolis, MN) (ASTM, 2005b). The testing conditions were 23 °C, 0% RH, and a permeant concentration of 100%. N_2 was used as a carrier gas.

All tests were run continuously until steady state was achieved with less than 5% variation for at least the last 10 data points. Three replicates were run per sample. The gases and water vapor permeabilities were calculated as follow:

$$\text{Gases and water permeability} = \frac{TR \times l}{A \times t \times p} \qquad \text{(Eq. 3-4)}$$

where *TR*= Transmission rate of each gas or vapor (kg); *l*= sample thickness (m); *A*= area of exposure (m^2); *t*=time (s); *p*=partial pressure (Pa).

3.1.9 Optical Properties

The light transmission of the PLA and PLA2M was performed by using a Perkin-Elmer Lambda 25 UV-Vis spectrophotometer (Waltham, MA, USA) with an integrating reflectance spectroscopy accessory (RSA-E-20, Labsphere, North Sulton, NH, USA). The measurements were carried out at a wavelength range of 200 to 800 nm in transmittance (%) mode with a rate of 240 nm/min. Samples were measured in triplicate.

Color measurements of PLA and PLA2M was done by a LabScan XE (HunterLab, Reston, VA, USA) and the *L**, *a**, *b** values were analyzed by Easymatch QC version 3.8. Samples were measured in triplicate. The ΔE value was calculated to measure the color differences between samples using Eq. 5:

$$\Delta E = \sqrt{\Delta L^2 + \Delta a^2 + \Delta b^2} \quad \text{(Eq. 3-5)}$$

where $\Delta L = L_{PLA2M} - L_{PLA}$, $\Delta a = a_{PLA2M} - a_{PLA}$, and $\Delta b = b_{PLA2M} - b_{PLA}$.

3.1.10 Fourier Transform Infrared Spectrophotometer (FTIR)

Fabricated membranes were scanned to assess their chemical structural properties by using a Fourier transform infrared spectrophotometer (Shimadzu IR Prestige-21, Shimadzu Scientific Instruments, Columbia, MD) with an attachment of attenuated total reflectance (ATR) set from 4000 to 650 cm^{-1} wavenumber with 40 scans at 4 cm^{-1}. The main and additional functional group absorption bands were identified and observed for any optical changes.

3.1.11 Oxidative Stability of Soybean Oil

Sample preparation: Deodorized soybean oil was added into 40 mL glass bottles (control) and pouches made of those fabricated membranes (6 x 4 cm) in the quantity of 15 mL for each package. Pouches formed resulting in a total contact area of 48 cm^2, in turns, volume-area ratio of 0.3125 mL/cm^2. These pouches were then kept at 30 ± 2 °C with exposure to fluorescence light (900-1000 lux (Luxometer SP 840020, Neurtek Instruments, Guizpucoa, Spain)) for 25 days of storage. The samples were analyzed for peroxide values (PV) at day 0, 3, 5, 7, 10, 15, and 25. While performing the test, the pouches were left sat still and the measurement was performed in triplicate.

Peroxide values (PV): Determination of peroxide values was conducted in accordance with the American Oils Chemists' Society (AOCS) official methods Cd-8b-90: Peroxide value acetic acid: isooctane method-Reapproved 2009 (AOCS, 2009). Approximately, 2.50 ± 0.01 g of each sample was weighed and kept under refrigerated condition until analyzed. The sample was first dissolved with 50 mL acetic acid: isooctane (3:2 (v/v)). A 0.5 mL of potassium iodide solution was added into the sample-acetic acid: isooctane solution and was continuously shaken for exactly 1 min, then 30 mL of distilled water was immediately added. This solution was then titrated gradually with 0.01 M sodium thiosulfate with constant and vigorous agitation until the color of the solution faded to light yellow. This solution was then added with 0.5 mL of 10% sodium dodecyl sulphate SDS (w/v) followed by 0.5 mL of starch indicator solution before further titration. When close to the end point, drops of the thiosulfate solution were added until the dark brown color just disappeared. The volume of thiosulfate solution used for each titration was then recorded for *PV* calculation. A blank determination of the reagents was also conducted in each

analyzed day. *PV* for each sample was expressed in milliequivalents peroxide/1000 g test portion unit and was calculated as follows:

$$PV = \frac{\text{(S-B)}\times\text{M}\times 1000}{\text{mass of test portion, g}} \quad \text{(Eq. 3-6)}$$

where *S* is the volume of titrant of test portion (mL); *B* is the volume of titrant of blank (mL); and *M* is the molarity of sodium thiosulfate solution.

3.2 Statistical Analysis

The data was analyzed by using one-way analysis of variance (ANOVA), and post-hoc pairwise comparisons were conducted by using Tukey-Kramer test with 95% level of confidence (α=0.05). All statistical models were fitted using the MIXED procedure of the statistical software SAS (Version 9.1, SAS Institute Inc., Cary, NC, US).

3.3 Results and Discussions

3.3.1 Quantification of astaxanthin in the fabricated membrane after processing

PLA2M originally contained 1.49 wt.% extract. From the extraction, it was found that fabricated PLA2M membrane had retained only 10.07 ± 2.58 μg/g of astaxanthin after processing, losing 82% due to processing. Antioxidant loss during processing was expected due to the nature of astaxanthin which is susceptible towards degradation with a decomposition temperature of approximately 200 °C as reported by Guo, Jones, & Ulrich (2010) (Guo, Jones, & Ulrich, 2010), and measured by TGA (Figure not shown). Even so, astaxanthin in oil-based extract was reported to have a considerable stability at room temperature (Rao, Sarada, & Ravishankar, 2007). Therefore, it can be expected that astaxanthin membrane are stable during typical packaging membrane storage conditions. Other reported studies have also shown that it is not uncommon to

lose antioxidant during processing. Butylated hydroxytoluene (BHT) incorporated into low density poly(ethylene), LDPE experienced losses from as low as 1.5% up to 58% (Galindo-Arcega, 2004; Soto-Cantú et al., 2008; Wessling et al., 1998). Lopez-de-Dicastillo et al. (2010) reported that 1 and 5 wt.% quercetin added into ethylene vinyl alcohol, EVOH, polymer experienced a loss of 19.9, and 24.4%, respectively, as well as 0.5, and 2 wt.% catechin added to that of EVOH had lost 32.9, and 33.2%, respectively (López-de-Dicastillo, Alonso, Catalá, Gavara, & Hernández-Muñoz, 2010). Losses of antioxidants such α-tocopherol, resveratrol, catechin, and epicatechin added to PLA has been reported in the range of 15 to 30% during processing. These losses were function of the extrusion process, processing temperature, residence time of PLA in the extruder, and the concentration of the antioxidants used (Iñiguez-Franco et al., 2012; Manzanarez-López, Soto-Valdez, Auras, & Peralta, 2011; Soto-Valdez, Auras, & Peralta, 2010). Colín-Chávez et al. (2012) used marigold flower extract as an antioxidant in LDPE, and co-extruded LDPE/HDPE membranes processed at 130, and 150 °C (temperature at which the molten polymer had entered the die), respectively, and they reported approximately 63 - 79% losses of astaxanthin with significant losses for the coextruded LDPE/HDPE than that of monolayer LDPE due to the higher processing temperature (Colín-Chávez et al., 2012).

Anderson & Sunderland (2002) reported that astaxanthin have a tendency to degrade in the presence of moisture during processing of extruded fish feed (Anderson & Sunderland, 2002). The amount of water content in PLA was below 0.02%, of which it could be speculated that during polymer processing the surrounding moisture level might as well contribute towards the loss of astaxanthin. Antioxidants are utilized to protect polymer degradation as a result of oxidation during its processing (Al-Malaika, Goodwin, Issenhuth, & Burdick, 1999; Byun, Kim, & Whiteside,

2010; Wessling et al., 1998). However, in this case, the loss of astaxanthin during processing could not be accounted for its mechanism to protect PLA from oxidation.

3.3.2 Migration of Astaxanthin into A Food Simulant (95% ETOH)

The migration of astaxanthin into 95% ETOH at both 30 and 40 °C followed the second Fick's law of diffusion (Figure 3-3). The partition coefficient, $K_{p,f}$ was calculated based on the ratio of the concentration of astaxanthin left in the PLA and the concentration of the astaxanthin migrated into 95% ETOH at equilibrium. The $K_{p,f}$ were found to be 61.75 and 18.7 at 30 and 40 °C, respectively (Table 3-1). A reduction of $K_{p,f}$ with temperature was expected since the solubility of the antioxidant in the food simulant increases as the temperature increases (Brandsch, Mercea, Rüter, Tosa, & Piringer, 2002).

Astaxanthin was released gradually into 95% ETOH before finally reached equilibrium at 8 d at 30 °C. Meanwhile, the release rate of astaxanthin at 40 °C reached equilibrium at 3 d (Figure 3-3). The diffusion coefficients were found to be $12.7 \pm 4.1 \times 10^{-11}$ cm^2/s (Figure 3-4a), and $22.8 \pm 4.7 \times 10^{-11}$ cm^2/s at 30 and 40 °C (Figure 3-4b), respectively. According to Van's Hoff Rule, an increment of temperature of 10 °C enhances the rate of diffusion by 2 to 3 fold. Likewise, as the rate of the diffusion increased, the intermolecular interaction between ethanol and PLA's polymeric chains was also enhanced (Lassalle & Ferreira, 2007; Peltonen, Koistinen, Karjalainen, Häkkinen, & Hirvonen, 2002). The sorption of ethanol by the polymer was conjectured to behave as a plasticizer by increasing the segmental mobility of the polymer chains (Mascheroni, Guillard, Nalin, Mora, & Piergiovanni, 2010), thus creating void that eventually diffuse the migrating compound as in this case astaxanthin into ethanol. Similar behavior was also reported by other studies with PLA-based functional membrane regarding the diffusivity of antioxidants like α-

tocopherol, resveratrol, catechin, epicatechin, and BHT into ethanol-based simulants (Iñiguez-Franco et al., 2012; Manzanarez-López et al., 2011; Ortiz-Vazquez et al., 2011; Soto-Valdez et al., 2010). However, it was found that the rate of astaxanthin released into 95% ETOH as a function of time was higher than the previously mentioned antioxidants at 30 °C (12.7×10^{-11} (astaxanthin) vs. 5.29×10^{-11} (α-tocopherol), 8.95×10^{-11} (BHT), $22.6\text{-}41.7 \times 10^{-11}$ (1-3% resveratrol), 13.1×10^{-11} (catechin), and 13.7×10^{-11} (epicatechin) cm^2/s). Meanwhile, at 40 °C, similar trend was also observed with the exception for the release of BHT that was higher than that of astaxanthin (22.8×10^{-11} (astaxanthin) vs. 38×10^{-11} (α-tocopherol), 190.4×10^{-11} (BHT), $85.1\text{-}82.6 \times 10^{-11}$ (1-3% resveratrol), 47.9×10^{-11} (catechin), and 51.2×10^{-11} (epicatechin) cm^2/s). In general, the diffusivity of BHT is expected to be fast due to its non-bulky structure with only one hydroxyl group as can be observed in the case of migration at 40 °C. Iñiguez-Franco et al. (2012) speculated that the presence of more number of hydroxyl group in the antioxidant structure may be the determinant factor that had caused the lower release rate of antioxidant into ethanol since more interaction could occur between PLA polymeric chains and the incorporated antioxidants. Since astaxanthin chemical structure contains two hydroxyl groups (Figure 3-2), it is expected to have higher release rate that that of resveratrol, catechin and epicatechin in which they consists of three and five hydroxyl groups, respectively. Despite both α-tocopherol and BHT consist of one hydroxyl group, the release rate of α-tocopherol was 4 to 5 magnitude lower than astaxanthin, which may be associated with its longer alkane chain with a methylated phenolic group.

On the other hand, the release of astaxanthin from monolayer LDPE and bilayer LDPE/HDPE was reported lower than the release of astaxanthin obtained in this study. Colín-Chávez et al. (2013) reported the D value of 7×10^{-11} cm^2/s of astaxanthin from monolayer LDPE membrane into ethanol at 30 °C. Meanwhile, a D value of 6×10^{-11} cm^2/s was reported for bilayer

LDPE/HDPE at 30 °C in the same study (Colín-Chávez, Soto-Valdez, Peralta, Lizardi-Mendoza, & Balandrán-Quintana, 2013). The large release in PLA and ethanol can be attributed to the modification of the membrane due the presence of ethanol, which disrupt the microstructure of PLA, and its further discussed in the next sections. In addition, it is worth mentioning that no degradation products of astaxanthin (*i.e.*, 9-*cis* and 13-*cis*) was detected during the migration test by HPLC.

Table 3-1 Migration data of produced functional membranes.

	Temperature (°C) ***	
	30	**40**
$K_{p,f}$*	61.75 ± 7.36[a]	18.7± 7.17[b]
α*	1.33 ± 0.15[a]	4.92 ± 2.36[b]
D × 10^{-11} (cm^2/s)**	12.7 ± 4.1[a]	22.8 ± 4.7[b]
D, Relative error	0.33	0.21
95% CI ×10^{-9}	0.04, 0.21	0.13, 0.32
$M_{inf/Predicted}$ × 10^{-8} (g Astaxanthin/ g ETOH) **	9.89 ± 0.64[a]	10.12 ± 0.63[b]
$M_{inf/Predicted,}$ Relative error	0.06	0.06
95%CI × 10^{-8}	8.61, 11.18	8.86, 11.38
$M_{inf/Experimental}$ × 10^{-8} (g Astaxanthin/ g ETOH)**	18.86 ± 2.35	52.16 ± 5.58[b]
RMSE × 10^{-8} (g Astaxanthin/ g ETOH)	2.19	1.43
Correlation coefficient, $\rho_{\beta_D \beta_{Minf}}$	0.53	0.76

*The values are reported as mean ± standard deviation.

** The values are reported as mean ± standard error.

*** Values in the same row with same alphabetic symbol are not statistically significantly different (p>0.05).

$M_{inf/Experimental}$= M_{total}-$M_{membrane\ extracted,inf}$; 95% CI is reported as asymptotic; RMSE= Root mean square error.

******** All measurements were performed in triplicate.

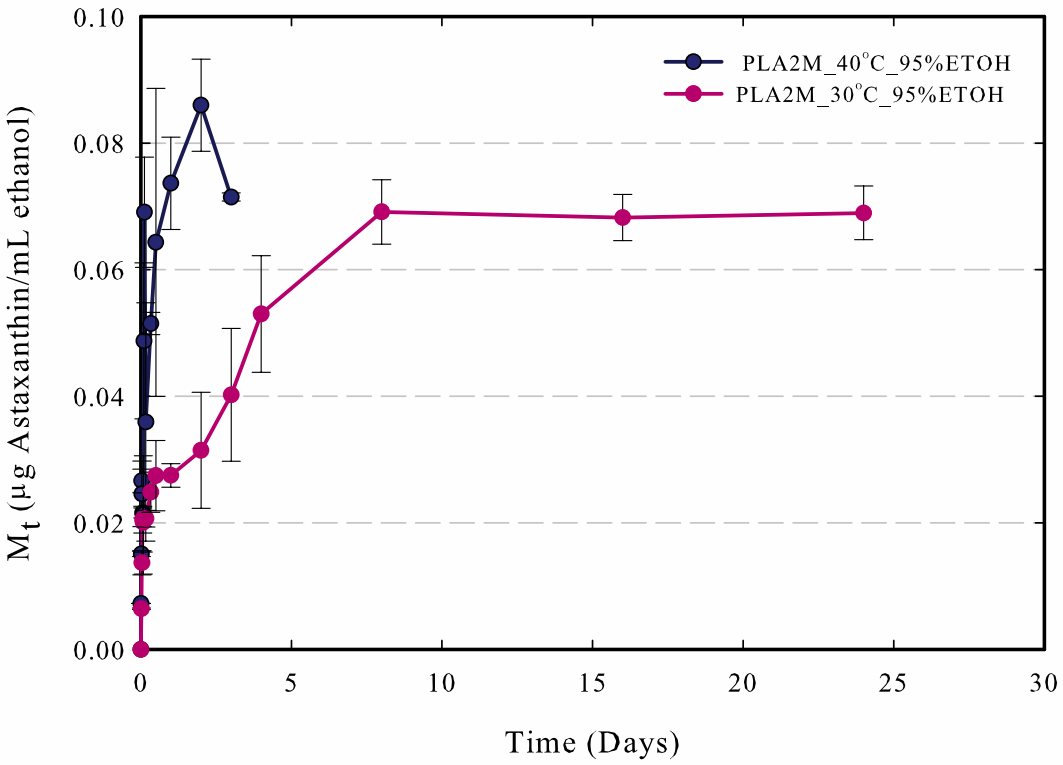

Figure 3-3 The concentration of astaxanthin migrated into 95% ETOH at 30 to 40 °C.

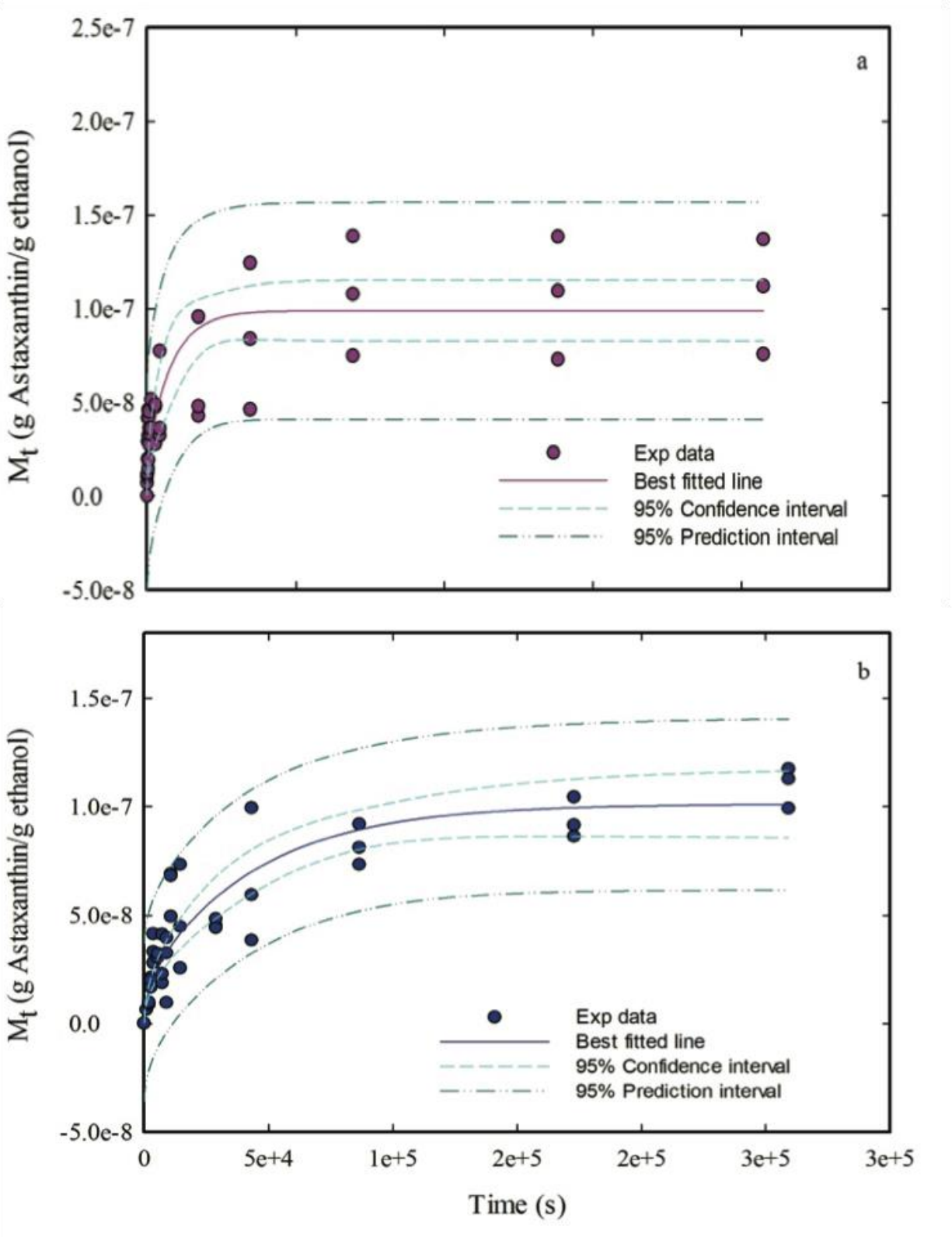

Figure 3-4 (a) Migration of astaxanthin into 95% ETOH at 30 °C and (b) 40 °C during storage.

3.3.3 Thermal Properties

Table 3-2 shows the T_g, T_m, and X_c between PLA and PLA2M. The addition of approximately 2 wt.% of marigold flower extract did not affect the T_g, T_m, and X_c. Similar observation was also reported by other studies (Manzanarez-López et al., 2011; Ortiz-Vazquez et al., 2011; Soto-Valdez et al., 2010). However, it is worth mentioning that a decrease of 1 °C in T_g was observed for all these systems. On the other hand, a slight and significant decrease in the T_g was reported for PLA-based membrane incorporated with either α-tocopherol, ascorbyl palmitate, BHT, or tert-butyl-hydroquinone (TBHQ) by other studies (Goncalves et al., 2012; Jamshidian, Tehrany, Imran, et al., 2012). These antioxidants were found responsible for a plasticization effect, thus resulted in the reduced T_g. A reduction of 3-5 °C was observed for PLA-based membrane added with both resveratrol and α-tocopherol when the antioxidants were introduced at a various combination of high concentration (1-4 wt.%) (Hwang et al., 2012)

The addition of no more than 2 wt.% of α-tocopherol, BHT, and TBHQ was reported to show no impact in the T_m of PLA-based membrane (Goncalves et al., 2012; Jamshidian, Tehrany, Imran, et al., 2012; Manzanarez-López et al., 2011; Ortiz-Vazquez et al., 2011), similar to this study. However, the incorporation of antioxidants (*i.e.*, α-tocopherol, BHT, TBHQ, and resveratrol) at a higher concentration (> 3 wt.%) was reported to induce lower T_m, which may possibly be due the greater plasticization effect (Goncalves et al., 2012; Hwang et al., 2012), as the antioxidants cause a hindrance in the formation of crystallites that resulted in less energy required for melting the crystallites. In addition, a study on the effect of different plasticizers (*i.e.*, glycerol, citrate ester, polyethylene glycol (PEG), PEG-monolaurate, and oligomeric lactic acid) on PLA found that the presence of those plastizers in the polymeric system did reduced the T_m of this polymer by 10-15 °C; however, the T_m reduction was not greatly affected by the plasticizer

concentration as it was observed in the T_g (Martin & Averous, 2001). No effect of marigold flower extract was also observed on the X_c of PLA2M. The difference effect of antioxidants on the X_c of PLA-based membrane was also explained in other studies (Goncalves et al., 2012; Hwang et al., 2012; Jamshidian, Tehrany, Cleymand, et al., 2012; Sawalha, Schroën, & Boom, 2010; Soto-Valdez et al., 2010).

Table 3-2 shows also detailed information about T_g, T_m, and $\%X_c$ of the PLA-based functional membranes before and after contact with 95% ETOH at 30 °C (24 d), and 40 °C (3 d). The T_g of PLA that was originally 57.8 °C reduced to 50.5 °C, and increased to 73.6 °C after being in contact with 95% ETOH at 30 and 40 °C, respectively. As for PLA2M, similar behavior was also demonstrated at both respective temperatures under similar condition. In terms of the T_m, it is worth noticing that two melting peaks appeared (Figure 3-5). This behavior was explained by Sato et al. (2012) from the differences type of crystalline formation due to solvent induced crystallization. This type of behavior was classified due to the degree of cloudiness produced by the solvent with 7-20% swelling. This type of behavior was observed and associated with PLA membrane that had been in contact with ethanol, methanol, 1-propanol, 2-propanol, butanol, and 3-methyl-1-butanol di-n-butylphthalate isopropyl ether (Sato, Gondo, Wada, Kanehashi, & Nagai, 2012). Even though two T_m was seen in this study, only the distinctive peak data was reported, and only slight changes were observed for both PLA and PLA2M that were in contact with 95% ETOH at 30, and 40 °C compared to that of counterpart membranes that were not in contact with 95%ETOH. For X_c, a significant increment was demonstrated comparing before and after both membranes had been in contact with 95% ETOH at both temperatures ($p<0.0001$); however, PLA2M exhibited significant increase in X_c than that of PLA ($p<0.0001$), confirming the solvent induced crystallization with ETOH. This effect can be clearly observed in Figure 3-5, of which the

cold crystallization diminished completely for both PLA and PLA2M after had been in contact with 95% ETOH. Similar phenomena was also observed by Chen et al. (2013), and was reported to be associated with the reduction of locally ordered structured as a result of hydrolytic degradation (Chen et al., 2013). It can also be seen that the presence of antioxidant did further induce the increment of X_c with the exposure to 95% ETOH at both temperatures. This circumstance could possibly be attributed to the presence of more -OH groups in the PLA2M membrane; thus introducing more intermolecular forces that consequently causing a greater increase in the X_c. This result has important regulatory implications for testing migration of fatty foods in PLA membranes using ETOH solution as simulant. Thus, a new simulant should be designed for testing migration in fatty foods for PLA membranes.

Both PLA and PLA2M exhibited no significant difference in their respective T_d ($p>0.05$). Some antioxidants like α-tocopherol and resveratrol showed significant enhancement in the thermal stability of PLA-based membrane, in which these antioxidants extended the temperature at which the mass loss of the sample can be observed (Hwang et al., 2012). However, an opposite behavior was observed for PLA-based membrane incorporated with BHT where the T_d of this membrane was reduced in comparison to the control PLA-based membrane (Ortiz-Vazquez et al., 2011). This phenomenon was reported to be as a result of the degradation product during processing (Ortiz-Vazquez et al., 2011).

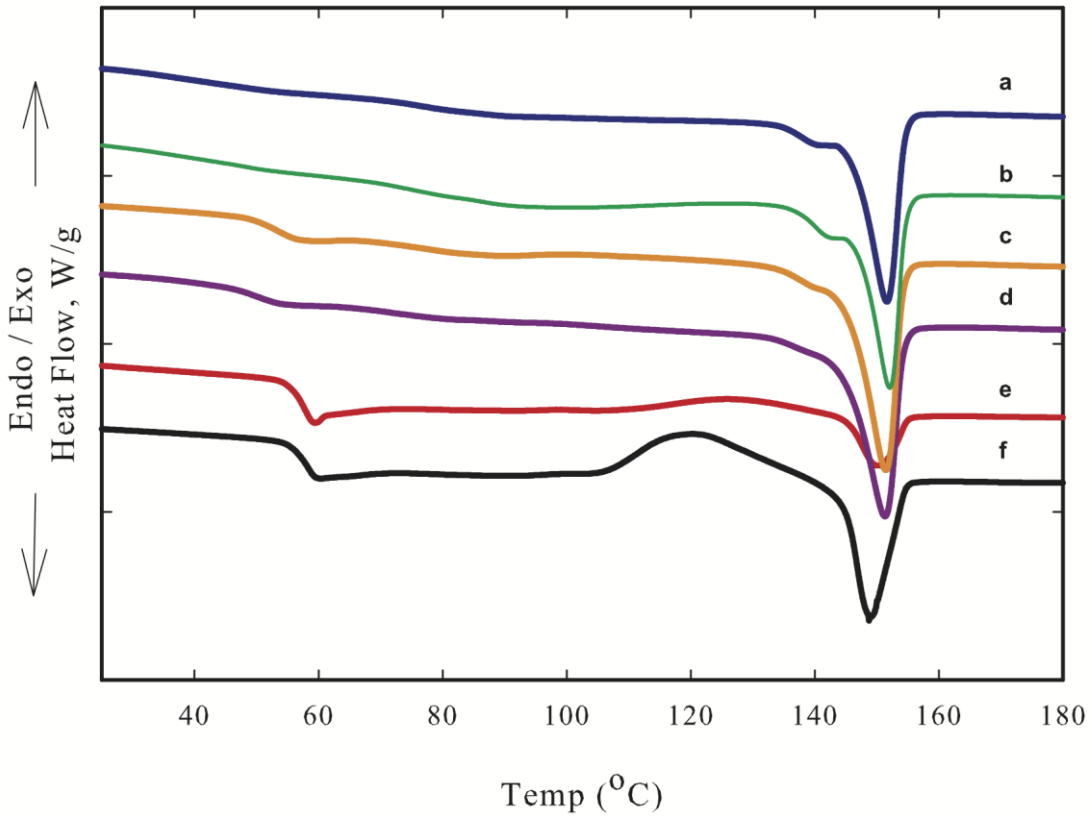

Figure 3-5 DSC thermogram of (a) PLA2M in contact with 95% ETOH at 40°C for 3 d; (b) PLA in contact with 95% ETOH at 40°C for 3 d; (c) PLA2M in contact with 95% ETOH at 30°C for 24 d; (d) PLA in contact with 95% ETOH at 30°C for 24 d; (e) PLA2M; and (f) PLA.

3.3.4 Number Average Molecular Weight (M_n), and Weight Average Molecular Weight (M_w)

In comparison with PLA resin, significant reduction in the M_n and M_w, was observed for both PLA and PLA2M of which could be attributed to the thermal, and possible hydrolytic degradation of PLA during processing ($p<0.0001$). Despite the fact that the PLA resin was truly dried prior to processing (moisture content: <0.02 wt.%), the presence of heat and residual moisture from the surrounding could reintroduce moisture during processing causing the chain scission of the polymer (Table 3-2). PLA2M experienced a slight decrease in its M_n and M_w than

that of PLA. The incorporation of the marigold flower extract seemed to induce the membrane degradation. It could be speculated that the presence of the extract containing astaxanthin enhanced the degradation of the PLA polymer chain via the 'backbiting' ester interchange reaction that occurred at the –OH chain ends. This phenomenon is a non-radical process that degrades the chain into a lactide molecule, an oligomeric ring, or acetaldehyde with carbon monoxide accordingly to the site in the backbone at which the reactions take place (Lim, Auras, & Rubino, 2008; McNeill & Leiper, 1985). Even though the occurrence of this phenomenon was reported at an excessive temperature (>270 °C) (McNeill & Leiper, 1985), and the maximum processing temperature used in this study was only at 155 °C, the presence of additional –OH groups from astaxanthin could be conjectured to cause the chain degradation that finally resulted in the decreased of M_w and M_n.

On the contrary, Ortiz-Vazquez et al. (2011) reported no significant impact on M_w and M_n of adding the pure antioxidant BHT in a PLA-based membrane (Ortiz-Vazquez et al., 2011). Meanwhile, Hwang et al. (2011) found that the M_w and M_n of PLA-based membrane incorporated with α-tocopherol and resveratrol increased gradually with increasing concentration of these antioxidants (*e.g.*, estimated relative change of 25%, and 11% of M_w, and M_n, respectively by comparison of 0% vs. 4% of α-tocopherol). This behavior was speculated to be due to the interaction that could have occurred between PLA, and antioxidant chains in the amorphous regions, thus increased the chain entanglements (Hwang et al., 2012). Physical crosslinking between PLA, and antioxidant chains was also conjectured as one of the reasons that resulted in the higher M_w and M_n (Hwang et al., 2012). The *PI* changed for PLA and PLA2M as it did for the studies by Ortiz-Vazquez et al. (2011) and Hwang et al. (2011) (Hwang et al., 2012; Ortiz-Vazquez et al., 2011).

Figure 3-6 shows molecular weight distribution of the fabricated functional membranes before and after had been in contact with 95% ETOH. It was observed that M_w of both PLA and PLA2M had reduced approximately by 67% and 69%, respectively (in comparison with their respective M_w after processing) after had been in contact with 95% ETOH at 30 and 40 °C during the experimental period ($p<0.0001$). The significant shift toward lower molecular weight for those membranes that had been in contact with 95% ETOH suggested the possibility of the chain scission phenomena. Meanwhile, M_n for both produced functional membranes indicated a decrease of approximately 69-73% under similar condition ($p<0.0001$). There was neither pronounced effect of the temperature seen, nor the contact time (Table 3-2).

In addition, it was observed that both PLA, and PLA2M had greater reduction in M_w compared to those of PLA-based membranes incorporated with antioxidants (*i.e.*, BHT, resveratrol, α-tocopherol, catechin, and epicatechin) after had been in contact with 95% ETOH at similarly reported temperatures (30 and 40 °C) (Iñiguez-Franco et al., 2012; Manzanarez-López et al., 2011; Ortiz-Vazquez et al., 2011; Soto-Valdez , Peralta, & Auras, 2008). In this study, it was found that the M_w of both membranes decrease by 3 orders of magnitude from its original M_w (after processing). In the other aforementioned studies, the decreased observed in the M_w of their membranes was not larger than 1 order of magnitude, regardless of the temperatures and contact times with ethanol. It could be speculated that the polymer processing method – bilayer blown extrusion - and the temperature conditions used in this study may be responsible for inducing these significant changes in the morphologies of the PLA surfaces. It can also be concluded that 95% ETOH is not a good food simulant for studying fatty foods migration in PLA membranes.

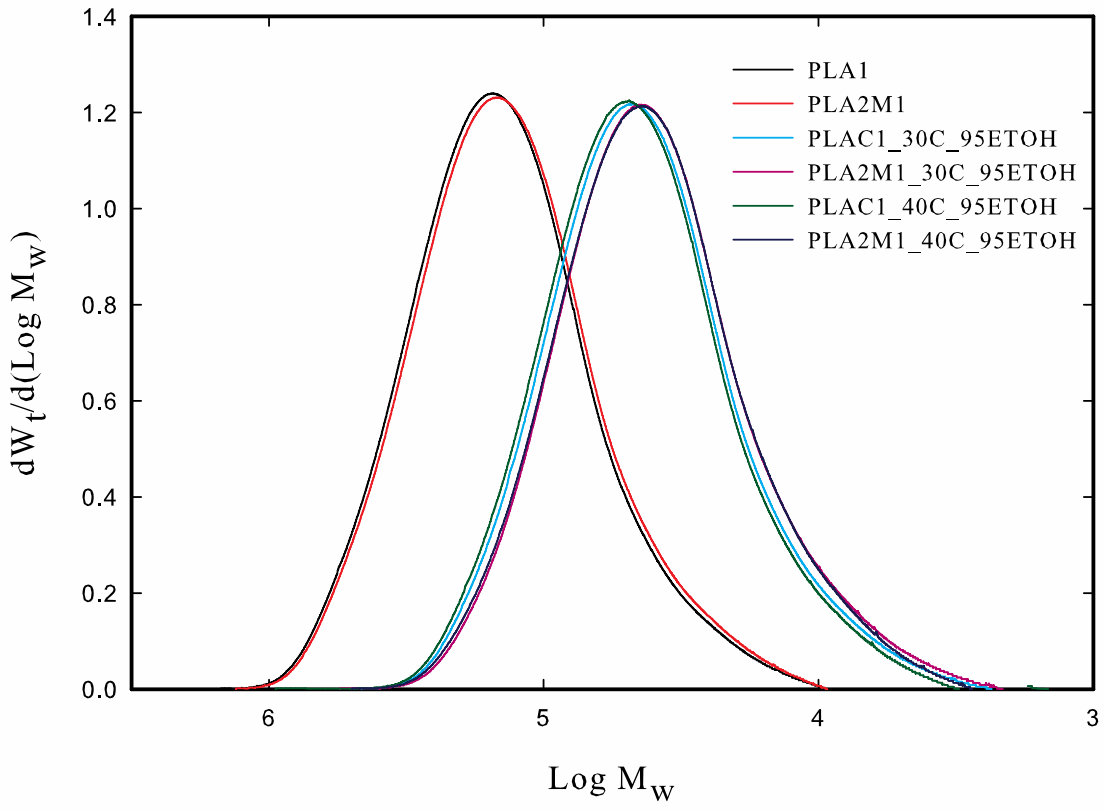

Figure 3-6 Molecular weight distributions of fabricated functional membranes PLA and PLA2M without and in contact with 95% ETOH at 30 and 40 °C for 24 and 3 d, respectively.

Table 3-2 Characterization of the fabricated functional membranes.

Properties	**After processing**		**After in contact with 95%ETOH 30 °C (24 d)**		**After in contact with 95% ETOH 40 °C (8 d)**	
Thermal	**PLA**	**PLA 2M**	**PLA**	**PLA 2M**	**PLA**	**PLA 2M**
T_g ,°C	56.8 ± 0.1^{a1}	56.9 ± 0.3^{a1}	50.5 ± 1.9^{a2}	51.7 ± 3.8^{a2}	73.6 ± 1.7^{a3}	75.5 ± 0.4^{a3}
T_m ,°C	151.05 ± 0.1^{a1}	150.5 ± 0.6^{a1}	$151.3 \pm 0.1^{a1,2}$	$151.5 \pm 0.5^{a1,2}$	152.1 ± 0.0^{a2}	151.8 ± 0.4^{a2}
X_c ,%	0.52 ± 0.3^{a1}	1.3 ± 0.4^{a1}	25.5 ± 0.7^{a2}	38.2 ± 1.5^{b2}	23.7 ± 0.8^{a2}	35.8 ± 1.02^{b2}
T_d ,°C	355.9 ± 0.4^{a}	354.7 ± 0.7^{a}	ND	ND	ND	ND
Molecular weight						
M_w , kDa	113.0 ± 0.5^{a1}	110.0 ± 1.6^{b1}	36.1 ± 0.1^{a2}	34.5 ± 0.1^{a2}	36.3 ± 0.9^{a2}	34.1 ± 1.1^{a2}
M_n , kDa	73.8 ± 1.0^{a1}	71.4 ± 1.7^{a1}	22.3 ± 0.5^{a2}	21.0 ± 0.7^{a2}	22.1 ± 2.2^{a2}	19.1 ± 2.7^{a2}
M_z , kDa	143.0 ± 0.3^{a1}	141.0 ± 1.2^{b1}	46.8 ± 0.1^{a2}	45.5 ± 0.1^{b2}	47.1 ± 0.3^{a3}	45.7 ± 0.5^{a2}
PI	1.53 ± 0.02^{a1}	1.55 ± 0.02^{a1}	1.62 ± 0.03^{a1}	$1.64 \pm 0.05^{a2,3}$	1.65 ± 0.13^{a1}	1.81 ± 0.21^{b3}
Barrier ***, kg.m/m^2.s.Pa						
Water vapor $\times 10^{-15}$	26.4 ± 6.8^{a}	20.7 ± 6.8^{b}	ND	ND	ND	ND
$O_2 \times 10^{-17}$	55.6 ± 53.6^{a}	45.9 ± 7.1^{a}	ND	ND	ND	ND
CO_2 x10^{-17}	4.7 ± 0.8	$> 4.7 \pm 0.8$	ND	ND	ND	ND

* Values are reported as mean ± standard deviation.

** Values with same alphabetic, and numerical symbol are not statistically significantly different ($p>0.05$).

Table 3-2 (Cont'd)

Alphabetic symbol indicates comparison between samples within the corresponding properties.

Numerical symbol indicates comparison between the corresponding properties within samples.

*** Water was measured at 37.8 °C, 100% RH, and O_2, CO_2 were measured at 23 °C, 0% RH. The CO_2 sensitivity limit for MoCON Permatran 4/41 Module C is 1.14×10^{-5} kg/ m^2.s based on standard masking area size (PLA= 4.39×10^{-8} kg/ m^2.s with smaller masking area size).

******** All measurements were performed in triplicate.

Note: PLA resin M_w= 121.8 ± 1.0 kDa; M_n= 81.2 ± 1.1kDa; M_z= 152.6 ± 0.7 kDa; PI= 1.5 ± 0.01

3.3.5 Scanning Electron Microscopy (SEM)

The SEM micrograph indicates initial homogenous surfaces for both PLA and PLA2M (Figure 3-7a and b). Both PLA and PLA2M showed a modified fracture-like morphology on their surface after being in contact with 95% ETOH at 30 °C (24 d) (Figure 3-7c and d). However, at 40 °C (3 d), more noticeable effect of 95% ETOH was observed on the surface of both membranes in terms of roughness and fracture-like effects compared to that of 30 °C (Figure 3-7e and f). These morphological changes were anticipated due to the strong chemical interaction between simulant and membrane, especially at 40 °C. Similar looking surfaces classified as rib-like structures were reported by Chen et al. (2013). These structures were found to be correlated with hydrolytic degradation that resulted in the formation of the α'-form lamellar structure. Chen et al. (2013) found more distinguishable pattern than those shown in this study since samples were subjected to an extreme condition of 60 °C, 40 h in sodium hydroxide (NaOH) solution (Chen et al., 2013). In addition, shish kebab like structure was also reported to be associated with the effect of ethanol-richer solvent mixtures on PLA surface (Gao et al., 2012). This type of structure is more of a resemblance of the structure found in this study and it could be justified that 95% ETOH greatly induced the morphological properties of the membranes by means of thermally assisted solvent degradation. This finding was also in conjunction with the data obtained in DSC (Figure 3-5), and molecular weight analysis (Figure 3-6), in which the absences of amorphous regions, and the reduction of molecular weight, respectively, were observed.

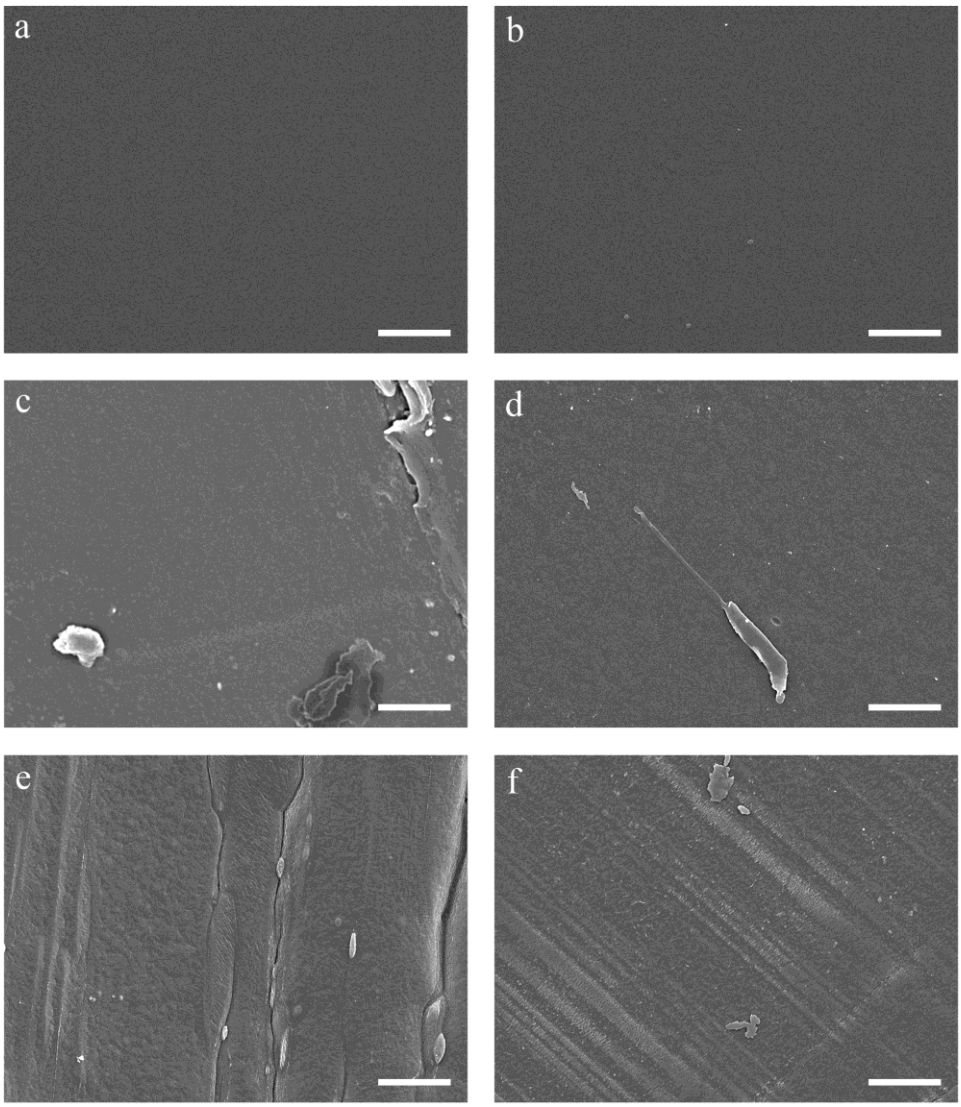

Figure 3-7 Top SEM surface section micrograph (a) PLA; (b) PLA2M; (c) PLA in contact with 95% ETOH at 30 °C for 24 d; (d) PLA2M in contact with 95% ETOH at 30 °C for 24 d; (e) PLA in contact with 95% ETOH at 40 °C for 3 d; (f) PLA2M in contact with 95% ETOH at 40 °C for 3 d. Bar=10 μm.

3.3.6 Barrier properties

3.3.6.1 Oxygen (O_2)

In general, antioxidant may introduce a plasticization effect into membrane, thus changing membrane crystallinity, increasing the amount of free volume, hence resulted in the increase of gas permeability. However, in this study the incorporation of marigold flower extract did not affect the X_c of the membrane, and this finding further confirming the non-significant different obtained in the O_2 permeability between PLA and PLA2M ($55.6 \pm 53.6 \times 10^{-17}$ vs. $45.9 \pm 7.1 \times 10^{-17}$ kg-m/m^2-Pa-s, respectively) (p=0.5784) (Table 3-2). Similarly, Ortiz-Vazquez et al. (2011) also reported that the addition of 1.5 wt.% BHT did not significantly affect the O_2 permeability of the PLA-based membrane at the same testing conditions (23 °C, 0 %RH) (Ortiz-Vazquez et al., 2011). Meanwhile, the O_2 permeability of PLA-based membranes added with 4 and 10 wt.% TBHQ were significantly lower than that of PLA-based membrane at 20 °C (Goncalves et al., 2012). However, of the same PLA-based membranes but with 2 wt.% α-tocopherol, and 4 wt.% BHT, no significant reduction were observed in their O_2 permeability. Gonçalves et al., (2012) reported that due to TBHQ lower molar volume (166.1 cm^3/mol) compared to α-tocopherol (453.4 cm^3/mol) and BHT (244.3 cm^3/mol), increase of free spaces are anticipated for the orientation of polymer chains, thus reducing the gas permeability of the membranes. This decreased was also attributed to the fast diffusivity of gas (Goncalves et al., 2012). Since astaxanthin has a molar volume of 557.0 cm^3/mol, the finding in this study matched the aforementioned explanation.

3.3.6.2 Water Vapor (WV)

WV permeability for both PLA and PLA2M were 26.4 ($\pm$ 6.79) $\times 10^{-15}$, and 20.7 ($\pm$ 6.80) $\times 10^{-15}$ kg.m/m^2.s.Pa, respectively at 37.8 °C and 100% RH (Table 3-2). These values were

comparable and of the same order of magnitude to those reported for PLA-based membrane with and without antioxidants. WVP of PLA-based membrane was widely reported and ranged from approximately 1.4 to 15 × 10^{-15} kg.m/m^2.s.Pa at 37-38 °C, 90-100% RH (Auras et al., 2004a; R. Auras, B. Harte, & S. E. M. Selke, 2004b; Jamshidian, Tehrany, Cleymand, et al., 2012; Jamshidian, Tehrany, Imran, et al., 2012; Ortiz-Vazquez et al., 2011). Meanwhile, PLA-based membrane with BHT were reported to have WVP between 1.2-2.5 × 10^{-15} kg.m/m^2.s.Pa, and PLA-based membranes with other antioxidants *i.e.*, α-tocopherol, ascorbyl palmitate, butylated hydroxyl-anisole (BHA), propyl gallate, TBHQ had WVP ranged from approximately 1.2-3.0 × 10^{-15} kg.m/m^2.s.Pa under the same condition (Jamshidian, Tehrany, Cleymand, et al., 2012; Jamshidian, Tehrany, Imran, et al., 2012; Ortiz-Vazquez et al., 2011). Other study performed at 23 °C, 45% RH, reported a value of 19.9 × 10^{-15} kg.m/m^2.s.Pa for PLA, and a range of value from 12-20 × 10^{-15} kg.m/m^2.s.Pa for PLA-based membranes added with α-tocopherol, BHT, and TBHQ at three different concentrations (2, 4, 10 wt.%) (Goncalves et al., 2012).

The incorporation of marigold flower extract was found to significantly reduce WVP of PLA, which could be attributed to the hydrophobic nature of this extract ($p=0.03$). On the contrary, no significant differences were observed for WVP of PLA-based membranes with α-tocopherol, BHT, BHA, propyl gallate (PG), TBHQ, and ascorbyl palmitate (Goncalves et al., 2012; Jamshidian, Tehrany, Cleymand, et al., 2012; Jamshidian, Tehrany, Imran, et al., 2012; Ortiz-Vazquez et al., 2011) except when the antioxidants were added at a concentration >2 wt.%. However, the addition of BHT or TBHQ at a nominal concentration >2 wt.% did not show any significant decrease in WVP of the PLA-based membranes (Goncalves et al., 2012). The reason behind this difference could be due to the chemical structure of α-tocopherol that contains a long hydrophobic side chain, thus possess greater hydrophobicity than that of BHT, and TBHQ.

Moreover, it can be observed that the addition of 2 wt.% marigold flower extract containing astaxanthin resulted in approximately 21 % decrease in WVP of PLA, while the addition of 2 wt.% α-tocopherol did not change WVP of the same membrane. The significant decreased of WVP of PLA-based membrane in this study ($p=0.03$) could be as well due to the presence of longer hydrophobic side chain possess by astaxanthin.

3.3.6.3 Carbon dioxide (CO_2)

CO_2 permeability of PLA was found to be 4.7 (± 0.77) × 10^{-17} kg.m/m^2.s.Pa at 23°C, 0% RH (Table 3-2). This value was closed to the value reported by Auras et al. (2004b) (1.99 (± 0.06) × 10^{-17} kg.m/m^2.s.Pa at 25°C, 0% RH) (Auras et al., 2004a). Gonçalves et al. (2012) also did report a value within this range (Goncalves et al., 2012). Meanwhile, the permeability value of PLA2M can only be assumed to be higher than the PLA since it was not possible to obtain the value due to the machine limitation. Gonçalves et al. (2012) also did report a higher permeability value for those PLA membranes added with 4 wt.% α-tocopherol and BHT, even though the opposite effect was demonstrated for PLA membranes added with 4 wt.% TBHQ. They speculated that the increment in the permeability value of PLA membranes added with α-tocopherol and BHT was due to this antioxidant higher molar volume compared to that of TBHQ (Goncalves et al., 2012). Therefore, it was reasonable that PLA2M showed higher permeability in comparison to that of PLA as had been described before.

3.3.7 Optical Properties

PLA and PLA2M were visually transparency with the latter pose a pale orange-like color. PLA and PLA2M did show slightly lower light transmission from 250 to 480 nm. PLA2M

indicated absorption behavior within the aforementioned region due to the chromophore compounds (conjugated double bonds) in the astaxanthin structure (Figure not shown). The CIELAB color parameters for PLA were *a*=-1.0 ± 0.0, *b*= 0.9 ± 0.0 and *L*=92.1 ± 0.2 and for PLA2M were *a*=-1.1 ± 0.1, *b*= 4.6 ± 0.8 and *L*=91.2 ± 0.2. The ΔE value between the PLA and PLA2M membranes was 3.8 ± 0.8 indicating that the samples were not much different in color, mainly attributed to the yellow (+*b*) difference.

3.3.8 Fourier Transform Infrared Spectrophotometer (FTIR)

The IR spectrum of PLA, PLA2M, and both membranes in contact with 95% ETOH at 40 °C is shown in Figure 3-8. The IR spectrum of PLA indicated the free –OH stretching around 3300-3600 cm^{-1} that reflects the –OH side chain end in the PLA chemical structure. The –CH stretch, and asymmetrical –CH stretch bands can also be observed around 2877 and 2997 cm^{-1}, respectively (Auras et al., 2004b). Meanwhile, at around 1749 cm^{-1}, the C=O carbonyl stretching appeared as a sharp and large band and the band was reported to be due to the A_1, and E_1 active modes (Gonçalves, Coutinho, & Marrucho, 2010). The $–CH_3$ bending was also observed at around 1458 cm^{-1}. The symmetric and asymmetric –CH deformation bending regions were also seen as a twin peaks at 1387, and 1366 cm^{-1}, respectively. The –C-O stretch was observed at around 1189 cm^{-1}. The -C-O-C aliphatic esters, and –C-O-C asymmetric stretching mode corresponded to the wavenumber at 1132, and 1076 cm^{-1}, respectively. The –OH bending mode can also be slightly observed around 1040 cm^{-1} (Auras et al., 2004a). Additionally, the $–CH_3$ rocking mode can be observed at 955 cm^{-1}, and this mode characterizes the helical backbone vibrations. The bands for amorphous, and crystalline regions of PLA were found at 870, and 757 cm^{-1}, respectively (Gonçalves et al., 2010).

The incorporation of 2 wt.% marigold flower extract was found to affect the PLA-based membrane, and the most profound changes can be observed for carbonyl band stretching, -C-O-C aliphatic esters stretching, and -C-O-C asymmetric stretching at 1744, 1132, and 1076 cm^{-1}, respectively (Colín-Chávez et al., 2012). The -C-O stretching of the ester group band was also found at 1210 cm^{-1}. All these changes were anticipated due to the presence of carbonyl group, and more polyunsaturated alkenes in the structure of astaxanthin as well as the fatty acids and triglycerides presence in the marigold flower extract (Figure 3-2).

In the case of PLA, and PLA2M that were in contact with 95% ETOH at 30 and 40 °C, more changes were observed especially for carbonyl band stretching, and -C-O stretching at 1749, and 1189 cm^{-1}, respectively. The –OH stretching band was observed to be broader for PLA2M that was in contact with 95% ETOH, and it could be attributed to the rapid penetration of the ethanol into the membrane at such a high temperature, hence modifying the membrane chains. A new and strong formation of peaks was also seen at 1968, and 2025 cm^{-1} PLA stored in 95% ETOH at 40 °C (indicated by arrows in Figure 3-8(b)). These peaks could be associated with C=C asymmetric stretching, and could possibly due to depolymerization of the membrane chains after an exposure at 40 °C with 95% ETOH for 3 days.

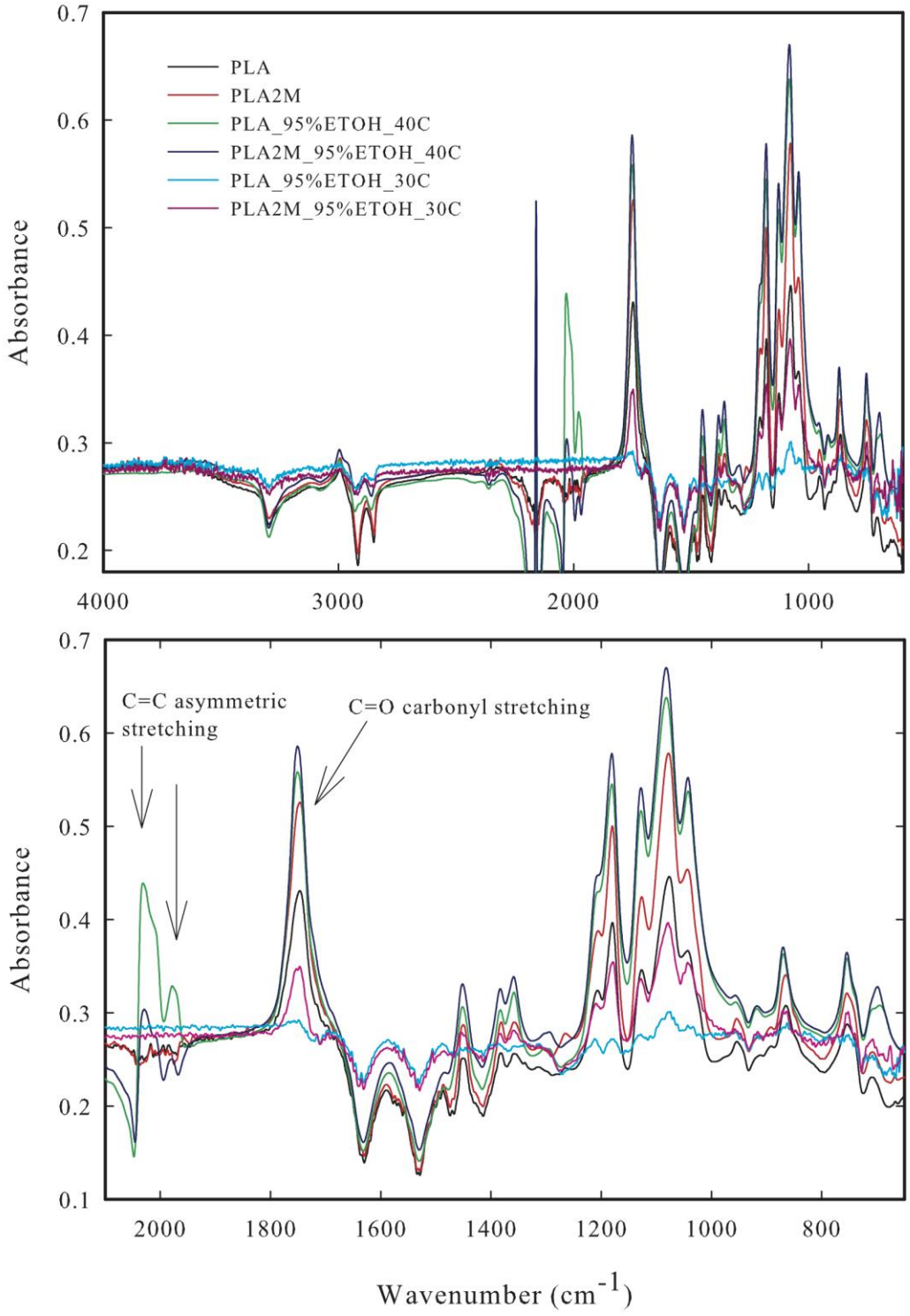

Figure 3-8 (a) FTIR spectrum of the fabricated functional membranes and (b) focused FTIR spectrum of the fabricated functional membranes.

3.3.9 Oxidative Stability of Soybean Oil

The most influential deteriorative reaction that could shorten the shelf life of oil in general is lipid degradation. Soybean oil that consists of significant amount of polyunsaturated fatty acids (PUFA) is highly susceptible to oxidation. In this study, the effectiveness of the fabricated membranes in the oxidative stability of soybean oil was investigated by the determination of peroxide value (PV). PV is one of the most commonly technique used to determine the degree of lipid degradation by measuring the formation of hydroperoxides, the primary product of lipid oxidation (Yildiz, Wehling, & Cuppett, 2003).

Soybean oil packaged in all pouches made of PLA and PLA2M underwent oxidation at more or less similar rate during the first 10 days as can be seen from Figure 3-9. This result was not surprising since these pouches were transparent in nature causing them susceptible towards oxidation due to light penetration, thus accelerating oxidation mechanism, in turns resulting in the formation of hydroperoxides. Light was also reported to have greater effect on singlet O_2 oxidation than the temperature. However, in the case of PLA2M pouches, it was expected that they could reduce the oxidation due to its antioxidant reaction with the oil by quenching of singlet O_2. Then, starting at day 15, the PV value of soybean oil in the PLA2M pouches was significantly lowered than that of PV of soybean oil in the glass bottle and PLA pouches (32.7 ± 2.58 vs 43.5 ± 2.89 and 41.5 ± 2.51 Meq/1000g test portion, respectively) ($p<0.0001$). It seemed that astaxanthin had migrated slowly from the membrane of the pouches to soybean oil before it accumulated sufficiently to slow down the oxidation.

Based on the results obtained, it can be concluded that the shelf life of soybean oil packaged in PLA2M pouches was 5 days or less, and in PLA and glass bottle was 3 days or less as compliance with Codex Alimentarius, in which the maximum acceptable level of PV for refined

vegetable oils is 10 milliequivalent/kg (Codex-Alimentarius, 1999). In an agreement, similar behavior was also observed for soybean oil packaged in the pouches made of mono- and bilayer LDPE, and LDPE/HDPE membranes containing marigold flower extract (Colín-Chávez et al., 2012). On the other hand, PLA incorporated with 2.5 wt.% α-tocopherol was reported to maintain the acceptable limit of PV of soybean oil for 60 days at 30 °C (Manzanarez-López et al., 2011). This difference could be associated with the concentration of antioxidant incorporated (2.5 wt.% α-tocopherol vs 1.49 wt.% marigold extract (of which contained only 0.7 % astaxanthin)), the nature of soybean oil (riched-additive vs additive-free oil), the compatibility of the antioxidant utilized with the membrane, and the nature of the contact surface of membrane (discs vs pouch).

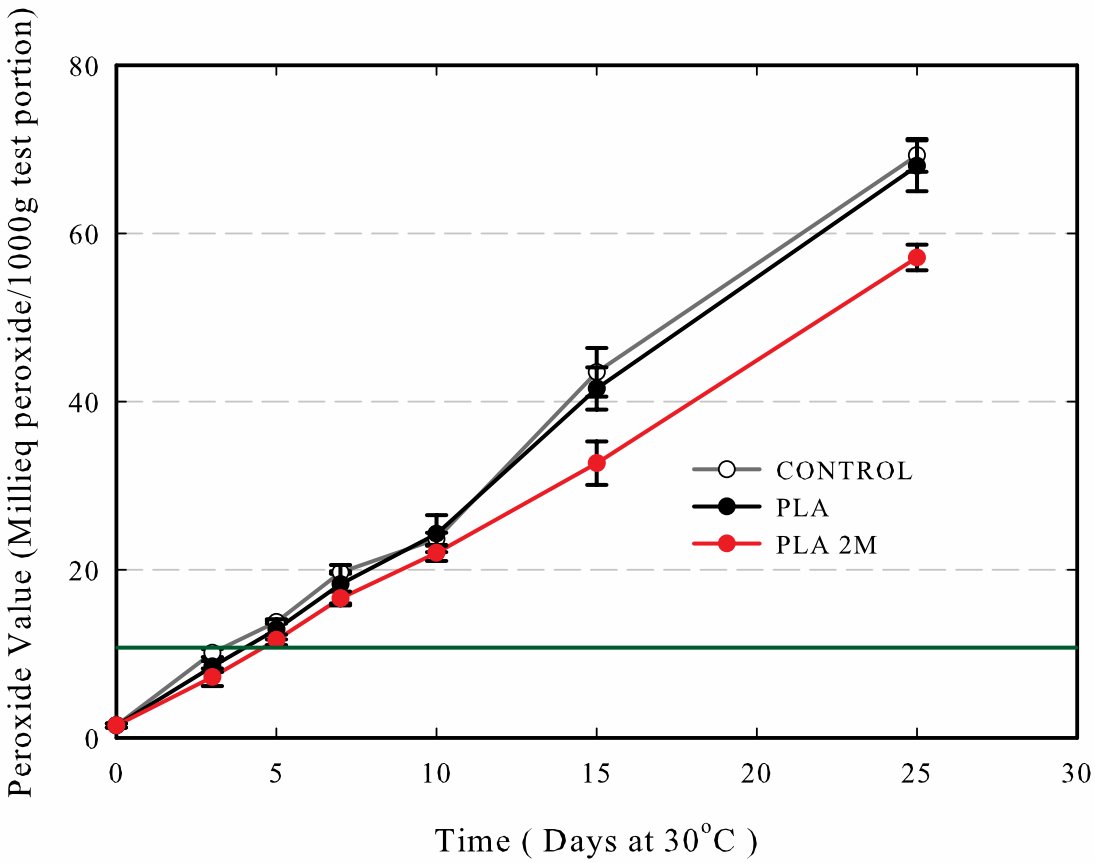

Figure 3-9 Oxidative stability of soybean oil packaged in the glass bottles, pouches made of PLA and pouches made of PLA2M at 30 °C during 25 d. Straight green line indicated the cut off point for Codex Alimentarius.

3.4 Conclusion

Bilayer antioxidant functional membrane made of PLA incorporated with Marigold flower extract was successfully fabricated. Migration study of astaxanthin towards 95% ETOH at 30 and 40 °C followed the Fick's second law of diffusion, with diffusion coefficient of 12.7 and 22.8 x 10^{-11} cm^2/s, respectively. No effect of marigold flower extract was seen in the thermal properties, and O_2 permeability of the PLA-based membrane. The incorporation of marigold flower extract was found to affect the molecular weight, IR spectra, and significantly reduced the WVP of PLA-

based membrane. However, it was also found that the gas permeability of this membrane was significantly increased possibly due to the presence of the components of the marigold flower extract introducing more free spaces for gas diffusivity to happen. In addition, PLA2M did not show any effect in prolonging the freshness of soybean oil within the Codex Alimentarius guideline (measured at 30 ± 2 °C, and 900-1000 lux of exposure) due to the slow release of astaxanthin. However, PLA2M did retard the oxidation of soybean oil from 15 to 25 d. Future work should be oriented to control the release of astaxanthin from PLA-based membrane by tailoring the membrane structure either by blending with another polymer or by incorporating another antioxidant that can facilitate the migration process optimizing the migration process, and extending the shelf life of the intended product. Ethanol at 95% is not a good food simulant for studying fatty foods release in PLA membranes. An alternative fatty food simulant for PLA membranes should be investigated in future studies.

REFERENCES

REFERENCES

Al-Malaika, S., Goodwin, C., Issenhuth, S., & Burdick, D. (1999). The antioxidant role of [alpha]-tocopherol in polymers II. Melt stabilising effect in polypropylene. *Polymer Degradation and Stability, 64*(1), 145-156.

Anderson, J. S., & Sunderland, R. (2002). Effect of extruder moisture and dryer processing temperature on vitamin C and E and astaxanthin stability. *Aquaculture, 207*(1-2), 137-149.

AOCS. (2009). Peroxide Value Acetic Acid-Isooctane Method-AOCS Official Method Cd 8b-90. In D. Firestone (Ed.), *Official Methods and Recommended Practices of the AOCS* (6 ed.). Illinois: American Oils Chemists' Society (AOCS) Press.

ASTM. (2003a). ASTM D4754-98 Standard Test Method for Two-Sided Liquid Extraction of Plastic Materials Using FDA Migration Cell (pp. 1-5). West Conshohocken, PA: ASTM International.

ASTM. (2003b). Standard test method for transition temperatures of polymers by differential scanning calorimetry. West Conshohocken, PA: ASTM International.

ASTM. (2005a). Standard test method for oxygen gas transmission rate through plastic film and sheeting using a coulometric sensor (Vol. ASTM D3985). West Conshohocken, PA: ASTM International.

ASTM. (2005b). Test Method for the Determination of Carbon Dioxide Gas Transmission Rate (Co 2TR) Through Barrier Materials Using An Infrared Detector (Vol. ASTM F2476 - 05). West Conshohocken, PA: ASTM International.

ASTM. (2006). Standard test method for water vapor transmission rate through plastic film and sheeting using a modulated infrared sensor (Vol. ASTM F1249). West Conshohocken, PA: ASTM International.

ASTM. (2008). Standard test method for compositional analysis by thermogravimetry. West Conshohocken, PA: ASTM International.

Auras, R., Harte, B., & Selke, S. (2004a). An overview of polylactides as packaging materials. *Macromolecular Bioscience, 4*(9), 835-864. doi: Doi 10.1002/Mabi.200400043

Auras, R., Harte, B., & Selke, S. E. M. (2004b). Effect of water on the oxygen barrier properties of poly(ethylene terephthalate) and polylactide films. *Journal of Applied Polymer Science, 92*(3), 1790-1803. doi: Doi 10.1002/App.20148

Balasubramanian, A. (2009, March 1, 2009). Antioxidant Packaging. *Packaging World Magazine*.

Baner, A. L. (2000). Partition coefficient. In A. L. Baner & O.-G. Piringer (Eds.), *Plastic Packaging Materials for Food, Barrier Function,Mass Transport, Quality Assurance and Legislation* (pp. 79-123). Weinheim: Wiley-VCH

Brandsch, J., Mercea, P., Rüter, M., Tosa, V., & Piringer, O. (2002). Migration modelling as a tool for quality assurance of food packaging. *Food Additives and Contaminants, 19*(S1), 29-41.

Byun, Y., Kim, Y. T., & Whiteside, S. (2010). Characterization of an antioxidant polylactic acid (PLA) film prepared with α-tocopherol, BHT and polyethylene glycol using film cast extruder. *Journal of Food Engineering, 100*(2), 239-244.

Camo, J., Beltrán, J. A., & Roncalés, P. (2008). Extension of the display life of lamb with an antioxidant active packaging. *Meat Science, 80*(4), 1086-1091.

Chen, H.-m., Shen, Y., Yang, J.-h., Huang, T., Zhang, N., Wang, Y., & Zhou, Z.-w. (2013). Molecular ordering and α'-form formation of poly (L-lactide) during the hydrolytic degradation. *Polymer*.

Codex-Alimentarius. (1999). Codex standard for named vegetable oils. *Codex-Stan, 210*, 1-13.

Colín-Chávez, C., Soto-Valdez, H., Peralta, E., Lizardi-Mendoza, J., & Balandrán-Quintana, R. R. (2012). Fabrication and Properties of Antioxidant Polyethylene-based Films Containing Marigold (Tagetes erecta) Extract and Application on Soybean Oil Stability. *Packaging Technology and Science*. doi: 10.1002/pts.1982

Colín-Chávez, C., Soto-Valdez, H., Peralta, E., Lizardi-Mendoza, J., & Balandrán-Quintana, R. R. (2013). Diffusion of natural astaxanthin from polyethylene active packaging films into a fatty food simulant. *Food Research International, 54*(1), 873-880.

Conn, R. E., Kolstad, J. J., Borzelleca, J. F., Dixler, D. S., Filer, L. J., LaDu, B. N., & Pariza, M. W. (1995). Safety assessment of polylactide (PLA) for use as a food-contact polymer. *Food and Chemical Toxicology, 33*(4), 273-283.

Crank, J. (1979). *The Mathematics of Diffusion* (2nd ed.). Bristol: Oxford University Press.

De Meulenaer, B. (2009). Migration from packaging materials. In R. Cósta & K. Kristbergsson (Eds.), *Predictive Modeling and Risk Assessment*. New york: Springer Science.

Dhoot, G., Auras, R., Rubino, M., Dolan, K. D., & Soto-Valdez, H. (2009). Determination of eugenol diffusion through LLDPE using FTIR-ATR flow cell and HPLC techniques. *Polymer, 50*(6), 1470-1482.

Endres, H.-J., Siebert, A., & Kaneva, Y. (2007). Overview of the current biopolymer market situation. *Bioplastic Magazine, 2*, 3.

Floros, J. D., Dock, L. L., & Han, J. H. (1997). Active packaging technologies and applications. *Food Cosmetics and Drug Packaging, 20*(1), 10-17.

Galindo-Arcega, C. E. (2004). *Migración del BHT de películas de PEBD y su efecto en la estabilidad del aceite de soya.* (MSc), Centro de Investigación en Alimentación y Desarrollo Hermosillo.

Gao, J., Duan, L., Yang, G., Zhang, Q., Yang, M., & Fu, Q. (2012). Manipulating poly (lactic acid) surface morphology by solvent-induced crystallization. *Applied Surface Science*.

Gavara, R., Lagarón, J. M., & Catalá, R. (2004). *Materiales poliméricos para en diseñyo de envases actives.* Paper presented at the Seminario Cyted-Technológico de Monterrey, Monterrey, México.

Gonçalves, C., Coutinho, J., & Marrucho, I. M. (2010). Optical properties. In R. Auras, L.-T. Lim, S. E. M. Selke & H. Tsuji (Eds.), *Poly(lactic acid): Synthesis, Structures, Properties, Processing, and Applications*. New Jersey: John Wiley and Sons, Inc.

Goncalves, C., Tomé, L. C., Garcia, H., Brandão, L., Mendes, A. M., & Marrucho, I. M. (2012). Effect of natural and synthetic antioxidants incorporation on the gas permeation properties of poly (lactic acid) films. *Journal of Food Engineering*.

Guo, J., Jones, M. J., & Ulrich, J. (2010). Polymorphism of 3, 3′-dihydroxy-β, β-carotene-4, 4′-dione (Astaxanthin). *Chemical Engineering Research and Design, 88*(12), 1648-1652.

Hamdani, M., Feigenbaum, A., & Vergnaud, J. M. (1997). Prediction of worst case migration from packaging to food using mathematical models. *Food Additives and Contaminants, 14*(5), 499-506.

Higuera-Ciapara, I., Félix-Valenzuela, L., & Goycoolea, F. M. (2006). Astaxanthin: A Review of its Chemistry and Applications. *Critical Reviews in Food Science and Nutrition, 46*(2), 185-196. doi: 10.1080/10408690590957188

Hwang, S. W., Shim, J. K., Selke, S. E. M., Soto-Valdez, H., Matuana, L., Rubino, M., & Auras, R. (2012). Poly (L-lactic acid) with added α-tocopherol and resveratrol: optical, physical, thermal and mechanical properties. *Polymer International, 61*(3), 418-425.

Iñiguez-Franco, F., Soto-Valdez, H., Peralta, E., Ayala-Zavala, J. F., Auras, R., & Gámez-Meza, N. (2012). Antioxidant Activity and Diffusion of Catechin and Epicatechin from Antioxidant Active Films Made of Poly (l-lactic acid). *Journal of Agricultural and Food Chemistry, 60*(26), 6515-6523.

Jamshidian, M., Tehrany, E. A., Cleymand, F., Leconte, S., Falher, T., & Desobry, S. (2012). Effects of synthetic phenolic antioxidants on physical, structural, mechanical and barrier properties of poly lactic acid film. *Carbohydrate Polymers, 87*(2), 1763-1773.

Jamshidian, M., Tehrany, E. A., Imran, M., Akhtar, M. J., Cleymand, F., & Desobry, S. (2012). Structural, mechanical and barrier properties of active PLA–antioxidant films. *Journal of Food Engineering, 110*(3), 380-389.

Lassalle, V., & Ferreira, M. L. (2007). PLA Nano-and Microparticles for Drug Delivery: An Overview of the Methods of Preparation. *Macromolecular Bioscience, 7*(6), 767-783.

Lim, L.-T., Auras, R., & Rubino, M. (2008). Processing technologies for poly (lactic acid). *Progress in Polymer Science, 33*(8), 820-852.

López-de-Dicastillo, C., Alonso, J. M., Catalá, R., Gavara, R., & Hernández-Muñoz, P. (2010). Improving the Antioxidant Protection of Packaged Food by Incorporating Natural Flavonoids into Ethylene− Vinyl Alcohol Copolymer (EVOH) Films. *Journal of Agricultural and Food Chemistry*.

Manzanarez-López, F., Soto-Valdez, H., Auras, R., & Peralta, E. (2011). Release of α-Tocopherol from Poly (lactic acid) films, and its effect on the oxidative stability of soybean oil. *Journal of Food Engineering, 104*(4), 508-517.

Martin, O., & Averous, L. (2001). Poly (lactic acid): plasticization and properties of biodegradable multiphase systems. *Polymer, 42*(14), 6209-6219.

Mascheroni, E., Guillard, V., Nalin, F., Mora, L., & Piergiovanni, L. (2010). Diffusivity of propolis compounds in Polylactic acid polymer for the development of anti-microbial packaging films. *Journal of Food Engineering, 98*(3), 294-301.

McNeill, I. C., & Leiper, H. A. (1985). Degradation studies of some polyesters and polycarbonates—2. Polylactide: degradation under isothermal conditions, thermal degradation mechanism and photolysis of the polymer. *Polymer Degradation and Stability, 11*(4), 309-326.

Miková, K. (2001). The regulation of antioxidants in food. *Antioxidants in food.(Pokorny, J., Yanishlieva, N. and Gordon, M., ed.)*, 287-284.

Mutsuga, M., Kawamura, Y., & Tanamoto, K. (2008). Migration of lactic acid, lactide and oligomers from polylactide food-contact materials. *Food Additives and Contaminants, 25*(10), 1283-1290.

Naguib, Y. M. A. (2000). Antioxidant Activities of Astaxanthin and Related Carotenoids. *Journal of Agricultural and Food Chemistry, 48*(4), 1150-1154. doi: 10.1021/jf991106k

Ortiz-Vazquez, H., Shin, J. M., Soto-Valdez, H., & Auras, R. (2011). Release of butylated hydroxytoluene (BHT) from Poly (lactic acid) films. *Polymer Testing, 30*(5), 463-471.

Peltonen, L., Koistinen, P., Karjalainen, M., Häkkinen, A., & Hirvonen, J. (2002). The effect of cosolvents on the formulation of nanoparticles from low-molecular-weight poly (I) lactide. *American Association of Pharmaceutical Scientists- Pharm Sci Tech, 3*(4), 52-58.

Rao, A. R., Sarada, R., & Ravishankar, G. A. (2007). Stabilization of astaxanthin in edible oils and its use as an antioxidant. *Journal of the Science of Food and Agriculture, 87*(6), 957-965.

Robertson, G. L. (2006). Active and intelligent packaging. In G. L. Robertson (Ed.), *Food Packaging: Principles and Practice* (2nd ed., pp. 292-294). Boca Raton: CRC Press

Rooney, M. L. (1995). *Active food packaging*: Blackie Academic & Professional.

Sato, S., Gondo, D., Wada, T., Kanehashi, S., & Nagai, K. (2012). Effects of various liquid organic solvents on solvent-induced crystallization of amorphous poly (lactic acid) film. *Journal of Applied Polymer Science*.

Sawalha, H., Schroën, K., & Boom, R. (2010). Addition of oils to polylactide casting solutions as a tool to tune film morphology and mechanical properties. *Polymer Engineering and Science, 50*(3), 513-519. doi: 10.1002/pen.21557

Smith, J. P., Hoshino, J., & Abe, Y. (1995). Active packaging in polymer films. In M. Rooney (Ed.), *Active Food Packaging* (pp. 143-172). Glasgow: Blackie Academic & Professional

Soto-Cantú, C. D., Graciano-Verdugo, A. Z., Peralta, E., Islas-Rubio, A. R., González-Córdova, A., González-León, A., & Soto-Valdez, H. (2008). Release of butylated hydroxytoluene from an active film packaging to asadero cheese and its effect on oxidation and odor stability. *Journal of Dairy Science, 91*(1), 11-19.

Soto-Valdez, H. (2011). Migration. In R. A. Auras, L. T. Lim, S. E. Selke & H. Tsuji (Eds.), *Poly(lactic acid): Synthesis, strucures, properties, processing, and applications* (Vol. 10, pp. 181-188). New Jersey: Wiley.

Soto-Valdez, H., Auras, R., & Peralta, E. (2010). Fabrication of Poly(lactic acid) Films with Resveratrol and the Diffusion of Resveratrol into Ethanol. *Journal of Applied Polymer Science*. doi: 10.1002/app.33687

Soto-Valdez , H., Peralta, E., & Auras, R. (2008). *Poly(lactic acid) films added with resveratrol as active packaging with potential application in the food industry.* Paper presented at the 16th IAPRI World Conference on Packaging Bangkok, Thailand.

Wessling, C., Nielsen, T., Leufvén, A., & Jägerstad, M. (1998). Mobility of α-tocopherol and BHT in LDPE in contact with fatty food simulants. *Food Additives and Contaminants, 15*(6), 709-715. doi: 10.1080/02652039809374701

Yildiz, G., Wehling, R. L., & Cuppett, S. L. (2003). Comparison of four analytical methods for the determination of peroxide value in oxidized soybean oils. *Journal of the American Oil Chemists' Society, 80*(2), 103-107.

Chapter 4

Parameter Estimation for Migration Studies of Antioxidant-Polymer Films

4.0 Introduction

Migration in packaging is referred as a diffusivity process of chemical substances from polymeric films into products. These chemical substances include but are not limited to surfactants, contaminants, polymer hydrolysis by-products such as monomers, oligomers and others, and regulated chemical additives such as antioxidants, antimicrobials, and heat stabilizers. Migration could be a desirable or an undesirable process. It is desirable when the incorporated additives are intended for a gradual release over time for protecting the product from any adverse chemical reactions, thus prolonging the product's shelf life. On the contrary, when the incorporated additives migrate into the product due to the incompatibility of polymer film-additives, *e.g.*, surfactants, unwanted organoleptic changes and/or unforeseen food safety hazards may occur, depending on the reactivity of the additives; thus this migration process is undesirable. Both types of migration have been widely investigated for multiple reasons, particularly shelf life extension and safety concerns of intended products. However, in recent years the development of antioxidant-functional film systems for food products has tremendously increased due to optimized packaging technology with dual functions: protection of the film and the food product during processing and storage, and also nutritional enhancement of intended products.

Developments in the area of antioxidant functional films have covered a wide range of polymers: petroleum-based and/or bio-based and various types of antioxidants: natural and/or synthetic (Barbosa-Pereira et al., 2013; Byun, Kim, & Whiteside, 2010; Calatayud et al., 2013; Chen, Lee, Zhu, & Yam, 2012; C. Colín-Chávez, H. Soto-Valdez, E. Peralta, J. Lizardi-Mendoza, & R.R. Balandrán-Quintana, 2013; Citlali Colín-Chávez, Herlinda Soto-Valdez, Elizabeth Peralta,

Jaime Lizardi-Mendoza, & René Renato Balandrán-Quintana, 2013; Goncalves et al., 2012; Graciano-Verdugo et al., 2010; Granda-Restrepo et al., 2009; Hwang et al., 2013; Iñiguez-Franco & Soto-Valdez 2011; M. Jamshidian, E. A. Tehrany, et al., 2012; M. Jamshidian, E.A. Tehrany, & S. Desobry, 2012; Majid Jamshidian, Elmira Arab Tehrany, & Stéphane Desobry, 2012; Lee, Shin, Han, Lee, & Giacin, 2004; Lopez de Dicastillo et al., 2011; López-de-Dicastillo, Gómez-Estaca, Catalá, Gavara, & Hernández-Muñoz, 2012; Manzanarez-López, Soto-Valdez, Auras, & Peralta, 2011; Nerín et al., 2006; Ortiz-Vazquez, Shin, Soto-Valdez, & Auras, 2011; Pereira de Abreu, Losada, Maroto, & Cruz, 2010; Sonkaew, Sane, & Suppakul, 2012; Soto-Valdez, Auras, & Peralta, 2010; Soto-Valdez , Peralta, & Auras, 2008; Wessling, Nielsen, & Giacin, 2001; Zhu, Lee, & Yam, 2012; Zhu, Schaich, Chen, & Yam, 2013). Most of these studies investigated the diffusion coefficient, *D*, of migrants from different polymeric films with some extended focus on the antioxidant capacity and shelf life of various products. Nevertheless, these studies were designed on a trial and error basis with limited fruitful findings. Even though this approach may have seemed feasible, a considerable amount of money, time, and effort could have been wasted on resources without meeting sufficient expectations. Therefore, a parameter estimation approach can be used to improve estimation of the parameters of interest, and to assist experimental design by providing insights into the physical process of the experiment.

The estimation of parameters involved in migration processes was often explored with little consideration of statistical assumptions and the accuracy of the estimation was scarcely reported and discussed with the exception of few works. In addition, to the best of the authors' knowledge, migration studies often focus on the *D* values. Only a few works investigated parameters like mass transfer coefficient, *h* (Reynier, Dole, & Feigenbaum, 2002a, 2002b; Vitrac & Hayert, 2006; Vitrac, Mougharbel, & Feigenbaum, 2007), other parameters are commonly neglected.

This study explored the parameter estimation aspects of three migration models addressing the following conditions: i) film in contact with a finite volume of food/simulant and negligible external mass transfer coefficient, ii) film in contact with an infinite volume of food/simulant and negligible external mass transfer coefficient, and iii) film in contact with infinite volume of food/simulant and non-negligible external mass transfer coefficient. The parameters considered for estimation were D, M_∞, and α.

4.1 Theoretical Background

4.1.1 Part A: Migration

4.1.1.1 Partition Coefficient, $K_{p,f}$

In a migration study, the partition coefficient is often determined when the concentration of migrant from the film that has migrated into the food/simulant reaches equilibrium. The partition coefficient, $K_{p,f}$ can be defined as the ratio of the migrant concentration left in the film to the migrant concentration in the food simulant/system (Poças, Oliveira, Oliveira, & Hogg, 2008). The value of $K_{p,f}$ is often used to calculate the α value that later determines the migration model for a film-food system. The value of $K_{p,f}$ can also be used to describe the anticipated physical process of the film-food system in terms of the chemical affinity of the migrant towards the film and the food system. Other factors such as temperature, film area of exposure to the food system, and the degree of solvency of the food system will also influence the value of $K_{p,f}$ (Tehrany & Desobry, 2004). A value of $K_{p,f}$ equal to 1 means that the migrant concentrations are similar in both the film and the food system at equilibrium. Meanwhile, $K_{p,f} > 1$, and $K_{p,f} < 1$ describe a higher affinity of the migrant towards the film, and a higher affinity of the migrant towards the food system, respectively. The former is commonly preferred when food safety is of concern, while the later is

preferred in the case of a functional film where the additives incorporated into the film are expected to provide controlled release into a food system for shelf life extension.

From $K_{p,f}$, one can determine α, which can also be estimated from the non-zero positive roots of q_n (tan q_n = - αq_n). α is also a ratio of the mass of migrant migrated into food/simulant to the mass of migrant left in the film, at equilibrium.

$$K_{p,f} = \frac{C_{p,\infty}}{C_{f,\infty}} \quad \text{(Eq. 4-1)}$$

$C_{p,\infty}$= the concentration of the migrant in the film at equilibrium (g of migrant/cm^3 film).

$C_{f,\infty}$= the concentration of migrant in the food/simulant at equilibrium (g of migrant/cm^3 food/simulant).

$$\alpha = \frac{C_{f,\infty}}{C_{p,\infty}}\frac{V_f}{V_p} = \frac{V_f}{K_{p.f}V_p} = \frac{M_{f,\infty}}{M_{p,\infty}} \quad \text{(Eq. 4-2)}$$

V_f =volume of food/simulant (cm^3)

V_p =volume of film (cm^3)

$M_{f,\infty}$= mass of the migrant in food/simulant at equilibrium (μg or g)

$M_{p,\infty}$ =mass of the migrant left in film at equilibrium (μg or g)

4.1.1.2 Biot number, *Bi*

Besides $K_{p,f}$, another important parameter that may affect migration is the convective mass transfer coefficient, *h*. This parameter describes the interfacial mass transfer coefficient with or without the presence of fluid flow (bulk convection). However, the importance of the parameter depends on the system, specifically in the case where resistance exists at the surface boundary between film and food/simulant. This parameter is embedded inside the *Biot* number together with the diffusion coefficient, *D* as the overall migration resistance series. *Bi* is a dimensionless number

representing a ratio between the convective mass transfer coefficient, *h* and the diffusion coefficient, *D*, taking into consideration the film thickness, *L* (Eq. 4-3) (Bird, Stewart, & Lightfoot, 2007; Galotto, Torres, Guarda, Moraga, & Romero, 2011; Vitrac et al., 2007).

$$Bi = \frac{Lh}{D} \quad \text{(Eq. 4-3)}$$

In addition, determination of *h* is crucial for a system of film-food/simulant that imposes resistance at the system's surface such as in a system where the thickness of the film is thicker (Vitrac et al., 2007) and in the case of hydrophilic polymer-oil like simulant system, thus increases the resistance of interfacial mass transfer.

4.1.1.3 Diffusion coefficient, *D*

The diffusion coefficient, *D* is a parameter used to describe the migration process that takes place between a film and a food/simulant. Fick's laws of diffusion are commonly used to interpret the diffusion process. Fick's first law of diffusion refers to steady state flow in a diffusion process that occurs from higher to lower migrant concentration with respect to spatial discretization (Eq. 4-4). Meanwhile, Fick's second law of diffusion describes a diffusion process that may take place in an unsteady state, where the concentration of the migrant changes as a function of time (Eq. 4-5) (Crank, 1979). The rate of diffusion is usually affected by the temperature, the partition coefficient, chemical affinity between film-food/simulant, and the effect of stirring, to name a few.

$$F = -D\frac{\partial C}{\partial x} \quad \text{(Eq. 4-4)}$$

$$\frac{\partial C}{\partial t} = D\frac{\partial^2 C}{\partial x^2} \quad \text{(Eq. 4-5)}$$

F= flow rate

D= diffusion coefficient

c= migrant concentration in the film

x= the distance (in the direction of the diffusion)

t=time

The determination of $K_{p,f}$, α, h, and D are among the most important parameters that describe migration. This phenomenon can be further described through established mathematical models with the following assumptions: i) initial concentration of the migrants is uniformly distributed in the film, ii) migration happens on the side of the film that is in contact with the food/simulant, iii) the food/simulant is well mixed and has large surface mass transfer coefficient, h (*Biot* no. >100), iv) Fickian diffusion controls the migration in the film, v) migration depends only on temperature, and the diffusion coefficient, D and the partition coefficient, $K_{p,f,}$ are constants, vi) the film interface and the food are always at equilibrium, and vii) no interaction occurs between the film and the food/simulant and the edge effect is negligible (Chung, Papadakis, & Yam, 2001, 2002; Crank, 1979; Poças et al., 2008).

Model A: Film in contact with finite volume of food/simulant and negligible external mass transfer coefficient

This model is commonly used for a migration study at relatively low temperature or in the case where the migrant has higher affinity towards the film than that of the food/simulant, which results in α <1 because $K_{p,f}$>1 (Figure 4-1). The final solution in this model is as follows:

$$\frac{M_{f,t}}{M_{f,\infty}} = 1 - \sum_{n=1}^{\infty} \frac{2\alpha(1+\alpha)}{1+\alpha+\alpha^2 q_n^2} exp\left[-\frac{Dq_n^2 t}{L^2}\right] \quad \textbf{(}\text{Eq. 4-6)}$$

Model B: Film in contact with an infinite volume of food/simulant and negligible external mass transfer coefficient

This model is applicable when most of the migrant in the film migrates into the food/simulant, resulting in $K_{p,f}$ <1, and thus $\alpha \geq 1$ (Figure 4-1). The final solution in this model is as follows:

$$\frac{M_{f,t}}{M_{f,\infty}} = 1 - \frac{8}{\pi^2}\sum_{n=1}^{\infty}\frac{1}{(2n+1)^2}\,exp\left[-\frac{(2n+1)^2}{4L^2}D\pi^2 t\right] \quad \text{(Eq.4-7)}$$

It is worth mentioning that in the case where the ratio of $V_f/V_p >> 20$, the same outcome will result from both Eq. 4-6 and Eq.4-7 (Hamdani, Feigenbaum, & Vergnaud, 1997).

Model C: Film in contact with an infinite volume of food/simulant and non-negligible external mass transfer coefficient

This type of model is commonly used when there is interfacial resistance at the boundary layer between the film and the food/simulant, like in the case of a film in contact with an oil-like food/simulant and/or when a thicker film is used (Bi<200) (Figure 4-1) (Vitrac et al., 2007). The final solution for this model is as follows:

$$\frac{M_{f,t}}{M_{f,\infty}} = 1 - \sum_{n=1}^{\infty}\frac{2\mathrm{Bi}}{(q_n^2+Bi+Bi^2)q_n^2}\,exp\left[-\frac{Dq_n^2 t}{L^2}\right] \quad \text{(Eq. 4-8)}$$

In the case that the food/simulant is stirred vigorously and/or a thin layer of film is used, thus resulting in Bi >200, Eq. 4-8 is reduced/simplified to Eq. 4-7 (Mascheroni, Guillard, Nalin, Mora, & Piergiovanni, 2010).

<table>
<tr><td>Migration controlled by diffusion in the film</td><td>Migration with boundary layer resistance</td></tr>
<tr><td> 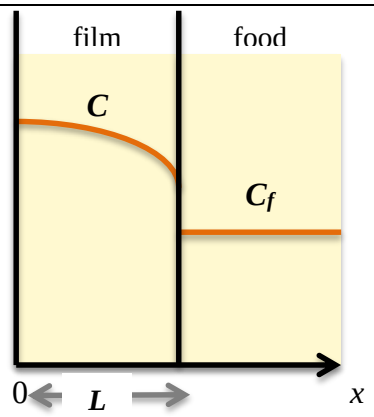
</td><td> 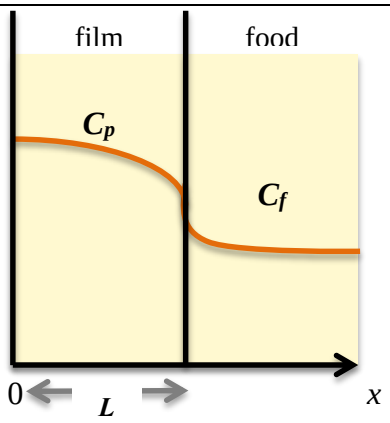
</td></tr>
<tr><td colspan="2">Fick's 2nd Law of Diffusion
$$\frac{\partial C_p}{\partial t} = D\frac{\partial^2 C_p}{\partial x^2}$$</td></tr>
<tr><td colspan="2">Initial conditions
$$C_p(x,0) = C_0 \qquad C_f(x,0) = 0$$</td></tr>
<tr><td>Boundary conditions
$$\left.\frac{\partial C_p}{\partial x}\right|_{x=0} = 0 \quad -D\left.\frac{\partial C_p}{\partial x}\right|_{x=L} = \frac{V_f}{A}\left.\frac{\partial C_f}{\partial t}\right|_{x=L}$$</td><td>Boundary conditions
$$\left.\frac{\partial C_p}{\partial x}\right|_{x=0} = 0 \qquad -D\left.\frac{\partial C_p}{\partial x}\right|_{x=L} = h(C_p - C_{p,\infty})$$</td></tr>
<tr><td>$\frac{M_{f,t}}{M_{f,\infty}} = 1 - \sum_{n=1}^{\infty}\frac{2\alpha(1+\alpha)}{1+\alpha+\alpha^2 q_n^2} exp\left[-\frac{Dq_n^2 t}{L^2}\right]$
q_n= the non-zero positive roots of
tan $q_n = -\alpha q_n$</td><td>$\frac{M_{f,t}}{M_{f,\infty}} = 1 - \sum_{n=1}^{\infty}\frac{2\mathrm{Bi}}{(q_n^2+Bi+Bi^2)q_n^2} exp\left[-\frac{Dq_n^2 t}{L^2}\right]$
q_n= the non-zero positive roots of
Biot # (*Bi*)= q_n tan q_n</td></tr>
<tr><td>If $\alpha \gg 1$ because $V_f \gg V_p$ and/ or $K_{p,f} < 1$, a simplified solution:</td><td>If Bi is very high (>100), a simplified solution:</td></tr>
<tr><td colspan="2">$$\frac{M_{f,t}}{M_{f,\infty}} = 1 - \frac{8}{\pi^2}\sum_{n=1}^{\infty}\frac{1}{(2n+1)^2} exp\left[-\frac{(2n+1)^2}{4L^2}D\pi^2 t\right]$$</td></tr>
</table>

Figure 4-1 Summary of migration models A, B, and C. Figure adapted from Poças et. al (2008) (Poças et al., 2008).

4.1.2 Part B: Parameter Estimation

Many migration models are available to determine the diffusion coefficient through mainly deterministic mathematical modeling. Deterministic models often have an input of variables as a single and constant value that results in the same output value of variables due to its zero error assumption (Poças et al., 2008). Some studies employ a curve-fitting or optimization approach; however this approach considers mostly minimizing the sum of squared errors rather than evaluating the importance of the parameters (Dolan & Mishra, 2013).

In reality, most experimental studies are designed by collecting observational data (dependent variable) with unknown functions or parameters. This approach is an inverse problem and is also known as parameter estimation. Parameter estimation helps to estimate the parameters/constants of interest using mathematical models, and to a certain extent it may provide some physical meaning for parameters that are relevant to the experiment. Beck and Arnold (1977) defined parameter estimation as "a discipline that provides tools for the efficient use of data in the estimation of constants appearing in mathematical models and for aiding in modeling of phenomena" (Beck & Arnold, 1977). Parameter estimation takes into consideration the importance of parameters and how these parameters affect each other, and in turn the whole experimental design.

Experimentally, in most cases, more than one parameter is estimated through mathematical models. Lack of information on how these parameters affect each other often results in higher variability in observational data, thus causing higher statistical error and/or overestimation or underestimation of parameters of interest. Therefore, the first step to consider in parameter estimation is to investigate the correlation among parameters through the sensitivity coefficients and scaled sensitivity coefficients.

4.1.2.1 Sensitivity Coefficient and Scaled Sensitivity Coefficient

Sensitivity coefficient and scaled sensitivity coefficient were described in Chapter 2 section 2.7.2.

4.1.2.2 Ordinary Least Squares (OLS) Estimation

Parameter estimation can be performed by an OLS using the non-linear regression (nlinfit) command in MATLAB®. Statistical assumptions need to be analyzed before data fitting. Statistical assumptions that need to be taken into account include (but are not limited to); i) the errors are additive in the measurement, ii) the errors in the measurement contain zero mean, iii) the measurement errors have constant variance, iv) the measurement errors are uncorrelated, v) the errors are normal, independent, and identically distributed, vi) the statistical parameters describing the errors are known, vii) the independent variables are errorless, and viii) the nature of the parameters (constant vs. random vector parameter; prior information vs. unknown statistics of parameter) (Beck & Arnold, 1977; Dolan & Mishra, 2013).

4.1.2.3 Corrected Akaike Information Criterion (AICc)

The corrected Akaike Information Criterion (AICc) was used to compare models with 1P, 2P and/or 3P. This approach is commonly used for the non-nested model comparison. Commonly, the higher the number of the parameters the more likely the goodness of fit seems to improve and vice versa. Thus, AICc eliminates the bias that may be caused by different numbers of parameters among models. The smaller the value of AICc is, the more likely the model is correct (Motulsky & Christopoulos, 2004).

$$AICc = n\ ln\left(\frac{SSE}{n}\right) + 2K + \frac{2K(K+1)}{n-K-1} \quad \text{(Eq. 4-9)}$$

where *n*=number of data; *p*=number of parameter; *K=p+1*

4.1.2.4 Optimal Experimental Design

Optimal experimental design helps in finding the optimal point at which the parameters can be estimated and have lower errors. The C matrix is needed in order to achieve a desirable maximum determinant (Eq. 4-15). By maximizing the determinant Δ^n (Eq. 4-16), the optimal time to perform an experimental study can be determined. This approach is beneficial in terms of optimizing not only the resources used, but also the time spent for a given experiment (Beck & Arnold, 1977; Dolan & Mishra, 2013).

$$\Delta^n = |X^T X| \quad \text{(Eq. 4-10)}$$

$$C_{ij} = \frac{1}{t_n}\int_0^{t_n} X_i'(t) X_j'(t) dt \quad \text{(Eq. 4-11)}$$

In addition, providing that all standard statistical assumptions are met, the OLS, maximum likelihood (ML), Gauss-Markov, and Maximum A Posteriori (MAP) method produce similar estimators and variance. Among all the criteria suggested for Δ^n, Beck & Arnold (1977) recommended the maximization of the determinant Δ^n due to its implications of minimizing the hypervolume of the confidence region (Beck & Arnold, 1977).

4.2 Case Study

A selected case study is presented to demonstrate the difference between estimation of 1, 2, and 3 parameters. Data analyses were performed using a non-linear regression fitting function in MATLAB® R2011b (MathWorks, Natick, MA, USA).

Statistical analysis was performed by using a SPSS Statistics (version 22, 2013, IBM Corporation©, Armonk, NY, USA). Mean comparison of more than two parameters was done using an analysis of variance (ANOVA) and post-hoc of Tukey's test. While, an independent t-test was performed for comparing means between two parameters.

4.2.1 A Selected Case Study: Poly(Lactic Acid), PLA-α-Tocopherol Functional Film in Contact With 100% Ethanol At 23 °C

A poly(lactic acid), PLA film incorporated with 2.58 ± 0.18 wt.% α-tocopherol was prepared in the form of round discs with a total area/disc of 6.28 cm^2. Six discs were separated by beads on a stainless steel wire and placed in a vial containing 30 mL 100% ethanol (volume-area ratio= 0.8 mL/ cm^2). The experiment was run at 23 °C and sampling was performed frequently during an interval of 8 days (Manzanarez-López et al., 2011). The $K_{p,f}$ was measured at the end of the experiment and was reported to be 796.62 ± 45.4. The α value was also calculated and was found to be 0.366 (Manzanarez-López et al., 2011), which meets the boundary conditions and the requirements of model A presented earlier. Thus, the analytical solution of Eq. 4-6 was used to fit the model. For this selected case study, three parameters (D, M_∞ and α) were estimated for 1, 2, and 3P models.

4.2.1.1 Initial Scaled Sensitivity Coefficient, *X'*

The initial scaled sensitivity coefficient, *X'* involving two and three parameters was analyzed and plotted based on initial parameter guesses by using an approximation of the forward difference method. Figure 4-2a and 4-2b show the *X'* plots for 2 and 3 parameters, respectively. From Figure 4-2a, it can be seen that D and M_∞ were not correlated, thus providing an initial

indication that they can be estimated easily and accurately. Since the absolute magnitude of change for M_∞ was larger, it was expected that the estimation for this particular parameter could be performed accurately with lower relative error than that of *D*. Meanwhile, Figure 4-2b indicates that based on the magnitude of the plots, M_∞ can be accurately estimated with the lowest relative error, followed by α and *D*. Even though it may have appeared on the plot that there could be some correlation between α, and *D*, the ratio between these two parameters was not constant. It is also worth noticing that a closer look into α provides an initial indication that this parameter would be best estimated at an early stage of the experiment due to its sensitivity towards perturbation as well as to avoid correlation with *D* (Figure 4-2b).

In addition, the *X'* plot can also be used to give an approximation of the duration actually needed to sufficiently estimate all parameters of interest. This approximation can later be compared with the optimal experimental design.

4.2.1.2 Ordinary Least Square (OLS) Estimation and the Corrected Akaike Information Criterion (AICc)

D values of 1.06 ± 0.04, 4.5 ± 0.23, and $0.79 \pm 0.08 \times 10^{-10}$ cm^2/s were obtained from OLS estimation of 1, 2, and 3P, respectively. No significant different ($p>0.05$) was observed between the M_∞ values of 2P vs. 3P estimation (0.36 ± 0.003 vs. $0.37 \pm 0.004 \times 10^{-4}$ g α-tocopherol/ g ethanol). Meanwhile, an estimated α value was found to be 0.30 ± 0.01 (Table 4-1). Root mean square errors (RMSE) of 1, 2, and 3P were 1.51×10^{-6}, 1.52×10^{-6} and 1.32×10^{-6} g α-tocopherol/ g ethanol, respectively. In general, the RMSE represents the accuracy of estimation by taking into consideration how much deviation occurs between predicted and observed data. A smaller RMSE value is often anticipated with an increasing number of parameters estimated as more factors are

being weighted into the model fitting, thus increasing the accuracy of estimation as can be seen from the results obtained. However, a limit on the number of parameters estimated should be considered carefully since over-parameterized models introduce more uncertainty; thus, the expected accuracy could be compromised. Therefore, to avoid the bias introduced by having different number of parameters in a model, AICc can provide better and more fair indication than that of RMSE. In this case, it was found that 3P estimation is more likely to be the correct one over 1P and 2P, since its AICc value was the lowest among the others (-2269). This result gave an indication that the estimation of those aforementioned three parameters should be considered for this particular case study. From an overall perspective, it can be concluded that 3P estimation did give a lower, better RMSE and lower AICc over 1P and 2P estimation. Therefore, by estimating three parameters, the accuracy of the estimation can be improved and additional insight on the kinetics behind the migration experiment can be obtained.

For 2P estimation, M_∞ had the lowest relative error (0.009) compared to D (0.052) as had been anticipated based on the initial X' plot. The asymptotic 95% confidence interval, for which indicates the reliability of the estimate, was found to be tighter for M_∞ than for D ($0.35\text{-}0.36 \times 10^{-4}$ vs. $4.04\text{-}4.97 \times 10^{-10}$, respectively). A similar expectation was also met for 3P estimation, which M_∞ had the lowest relative error (0.012), followed by α (0.039), and D (0.097). The correlation coefficient between the parameters estimated for both models (2P and 3P) was also in an agreement with the initial X' plot (Figure 4-2a,b), which demonstrated that they were all not correlated (Table 4-1). Figure 4-3a,b,c shows the migration plots of this case study for all 3 estimations.

Residual plots were also plotted for 1P, 2P, and 3P estimation for visual interpretation of how the assumption of normal, identically, independent distribution of data was met (Figure 4-3d,e,f). A signature residual was found visually apparent for 1P estimation in comparison to that

of the residual distribution observed for 2P and 3P. For this particular case study, it was observed that the addition of extra parameters increased the accuracy of the estimates based on the results obtained from OLS estimation.

A final X' plot was also constructed based on the estimated values obtained from OLS estimation to demonstrate the final outcomes (Figure 4-4a,b).

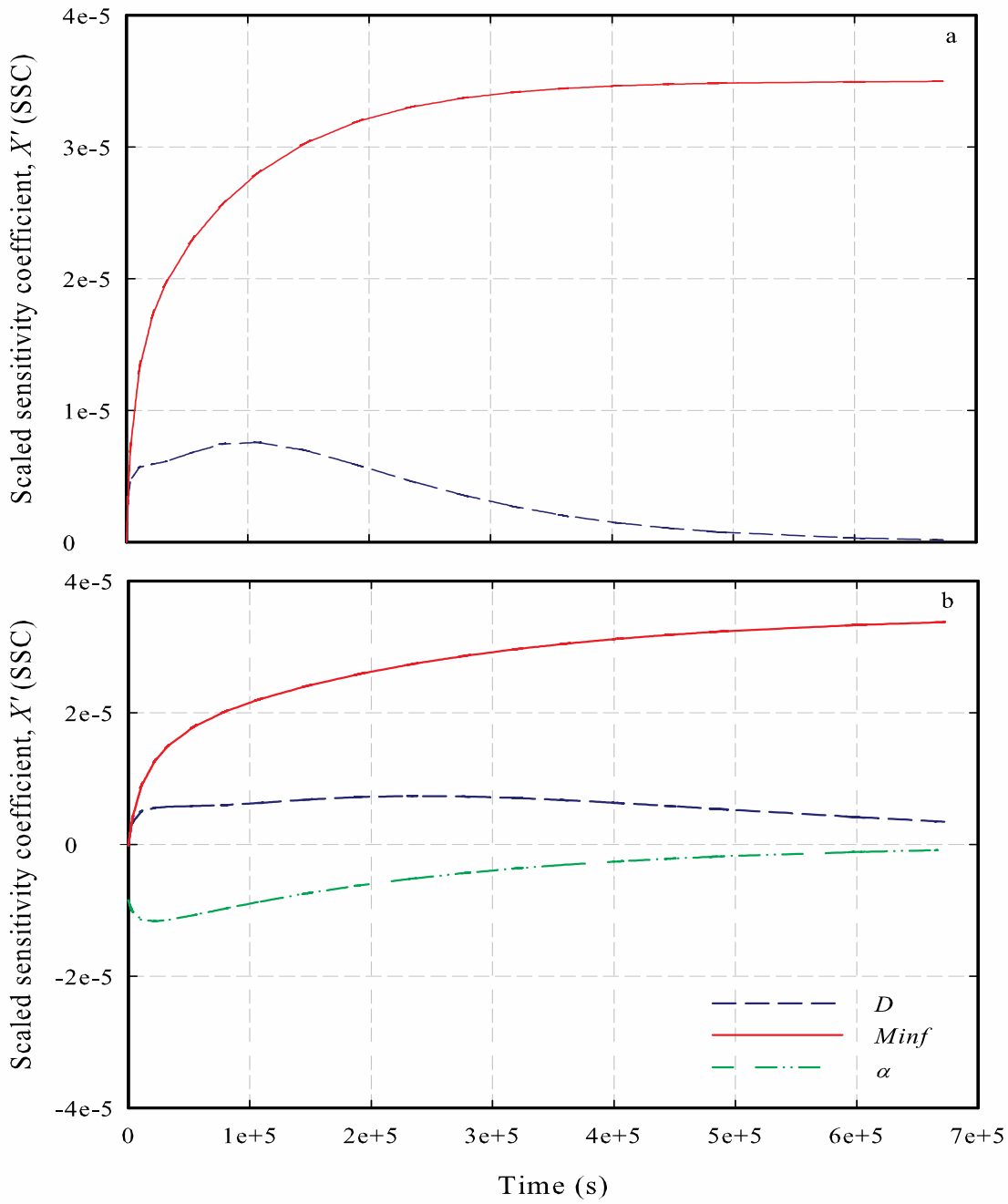

Figure 4-2 (a) Scaled sensitivity coefficients for 2P, and (b) for 3P of migration study of PLA-α-tocopherol system at 23 °C using forward difference approximation. Initial guesses used were: D= 0.06×10^{-9} cm^2/s, M_{inf}=3.95×10^{-5} g α-tocopherol/g ethanol, and α=0.35.

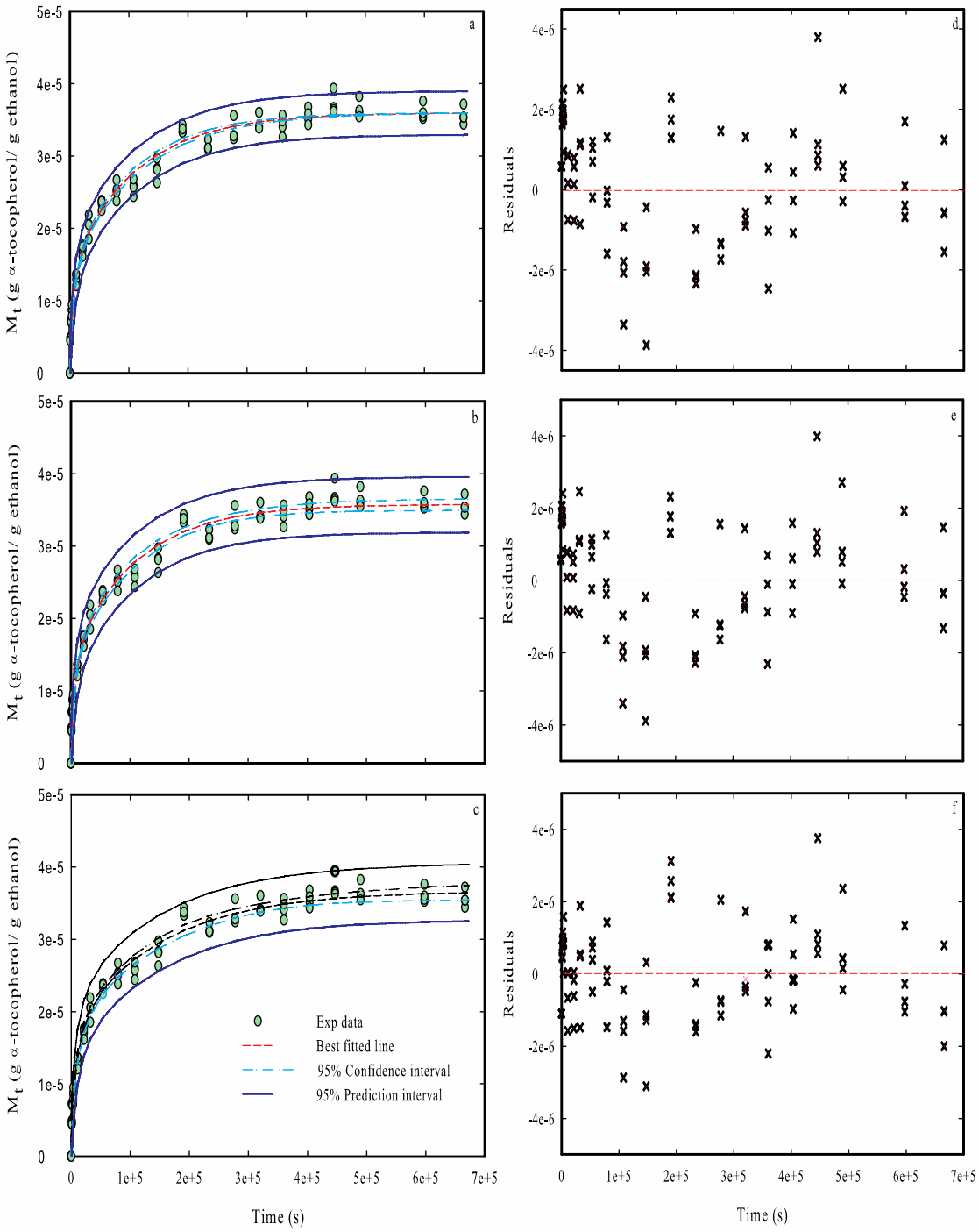

Figure 4-3 Migration of α-tocopherol into 100% ethanol at 23 °C during storage for (a) 1P, (b) 2P, and (c) 3P using OLS estimation and their corresponding residuals plot (d), (e), and (f), respectively.

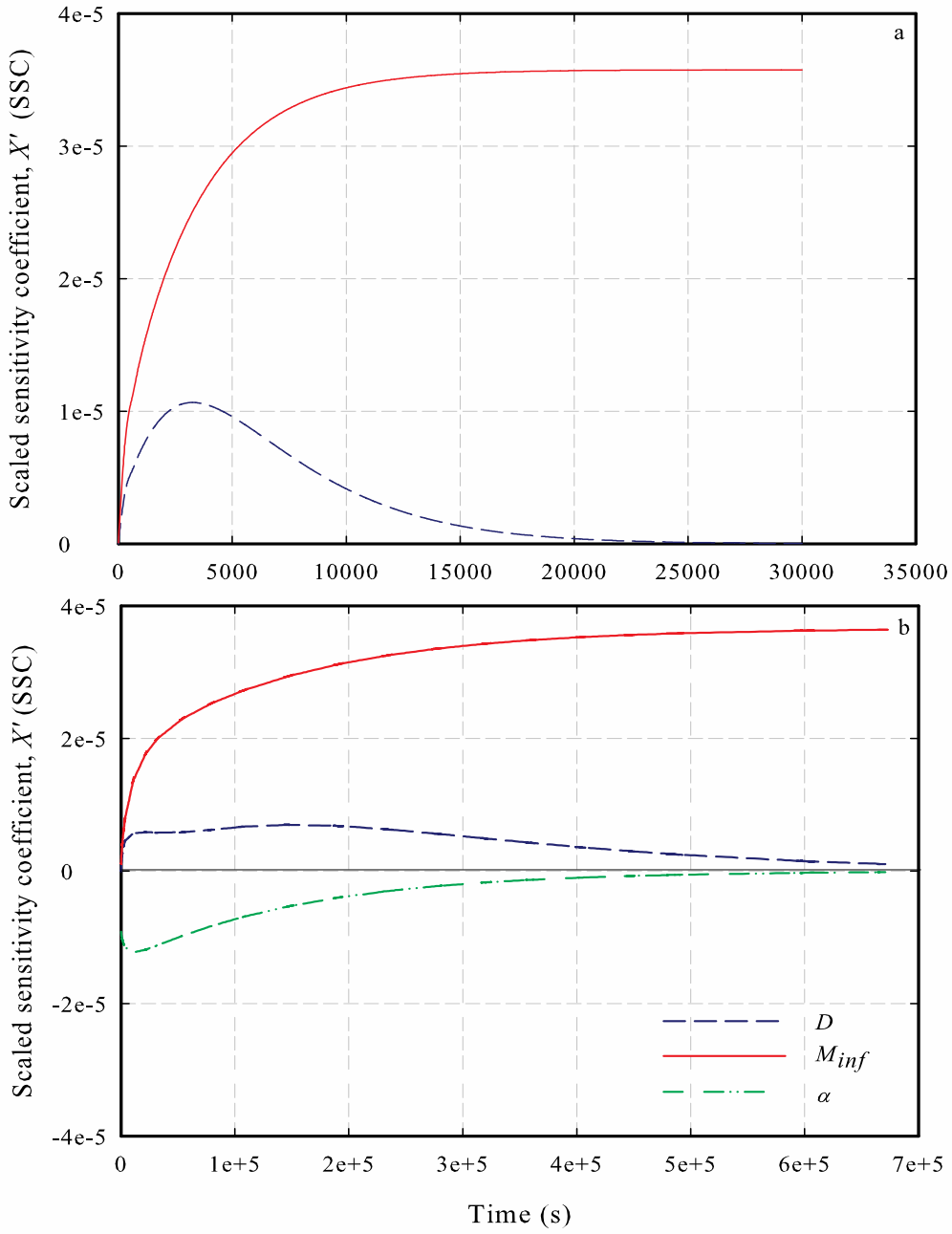

Figure 4-4 (a) Final scaled sensitivity coefficients for 2P, and (b) for 3P of migration study of PLA-α-tocopherol system at 23 °C using forward difference approximation. Estimated values used for 2P were: D= 4.05 × 10^{-10} cm^2/s, M_{inf}=0.36 × 10^{-4} g α-tocopherol/g ethanol. Estimated values used for 3P were: D= 0.79 × 10^{-10} cm^2/s, M_{inf}=0.37 × 10^{-4} g α-tocopherol/g ethanol, and α=0.30.

4.2.1.3 Optimal Experimental Design

A plot of the optimal experimental design for 2P was constructed to demonstrate the sufficient time required for collecting observational data with increased parameters' accuracy (Figure 4-5). It was observed that the required time to collect enough data to obtain the best estimates of D and M_∞ was approximately 2 d and 8 d, respectively. However, it was also apparent that the delta (Δ) was maximized at approximately 8 d, which suggested that to estimate both parameters simultaneously, at least 8 d of experimental duration was needed. Therefore, it can be concluded that both the X' and the optimal experimental design were in agreement, and were informative and beneficial for designing experimental plans.

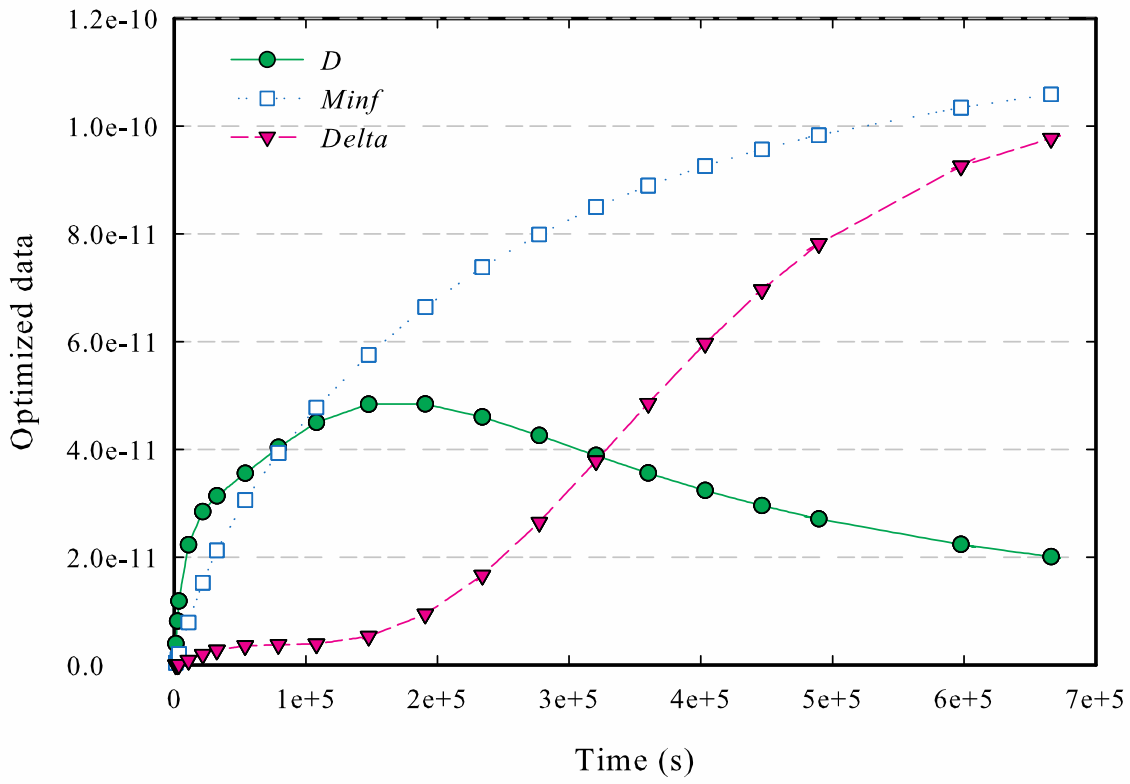

Figure 4-5 Optimal experimental designs for 2P of migration study of PLA-α-tocopherol system at 23 °C.

4.2.2 Other Case Studies

Other case studies are summarized in Table 4-1. All data were extracted from published and unpublished works from our research group and reanalyzed to showcase different scenarios of migration of antioxidants from PLA-based films into food simulants based on the parameter estimation approach (Table 4-1). Overall, the introduction of more than one parameter did show an improvement in models by resulting in a significant decrease in RMSE. However, in some cases (*i.e.*, PLA-catechin at 20 °C, PLA-epicatechin at 20 °C, and PLA-rutin at 40 °C), a detail observation is needed due to the high correlation coefficient values obtained (>0.93), which could affect the accuracy of estimating those parameters (*i.e.*, D and M_∞. It was also observed that there

was not much difference between the AICc values when comparing 1P versus 2P estimations. This indicates that the additional parameter of M_∞ might not really contribute much to the overall physical interpretation of the experiments.

In addition, the optimal experimental design was found useful to predict the sufficient time needed for an experiment to be able to accurately estimate parameters of interest. For example, in the case of PLA-3 wt. % resveratrol at 23 °C, the experiment was performed beyond necessary since it was found the time needed for this experiment is actually around 17 d instead of 43 d. In contrast, PLA-3 wt. % resveratrol at 9 °C that was performed for 278 d, longer experimental time (417 d) is needed in order to achieve better estimation of all parameters. Thus, optimal experimental design should be implemented to efficiently use the resources (*i.e.*, cost and labor) with compromising the accuracy of the parameters estimated.

Table 4-1 Summarized of estimated parameters for different migration studies of antioxidant-PLA film systems.

Case studies					
PLA-α-tocopherol (L= 5.46 × 10^{-3} cm) (Manzanarez-López et al., 2011)					
Temperature (°C)	**Number of estimation (P)**	**Criteria estimated**	***D*** **× 10^{-10} (cm^2/s)**	***M_∞*** **× 10^{-4} g AOx/g ETOH**	***α***
23	1P	Estimated value ± Standard error	1.0582 ± 0.036[a]		
α=0.366		(95% Asymptotic CI)	(0.987-1.129)		
		RMSE ×10^{-6} (g AOx/g ETOH)	1.5107		
		Relative error	0.034		
		Correlation coefficient, ρ		NA	
		AICc		-2249	

Table 4-1 (Cont'd)

Case studies					
PLA-α-tocopherol (L= 5.46 × 10^{-3} cm) (Manzanarez-López et al., 2011)					
Temperature (°C)	**Number of estimation (P)**	**Criteria estimated**	***D*** **× 10^{-10} (cm^2/s)**	***M_∞*** **× 10^{-4} g AOx/g ETOH**	***α***
23	2P	Estimated value ± Standard error	4.5025 ± 0.23[b]	0.3576 ± 0.0033[1]	
α=0.366		(95% Asymptotic CI)	(4.037-4.968)	(0.3511-0.3641)	
		RMSE ×10^{-6} (g AOx/g ETOH)	1.5153		
		Relative error	0.052	0.009	
		Correlation coefficient, ρ	0.7507		
		AICc	-2247		

Table 4-1 (Cont'd)

Case studies					
PLA-α-tocopherol (L= 5.46 × 10^{-3} cm) (Manzanarez-López et al., 2011)					
Temperature (°C)	**Number of estimation (P)**	**Criteria estimated**	***D*** **× 10^{-10} (cm^2/s)**	***M_∞*** **× 10^{-4} g AOx/g ETOH**	***α***
23	3P	Estimated value ± Standard error	0.7894 ± 0.076[a]	0.3664 ± 0.0044[1]	0.3034 ± 0.012
α=0.366		(95% Asymptotic CI)	(0.638-0.941)	(0.3577-0.3751)	(0.28-0.3268)
		RMSE ×10^{-6} (g AOx/g ETOH)		1.322	
		Relative error	0.0963	0.012	0.0387
		Correlation coefficient, ρ		0.8627; 0.8132; 0.5560	
		AICc		-2269	

Table 4-1 (Cont'd)

Case studies					
PLA-α-tocopherol (L= 5.46 × 10^{-3} cm) (Manzanarez-López et al., 2011)					
Temperature (°C)	**Number of estimation (P)**	**Criteria estimated**	**$D \times 10^{-10}$ (cm^2/s)**	**$M_\infty \times 10^{-4}$ g AOx/g ETOH**	**α**
33	1P	Estimated value ± Standard error	0.4855 ± 0.036[a]		
α=2.5306		(95% Asymptotic CI)	(0.4185-0.5525)		
		RMSE $\times 10^{-6}$ (g AOx/g ETOH)	9.050		
		Relative error	0.0691		
		Correlation coefficient, ρ		NA	
		AICc		-1576	

Table 4-1 (Cont'd)

Case studies					
PLA-α-tocopherol (L= 5.46 × 10^{-3} cm) (Manzanarez-López et al., 2011)					
Temperature (°C)	**Number of estimation (P)**	**Criteria estimated**	***D*** **× 10^{-10} (cm^2/s)**	***M_∞*** **× 10^{-4} g AOx/g ETOH**	***α***
33	2P	Estimated value ± Standard error	0.4857 ± 0.0055[a]	0.9251 ± 0.027	
α=2.5306		(95% Asymptotic CI)	(0.3753-0.5962)	(0.8701-0.98)	
		RMSE ×10^{-6} (g AOx/g ETOH)	9.118		
		Relative error	0.1139	0.0298	
		Correlation coefficient, ρ	0.7912		
		AICc	-1574		

Table 4-1 (Cont'd)

Case studies					
PLA-α-tocopherol (L= 5.46 × 10^{-3} cm) (Manzanarez-López et al., 2011)					
Temperature (°C)	**Number of estimation (P)**	**Criteria estimated**	**$D \times 10^{-10}$ (cm^2/s)**	**$M_\infty \times 10^{-4}$ g AOx/g ETOH**	**α**
43	1P	Estimated value ± Standard error	3.8023 ± 0.2298[a]		
α=108.38		(95% Asymptotic CI)	(3.343-4.262)		
		RMSE ×10^{-6} (g AOx/g ETOH)	9.4088		
		Relative error	0.0604		
		Correlation coefficient, ρ		NA	
		AICc		-1386	

Table 4-1 (Cont'd)

Case studies					
PLA-α-tocopherol (L= 5.46 × 10^{-3} cm) (Manzanarez-López et al., 2011)					
Temperature (°C)	**Number of estimation (P)**	**Criteria estimated**	***D*** **× 10^{-10} (cm^2/s)**	***M_∞*** **× 10^{-4} g AOx/g ETOH**	***α***
43	2P	Estimated value ± Standard error	3.8038 ± 0.288 [a]	1.3179 ± 0.0205	
α=108.38		(95% Asymptotic CI)	(3.2256-4.3820)	(1.2769-1.3588)	
		RMSE ×10^{-6} (g AOx/g ETOH)	9.4896		
		Relative error	0.0759	0.0155	
		Correlation coefficient, ρ	0.5966		
		AICc	-1383		

Table 4-1 (Cont'd)

Case studies					
PLA-BHT (L= 5.08 × 10^{-3} cm) (Ortiz-Vazquez et al., 2011)					
Temperature (°C)	**Number of estimation (P)**	**Criteria estimated**	***D*** **× 10^{-10} (cm^2/s)**	***M_∞*** **× 10^{-4} g AOx/g 95%ETOH**	***α***
23	1P	Estimated value ± Standard error	0.2224 ± 0.0103[a]		
α=2.1961		(95% Asymptotic CI)	(0.2017-0.2430)		
		RMSE ×10^{-6} (g AOx/g ETOH)	9.3148		
		Relative error	0.0464		
		Correlation coefficient, ρ		NA	
		AICc		-1480	

Table 4-1 (Cont'd)

Case studies					
PLA-BHT (L= 5.08 × 10^{-3} cm) (Ortiz-Vazquez et al., 2011)					
Temperature (°C)	**Number of estimation (P)**	**Criteria estimated**	***D*** **× 10^{-10} (cm^2/s)**	***M_∞*** **× 10^{-4} g AOx/g 95%ETOH**	***α***
23	2P	Estimated value ± Standard error	0.223 ± 0.013[a]	1.622 ± 0.018	
α=2.1961		(95% Asymptotic CI)	(0.1966-0.2485)	(1.5840-1.6591)	
		RMSE ×10^{-6} (g AOx/g ETOH)	9.3896		
		Relative error	0.0583	0.0116	
		Correlation coefficient, ρ	0.596		
		AICc	-1477		

Table 4-1 (Cont'd)

Case studies					
PLA-BHT (L= 5.08 × 10^{-3} cm) (Ortiz-Vazquez et al., 2011)					
Temperature (°C)	**Number of estimation (P)**	**Criteria estimated**	***D*** **× 10^{-10} (cm^2/s)**	***M_∞*** **× 10^{-4} g AOx/g 95%ETOH**	***α***
33	1P	Estimated value ± Standard error	0.6780 ± 0.0483[a]		
α=6.5384		(95% Asymptotic CI)	(0.5820-0.7741)		
		RMSE ×10^{-6} (g AOx/g ETOH)	19.3447		
		Relative error	0.0712		
		Correlation coefficient, ρ		NA	
		AICc		-1798	

Table 4-1 (Cont'd)

Case studies					
PLA-BHT (L= 5.08 × 10^{-3} cm) (Ortiz-Vazquez et al., 2011)					
Temperature (°C)	**Number of estimation (P)**	**Criteria estimated**	***D*** **× 10^{-10} (cm^2/s)**	***M_∞*** **× 10^{-4} g AOx/g 95%ETOH**	***α***
33	2P	Estimated value ± Standard error	0.678 ± 0.06[a]	2.085 ± 0.034	
α=6.5384		(95% Asymptotic CI)	(0.5586-0.7975)	(2.0174-2.1527)	
		RMSE ×10^{-6} (g AOx/g ETOH)	19.464		
		Relative error	0.0866	0.0163	
		Correlation coefficient, ρ	0.588		
		AICc	-1796		

Table 4-1 (Cont'd)

Case studies					
PLA-BHT (L= 5.08 × 10^{-3} cm) (Ortiz-Vazquez et al., 2011)					
Temperature (°C)	**Number of estimation (P)**	**Criteria estimated**	***D*** **× 10^{-10} (cm^2/s)**	***M_∞*** **× 10^{-4} g AOx/g 95%ETOH**	***α***
43	1P	Estimated value ± Standard error	19.0376 ± 0.5073[a]		
α=10.6506		(95% Asymptotic CI)	(18.032-20.044)		
		RMSE ×10^{-6} (g AOx/g ETOH)	8.2746		
		Relative error	0.0267		
		Correlation coefficient, ρ		NA	
		AICc		-2431	

Table 4-1 (Cont'd)

Case studies					
PLA-BHT (L= 5.08 × 10^{-3} cm) (Ortiz-Vazquez et al., 2011)					
Temperature (°C)	**Number of estimation (P)**	**Criteria estimated**	***D*** **× 10^{-10} (cm^2/s)**	***M_∞*** **× 10^{-4} g AOx/g 95%ETOH**	***α***
43	2P	Estimated value ± Standard error	19.04 ± 0.617[a]	1.9635 ± 0.011	
α=10.6506		(95% Asymptotic CI)	(17.812-20.26)	(1.9414-1.9857)	
		RMSE ×10^{-6} (g AOx/g ETOH)	8.3151		
		Relative error	0.0324	0.0057	
		Correlation coefficient, ρ	0.5639		
		AICc	-2429		

Table 4-1 (Cont'd)

Case studies					
PLA-catechin (L= 6.49 × 10^{-3} cm) (Iñiguez-Franco et al., 2012)					
Temperature (°C)	**Number of estimation (P)**	**Criteria estimated**	***D*** **× 10^{-10} (cm^2/s)**	***M_∞*** **× 10^{-4} g AOx/g 95%ETOH**	***α***
20	1P	Estimated value ± Standard error	0.4329 ± 0.016[a]		
α=0.36		(95% Asymptotic CI)	(0.4006-0.4652)		
		RMSE×10^{-6} (g AOx/g ETOH)	0.2095		
		Relative error	0.0371		
		Correlation coefficient, ρ		NA	
		AICc		-1473	

Table 4-1 (Cont'd)

Case studies					
PLA-catechin (L= 6.49 × 10^{-3} cm) (Iñiguez-Franco et al., 2012)					
Temperature (°C)	**Number of estimation (P)**	**Criteria estimated**	***D*** **× 10^{-10} (cm^2/s)**	***M_∞*** **× 10^{-4} g AOx/g 95%ETOH**	***α***
20	2P	Estimated value ± Standard error	0.407 ± 0.051[a]	0.049 ± 0.0016 [1]	
α=0.36		(95% Asymptotic CI)	(0.304-0.511)	(0.046-0.052)	
		RMSE ×10^{-6} (g AOx/g ETOH)	0.211		
		Relative error	0.126	0.033	
		Correlation coefficient, ρ	0.9572		
		AICc	-1471		

Table 4-1 (Cont'd)

Case studies					
PLA-catechin (L= 6.49 × 10^{-3} cm) (Iñiguez-Franco et al., 2012)					
Temperature (°C)	**Number of estimation (P)**	**Criteria estimated**	***D*** **× 10^{-10} (cm^2/s)**	***M_∞*** **× 10^{-4} g AOx/g 95%ETOH**	***α***
20	3P	Estimated value ± Standard error	0.4794 ± 0.11[a]	0.0476 ± 0.0021[1]	0.3869 ± 0.0288
α=0.36		(95% Asymptotic CI)	(0.2638-0.6949)	(0.0434-0.0518)	(0.329-0.4448)
		RMSE ×10^{-6} (g AOx/g ETOH)		0.2095	
		Relative error	0.2233	0.0434	0.0743
		Correlation coefficient, ρ		0.9623; 0.8763;0.7661	
		AICc		-1471	

Table 4-1 (Cont'd)

Case studies					
PLA-catechin (L= 6.49 × 10^{-3} cm) (Iñiguez-Franco et al., 2012)					
Temperature (°C)	**Number of estimation (P)**	**Criteria estimated**	***D*** **× 10^{-10} (cm^2/s)**	***M_∞*** **× 10^{-4} g AOx/g 95%ETOH**	***α***
30	1P	Estimated value ± Standard error	0.9734 ± 0.1016[a]		
α=5.33		(95% Asymptotic CI)	(0.7683-1.1785)		
		RMSE ×10^{-6} (g AOx/g ETOH)	1.9495		
		Relative error	0.104		
		Correlation coefficient, ρ		NA	
		AICc		-1101	

Table 4-1 (Cont'd)

Case studies					
PLA-catechin (L= 6.49 × 10^{-3} cm) (Iñiguez-Franco et al., 2012)					
Temperature (°C)	**Number of estimation (P)**	**Criteria estimated**	***D*** **× 10^{-10} (cm^2/s)**	***M_∞*** **× 10^{-4} g AOx/g 95%ETOH**	***α***
30	2P	Estimated value ± Standard error	0.9744 ± 0.131[a]	0.2234 ± 0.005	
α=5.33		(95% Asymptotic CI)	(0.7105-1.238)	(0.2126-0.2342)	
		RMSE ×10^{-6} (g AOx/g ETOH)	1.974		
		Relative error	0.134	0.0239	
		Correlation coefficient, ρ	0.6153		
		AICc	-1099		

Table 4-1 (Cont'd)

Case studies					
PLA-catechin (L= 6.49 × 10^{-3} cm) (Iñiguez-Franco et al., 2012)					
Temperature (°C)	**Number of estimation (P)**	**Criteria estimated**	***D*** **× 10^{-10} (cm^2/s)**	***M_∞*** **× 10^{-4} g AOx/g 95%ETOH**	***α***
40	1P	Estimated value ± Standard error	6.8511 ± 0.276[a]		
α=158.09		(95% Asymptotic CI)	(6.289-7.413)		
		RMSE ×10^{-6} (g AOx/g ETOH)	0.9691		
		Relative error	0.0403		
		Correlation coefficient, ρ		NA	
		AICc		-911	

Table 4-1 (Cont'd)

Case studies					
PLA-catechin (L= 6.49 × 10^{-3} cm) (Iñiguez-Franco et al., 2012)					
Temperature (°C)	**Number of estimation (P)**	**Criteria estimated**	***D*** **× 10^{-10} (cm^2/s)**	***M_∞*** **× 10^{-4} g AOx/g 95%ETOH**	***α***
40	2P	Estimated value ± Standard error	6.853 ± 0.3895[a]	0.2438 ± 0.0032	
α=158.09		(95% Asymptotic CI)	(6.0581-7.647)	(0.2373-0.2503)	
		RMSE ×10^{-6} (g AOx/g ETOH)	0.9846		
		Relative error	0.0568	0.0131	
		Correlation coefficient, ρ	0.6939		
		AICc	-908		

Table 4-1 (Cont'd)

Case studies					
PLA-catechin (L= 6.49 × 10^{-3} cm) (Iñiguez-Franco et al., 2012)					
Temperature (°C)	**Number of estimation (P)**	**Criteria estimated**	***D* × 10^{-10} (cm^2/s)**	***M_∞*× 10^{-4} g AOx/g 95%ETOH**	***α***
50	1P	Estimated value ± Standard error	3.7609 ± 0.1525[a]		
α=220.96		(95% Asymptotic CI)	(3.449-4.073)		
		RMSE×10^{-6} (g AOx/g ETOH)	1.2862		
		Relative error	0.0406		
		Correlation coefficient, ρ		NA	
		AICc		-810	

Table 4-1 (Cont'd)

Case studies					
PLA-catechin (L= 6.49 × 10^{-3} cm) (Iñiguez-Franco et al., 2012)					
Temperature (°C)	**Number of estimation (P)**	**Criteria estimated**	***D*** **× 10^{-10} (cm^2/s)**	***M_∞*** **× 10^{-4} g AOx/g 95%ETOH**	***α***
50	2P	Estimated value ± Standard error	3.769 ± 0.396[a]	0.271± 0.009	
α=220.96		(95% Asymptotic CI)	(2.9582-4.5806)	(0.252-0.2895)	
		RMSE ×10^{-6} (g AOx/g ETOH)	1.3089		
		Relative error	0.1051	0.0337	
		Correlation coefficient, ρ	0.9194		
		AICc	-808		

Table 4-1 (Cont'd)

Case studies					
PLA-catechin (L= 6.49 × 10^{-3} cm) (Iñiguez-Franco et al., 2012)					
Temperature (°C)	**Number of estimation (P)**	**Criteria estimated**	***D*** **× 10^{-10} (cm^2/s)**	***M_∞*** **× 10^{-4} g AOx/g 95%ETOH**	***α***
*40	1P	Estimated value ± Standard error	0.8840 ± 0.04[a]		
α=3.97		(95% Asymptotic CI)	(0.799-0.9693)		
		RMSE ×10^{-6} (g AOx/g ETOH)	0.6394		
		Relative error	0.0478		
		Correlation coefficient, ρ		NA	
		AICc		-1195	

Table 4-1 (Cont'd)

Case studies					
PLA-catechin (L= 6.49 × 10^{-3} cm) (Iñiguez-Franco et al., 2012)					
Temperature (°C)	**Number of estimation (P)**	**Criteria estimated**	***D*** **× 10^{-10} (cm^2/s)**	***M_∞*** **× 10^{-4} g AOx/g 95%ETOH**	***α***
*40	2P	Estimated value ± Standard error	0.8831 ± 0.0744[a]	0.1136 ± 0.0029	
α=3.97		(95% Asymptotic CI)	(0.7328-1.033)	(0.1077-0.1196)	
		RMSE ×10^{-6} (g AOx/g ETOH)	0.065		
		Relative error	0.0842	0.0258	
		Correlation coefficient, ρ	0.8187		
		AICc	-1192		

Table 4-1 (Cont'd)

Case studies					
PLA-epicatechin (L= 6.19 × 10^{-3} cm) (Iñiguez-Franco et al., 2012)					
Temperature (°C)	**Number of estimation (P)**	**Criteria estimated**	***D*** **× 10^{-10} (cm^2/s)**	***M_∞*** **× 10^{-4} g AOx/g 95%ETOH**	***α***
20	1P	Estimated value ± Standard error	0.3492 ± 0.013[a]		
α=0.32		(95% Asymptotic CI)	(0.3229-0.3755)		
		RMSE ×10^{-6} (g AOx/g ETOH)	0.1952		
		Relative error	0.0374		
		Correlation coefficient, ρ		NA	
		AICc		-1387	

Table 4-1 (Cont'd)

Case studies					
PLA-epicatechin (L= 6.19 × 10^{-3} cm) (Iñiguez-Franco et al., 2012)					
Temperature (°C)	**Number of estimation (P)**	**Criteria estimated**	***D*** **× 10^{-10} (cm^2/s)**	***M_∞*** **× 10^{-4} g AOx/g 95%ETOH**	***α***
20	2P	Estimated value ± Standard error	0.3226 ± 0.048[a]	0.04795 ± 0.0018[1]	
α=0.32		(95% Asymptotic CI)	(0.2246-0.4206)	(0.0443-0.05161)	
		RMSE ×10^{-6} (g AOx/g ETOH)	0.197		
		Relative error	0.1507	0.0378	
		Correlation coefficient, ρ	0.97		
		AICc	-1385		

Table 4-1 (Cont'd)

Case studies					
PLA-epicatechin (L= 6.19 × 10^{-3} cm) (Iñiguez-Franco et al., 2012)					
Temperature (°C)	**Number of estimation (P)**	**Criteria estimated**	***D*** **× 10^{-10} (cm^2/s)**	***M_∞*** **× 10^{-4} g AOx/g 95%ETOH**	***α***
20	3P	Estimated value ± Standard error	0.525 ± 0.091[b]	0.044 ± 0.0013[1]	0.3767 ± 0.026
α=0.32		(95% Asymptotic CI)	(0.3415-0.709)	(0.042-0.047)	(0.3251-0.4284)
		RMSE ×10^{-6} **(**g AOx/g ETOH)		0.1886	
		Relative error	0.1734	0.0296	0.068
		Correlation coefficient, ρ		0.932; 0.8318; 0.6599	
		AICc		-1388	

Table 4-1 (Cont'd)

Case studies					
PLA-epicatechin (L= 6.19 × 10^{-3} cm) (Iñiguez-Franco et al., 2012)					
Temperature (°C)	**Number of estimation (P)**	**Criteria estimated**	***D*** **× 10^{-10} (cm^2/s)**	***M_∞*** **× 10^{-4} g AOx/g 95%ETOH**	***α***
30	1P	Estimated value ± Standard error	1.168 ± 0.122[a]		
α=3.68		(95% Asymptotic CI)	(0.9195-1.4161)		
		RMSE×10^{-6} (g AOx/g ETOH)	1.5292		
		Relative error	0.105		
		Correlation coefficient, ρ		NA	
		AICc		-961	

Table 4-1 (Cont'd)

Case studies					
PLA-epicatechin (L= 6.19 × 10^{-3} cm) (Iñiguez-Franco et al., 2012)					
Temperature (°C)	**Number of estimation (P)**	**Criteria estimated**	***D*** **× 10^{-10} (cm^2/s)**	***M_∞*** **× 10^{-4} g AOx/g 95%ETOH**	***α***
30	2P	Estimated value ± Standard error	1.168 ± 0.143[a]	0.1824 ± 0.004	
α=3.68		(95% Asymptotic CI)	(0.8764-1.460)	(0.1748-0.1899)	
		RMSE ×10^{-6} (g AOx/g ETOH)	1.5515		
		Relative error	0.123	0.0204	
		Correlation coefficient, ρ	0.5021		
		AICc	-958		

Table 4-1 (Cont'd)

Case studies					
PLA-epicatechin (L= 6.19 × 10^{-3} cm) (Iñiguez-Franco et al., 2012)					
Temperature (°C)	**Number of estimation (P)**	**Criteria estimated**	***D*** **× 10^{-10} (cm^2/s)**	***M_∞*** **× 10^{-4} g AOx/g 95%ETOH**	***α***
40	1P	Estimated value ± Standard error	5.349 ± 0.214[a]		
α=94.08		(95% Asymptotic CI)	(4.912-5.785)		
		RMSE ×10^{-6} (g AOx/g ETOH)	1.003		
		Relative error	0.040		
		Correlation coefficient, ρ		NA	
		AICc		-908	

Table 4-1 (Cont'd)

Case studies					
PLA-epicatechin (L= 6.19 × 10^{-3} cm) (Iñiguez-Franco et al., 2012)					
Temperature (°C)	**Number of estimation (P)**	**Criteria estimated**	***D*** **× 10^{-10} (cm^2/s)**	***M_∞*** **× 10^{-4} g AOx/g 95%ETOH**	***α***
40	2P	Estimated value ± Standard error	5.348 ± 0.3023[a]	0.2538 ± 0.003	
α=94.08		(95% Asymptotic CI)	(4.732-5.965)	(0.2471-0.2605)	
		RMSE ×10^{-6} (g AOx/g ETOH)	1.019		
		Relative error	0.057	0.013	
		Correlation coefficient, ρ	0.6943		
		AICc	-906		

Table 4-1 (Cont'd)

Case studies					
PLA-epicatechin (L= 6.19 × 10^{-3} cm) (Iñiguez-Franco et al., 2012)					
Temperature (°C)	**Number of estimation (P)**	**Criteria estimated**	***D*** **× 10^{-10} (cm^2/s)**	***M_∞*** **× 10^{-4} g AOx/g 95%ETOH**	***α***
*40	1P	Estimated value ± Standard error	0.7746 ± 0.032[a]		
α=32.23		(95% Asymptotic CI)	(0.7104-0.8388)		
		RMSE ×10^{-6} (g AOx/g ETOH)	5.6021		
		Relative error	0.041		
		Correlation coefficient, ρ		NA	
		AICc		-1206	

Table 4-1 (Cont'd)

Case studies					
PLA-epicatechin (L= 6.19 × 10^{-3} cm) (Iñiguez-Franco et al., 2012)					
Temperature (°C)	**Number of estimation (P)**	**Criteria estimated**	***D*** **× 10^{-10} (cm^2/s)**	***M_∞*** **× 10^{-4} g AOx/g 95%ETOH**	***α***
*40	2P	Estimated value ± Standard error	0.7751 ± 0.0547[a]	0.1113 ± 0.0023	
α=32.23		(95% Asymptotic CI)	(0.6644-0.8857)	(0.1067-0.1159)	
		RMSE ×10^{-6} (g AOx/g ETOH)	0.5672		
		Relative error	0.0706	0.0203	
		Correlation coefficient, ρ	0.8085		
		AICc	-1204		

Table 4-1 (Cont'd)

Case studies					
PLA-Resveratrol 1% (L= 5.08 × 10^{-3} cm) (Soto-Valdez et al., 2010)					
Temperature (°C)	**Number of estimation (P)**	**Criteria estimated**	***D*** **× 10^{-10} (cm^2/s)**	***M_∞*** **× 10^{-4} g AOx/g 95%ETOH**	***α***
23	1P	Estimated value ± Standard error	0.2389 ± 0.0033[a]		
α=2.877		(95% Asymptotic CI)	(0.232-0.245)		
		RMSE×10^{-6} (g AOx/g ETOH)	0.666		
		Relative error	0.0140		
		Correlation coefficient, ρ		NA	
		AICc		-1817	

Table 4-1 (Cont'd)

Case studies					
PLA-Resveratrol 1% (L= 5.08 × 10^{-3} cm) (Soto-Valdez et al., 2010)					
Temperature (°C)	**Number of estimation (P)**	**Criteria estimated**	***D*** **× 10^{-10} (cm^2/s)**	***M_∞*** **× 10^{-4} g AOx/g 95%ETOH**	***α***
23	2P	Estimated value ± Standard error	0.2385 ± 0.0048[a]	0.3562 ± 0.0015	
α=2.877		(95% Asymptotic CI)	(0.2289-0.2480)	(0.3531-0.3593)	
		RMSE ×10^{-6} (g AOx/g ETOH)	0.671		
		Relative error	0.02	0.0043	
		Correlation coefficient, ρ	0.7113		
		AICc	-1815		

Table 4-1 (Cont'd)

Case studies					
PLA-Resveratrol 1% (L= 5.08 × 10^{-3} cm) (Soto-Valdez et al., 2010)					
Temperature (°C)	**Number of estimation (P)**	**Criteria estimated**	***D*** **× 10^{-10} (cm^2/s)**	***M_∞*** **× 10^{-4} g AOx/g 95%ETOH**	***α***
33	1P	Estimated value ± Standard error	2.8025 ± 0.184[a]		
α=17.74		(95% Asymptotic CI)	(2.4359-3.1692)		
		RMSE ×10^{-6} (g AOx/g ETOH)	3.5020		
		Relative error	0.0655		
		Correlation coefficient, ρ		NA	
		AICc		-1705	

Table 4-1 (Cont'd)

Case studies					
PLA-Resveratrol 1% (L= 5.08 × 10^{-3} cm) (Soto-Valdez et al., 2010)					
Temperature (°C)	**Number of estimation (P)**	**Criteria estimated**	***D*** **× 10^{-10} (cm^2/s)**	***M_∞*** **× 10^{-4} g AOx/g 95%ETOH**	***α***
33	2P	Estimated value ± Standard error	2.8036 ± 0.21[a]	0.4708 ± 0.0056	
α=17.74		(95% Asymptotic CI)	(2.384-3.223)	(0.4596-0.4819)	
		RMSE ×10^{-6} (g AOx/g ETOH)		3.5284	
		Relative error	0.075	0.012	
		Correlation coefficient, ρ		0.4735	
		AICc		-1703	

Table 4-1 (Cont'd)

Case studies					
PLA-Resveratrol 1% (L= 5.08 × 10^{-3} cm) (Soto-Valdez et al., 2010)					
Temperature (°C)	**Number of estimation (P)**	**Criteria estimated**	***D*** **× 10^{-10} (cm^2/s)**	***M_∞*** **× 10^{-4} g AOx/g 95%ETOH**	***α***
43	1P	Estimated value ± Standard error	9.5287 ± 0.4481[a]		
α=51.99		(95% Asymptotic CI)	(8.627-10.430)		
		RMSE ×10^{-6} (g AOx/g ETOH)	1.956		
		Relative error	0.047		
		Correlation coefficient, ρ		NA	
		AICc		-1259	

Table 4-1 (Cont'd)

Case studies					
PLA-Resveratrol 1% (L= 5.08 × 10^{-3} cm) (Soto-Valdez et al., 2010)					
Temperature (°C)	**Number of estimation (P)**	**Criteria estimated**	***D*** **× 10^{-10} (cm^2/s)**	***M_∞*** **× 10^{-4} g AOx/g 95%ETOH**	***α***
43	2P	Estimated value ± Standard error	9.56 ± 0.56[a]	0.421 ± 0.004	
α=51.99		(95% Asymptotic CI)	(8.44-10.68)	(0.4128-0.4285)	
		RMSE ×10^{-6} (g AOx/g ETOH)		1.977	
		Relative error	0.0581	0.0093	
		Correlation coefficient, ρ		0.5733	
		AICc		-1256	

Table 4-1 (Cont'd)

Case studies					
PLA-Resveratrol 3% (L= 5.08 × 10^{-3} cm) (Soto-Valdez et al., 2010)					
Temperature (°C)	**Number of estimation (P)**	**Criteria estimated**	***D*** **× 10^{-10} (cm^2/s)**	***M_∞*** **× 10^{-4} g AOx/g 95%ETOH**	***α***
23	1P	Estimated value ± Standard error	0.3988 ± 0.017[a]		
α=2.099		(95% Asymptotic CI)	(0.3649-0.4327)		
		RMSE ×10^{-6} (g AOx/g ETOH)	4.6825		
		Relative error	0.0423		
		Correlation coefficient, ρ		NA	
		AICc		-1666	

Table 4-1 (Cont'd)

Case studies					
PLA-Resveratrol 3% (L= 5.08 × 10^{-3} cm) (Soto-Valdez et al., 2010)					
Temperature (°C)	**Number of estimation (P)**	**Criteria estimated**	***D*** **× 10^{-10} (cm^2/s)**	***M_∞*** **× 10^{-4} g AOx/g 95%ETOH**	***α***
23	2P	Estimated value ± Standard error	0.3988 ± 0.021[a]	0.9756 ± 0.0083	
α=2.099		(95% Asymptotic CI)	(0.3576-0.44)	(0.959-0.9921)	
		RMSE ×10^{-6} (g AOx/g ETOH)	4.7179		
		Relative error	0.0517	0.0085	
		Correlation coefficient, ρ	0.559		
		AICc	-1664		

Table 4-1 (Cont'd)

Case studies					
PLA-Resveratrol 3% (L= 5.08 × 10^{-3} cm) (Soto-Valdez et al., 2010)					
Temperature (°C)	**Number of estimation (P)**	**Criteria estimated**	***D*** **× 10^{-10} (cm^2/s)**	***M_∞*** **× 10^{-4} g AOx/g 95%ETOH**	***α***
33	1P	Estimated value ± Standard error	4.8085 ± 0.2960[a]		
α=9.855		(95% Asymptotic CI)	(4.2170-5.3999)		
		RMSE ×10^{-6} (g AOx/g ETOH)	8.0134		
		Relative error	0.06		
		Correlation coefficient, ρ		NA	
		AICc		-1499	

Table 4-1 (Cont'd)

Case studies					
PLA-Resveratrol 3% (L= 5.08 × 10^{-3} cm) (Soto-Valdez et al., 2010)					
Temperature (°C)	**Number of estimation (P)**	**Criteria estimated**	***D*** **× 10^{-10} (cm^2/s)**	***M_∞*** **× 10^{-4} g AOx/g 95%ETOH**	***α***
33	2P	Estimated value ± Standard error	4.8084 ± 0.3321[a]	1.2735 ± 0.013	
α=9.855		(95% Asymptotic CI)	(4.1446-5.4723)	(1.2484-1.2986)	
		RMSE ×10^{-6} (g AOx/g ETOH)	8.0778		
		Relative error	0.0691	0.0099	
		Correlation coefficient, ρ	0.4393		
		AICc	-1497		

Table 4-1 (Cont'd)

Case studies					
PLA-Resveratrol 3% (L= 5.08 × 10^{-3} cm) (Soto-Valdez et al., 2010)					
Temperature (°C)	**Number of estimation (P)**	**Criteria estimated**	***D*** **× 10^{-10} (cm^2/s)**	***M_∞*** **× 10^{-4} g AOx/g 95%ETOH**	***α***
43	1P	Estimated value ± Standard error	8.9965 ± 0.470[a]		
α=53.85		(95% Asymptotic CI)	(8.0508-9.9421)		
		RMSE×10^{-6} (g AOx/g ETOH)	7.2709		
		Relative error	0.052		
		Correlation coefficient, ρ		NA	
		AICc		-1133	

Table 4-1 (Cont'd)

Case studies					
PLA-Resveratrol 3% (L= 5.08 × 10^{-3} cm) (Soto-Valdez et al., 2010)					
Temperature (°C)	**Number of estimation (P)**	**Criteria estimated**	***D*** **× 10^{-10} (cm^2/s)**	***M_∞*** **× 10^{-4} g AOx/g 95%ETOH**	***α***
43	2P	Estimated value ± Standard error	8.9968 ± 0.5684[a]	1.2279 ± 0.015	
α=53.85		(95% Asymptotic CI)	(7.8527-10.14)	(1.1973-1.2585)	
		RMSE ×10^{-6} (g AOx/g ETOH)	7.3495		
		Relative error	0.0632	0.0124	
		Correlation coefficient, ρ	0.5487		
		AICc	-1130		

Table 4-1 (Cont'd)

Case studies					
PLA-Resveratrol 3% (L= 5.08 × 10^{-3} cm) (Soto-Valdez et al., 2010)					
Temperature (°C)	**Number of estimation (P)**	**Criteria estimated**	***D*** **× 10^{-10} (cm^2/s)**	***M*∞× 10^{-4} g AOx/g 95%ETOH**	***α***
**43	1P	Estimated value ± Standard error	8.9959 ± 0.4700[a]		
α=6.51		(95% Asymptotic CI)	(8.0503-9.9415)		
		RMSE ×10^{-6} (g AOx/g ETOH)	5.7834		
		Relative error	0.052		
		Correlation coefficient, ρ		NA	
		AICc		-1155	

Table 4-1 (Cont'd)

Case studies					
PLA-Resveratrol 3% (L= 5.08 × 10^{-3} cm) (Soto-Valdez et al., 2010)					
Temperature (°C)	**Number of estimation (P)**	**Criteria estimated**	***D*** **× 10^{-10} (cm^2/s)**	***M_∞*** **× 10^{-4} g AOx/g 95%ETOH**	***α***
**43	2P	Estimated value ± Standard error	8.9968 ± 0.5684[a]	0.9691 ± 0.012	
α=6.51		(95% Asymptotic CI)	(7.8527-10.14)	(0.945-0.993)	
		RMSE ×10^{-6} (g AOx/g ETOH)	5.8		
		Relative error	0.0632	0.0124	
		Correlation coefficient, ρ	0.5487		
		AICc	-1153		

Table 4-1 (Cont'd)

Case studies					
***PLA-Rutin (L= 4.83 × 10^{-3} cm)					
Temperature (°C)	**Number of estimation (P)**	**Criteria estimated**	***D*** **× 10^{-10} (cm^2/s)**	***M_∞*** **× 10^{-4} g AOx/g 95%ETOH**	***α***
40	1P	Estimated value ± Standard error	0.2127 ± 0.022[a]		
α=0.3693		(95% Asymptotic CI)	(0.1687-0.2567)		
		RMSE ×10^{-6} (g AOx/g ETOH)	0.5640		
		Relative error	0.1032		
		Correlation coefficient, ρ		NA	
		AICc		-1637	

Table 4-1 (Cont'd)

Case studies					
***PLA-Rutin (L= 4.83 × 10^{-3} cm)					
Temperature (°C)	**Number of estimation (P)**	**Criteria estimated**	***D*** **× 10^{-10} (cm^2/s)**	***M_∞*** **× 10^{-4} g AOx/g 95%ETOH**	***α***
40	2P	Estimated value ± Standard error	0.1003 ± 0.036[a]	0.052 ± 0.0068[1]	
α=0.3693		(95% Asymptotic CI)	(0.028-0.1726)	(0.0383-0.0657)	
		RMSE ×10^{-6} (g AOx/g ETOH)	0.5533		
		Relative error	0.3593	0.1313	
		Correlation coefficient, ρ	0.9699		
		AICc	-1638		

Table 4-1 (Cont'd)

Case studies					
***PLA-Rutin (L= 4.83 × 10^{-3} cm)					
Temperature (°C)	**Number of estimation (P)**	**Criteria estimated**	$D \times 10^{-10}$ **(cm^2/s)**	$M_\infty \times 10^{-4}$ **g AOx/g 95%ETOH**	α
40	3P	Estimated value ± Standard error	0.7695 ± 0.278[b]	0.0322 ± 0.0021[1]	0.8086 ± 0.4324
α=0.3693		(95% Asymptotic CI)	(0.2123-1.3267)	(0.028-0.036)	(0.0583-1.6756)
		RMSE ×10^{-6} (g AOx/g ETOH)		0.5514	
		Relative error	0.3611	0.0653	0.5348
		Correlation coefficient, ρ		0.8236; 0.8778; 0.5839	
		AICc		-1637	

Table 4-1 (Cont'd)

Case studies					
***PLA-Quercetin (L= 4.83 × 10^{-3} cm)					
Temperature (°C)	**Number of estimation (P)**	**Criteria estimated**	$D \times 10^{-10}$ **(cm^2/s)**	$M_\infty \times 10^{-4}$ **g AOx/g 95%ETOH**	α
40	1P	Estimated value ± Standard error	0.6248 ± 0.028[a]		
α=23.19		(95% Asymptotic CI)	(0.5670-0.6825)		
		RMSE ×10^{-6} (g AOx/g ETOH)	0.4262		
		Relative error	0.0463		
		Correlation coefficient, ρ		NA	
		AICc		-2021	

Table 4-1 (Cont'd)

Case studies					
***PLA-Quercetin (L= 4.83 × 10^{-3} cm)					
Temperature (°C)	**Number of estimation (P)**	**Criteria estimated**	***D*** **× 10^{-10} (cm^2/s)**	***M_∞*** **× 10^{-4} g AOx/g 95%ETOH**	***α***
40	2P	Estimated value ± Standard error	0.6362 ± 0.039[a]	0.061 ± 0.0008	
α=23.19		(95% Asymptotic CI)	(0.5584-0.7140)	(0.059-0.0623)	
		RMSE ×10^{-6} (g AOx/g ETOH)	0.4288		
		Relative error	0.0613	0.0135	
		Correlation coefficient, ρ	0.6402		
		AICc	-2019		

Table 4-1 (Cont'd)

Case studies					
PLA-Astaxanthin (L= 5.02 × 10^{-3} cm)					
Temperature (°C)	**Number of estimation (P)**	**Criteria estimated**	***D*** **× 10^{-10} (cm^2/s)**	***M_∞*** **× 10^{-8} g AOx/g 95%ETOH**	***α***
30	1P	Estimated value ± Standard error	1.269 ± 0.347[a]		
α=1.33		(95% Asymptotic CI)	(0.5694-1.9683)		
		RMSE ×10^{-6} (g AOx/g ETOH)	0.022		
		Relative error	0.2735		
		Correlation coefficient, ρ		NA	
		AICc		-1585	

Table 4-1 (Cont'd)

Case studies					
PLA-Astaxanthin (L= 5.02 × 10^{-3} cm)					
Temperature (°C)	**Number of estimation (P)**	**Criteria estimated**	***D*** **× 10^{-10} (cm^2/s)**	***M_∞*** **× 10^{-8} g AOx/g 95%ETOH**	***α***
30	2P	Estimated value ± Standard error	1.269 ± 0.4145[a]	9.8946 ± 0.637	
α=1.33		(95% Asymptotic CI)	(0.4332-2.1051)	(8.6086-11.18)	
		RMSE ×10^{-6} (g AOx/g ETOH)	0.022		
		Relative error	0.3266	0.0644	
		Correlation coefficient, ρ	0.5311		
		AICc	-1583		

Table 4-1 (Cont'd)

Case studies					
PLA-Astaxanthin (L= 5.02 × 10^{-3} cm)					
Temperature (°C)	**Number of estimation (P)**	**Criteria estimated**	**$D \times 10^{-10}$ (cm^2/s)**	**$M_\infty \times 10^{-8}$ g AOx/g 95%ETOH**	**α**
40	1P	Estimated value ± Standard error	2.2838 ± 0.299[a]		
α=4.92		(95% Asymptotic CI)	(1.6811-2.8864)		
		RMSE ×10^{-6} (g AOx/g ETOH)	0.014		
		Relative error	0.1309		
		Correlation coefficient, ρ		NA	
		AICc		-1623	

Table 4-1 (Cont'd)

Case studies					
PLA-Astaxanthin (L= 5.02 × 10^{-3} cm)					
Temperature (°C)	**Number of estimation (P)**	**Criteria estimated**	***D*** **× 10^{-10} (cm^2/s)**	***M_∞*** **× 10^{-8} g AOx/g 95%ETOH**	***α***
40	2P	Estimated value ± Standard error	2.2816 ± 0.4677[a]	10.12 ± 0.63	
α=4.92		(95% Asymptotic CI)	(1.3385-3.2247)	(8.861-11.39)	
		RMSE ×10^{-6} (g AOx/g ETOH)	0.014		
		Relative error	0.205	0.062	
		Correlation coefficient, ρ	0.7632		
		AICc	-1621		

* Simulant used was 50% ETOH.

** Simulant used was 100% water.

Table 4-1 (Cont'd)

*** Residuals for these studies did show a significant signature. The data needs to be log transformed to meet the standard statistical assumptions.

Remarks:

Values within a case study of a particular temperature in the same row with same alphabetic or numeric symbol are not statistically significantly different ($p>0.05$).

RMSE=Root mean square error.

4.3 Conclusion

Parameter estimation was implemented to analyze selected published and unpublished data for migration of antioxidant(s) from PLA-based polymeric films into fatty food simulants, and in limited cases into an aqueous food simulant based on 1P, 2P, and 3P estimations. Significant improvement in terms of meeting standard statistical assumptions was observed in the case where additional parameters were being considered for model fitting (*i.e.*, 3P estimation) based on the residual scatter plot, RMSE and the AICc observations. Initial X', and optimal experimental design were found helpful in predicting and designing the right time for collecting sufficient data to obtain better P estimates with lower errors. Models A and B presented in this chapter were successfully integrated into fitting the data. Even though model C was not considered in this chapter, the h as the third kinetic migration parameter cannot simply be neglected since it does control the overall resistance series in addition to D.

In the next chapter, three kinetic migration parameters, D, $K_{p,f}$ and h, are considered. The solutions of the migration models are expressed as functions of $K_{p,f}$ in place of α since it can be easily interpreted during the kinetics of migration phenomenon.

REFERENCES

REFERENCES

Barbosa-Pereira, L., Cruz, J. M., Sendón, R., Rodríguez Bernaldo de Quirós, A., Ares, A., Castro-López, M., . . . Paseiro-Losada, P. (2013). Development of antioxidant active films containing tocopherols to extend the shelf life of fish. *Food Control, 31*(1), 236-243.

Beck, J. V., & Arnold, K. J. (1977). *Parameter Estimation in Engineering and Science* (Vol. 8): Wiley New York.

Bird, R. B., Stewart, W. E., & Lightfoot, E. N. (2007). *Transport phenomena*: John Wiley & Sons.

Byun, Y., Kim, Y. T., & Whiteside, S. (2010). Characterization of an antioxidant polylactic acid (PLA) film prepared with α-tocopherol, BHT and polyethylene glycol using film cast extruder. *Journal of Food Engineering, 100*(2), 239-244.

Calatayud, M., López-de-Dicastillo, C., López-Carballo, G., Vélez, D., Muñoz, P. H., & Gavara, R. (2013). Active films based on cocoa extract with antioxidant, antimicrobial and biological applications. *Food Chemistry*.

Chen, X., Lee, D. S., Zhu, X., & Yam, K. L. (2012). Release kinetics of tocopherol and quercetin from binary antioxidant controlled-release packaging films. *Journal of Agricultural and Food Chemistry, 60*(13), 3492-3497.

Chung, D., Papadakis, S. E., & Yam, K. L. (2001). Release of propyl paraben from a polymer coating into water and food simulating solvents for antimicrobial packaging applications. *Journal of Food Processing and Preservation, 25*(1), 71-87.

Chung, D., Papadakis, S. E., & Yam, K. L. (2002). Simple models for assessing migration from food-packaging films. *Food Additives and Contaminants, 19*(6), 611-617.

Colín-Chávez, C., Soto-Valdez, H., Peralta, E., Lizardi-Mendoza, J., & Balandrán-Quintana, R. R. (2013). Diffusion of natural astaxanthin from polyethylene active packaging films into a fatty food simulant. *Food Research International, 54*(1), 873-880.

Colín-Chávez, C., Soto-Valdez, H., Peralta, E., Lizardi-Mendoza, J., & Balandrán-Quintana, R. R. (2013). Fabrication and Properties of Antioxidant Polyethylene-based Films Containing Marigold (Tagetes erecta) Extract and Application on Soybean Oil Stability. *Packaging Technology and Science, 26*(5), 267-280. doi: 10.1002/pts.1982

Crank, J. (1979). *The Mathematics of Diffusion* (2nd ed.). Bristol: Oxford University Press.

Dolan, K. D., & Mishra, D. K. (2013). Parameter estimation in food science. *The Annual Review of Food Science and Technology, 4*, 401-422.

Galotto, M. J., Torres, A., Guarda, A., Moraga, N., & Romero, J. (2011). Experimental and theoretical study of LDPE: Evaluation of different food simulants and temperatures. *Food Research International, 44*(9), 3072-3078.

Goncalves, C., Tomé, L. C., Garcia, H., Brandão, L., Mendes, A. M., & Marrucho, I. M. (2012). Effect of natural and synthetic antioxidants incorporation on the gas permeation properties of poly (lactic acid) films. *Journal of Food Engineering*.

Graciano-Verdugo, A. Z., Soto-Valdez, H., Peralta, E., Islas-Rubio, A. R., Sánchez-Valdes, S., Sánchez-Escalante, A., . . . González-Ríos, H. (2010). Migration of α-tocopherol from LDPE films to corn oil and its effect on the oxidative stability. *Food Research International, 43*(4), 1073-1078.

Granda-Restrepo, D. M., Soto-Valdez, H., Peralta, E., Troncoso-Rojas, R., Vallejo-Córdoba, B., Gámez-Meza, N., & Graciano-Verdugo, A. Z. (2009). Migration of α-tocopherol from an active multilayer film into whole milk powder. *Food Research International, 42*(10), 1396-1402.

Hamdani, M., Feigenbaum, A., & Vergnaud, J. M. (1997). Prediction of worst case migration from packaging to food using mathematical models. *Food Additives and Contaminants, 14*(5), 499-506.

Hwang, S. W., Shim, J. K., Selke, S., Soto-Valdez, H., Matuana, L., Rubino, M., & Auras, R. (2013). Migration of α-Tocopherol and Resveratrol from Poly (L-lactic acid)/Starch Blends Films into Ethanol. *Journal of Food Engineering*.

Iñiguez-Franco, F., Soto-Valdez, H., Peralta, E., Ayala-Zavala, J. F., Auras, R., & Gámez-Meza, N. (2012). Antioxidant Activity and Diffusion of Catechin and Epicatechin from Antioxidant Active Films Made of Poly (l-lactic acid). *Journal of Agricultural and Food Chemistry, 60*(26), 6515-6523.

Iñiguez-Franco, F. M., & Soto-Valdez , H. (2011). *Vida de Anaquel de Plátano A Diferentes Temperaturas.* Paper presented at the Sociedad Mexicana de Ciencias Horticolas A.C (SOMECH), Cualiacan, Sinaloa.

Jamshidian, M., Tehrany, E. A., Cleymand, F., Leconte, S., Falher, T., & Desobry, S. (2012). Effects of synthetic phenolic antioxidants on physical, structural, mechanical and barrier properties of poly lactic acid film. *Carbohydrate Polymers, 87*(2), 1763-1773.

Jamshidian, M., Tehrany, E. A., & Desobry, S. (2012). Antioxidants release from solvent-cast pla film: investigation of pla antioxidant-active packaging. *Food and Bioprocess Technology,* 1-14.

Jamshidian, M., Tehrany, E. A., & Desobry, S. (2012). Release of synthetic phenolic antioxidants from extruded poly lactic acid (PLA) film. *Food Control*.

Lee, Y. S., Shin, H.-S., Han, J.-K., Lee, M., & Giacin, J. R. (2004). Effectiveness of antioxidant-impregnated film in retarding lipid oxidation. *Journal of the Science of Food and Agriculture, 84*(9), 993-1000.

Lopez de Dicastillo, C., Nerin, C., Alfaro, P., Catalá, R., Gavara, R., & Hernandez-Muñoz, P. (2011). Development of new antioxidant active packaging films based on ethylene vinyl alcohol copolymer (EVOH) and green tea extract. *Journal of Agricultural and Food Chemistry, 59*(14), 7832-7840.

López-de-Dicastillo, C., Gómez-Estaca, J., Catalá, R., Gavara, R., & Hernández-Muñoz, P. (2012). Active antioxidant packaging films: Development and effect on lipid stability of brined sardines. *Food Chemistry, 131*(4), 1376-1384.

Manzanarez-López, F., Soto-Valdez, H., Auras, R., & Peralta, E. (2011). Release of α-Tocopherol from Poly (lactic acid) films, and its effect on the oxidative stability of soybean oil. *Journal of Food Engineering, 104*(4), 508-517.

Mascheroni, E., Guillard, V., Nalin, F., Mora, L., & Piergiovanni, L. (2010). Diffusivity of propolis compounds in Polylactic acid polymer for the development of anti-microbial packaging films. *Journal of Food Engineering, 98*(3), 294-301.

Motulsky, H., & Christopoulos, A. (2004). Comparing models using Akaike's Information Criterion (AIC) In: Fitting models to biological data using linear and nonlinear regression: A practical guide to curve fitting: Oxford Univ. Press, New York.

Nerín, C., Tovar, L., Djenane, D., Camo, J., Salafranca, J., Beltrán, J. A., & Roncalés, P. (2006). Stabilization of beef meat by a new active packaging containing natural antioxidants. *Journal of Agricultural and Food Chemistry, 54*(20), 7840-7846.

Ortiz-Vazquez, H., Shin, J. M., Soto-Valdez, H., & Auras, R. (2011). Release of butylated hydroxytoluene (BHT) from Poly (lactic acid) films. *Polymer Testing, 30*(5), 463-471.

Pereira de Abreu, D. A., Losada, P. P., Maroto, J., & Cruz, J. M. (2010). Evaluation of the effectiveness of a new active packaging film containing natural antioxidants (from barley husks) that retard lipid damage in frozen Atlantic salmon (Salmo salar). *Food Research International, 43*(5), 1277-1282.

Poças, M. F., Oliveira, J. C., Oliveira, F. A. R., & Hogg, T. (2008). A critical survey of predictive mathematical models for migration from packaging. *Critical Reviews in Food Science and Nutrition, 48*(10), 913-928.

Reynier, A., Dole, P., & Feigenbaum, A. (2002a). Integrated approach of migration prediction using numerical modelling associated to experimental determination of key parameters. *Food Additives & Contaminants, 19*(S1), 42-55.

Reynier, A., Dole, P., & Feigenbaum, A. (2002b). Migration of additives from polymers into food simulants: numerical solution of a mathematical model taking into account food and polymer interactions. *Food Additives & Contaminants, 19*(1), 89-102.

Sonkaew, P., Sane, A., & Suppakul, P. (2012). Antioxidant activities of curcumin and ascorbyl dipalmitate nanoparticles and their activities after incorporation into cellulose-based packaging films. *Journal of Agricultural and Food Chemistry, 60*(21), 5388-5399.

Soto-Valdez, H., Auras, R., & Peralta, E. (2010). Fabrication of Poly(lactic acid) Films with Resveratrol and the Diffusion of Resveratrol into Ethanol. *Journal of Applied Polymer Science*. doi: 10.1002/app.33687

Soto-Valdez , H., Peralta, E., & Auras, R. (2008). *Poly(lactic acid) films added with resveratrol as active packaging with potential application in the food industry.* Paper presented at the 16th IAPRI World Conference on Packaging Bangkok, Thailand.

Tehrany, E. A., & Desobry, S. (2004). Partition coefficients in food/packaging systems: a review. *Food Additives and Contaminants, 21*(12), 1186-1202.

Vitrac, O., & Hayert, M. (2006). Identification of diffusion transport properties from desorption/sorption kinetics: an analysis based on a new approximation of fick equation during solid-liquid contact. *Industrial & Engineering Chemistry Research, 45*(23), 7941-7956.

Vitrac, O., Mougharbel, A., & Feigenbaum, A. (2007). Interfacial mass transport properties which control the migration of packaging constituents into foodstuffs. *Journal of Food Engineering, 79*(3), 1048-1064.

Wessling, C., Nielsen, T., & Giacin, J. R. (2001). Antioxidant ability of BHT‐and α‐tocopherol‐impregnated LDPE film in packaging of oatmeal. *Journal of the Science of Food and Agriculture, 81*(2), 194-201.

Zhu, X., Lee, D. S., & Yam, K. L. (2012). Release property and antioxidant effectiveness of tocopherol-incorporated LDPE/PP blend films. *Food Additives and Contaminants: Part A, 29*(3), 461-468.

Zhu, X., Schaich, K. M., Chen, X., & Yam, K. L. (2013). Antioxidant Effects of Sesamol Released from Polymeric Films on Lipid Oxidation in Linoleic Acid and Oat Cereal. *Packaging Technology and Science, 26*(1), 31-38. doi: 10.1002/pts.1964

Chapter 5

A Two-Step Solution to Estimate Mass Transfer Parameters of Migration Experiments Controlled by Diffusion, Partition and Convective Mass Transfer Coefficients

5.0 Introduction

Migration in food packaging applications involves mass transfer phenomenon of additives from polymeric membranes into products and/or simulants. These additives could be antimicrobials, antioxidants, or any chemical substances that may serve multifunctional purposes to a food-package system. Normally, these additives are intended for prolonging the shelf life of a food product by means of inhibiting microbial growth, retarding lipid oxidation, etc. Often times, these additives add extra value such as enhancing the flavor or nutritional aspects of the product or protecting the polymer from degradation during processing (Iñiguez-Franco et al., 2012; Ortiz-Vazquez, Shin, Soto-Valdez, & Auras, 2011; Samsudin, Valdez, & Auras, 2014), or they are introduced to improve the polymeric membrane's ageing properties. Despite all the positive outcomes, these additives or the by-products of the interaction between polymer and additives can migrate into the food, thus reaching a safety threshold limit, which may adversely affect consumers' safety. As a result, it is important to conduct migration experiments and determine the migration parameters determining this mass transfer phenomenon, which may have safety concern and implications for shelf life determination.

Since migration study is complex and time consuming, an increasing number of researchers have focused on investigating the kinetics of migration by means of mathematical modeling. In depth physical understanding of the particular factor/parameters that govern the kinetics of migration can be obtained by solving the mathematical models describing these experiments. There are various types of mathematical models available, including deterministic, stochastic,

mechanistic, dynamic, etc. In the area of mass transfer, most of the mathematical models available are based on Crank's solutions (Crank, 1979) in addition to Carslaw and Jaeger's solutions (Carslaw & Jaeger, 1959) of the governing equations for the diffusion of chemical compounds through thin membranes. These solutions are all based on the Fick's second law of diffusion by using a deterministic approach and are expressed analytically. Even though several numerical approximation techniques have been developed and are available to estimate the kinetics of migration, the use of analytical solutions is favored due to their simplicity and relationship to the physical phenomena driving the migration. Most of these mass transfer analytical solutions describe migration by solving for two kinetic migration parameters, the diffusion (D) and the partition coefficients ($K_{p,f}$) (Dhoot, Auras, Rubino, Dolan, & Soto-Valdez, 2009; Granda-Restrepo et al., 2009; Hwang et al., 2013; Iñiguez-Franco et al., 2012; Manzanarez-López, Soto-Valdez, Auras, & Peralta, 2011; Mascheroni, Guillard, Nalin, Mora, & Piergiovanni, 2010; Ortiz-Vazquez et al., 2011; Reinas, Oliveira, Pereira, Machado, & Poças, 2012; Samsudin et al., 2014). To the best of the author's knowledge, few solutions describing the migration process consider the convective mass transfer coefficient (h) between the films and the food / simulant (Galotto, Torres, Guarda, Moraga, & Romero, 2011; Gandek, Hatton, & Reid, 1989; Mascheroni et al., 2010; Pocas, Oliveira, Brandsch, & Hogg, 2012; Vitrac, Mougharbel, & Feigenbaum, 2007). The existence of one analytical solution capable of assessing the three kinetic migration parameters (D, $K_{p,f}$ and h) can provide a method to understand the physical process driving these experiments. Since there are many combinations of these parameters that can satisfy the solution of this equation, it is difficult to be sure that the solution used has the right global minimum that minimizes the sums of squared errors (SSE). Often times, a complex non-linear mathematical equation results in many

local minima (Figure 5-1); thus finding the right global minimum region that provides the true solution can be a challenge.

Therefore, the aims of this work are: *i*) to propose a two-step solution to estimate the *D*, $K_{p,f}$ and *h* kinetic migration parameters, *ii*) to assess the proposed two-step solution by using experimental migration data, *iii*) to introduce the kinetic phase diagram (KPD) as previously presented by Vitrac and Hayert (2006) based on the forward approximation, and *iv*) to use a bootstrapping technique on the residuals to find the true data distribution.

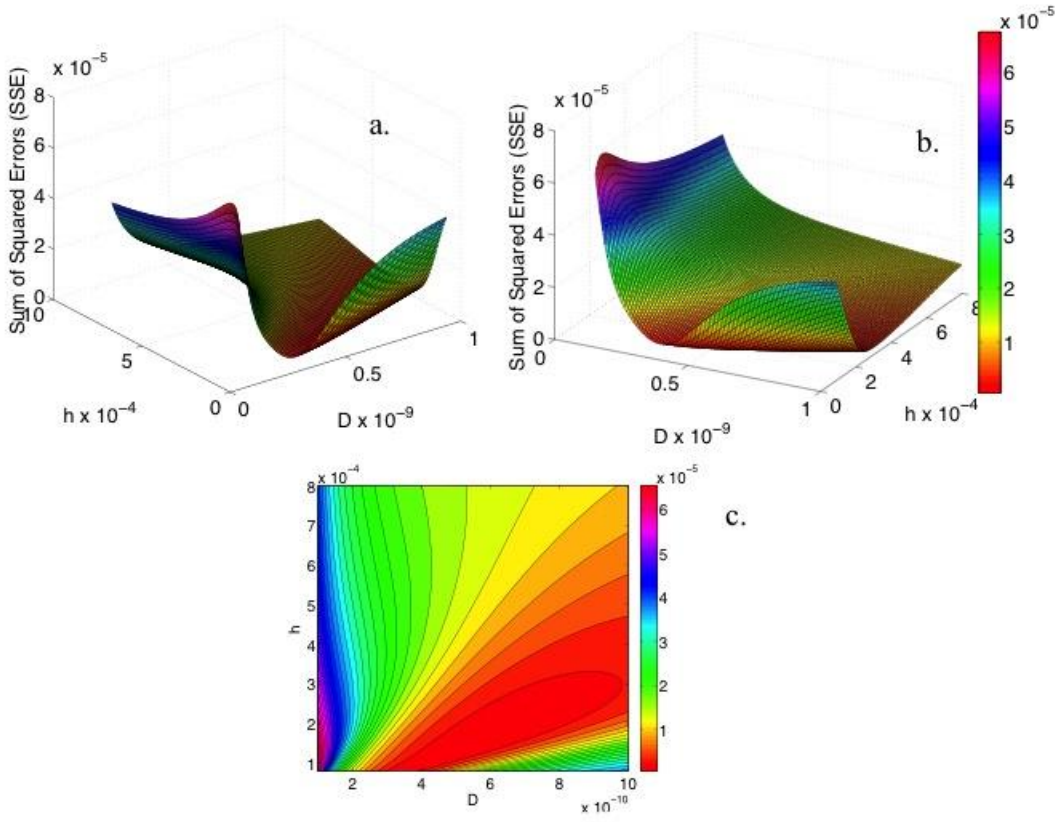

Figure 5-1 Example of multiple local minima for SSE in non-linear estimation. (a) Surface plot with default view, (b) surface plot view set at azimuth and elevation of 28, and 28, respectively, and (c) contour plot for minimum region of SSE.

5.1 Theoretical Development

A two-step solution consists of step 1: a simplified model, and step 2: an ordinary least square estimation, presented in the next section. Step 1 is used to determine the initial guess for step 2.

5.1.1 Assumptions and Boundary Conditions

Let us assume that we are conducting a migration experiment where a piece of film added with an additive or chemical compound is in contact with a food or a simulant on two sides (Figure 5-2). To find the concentration of the additive as a function of time in the polymeric membrane and/or in the food simulant, we need to make a number of assumptions to satisfy the boundary conditions used to derive the analytical solution. These assumptions include, but are not limited to:

i) the initial concentration of additive is uniformly distributed inside of the film

ii) the food/food simulant is assumed well-mixed

iii) the overall mass transfer is balanced

iv) the system of film-liquid food simulant is closed

v) no interaction occurs between the film and food/food simulant

vi) the concentration profile is symmetrical across the film

vii) the concentration of the additive far away from the film in the simulant is homogenous

viii) the diffusion coefficient (D) is constant throughout the experiment and it does not depend on the concentration of the additive

ix) the partition coefficient, $K_{p,f}$ is constant.

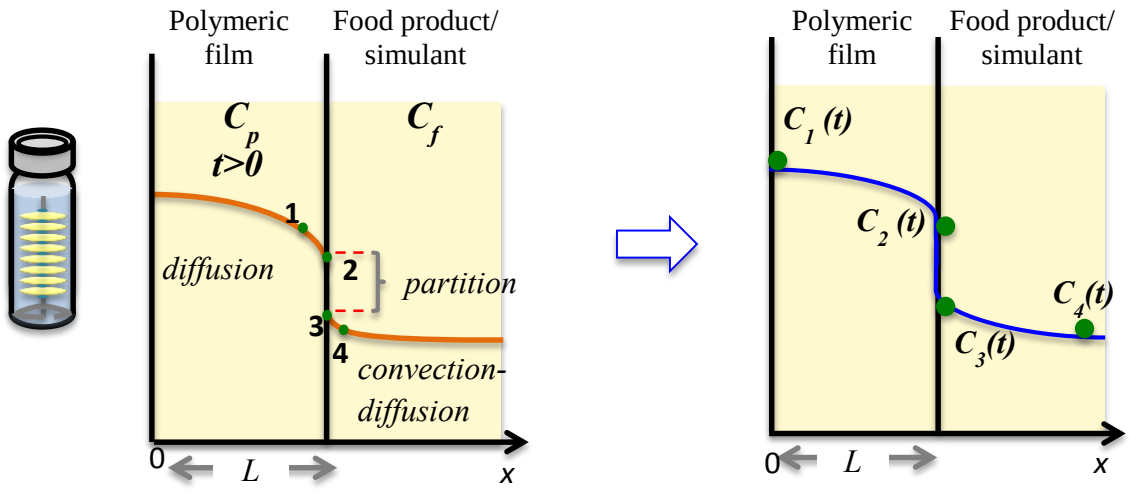

Figure 5-2 Graphical representation of the kinetics of migration.

Initial conditions;

$$C_p(x,0) = C_0 \qquad \text{(Eq. 5-1)}$$

$$C_f(x,0) = 0 \qquad \text{(Eq. 5-2)}$$

Boundary conditions;

$$\left.\frac{\partial C_p}{\partial x}\right|_{x=0} = 0 \qquad \text{(Eq. 5-3)}$$

$$-D\left.\frac{\partial C_p}{\partial x}\right|_{x=L} = h\left(C_{2,3} - K_{p,f}C_f\right) = \frac{V_f}{A}\frac{\partial C_f}{\partial t} \qquad \text{(Eq. 5-4)}$$

Now, the main differential equation describing the mass transfer process is provided by:

$$\frac{\partial C_p}{\partial t} = D\frac{\partial^2 C_p}{\partial x^2} \qquad \text{(Eq. 5-5)}$$

5.1.2.1 Step 1

In this step, a simplified model is proposed based on the homogeneous constant-coefficient linear differential equation by using the mass balance. The motivation of proposing step 1 is to be able to find the right region of SSE global minimum for obtaining robust order magnitude

approximation for simultaneously estimate of all kinetic migration parameters (*i.e.*, $K_{p,f}$, D, h) before estimating the parameters by using the ordinary least square (OLS) estimation method. By using step 1, the accuracy of the estimation is obtained since deviation from the true solution is avoided as the right region of SSE global minimum can be identified. Consequently, the initial guesses for the kinetic migration parameters can be obtained. Finding an appropriate initial guess for h in the mass transfer area is particularly challenging since this property imposes experimental difficulty due to the need to measure the additive concentration at the initial time of the experiment, resulting in two main issues: *i*) high possibility of introducing significant experimental error, and *ii*) the values obtained experimentally do not represent the true value at the interfacial boundary layer (since the concentration of additives is obtained via mathematical expressions assuming the spatial coordinate). Meanwhile, approximate values for D and $K_{p,f}$ can be obtained from published/known data for a similar polymer-additive-food simulant system. Although the quest of initial guesses for D and $K_{p,f}$ are not quite as challenging as for h, the importance of having robust initial guesses when estimating these parameters simultaneously cannot be neglected to avoid over and/or under fitting estimation.

The mass balance for the additive between the membrane and the food and/or simulant can initially be expressed as a linear relation between the different concentrations as shown:

$$DA\frac{C_1-C_2}{L} = hA(C_3 - C_4) = \frac{d}{dt}(VC_4) = -\frac{d}{dt}(AL\frac{C_1+C_2}{2}) \qquad \text{(Eq. 5-6)}$$

Although this is a large simplification since we are assuming that the mass coming out of the membrane is an average between C_1 and C_2.,we can use this initial approach to calculate initial guesses to be used in step 2. Vitrac and Hayert (2006), for example, used one linear and quadratic solution to determine the concentration profile of additives inside a membrane to avoid this initial

simplification. However, an initial parabolic profile does not produce guesses that are much different from this initial assumption.

The interface property is expressed as follows:

$$C_2 = K_{p,f} C_3 \quad \text{(Eq. 5-7)}$$

Solving for C_4 (C_f at time t):

$$C_1 = C_2 + \frac{LV}{DA}\frac{dC_4}{dt} \quad \text{(Eq. 5-8)}$$

$$C_2 = K_{p,f} C_4 + \frac{K_{p,f} V}{hA}\frac{dC_4}{dt} \quad \text{(Eq. 5-9)}$$

$$C_3 = C_4 + \frac{V}{hA}\frac{dC_4}{dt} \quad \text{(Eq. 5-10)}$$

$$\frac{d^2}{dt^2}(C_4) + R\frac{d}{dt}(C_4) = 0 \text{ ; where } R\ (rate\ constant) = \frac{2(K_{p,f} + \frac{V_f}{AL})}{\frac{V_f}{A}(\frac{L}{D} + \frac{2K_{p,f}}{h})} \quad \text{(Eq. 5-11)}$$

Assuming a solution of the type $f(x) = e^{mt}$ for Eq. 5-11

$$\frac{df}{dt} = m\, e^{mt} \quad \text{(Eq. 5-12)}$$

$$\frac{d^2 f}{dt^2} = m^2\, e^{mt} \quad \text{(Eq. 5-13)}$$

By substituting Eq. 5-12 and 5-13 into Eq. 5-11, the following equation is obtained;

$$m^2\, e^{mt} + Rm\, e^{mt} = 0 \quad \text{(Eq. 5-14)}$$

$$m(m + R) = 0; m = 0, m = -R \quad \text{(Eq. 5-15)}$$

$$C_4 = P + Qe^{-Rt} \ where\ P = \frac{C_0}{K_{p,f} + \frac{V}{AL}}\ and\ Q = -P\ as\ at\ t = 0^+, C_4 = 0 \quad \text{(Eq. 5-16)}$$

Thus, Eq. 5-16 becomes Eq.5-17;

$$C_4 = P(1 - e^{-Rt}) \quad \text{(Eq. 5-17)}$$

Then;

$C_3 = \mathrm{P} + \mathrm{P}\left(\frac{VR}{hA} - 1\right)e^{-Rt}$; $C_2 = \mathrm{K}_{p,f}C_3$; $C_1 = \mathrm{K}_{p,f}P + P\left[\frac{V}{A}\left(\frac{K_{p,f}}{h} + \frac{L}{D}\right)R - K_{p,f}\right]e^{-Rt}$

Thus, at $t^* = 0^+$, $\frac{C_1+C_2}{2} = C_0$, resulting in $P = \frac{C_0}{K_{p,f}+\frac{V}{AL}}$

By substituting $P = \frac{C_0}{K_{p,f}+\frac{V}{AL}}$ into Eq. 5-17, Eq. 5-18 is obtained;

$$\frac{\boldsymbol{C_4(t)}}{\boldsymbol{C_0}} = \frac{\boldsymbol{(1-e^{-Rt})}}{\boldsymbol{\left(K_{p,f}+\frac{V}{AL}\right)}} \qquad \text{(Eq. 5-18)}$$

The right side of Eq. 5-18 is equivalent to concentration of additives in the food or food simulant at equilibrium similar to what can be obtained by the exact analytical solution.

Note for $t^* = 0^+$; at $t = 0, C_1 = C_2 = C_0$ *and* $C_3 = C_4 = 0,$ therefore Eq. $5-9$ can't be satisfied after a short time ($t = 0^+$) since C_2 has decreased and C_3 has increased resulting in Eq.5-7. Therefore, at $t^* = 0^+$, $C_4 = 0, C_3 = \frac{C_0}{K_{p,f}+\frac{hL}{2D}}, C_2 = \frac{K_{p,f}C_0}{K_{p,f}+\frac{hL}{2D}} < C_0, C_1 = \frac{C_0(K_{p,f}+\frac{hL}{D})}{K_{p,f}+\frac{hL}{2D}} > C_0.$

As a result, a simplified model (Eq. 5-19) is obtained;

$$\frac{C_4}{C_0} = P(1 - e^{-Rt}) \text{ where } C_4 \equiv C_f \qquad \text{(Eq. 5-19)}$$

By fitting Eq. 5-19 to the experimental data, a combination of P and R with the lowest sums of squared errors (SSE)= $\sum\left[\frac{C_{f,i}}{C_0} - P(1 - e^{-Rt_i})\right]^2$ can be obtained. The best range of *R* can be selected accordingly to $\frac{\partial SSE}{\partial P} = 0$ resulting in the best fit of *P* (Eq. 5-20) for a given range of *R.*

$$P = \frac{\sum\frac{C_{f,i}}{C_0}(1-e^{-Rt,i})}{\sum(1-e^{-Rt,i})^2} \qquad \text{(Eq. 5-20)}$$

The combination of values of *P* and *R* that give the lowest SSE is used to first obtain the initial guess of $K_{p,f}$ by using $P = \frac{C_0}{K_{p,f}+\frac{V}{AL}}$. Then by substituting $K_{p,f}$ inside of $R = \frac{2(K_{p,f}+\frac{V_f}{AL})}{\frac{V_f}{A}(\frac{L}{D}+\frac{2K_{p,f}}{h})}$, the initial guesses of *D* and *h* can be obtained as follows ;

$$\frac{x_1}{D} + \frac{x_2}{h} = 1 \qquad \text{(Eq. 5-21)}$$

where x_1 and x_2 are numerical values.

The expression above (Eq. 5-21) is extracted from *R* since $\frac{L}{D}$ and $\frac{2K_{p,f}}{h}$ are two resistance in the series with only the total resistance determined by the rate of *R*. Thus *D* and *h* cannot be separated or obtained individually to establish the order of magnitude approximations as they both are physically influencing each other. The approximation of the initial guesses of both *D* and *h* based on Eq. 5-21 are $D \geq x_1$ and $h \geq x_2$, respectively. The initial guesses obtained for $K_{p,f}$, *D* and *h* are then used as the starting point of parameter estimation via the ordinary least squares estimation using the analytical solution in step 2.

5.1.2.2 Step 2

By using the Laplace transform, the analytical solution that satisfies the boundary conditions previously described in Eqs. 5-1 to 5-4 is derived.

Laplace transforms:

$$\phi(x,s) = L\{C(x,t)\} \rightarrow \bar{f}(s) = \int_0^\infty e^{st} f(t) dt$$

Partial differential equation:

$$s\phi - C_0 = D\phi'' \qquad \text{(Eq. 5-22)}$$

By rearranging Eq. 5-22, the following equation is obtained:

$\phi'' - \frac{s}{D}\phi = -\frac{C_0}{D}$, which has the solution $= C_1 e^{x\sqrt{s/D}} + C_2 e^{-x\sqrt{s/D}} + \frac{C_0}{s}$, from which $\phi' =$

$$\sqrt{\frac{s}{D}}\left[C_1 e^{x\sqrt{s/D}} - C_2 e^{-x\sqrt{s/D}}\right]; \phi' = \frac{\partial C_p}{\partial x} \qquad \text{(Eq. 5-23)}$$

Boundary conditions;

$$\phi'|_{x=0} = 0 \ \therefore \ C_1 = C_2 \qquad \text{(Eq. 5-24)}$$

$$D\phi'|_{x=L} = h\left(\frac{\phi}{K_{p,f}} - \phi_f\right) = \frac{V_f}{A}(s\phi_f - 0) \qquad \text{(Eq. 5-25)}$$

Laplace transforms (side of food/food simulant):

$$\phi_f = L\{C_f(t)\}$$

From Eq. 5-25;

$$\phi_f = \frac{\phi}{K_{p,f}(1+\frac{V_f}{Ah}s)} \qquad \text{(Eq. 5-26)}$$

Substituting this and Eq. 5-23 back into Eq. 5-25, the following equation is obtained:

$$-D\sqrt{\frac{s}{D}}2C_1 \sinh\left(L\sqrt{\frac{s}{D}}\right) = \frac{V_f s}{A}\frac{2C_1\cosh(L\sqrt{\frac{s}{D}})+\frac{C_0}{s}}{K_{p,f}(1+\frac{V_f}{Ah}s)} \qquad \text{(Eq. 5-27)}$$

$$C_1 = -\frac{\frac{C_0}{2}}{s*\cosh\left(L\sqrt{\frac{s}{D}}\right)+D(\frac{K_{p,f}A}{V_f}+\frac{K_{p,f}s}{h})\sqrt{\frac{s}{D}}sinh\left(L\sqrt{\frac{s}{D}}\right)} \qquad \text{(Eq. 5-28)}$$

$$\phi(x,s) = \frac{C_0}{s} - \frac{C_0\cosh(x\sqrt{\frac{s}{D}})}{s*\cosh\left(L\sqrt{\frac{s}{D}}\right)+D(\frac{K_{p,f}A}{V_f}+\frac{K_{p,f}s}{h})\sqrt{\frac{s}{D}}sinh\left(L\sqrt{\frac{s}{D}}\right)} \qquad \text{(Eq. 5-29)}$$

By using the residue theorem (complex variable theory), the inverse Laplace transform can be performed (to change to time domain):

$$C(x,t) = L^{-1}\{\phi(x,s)\} = C_0 - C_0\sum_{q_n}^{\infty}\left\{residues\ of\ \frac{\cosh(x\sqrt{\frac{s}{D}})e^{st}}{s*\cosh\left(L\sqrt{\frac{s}{D}}\right)+D(\frac{K_{p,f}A}{V_f}+\frac{K_{p,f}s}{h})\sqrt{\frac{s}{D}}sinh\left(L\sqrt{\frac{s}{D}}\right)}\right\}$$

(Eq. 5-30)

where the poles of ϕ in Eq. 5-29 are the roots of $\tanh\left(L\sqrt{\frac{s}{D}}\right) = -\frac{\sqrt{\frac{s}{D}}}{K_{p,f}(\frac{A}{V_f}+\frac{s}{h})}$; s is an infinite complex number corresponding to infinite number of roots of eigenvalues

Let $z = L\sqrt{\frac{s}{D}} \Rightarrow \tanh z = -\frac{\alpha Biz}{K_{p,f}\alpha z^2+Bi}$ where $\alpha = \frac{V_f}{K_{p,f}AL}$ and $Bi = \frac{hL}{D}$

By anticipating purely imaginary roots, set $z = iq_n \Rightarrow tan\, q_n = -\frac{\alpha Bi q_n}{Bi - K_{p,f}\alpha q_n^2}$ with $s_n = -\frac{Dq_n^2}{L^2}$

where $n = 1,2,3 \ldots . \infty$

Residue at *s*=0;

$$\lim_{s\to 0} \frac{(s-0)\cosh(x\sqrt{\frac{s}{D}})e^{st}}{s*\cosh\left(L\sqrt{\frac{s}{D}}\right)+D(\frac{K_{p,fA}}{V_f}+\frac{K_{p,fs}}{h})\sqrt{\frac{s}{D}}sinh\left(L\sqrt{\frac{s}{D}}\right)} \qquad \text{(Eq. 5-31)}$$

By dividing Eq. 5-31 with s, the following is obtained;

$$\frac{1}{1+\lim_{s\to 0} D(\frac{K_{p,fA}}{V_f}+\frac{K_{p,fs}}{h})\sqrt{\frac{s}{D}}sinh\left(L\sqrt{\frac{s}{D}}\right)} = \frac{1}{1+\frac{K_{p,fA}\sqrt{D}}{V_f}\lim_{s\to 0}\frac{sinh\left(L\sqrt{\frac{s}{D}}\right)}{\sqrt{s}}} \qquad \text{(Eq. 5-32)}$$

Since the last limit is indeterminate (0/0), $L'H\hat{o}pital's$ rule is employed:

$$lim = \frac{\frac{L}{\sqrt{D}}\cosh(L\sqrt{\frac{s}{D}})\frac{s^{-1/2}}{2}}{\frac{s^{-1/2}}{2}} = \frac{L}{\sqrt{D}} \qquad \text{(Eq. 5-33)}$$

$$\text{Residue (s=0)}=\frac{\mathbf{1}}{\mathbf{1}+\frac{\boldsymbol{K_{p,fAL}}}{\boldsymbol{V_f}}} = \frac{\boldsymbol{\alpha}}{\boldsymbol{\alpha+1}} \qquad \text{(Eq. 5-34)}$$

Residue at $s=s_n$;

$$\frac{cosh(x\sqrt{\frac{s_n}{D}})e^{s_n t}}{s_n}\lim_{s\to s_n}\frac{s-s_n}{\cosh(L\sqrt{\frac{s}{D}})+\sqrt{D}\,(\frac{K_{p,fA}s^{-\frac{1}{2}}}{V_f}+\frac{K_{p,fs^{\frac{1}{2}}}}{h})sinh(L\sqrt{\frac{s}{D}})} \qquad \text{(Eq. 5-35)}$$

Since s_n is the root of the denominator $L'H\hat{o}pital's$ rule is employed:

$$\lim_{s\to s_n} = \frac{1}{\sinh\left(L\sqrt{\frac{s}{D}}\right)\frac{L}{\sqrt{D}2}\frac{1}{s^{-1/2}}+\sqrt{D}(\frac{K_{p,fA}}{V_f}s^{-\frac{1}{2}}+\frac{K_{p,fs^{\frac{1}{2}}}}{h})\cosh\left(L\sqrt{\frac{s}{D}}\right)\frac{L}{\sqrt{D}2}\frac{1}{s^{-\frac{1}{2}}}+\sqrt{D}(-\frac{1}{2}\frac{K_{p,fA}}{V_f}s^{-\frac{3}{2}}+\frac{K_{p,fs^{-1/2}}}{2h})sinh\left(L\sqrt{\frac{s}{D}}\right)} \text{ (Eq. 5-36)}$$

$$\lim_{s\to s_n} = \frac{2s}{\sinh\left(L\sqrt{\frac{s}{D}}\right)\left[L\sqrt{\frac{s}{D}}-\frac{K_{p,fAL}}{V_f}\frac{1}{\left(L\sqrt{\frac{s}{D}}\right)}+\frac{K_{p,f\sqrt{Ds}}}{h}\right]+cosh\left(L\sqrt{\frac{s}{D}}\right)\left[\frac{K_{p,fAL}}{V_f}+\frac{K_{p,fLs}}{h}\right]} \qquad \text{(Eq. 5-37)}$$

Substitute Eq. 5-37 into Eq. 5-35, where $s(=s_n)=-D\frac{q_n^2}{L^2}$;

Residue at $s=s_n=\frac{2cosh\left(x\sqrt{\frac{-q_n^2}{L^2}}\right)e^{\frac{-q_n^2Dt}{L^2}}}{\sinh\left(L\sqrt{\frac{-q_n^2}{L^2}}\right)\left[L\sqrt{\frac{-q_n^2}{L^2}}-\frac{K_{p,f}AL}{V_fL\sqrt{\frac{-q_n^2}{L^2}}}+\frac{K_{p,f}}{h}\sqrt{\frac{-D^2q_n^2}{L^2}}\right]+\cosh\left(L\sqrt{\frac{-q_n^2}{L^2}}\right)\left[\frac{K_{p,f}AL}{V_f}-\frac{K_{p,f}Dq_n^2}{hL}\right]}$

$$=\frac{2cosh\left(\frac{iqx}{L}\right)e^{\frac{-q_n^2Dt}{L^2}}}{\sinh(iq)\left[iq_n-\frac{K_{p,f}AL}{V_fL}\frac{1}{iq_n}+\frac{K_{p,f}}{h}i\frac{Dq_n}{L}\right]+\cosh(iq_n)\left[\frac{K_{p,f}AL}{V_f}-\frac{K_{p,f}Dq_n^2}{hL}\right]} \quad \text{(Eq.5-38)}$$

Substitute Eq. 5-34 and $Bi=\frac{hL}{D}$ into Eq. 5-38;

$$\frac{2\alpha Bicos\left(\frac{qx}{L}\right)e^{\frac{-q_n^2Dt}{L^2}}}{\cos(q)[Bi-K_{p,f}\alpha Bq_n^2]-sin(q_n)\left[\alpha(K_{p,f}+Bi)q_n^2+\frac{Bi}{q_n^2}\right]} \quad \text{(Eq.5-39)}$$

Substitute Eq. 5-39 into Eq. 5-30;

$$\frac{C(x,t)}{C_0}=\frac{1}{\alpha+1}+2\alpha Bi\sum_{q_n}^{\infty}\frac{cos\left(\frac{q_nx}{L}\right)e^{\frac{-q_n^2Dt}{L^2}}}{\sin(q_n)\left[\alpha(K_{p,f}+Bi)q_n+\frac{Bi}{q_n}\right]-\cos(q_n)[Bi-K_{p,f}\alpha q_n^2]} \quad \text{(Eq. 5-40)}$$

The mass that remains in the polymer at time *t* is:

$$M(t)=\int_0^L C(x,t)\,A\,dx$$

$$=C_0A\int_0^L\left[\frac{1}{1+\alpha}+2\alpha Bi\sum_{q_n}^{\infty}\frac{cos\left(\frac{q_nx}{L}\right)e^{\frac{-q_n^2Dt}{L^2}}}{\sin(q_n)\left[\alpha(K_{p,f}+Bi)q_n+\frac{Bi}{q_n}\right]-\cos(q_n)[Bi-K_{p,f}\alpha q_n^2]}\right]\,dx \quad \text{(Eq. 5-41)}$$

$$=C_0AL\left[\frac{1}{\alpha+1}+2\alpha Bi\sum_{q_n}^{\infty}\frac{\sin q_n\,e^{\frac{-q_n^2Dt}{L^2}}}{\sin(q_n)\left(Bi+\alpha(K_{p,f}+Bi)q_n^2\right)-q_n\cos q_n(Bi-K_{p,f}\alpha q_n^2)}\right] \quad \text{(Eq. 5-42)}$$

Now, if we divide numerator and denominator of Eq. 5-42 by $cos\ q_n$, where $M_0=C_0AL$ and q_n is the non-zero roots of $tan\ q_n=-\frac{\alpha Biq_n}{Bi-K_{p,f}\alpha q_n^2}$;

$$\frac{M(t)}{M_0} = \frac{1}{\alpha+1} + 2\alpha^2 Bi^2 \sum_{q_n}^{\infty} \frac{e^{\frac{-q_n^2 Dt}{L^2}}}{Bi^2(1+\alpha)+\alpha Bi\left[K_{p,f}\alpha+\alpha Bi-2K_{p,f}\right]q_n^2+K_{p,f}^2\alpha^2 q_n^4} \quad \text{(Eq. 5-43)}$$

Since $M_f(t) = M_0 - M(t) \longrightarrow \frac{M_f}{M_0} = 1 - \frac{M}{M_0}$, the following equation is obtained;

$$\frac{M_f(t)}{M_0} = \frac{\alpha}{\alpha+1} - 2\alpha^2 Bi^2 \sum_{q_n}^{\infty} \frac{e^{\frac{-q_n^2 Dt}{L^2}}}{Bi^2(1+\alpha)+\alpha Bi\left[K_{p,f}\alpha+\alpha Bi-2K_{p,f}\right]q_n^2+K_{p,f}^2\alpha^2 q_n^4} \quad \text{(Eq. 5-44)}$$

As $t \longrightarrow \infty, \frac{M_{f,\infty}}{M_0} = \frac{\alpha}{\alpha+1}$, thus Eq. 5-44 becomes;

$$\frac{M_f(t)}{M_{f,\infty}} = 1 - 2\alpha(\alpha+1)Bi^2 \sum_{q_n}^{\infty} \frac{e^{\frac{-q_n^2 Dt}{L^2}}}{Bi^2(1+\alpha)+\alpha Bi\left[K_{p,f}\alpha+\alpha Bi-2K_{p,f}\right]q_n^2+K_{p,f}^2\alpha^2 q_n^4} \quad \text{(Eq. 5-45)}$$

Since $C_f(t) = \frac{M_f(t)}{V_f} = \frac{M_f}{M_0}\frac{C_0 AL}{V_f} = \frac{M_f}{M_0}\frac{C_0}{K_{p,f}}\frac{K_{p,f}AL}{V_f} = \frac{C_0}{\alpha K_{p,f}}\frac{M_f}{M_0}$, the following analytical solution is obtained;

$$\frac{\boldsymbol{C_f(t)}}{\boldsymbol{C_0}} = \frac{\mathbf{1}-\sum_{\boldsymbol{q_n}}^{\infty} \boldsymbol{f_q} \boldsymbol{e}^{\frac{-q_n^2 Dt}{L^2}}}{\boldsymbol{K_{p,f}(\alpha+1)}} \quad \text{(Eq. 5-46)}$$

where $f_q = \frac{2\alpha(\alpha+1)Bi^2}{Bi^2(1+\alpha)+\alpha Bi\left[K_{p,f}\alpha+\alpha Bi-2K_{p,f}\right]q_n^2+K_{p,f}^2\alpha^2 q_n^4}$;

The eigenvalue's root solutions= $tan\ q_n = -\frac{\alpha Bi q_n}{Bi-K_{p,f}\alpha q_n^2}$; $\alpha = \frac{V_f}{K_{p,f}AL}$ and $Bi = \frac{hL}{D}$

In order to ensure the analytical solution of Eq. 5-46 converge, the number of terms needed for a given accuracy (~98%) can be calculated as follows:

Let z = $e^{\frac{-Dt}{L^2}}$ where $0 < z \leq 1$

The solution converges faster when z decreases, thus in the worst case scenario is when z = 1 (slowest convergence).

% Accuracy=$\frac{sum\ of\ finite\ series}{sum\ of\ infinite\ series} \times 100$ where sum of finite series=$\sum_{n=1}^{n=20} f_q\, z^{qn^2}$ and sum of infinite series = $\sum_{n=1}^{n=\infty} f_q\, z^{qn^2}$**.** The infinite series was estimated with 100,000 terms, which is a good estimation.

Table 5-1 Number of terms with its corresponding percent accuracy.

Number of terms	% Accuracy
1	99.99
2	100.00
3	100.00
.	.
.	.
20	100.00

5.2 A Case Study Analysis

A case study was selected to assess the proposed two-step solutions model. A data set of poly(lactic acid) (PLA) polymer incorporated with 3 wt.% resveratrol in contact with 100% ethanol and kept at 9 °C (Soto-Valdez , Peralta, & Auras, 2008) was chosen to demonstrate the kinetics migration of the parameter estimation. The data was analyzed with different approaches by using MATLAB® R2011b (MathWorks, Natick, MA, USA).

Statistical analysis was performed using an independent t-test (SPSS Statistics, version 22, 2013, IBM Corporation©, Armonk, NY, USA) to compare means between two parameters.

5.3 Assessment of the Two-Step Solutions Model

5.3.1 Step 1

Step 1 was performed by employing Eq. 5-19 using a code developed for MATLAB (see Appendix 5C). The combination of P and R that resulted in the lowest SSE was then used to determine the initial guesses of the kinetics migration parameters (*i.e.*, $K_{p,f}$, D, and h).

5.3.2 Scaled Sensitivity Coefficient, *X'*

Sensitivity coefficient and scaled sensitivity coefficient are as described in Chapter 2 section 2.7.2.

5.3.3 Step 2

5.3.3.1 Ordinary Least Square (OLS) Estimation

For step 2, Eq. 5-46 was employed. The parameters were estimated by minimizing the SSE using the non-linear regression fitting function (nlinfit) of MATLAB. Additional information such as residuals, correlation coefficient matrix and asymptotic confidence interval (CI), to name a few, were also obtained. The relative error of each parameter was calculated by dividing the standard error of the parameter with the parameter's estimated.

5.3.3.2 Sequential Estimation

Sequential estimation is a powerful and generic method for parameter estimation. It was developed based on the Gauss minimization method by using the matrix inversion lemma (Beck & Arnold, 1977). This method updates parameters each time new responses are added and is particularly relevant for a time-dependent experiment. This method does rely on prior information such as good initial guesses, the covariance matrix of the parameter, etc. (Beck & Arnold, 1977; Dolan & Mishra, 2013). The sequential estimation method can be used to validate the OLS estimation. It can also offer additional insight (*i.e.,* time needed to collect sufficient data) in comparison to that of OLS estimation. The sequential estimation method was performed on the data set and the results were compared with the OLS results.

5.4 Kinetic Phase Diagram (KPD)

The idea behind the kinetic phase diagram (KPD) is to extrapolate the migration phenomenon at equilibrium (*i.e.,* concentration of additives at time=t_∞). It is an algebraic differential equation that substitutes for the commonly used partial differential equation to describe physical relationships among parameters, kinetic parameters and measurement. This concept helps to avoid many difficulties encountered in solving partial differential equations (Vitrac & Hayert, 2006). A dimensionless analytical expression of KPD is obtained by taking the first derivative of the concentration changes with respect to time and as a function of the residual concentration in the polymer phase (Eq. 5-47). The dimensionless analytical expression was developed by Vitrac and Hayert (2006) by using the parabolic solution.

$$j^* = f(\bar{u}) = \frac{dC_f}{dt} = \int C_f \qquad \text{(Eq. 5-47)}$$

$$\text{Residual concentration, } \bar{u} = \int_0^1 u(x)dx \qquad \text{(Eq. 5-48)}$$

Dimensionless Fick's second law of diffusion (Vitrac & Hayert, 2006):

$$\frac{\partial u}{\partial \theta} = \frac{\partial^2 u}{\partial x^{*2}} \qquad \text{(Eq. 5-49)}$$

where $u = \frac{C_p(x,t)}{C_0}$ (dimensionless concentration) ; $x^* = \frac{x}{L}$ (dimensionless position); $\theta = \frac{tD}{L^2}$ (dimensionless time or Fourier, F_o number)

The parabolic profile is defined based on its boundary conditions:

$$j^* = -\frac{\partial u}{\partial x^*}\Big|_{x^*=1} = Bi\mathrm{K}(u|_{x^*=1} - u|_{x^*=\infty}) \qquad \text{(Eq. 5-50)}$$

Mass balance approximation is as follows:

$$u|_{x^*\to\infty} = u|_{x^*\to\infty}^{\theta=0} + \frac{1}{K_{p,f}}\frac{1}{C_0}\frac{1}{L_l}\int_0^t j(\tau)\, d\,\tau = u|_{x^*\to\infty}^{\theta=0} + \frac{1}{K_{p,f}} L^* \int_0^\theta j^*(\tau)\, d\tau \qquad \text{(Eq. 5-51)}$$

where $Ku|_{x^*\to\infty}^{\theta=0}$ (the initial concentration in food/food simulant); $L_l = \frac{S_{sL}}{V_f}$ (characteristic of reservoir volume of food/food simulant); $L^* = \frac{L}{L_l}$ (dimensionless length/thickness).

By combining Eq. 5-50 and Eq. 5-51, a more practical form of the boundary conditions is obtained;

$$j^* = -\frac{\partial u}{\partial x^*}\Big|_{x^*=1} = Bi\mathrm{K}\left(u|_{x^*=1} - u|_{x^*\to\infty}^{\theta=0}\right) - BiL^* \int_0^\theta j^*(\tau)\, d\tau \qquad \text{(Eq. 5-52)}$$

$$\frac{\partial u}{\partial x^*}\Big|_{x^*=0} = 0 \qquad \text{(Eq.5-53)}$$

where $j^* = \frac{L}{DC_0}$ (dimensionless flux); $x^* = 1$ (concentration at the interface based on the assumption of local thermodynamic equilibrium); $x^* = \infty$ (concentration in the food/food simulant at equilibrium).

$$u(x^*) = \frac{1}{2}\frac{\partial u}{\partial x^*}\Big|_{x^*=1} x^{*2} + u|_{x^*=0} \qquad \text{(Eq. 5-54)}$$

By taking the dimensionless flux of $\boldsymbol{j^* = \frac{\partial u}{\partial x^*}\Big|_{x^*=1}}$ and Eq. 5-48, Eq. 5-54 becomes;

$$u(x^*) = \left(\frac{1}{6} - \frac{1}{2}x^{*2}\right) j^* + \bar{u} \qquad \text{(Eq. 5-55)}$$

The KPD expression (Eq. 5-47) is implied from Eq. 5-52 and by substituting $\bar{u}|_{x^*=1}$ with its calculated value using Eq. 5-56. The mass balance for the polymer phase is also defined from $\bar{u}$ as it changes with time;

$$\int_0^{\theta} j^*(\tau)\, d\tau = \bar{u}|_{\theta=0} - \bar{u} \qquad \text{(Eq. 5-56)}$$

Thus, Eq. 5-58 becomes;

$$j^*(\bar{u}) = -\frac{d\bar{u}}{d\theta} = BiK_{p,f}\frac{\left(1+\frac{L^*}{K_{p,f}}\right)\bar{u}-\left(\frac{L^*}{K_{p,f}}\bar{u}|_{\theta=0}+u|_{x^*\to\infty}^{\theta=0}\right)}{1+\frac{1}{3}BiK_{p,f}} = \underbrace{\alpha\bar{u}}_{j_D^*} - j_R^* \qquad \text{(Eq. 5-57)}$$

More details on the KPD profile solution can be found in Vitrac and Hayert (2006).

The data set of the selected case study was analyzed using the KPD approach to acquire additional understanding of experiment kinetics, in turns, the kinetic migration parameters.

5.5 Bootstrap Method

Bootstrap is a random resampling method based on statistical inference. This method is very powerful and useful since it better approximates the true distribution of the population in the case of an insufficient data set. This method counteracts any experimental errors that could have caused any disproportionate skewness of the data/and or residual distribution. There are many types of bootstrapping methods and residual bootstrapping is one of them. This method in particular is beneficial for a small data set and for when the magnitude of response of a parameter is large at a short time interval.

$$\hat{\varepsilon}_i = y_i - \hat{y}_i$$

where $\hat{\varepsilon}_i$ (residual); y_i (response variable); $\hat{y}_i$(predicted value).

Synthetic data ($y^*_{i=1,2,3\ldots n}$) is created by adding a random and resampled error term ($\widehat{\varepsilon}_{k=1,2,3\ldots n}$):

$$y^*_{i=1,2,3\ldots n} = \hat{y}_i + \hat{\varepsilon}_{k=1,2,3\ldots n}$$

This synthetic data is then generated for n=1000 and is run through the model for estimated bootstrap parameters.

5.6 Results and Discussions

The case study chosen to illustrate the two-step solution was PLA film incorporated with 3% wt. resveratrol tested at 9 °C in ethanol. The thickness of the film was 2 mil (5.08×10^{-5} m) and eight round discs of film attached to a stainless steel wire and separated by glass beads were used for the migration study (Soto-Valdez et al., 2008). Additional case studies were also analyzed and the results can be found in Appendix 5A and 5B.

5.6.1 Step 1

The newly proposed simplified model provided a good fit to the experimental data. Figure 5-3 shows experimental data sets with fitted values computed using Eq. 5-19. The combination of P and R values that gave the lowest SSE ($4.08\times\ 10^{-5}$) from Eq.5-19 was found to be 0.0013 and $9.00 \times\ 10^{-6}$, respectively. These values were then used to compute the initial guesses for $K_{p,f}$, D, and h, which were found to be 605.63 cm^3 PLA/cm^3 ethanol, $\geq 5.88 \times\ 10^{-12}$ cm^2/min, and $\geq$ $2.80 \times\ 10^{-6}$, respectively. It is worth mentioning that the $K_{p,f}$ value that is always experimentally determined at the end of the experiment by extracting the total amount of additive remaining in the film can be estimated using early data and at the beginning of the migration process.

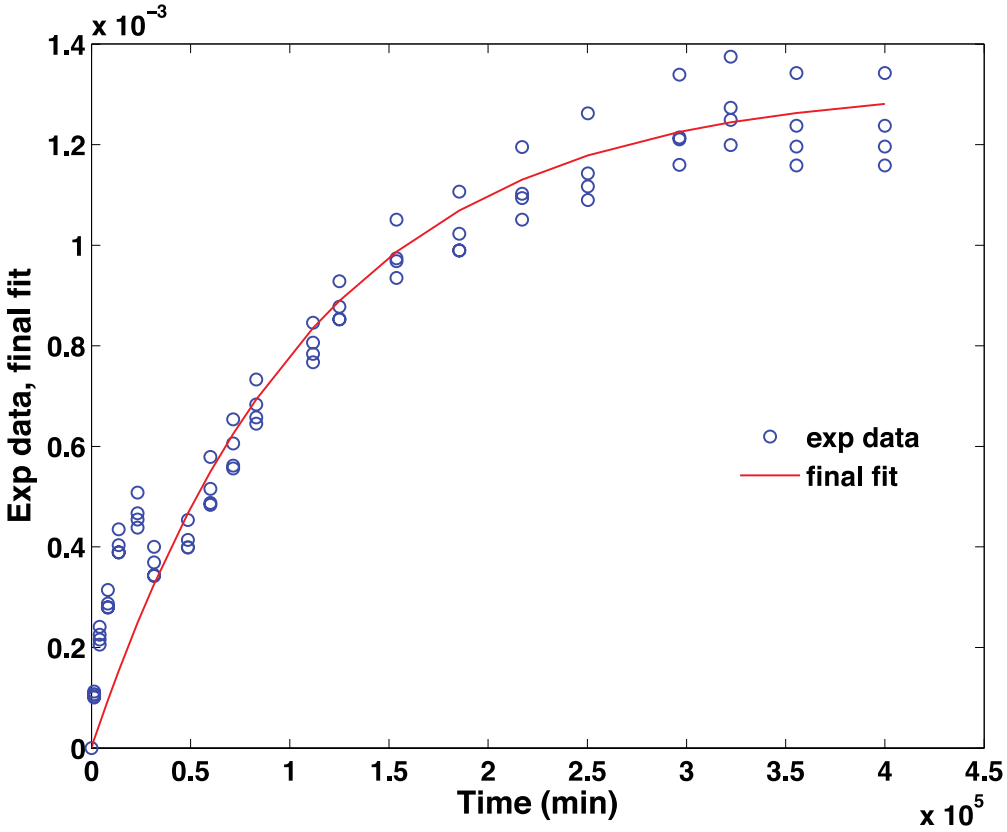

Figure 5-3 Experimental data fitting by using the simplified model of step 1. Initial approximation values obtained from this step were: D=5.88 × 10^{-12} cm^2/min, $K_{p,f}$=605.63 cm^3 PLA/cm^3 ethanol, and h=2.80 × 10^{-6} cm/min.

5.6.2 Scaled Sensitivity Coefficient, *X'*

Figure 5-4 shows the scaled sensitivity coefficient, *X'* of all the kinetic migration parameters. Based on this figure, it was found that $K_{p,f}$ had the highest absolute magnitude of response; thus this parameter can be estimated easier with highest accuracy, followed by D and h. There were no high correlations ($\rho \geq 0.99$) found among the parameters (Table 5-2). The highest correlation coefficient observed among the parameters was between D and $K_{p,f}$, which was 0.95.

From initial observation, it can be anticipated that $K_{p,f}$ will have the lowest relative error followed by D and h. Consequently, all these parameters were then estimated simultaneously by using the OLS estimation method.

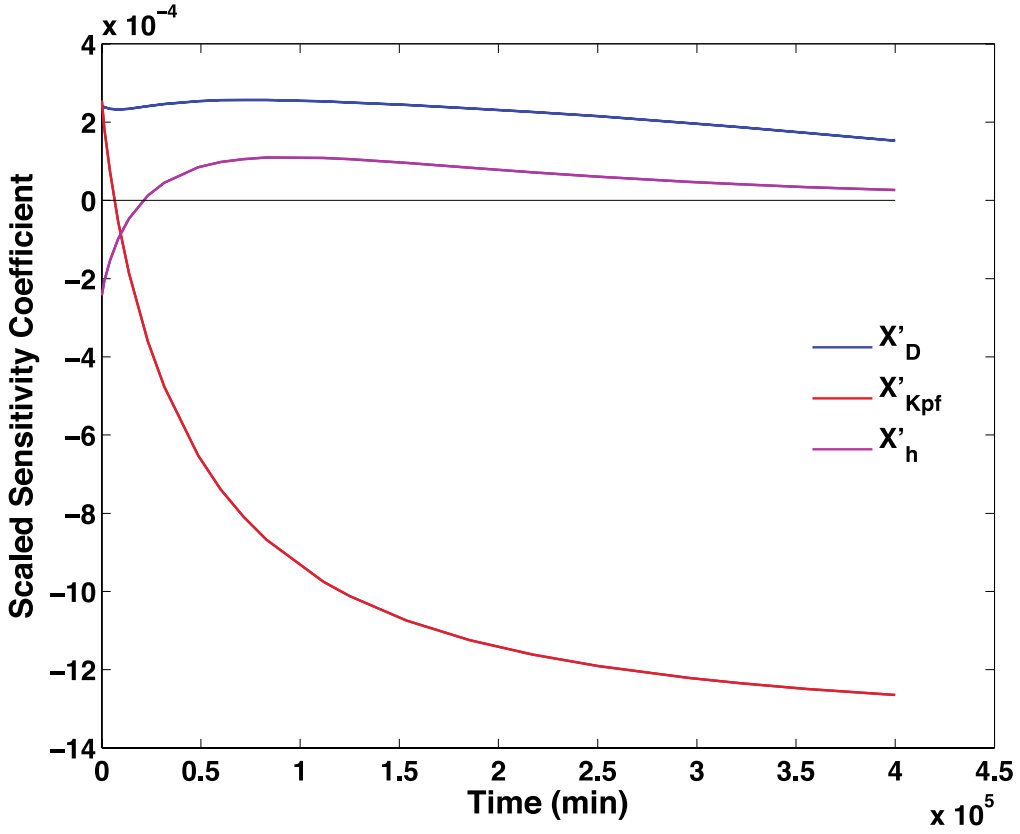

Figure 5-4 Scaled sensitivity coefficient of the kinetics migration parameters using initial guesses obtained from step 1. Initial guesses were: D=6.50 × 10^{-12} cm^2/min, $K_{p,f}$=605.00 cm^3 PLA/cm^3 ethanol, and h=5.90 × 10^{-6} cm/min.

5.6.3 Step 2

5.6.3.1 Ordinary Least Square (OLS) Estimation

All three kinetic migration parameters were successfully estimated by the proposed analytical solution (Eq. 5-46) (Figure 5-5). The estimated $K_{p,f}$, D and h values were 548.87 $\pm$ 21.76 cm^3 PLA/cm^3 ethanol, 5.42 $\pm$ 0.62 $\times$ 10^{-12} cm^2/min, and 2.56 $\pm$ 0.38 $\times$ 10^{-6} cm/min, respectively. The reported experimental $K_{p,f}$ value of this case study was 506.10 cm^3 PLA/cm^3 ethanol, which was not too far off from the estimated $K_{p,f}$ value, thus indicating an advantage from using the newly proposed model. Additionally, h was estimated for the first time without having an experimental set up. The importance of estimating h may have not be great for this particular case study since it seems not to be controlling the mass transfer process; however, it can be neglected since it could lead to overestimation or underestimation of a migration scenario. The feasibility of estimating h helps in reducing the experimental error due to the difficulty in measuring this parameter at the initial time. Vitrac et al. (2007) reported h of a range of 1.2 $\times 10^{-4}$ to 1.2 $\times 10^{-3}$ cm/min for alcohol homologous from a low density poly(ethylene), (LDPE) film into ethanol at 40 °C, which was higher than that estimated in this study. The low affinity of the migrant (*i.e.,* alcohol homologous) to ethanol besides the higher experimental temperature used could be responsible for the higher h value than that observed in this study. The existence of a slight interfacial resistance at the food simulant-PLA polymer interface was observed as shown by the kinetic desorption plot (Figure 5-6). On the other hand, the estimated D value found in this study was significantly lower by one magnitude order than that reported by Soto-Valdez et al. (2010) (5.42 $\times$ 10^{-12} cm^2/min vs. 2.04 $\times$ 10^{-11} cm^2/min. This discrepancy could be due to the different model selection. The accuracy of model selection can be assessed using the corrected Akaike information criterion (AICc) as a guideline. Further discussion can be found in Chapter 6.

Relative errors of $K_{p,}$, D and h were found to be 3.97, 11.38, and 14.97 %, respectively, thus confirming the indication observed from the scaled sensitivity coefficient plot (Figure 5-3). Residual plot (Figure 5-7) appears to be normally scattered with constant variance and additive errors, although a slight signature can be seen at time < 1×10^5 min. This issue could be due to experimental error as can be observed in Figure 5-5. Additional information such as correlation coefficients and confidence interval can be found in Table 5-2.

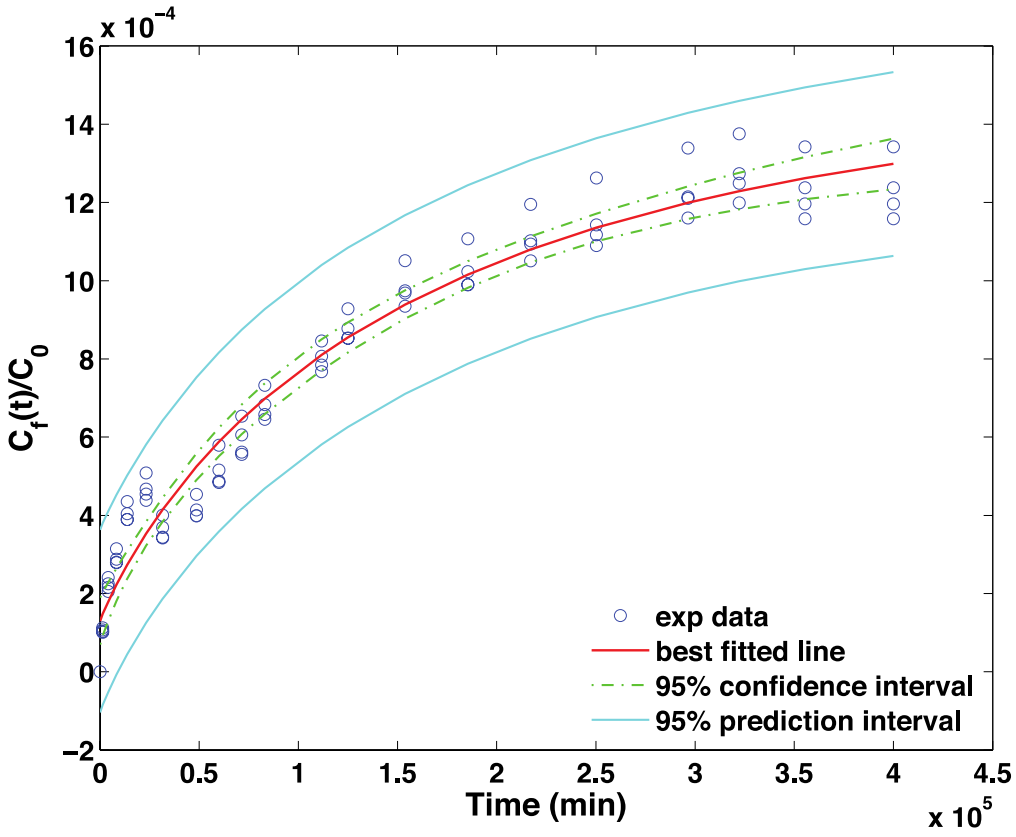

Figure 5-5 Migration of 3 wt.% of resveratrol into ethanol at 9 °C.

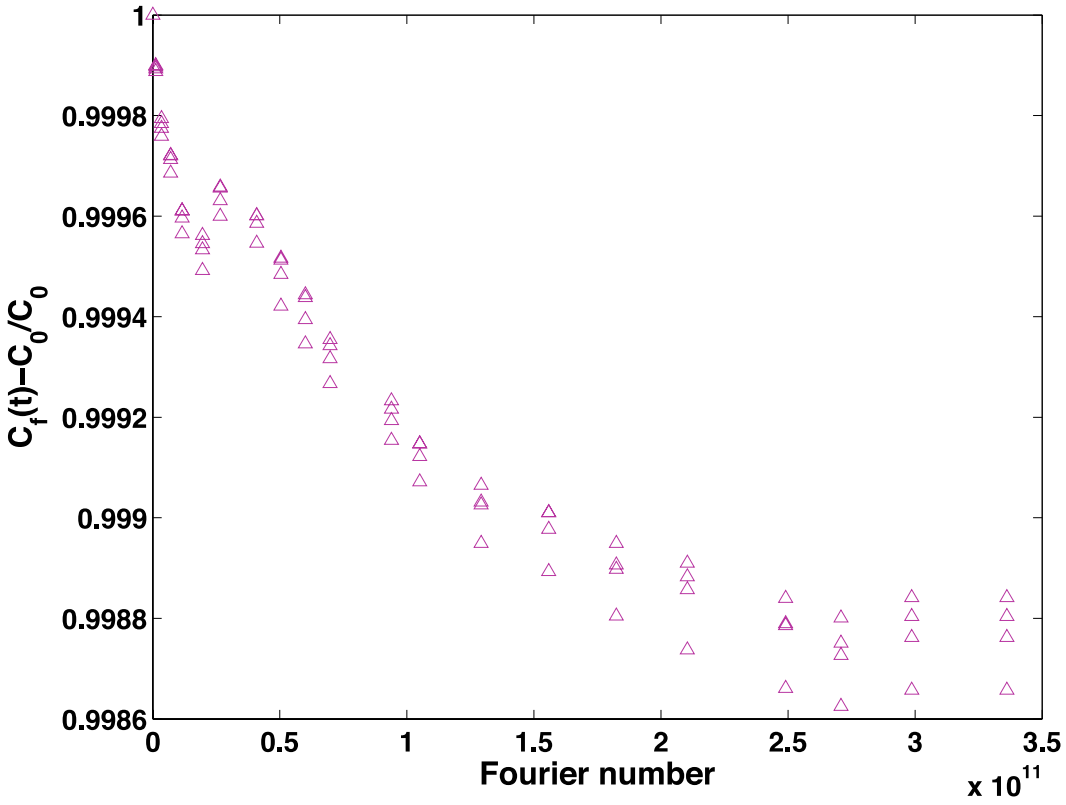

Figure 5-6 Desorption kinetics of PLA-3 wt.% resveratrol at 9 °C in the dimensionless time space (Fourier number=$\frac{Dt}{L^2}$).

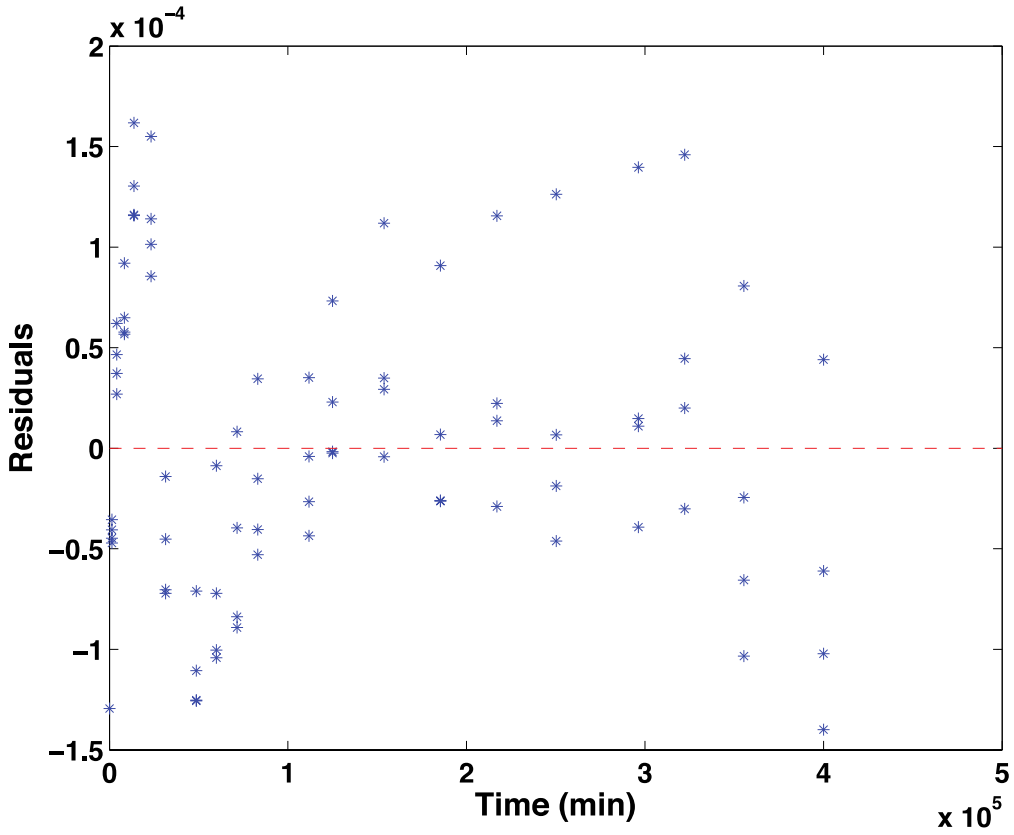

Figure 5-7 Residual plot for migration of 3 wt.% of resveratrol into ethanol at 9 °C.

Table 5-2 Additional information of OLS estimation.

Parameters	**95% Confidence interval**	**Correlation coefficients, ρ**		
		D **(cm^2/min)**	***Kp,f*** **(cm^3 PLA/cm^3 ethanol)**	***h*** **(cm/min)**
D (cm^2/min)	$4.19 – 6.65 \times 10^{-12}$			
Kp,f (cm^3 PLA/cm^3 ethanol)	505.56 – 592.17	0.95	Symmetric	
h (cm/min)	$1.80 - 3.33 \times 10^{-6}$	0.72	0.83	

5.7 Sequential Estimation

Sequential estimation results for each parameter were normalized by the estimates of dividing the i^{th} parameter by its final value to counteract the magnitude order differences among parameters. Figure 5-8 demonstrates the normalized sequential result for each parameter. All the estimated parameters were found to reach a constant state at around 2.0×10^5 min (~139 days); thus implying that the measurement does not need to be continued for much longer time afterward since it did not affect the parameters. Additionally, the parameters are expected to reach a constant state before an experiment ends. In the case that the constant state is not reached for a parameter, among the reasons that could have been responsible are insufficient data, number of parameters (too little or too many), and an imperfect physical model (Beck & Arnold, 1977). This particular information is an added insight that could not be gained from the OLS. Besides, the additional effect of new responses can be observed through the sequential estimation method since it continuously updates the parameters (Beck & Arnold, 1977). Table 5-2 shows the comparison between the OLS and the sequential estimation results. The results from both methods were in an agreement with each other.

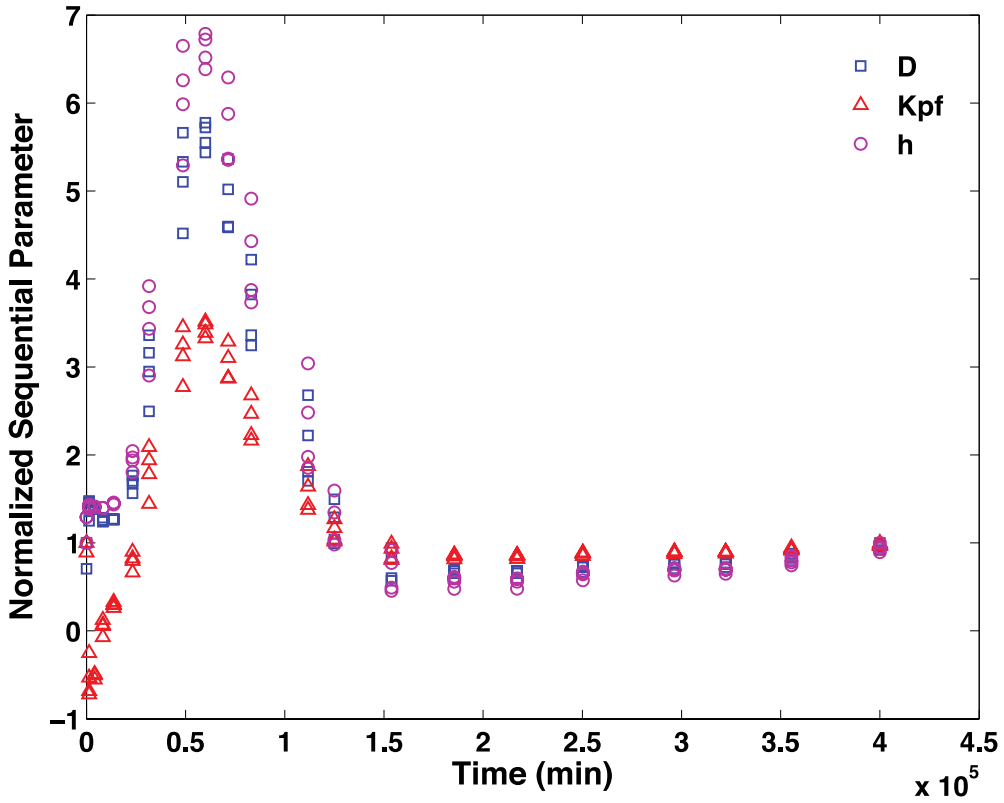

Figure 5-8 Normalized sequential parameters as a function of time for migration of 3 wt.% of resveratrol into ethanol at 9 °C.

Table 5-3 Comparison between OLS and sequential results.

Parameters	OLS			Sequential		
	Estimates ± Standard error	**Relative errors (%)**	**RMSE × 10^{-5}**	**Estimates ± Standard error**	**Relative errors (%)**	**RMSE × 10^{-5}**
$D \times 10^{-12}$ (cm^2/min)	5.42±0.62[a]	11.38		5.42±0.62[a]	11.47	
Kp,f (cm^3 PLA/cm^3 ethanol)	548.87±21.76[a]	3.97	7.91	548.87±21.95[a]	3.99	7.91
$h \times 10^{-6}$ (cm/min)	2.56±0.38[a]	14.97		2.56±0.39[a]	15.07	

Note: RMSE (Root mean square errors) unit= cm^3 ethanol/cm^3 PLA; Data is presented as mean ± standard error; similar superscripts represent no statistical difference at $p>0.05$ within the same row.

5.8 Kinetic Phase Diagram (KPD)

An approximation space, known as kinetic phase diagram (KPD) was used to assess information of the kinetics of migration (Vitrac & Hayert, 2006). This approach allows an easy approximation for sorption and desorption kinetics of migration. In a case where equilibrium state is not reached, this approach may be used to extrapolate the equilibrium state values by a linear approximation theory. Figure 5-9 (a) shows the sorption (migration) kinetic of 3 wt.% resveratrol

into ethanol, and its corresponding KPD. The noise due to experimental errors was filtered using a non-deterministic filtering method (weighting kernels) based on the local polynomial approximants (Ducruet et al., 2007; Vitrac & Hayert, 2006). As a result, the noise seen at time < 57 days becomes smoother as indicated by the filtered data (square dark cyan symbol) (Figure 5-9 (a)). Figure 5-9(b) shows the derivative of concentration as a function of time plotted vs concentration (C_f). A linear extrapolation that can be used to predict the theoretical equilibrium state (*i.e.*, the concentration of additive at equilibrium) by making the first derivative of the concentration as a function of time equal to zero is indicated by the blue line intersection in Figure 5-9 (a and b). Also, the initial slope of the KPD (Figure 5-9 (b)) provides an initial estimation of the rate of the compound leaving the polymer film. Additional interpretation of the KPD method can be obtained elsewhere (Ducruet et al., 2007; Vitrac & Hayert, 2006).

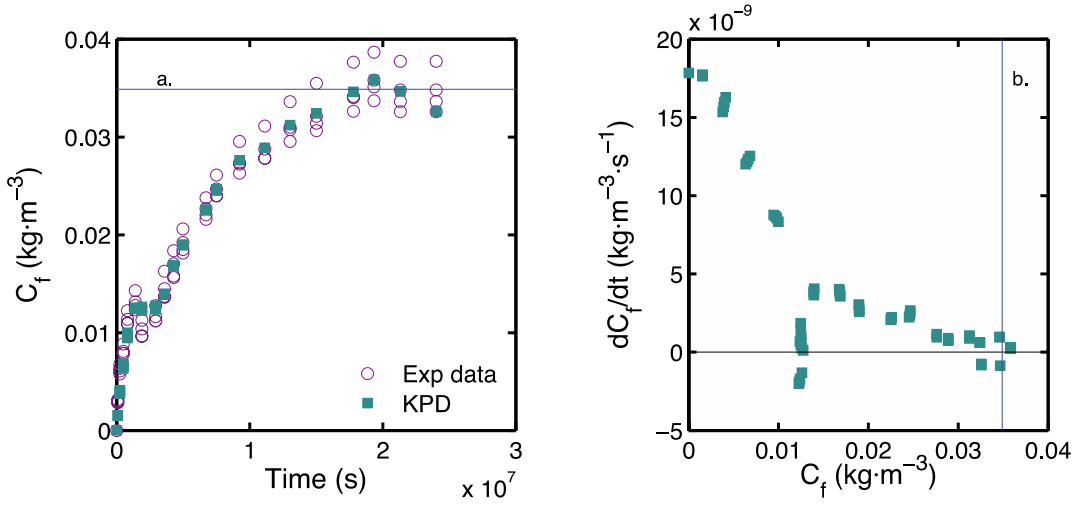

Figure 5-9 (a) Sorption kinetic of 3 wt.% resveratrol into ethanol, and (b) KPD. The blue line indicates the equilibrium state.

5.9 Residual Bootstrap

Residual bootstrap was performed and the results as expected did improve in terms of confidence interval (Table 5-3) and residual distribution (Figure 5-10) in comparison to the OLS results. However, a slight shift was observed in the lower bound of the bootstrap confidence interval and the upper bound shifted to lower levels than that of the asymptotic confidence interval for *D* and *h*. Similar outcomes were reported for the kinetic degradation of anthocyanins in grape pomace, indicating the flexibility of bootstrap from constrained need of being symmetric (Mishra, Dolan, & Yang, 2011). Clear improvement of the bootstrap method can be visualized in Figure 5-11. The bootstrap bands for both confidence and prediction are tighter than the asymptotic ones. Therefore, accuracy of estimation can be improved since the bootstrap method did statistical inference based on the size of the population (*i.e.*, for the 84 experimental data points and n=1000, we obtained 84,000 new resampling residual points), thus apparent results can be anticipated. Specifically, the information from bootstrap provides higher accuracy of a migration limit since it represents the population size with a tighter bandwidth of confidence and prediction intervals. Therefore, the information generated by this method could be used improve the uncertainty on migration limit that are of concern in food safety and provide tighter shelf life determination. Additionally, the bootstrap method does not rely on the distribution assumption, thus providing the actual representation of residuals, even when the sample size is insufficient and the data is ill-posed.

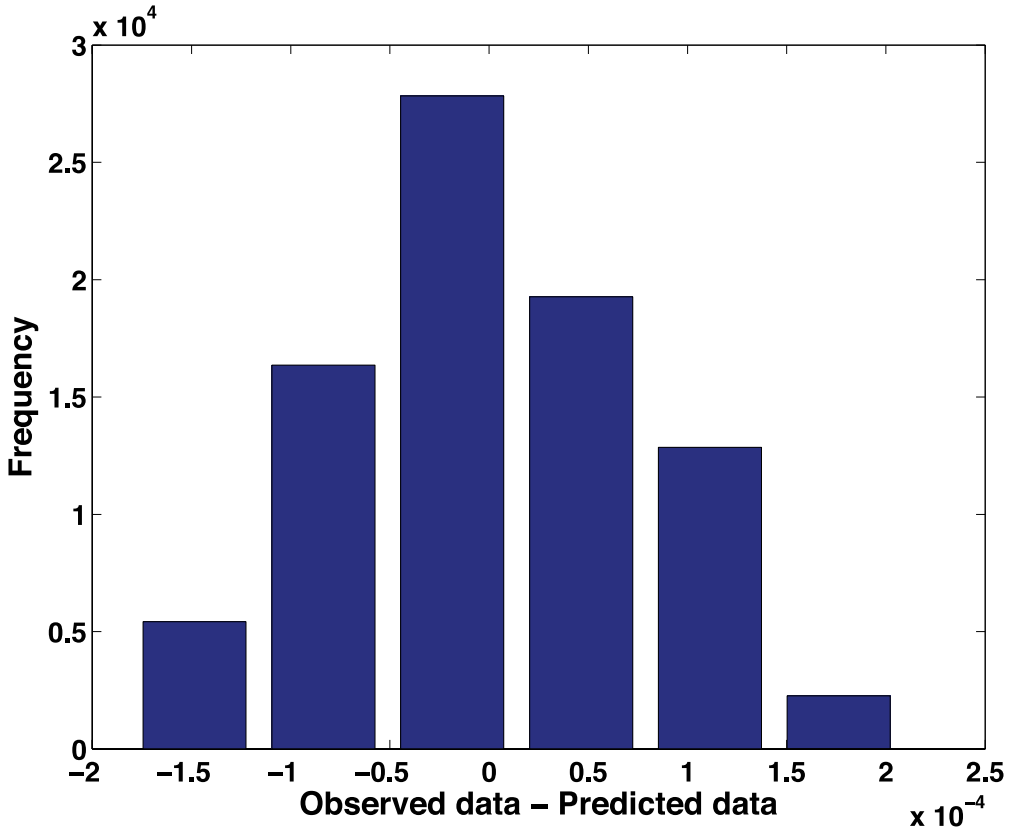

Figure 5-10 Histogram of the bootstrap residuals.

Table 5-4 Comparison between 95% asymptotic and 95% bootstrap confidence intervals of each parameter.

Parameters	**95% Asymptotic confidence interval**	**95% Bootstrap confidence interval**
$D\times 10^{-12}$ (cm^2/min)	4.19-6.65	4.46-6.55
$K_{p,f}$ (cm^3 PLA/cm^3 ethanol)	505.56-592.17	513.02-584.87
$h\times 10^{-6}$ (cm/min)	1.80-3.33	1.97-3.31

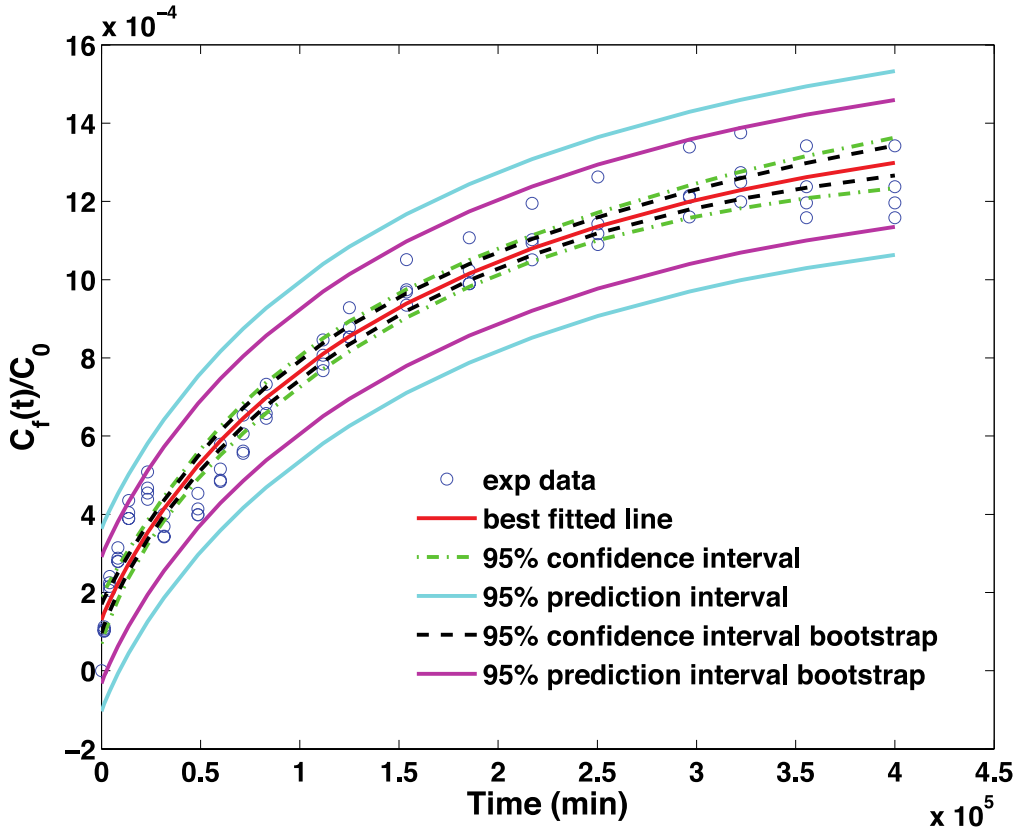

Figure 5-11 Migration of 3 wt.% of resveratrol into ethanol at 9 °C with added bootstrap results.

5.10 Conclusion

A two-step solution model was developed based on Crank's initial theoretical solution to obtain an analytical solution that provides a reasonable approximation for initial guesses needed for simultaneous parameter estimation allowing the estimation of three important kinetic migration parameters (D, $K_{p,f}$, and h) whenever possible (depend on the parameters' correlation based on the X') . This model was used to determine the D, $K_{p,f}$, and h of the migration of PLA added with 3%wt resveratrol. The new two-step solution was also successfully used to analyze a few selected case studies (*i.e.*, PLA incorporated with 2.6 wt.% α-tocopherol into ethanol at 23 °C and PLA incorporated with 1.28 wt.% catechin into 95% ethanol at 40 °C) that are shown in the Appendix

5A and 5B. The KPD approach was used to give additional insight on the sorption and desorption kinetics of the migration phenomenon. The residual bootstrap method provides insight information regarding the parameter estimation since they are estimated from a larger sample size population. This technique is particularly important since most of the data sets analyzed had a small sample size and large magnitude response was concentrated at the small region of time space. Further data validation is needed to ensure the robustness of the two-step solution model.

APPENDICES

APPENDIX 5A: Migration of poly(lactic acid), PLA incorporated with 2.6 wt.% α-tocopherol into ethanol at 23 °C.

Step 1

Figure 5A-1 shows the fitting of the step 1 solution Eq. 5-19 to PLA incorporated with 2.6 wt.% α-tocopherol into ethanol at 23 °C.

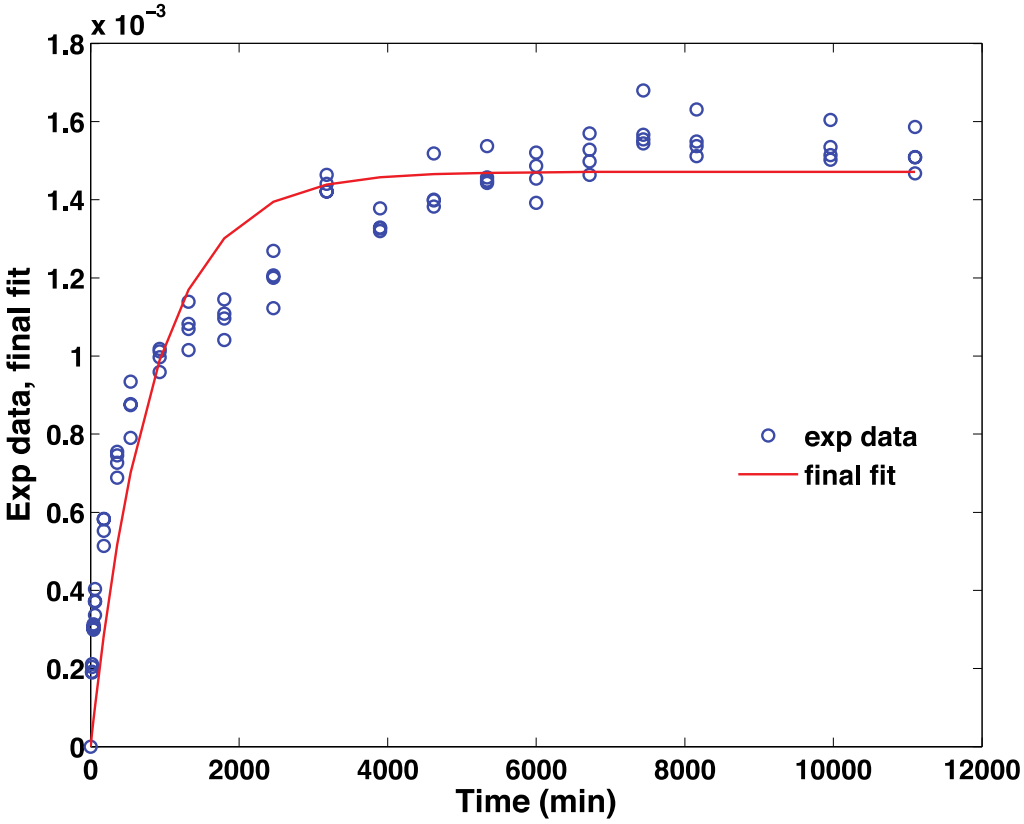

Figure 5A- 1 Experimental data fitting by using the simplified model of step 1. Initial approximation values obtained from this step were: D=1.88× 10^{-9} cm^2/min, $K_{p,f}$=608.11 cm^3 PLA/cm^3 ethanol, and h=4.19× 10^{-4} cm/min.

Scaled Sensitivity Coefficient, *X'*

Figure 5A-2 demonstrates the *X'* for PLA incorporated with 2.6 wt.% α-tocopherol into ethanol at 23 °C for three parameters. Since *D* and *h* are highly correlated ($\rho_{D,h} = 0.99$), only *D* and $K_{p,f}$ were estimated. *h* was not estimated due to it having the smallest magnitude of response. Figure 5A-3 shows the for *X'* for *D* and $K_{p,f}$.

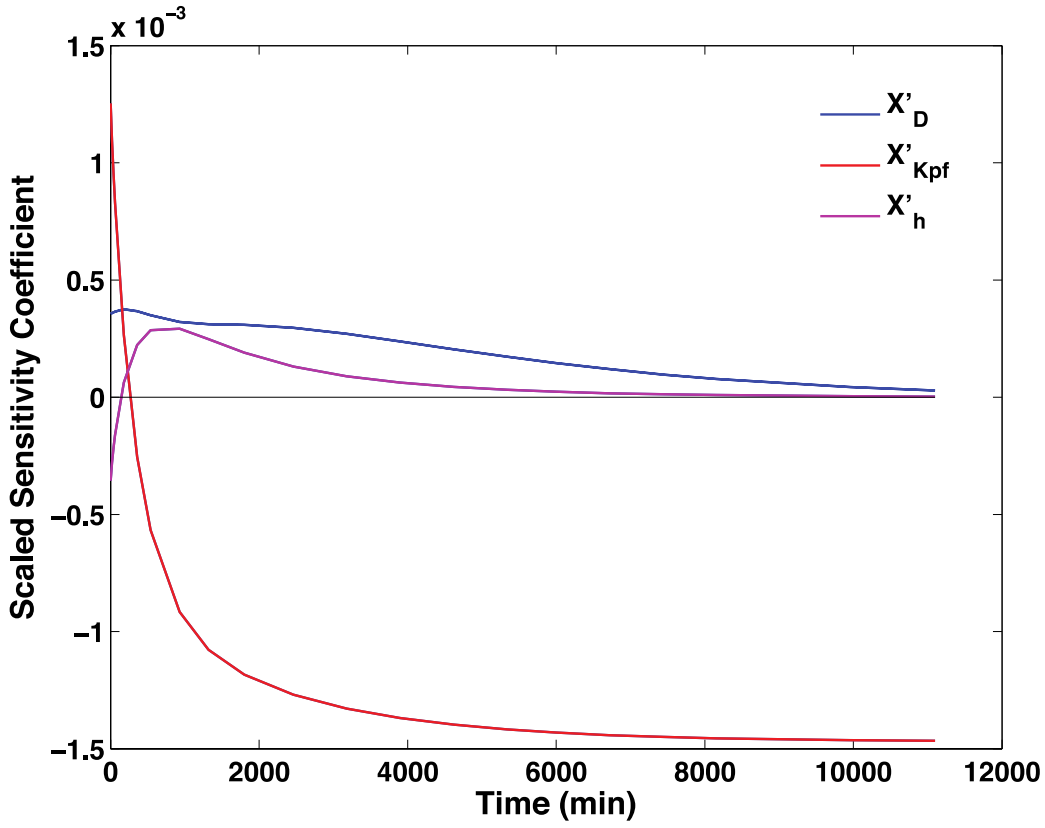

Figure 5A- 2 Scaled sensitivity coefficient of the kinetics migration parameters using initial guesses obtained from step 1. Initial guesses were: D=1.90 × 10^{-9} cm^2/min, $K_{p,f}$=608.11 cm^3 PLA/cm^3 ethanol, and h=8.00× 10^{-4} cm/min.

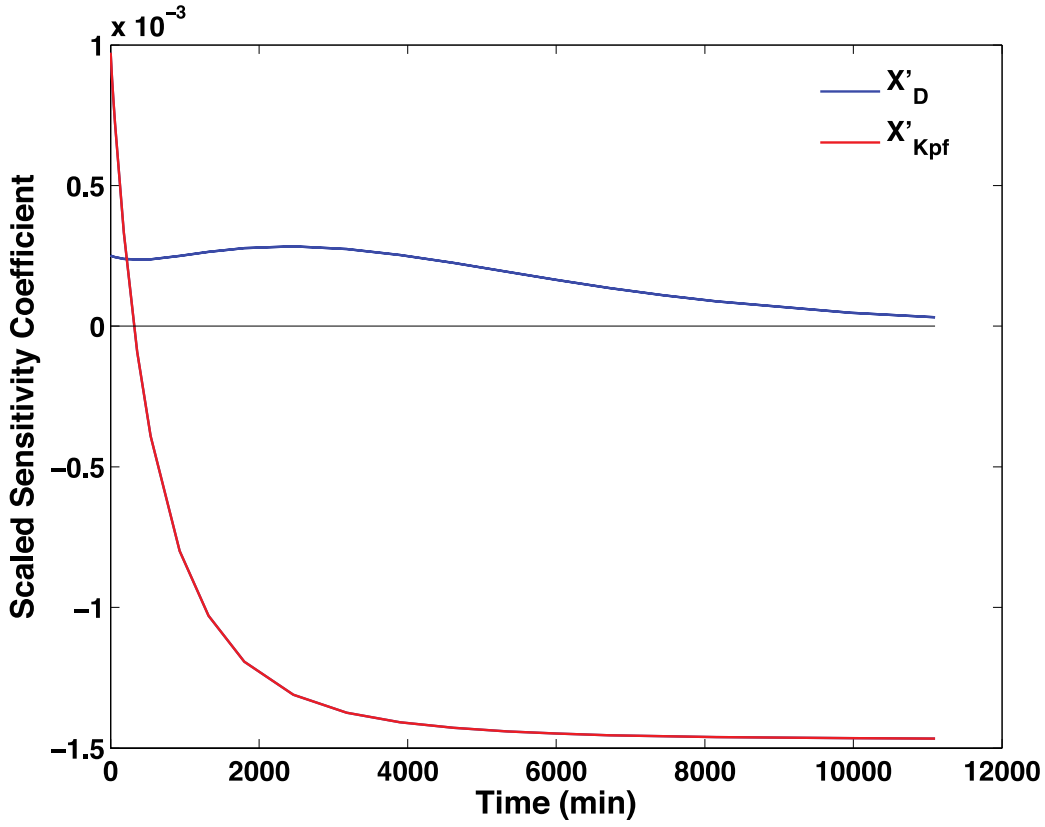

Figure 5A- 3 Scaled sensitivity coefficient of the kinetics migration parameters (D and $K_{p,f}$) using initial guesses obtained from step 1. Initial guesses were: D=2.00 × 10^{-9} cm^2/min, $K_{p,f}$=609.00 cm^3 PLA/cm^3 ethanol.

Step 2

Figure 5A-4 shows the migration of 2.6 wt.% α-tocopherol into ethanol at 23 °C with the predicted values, 95% confidence and prediction intervals. Meanwhile, Figure 5A-5 shows the desorption kinetic of the aforementioned migration in the dimensionless time.

Ordinary Least Square (OLS) Estimation

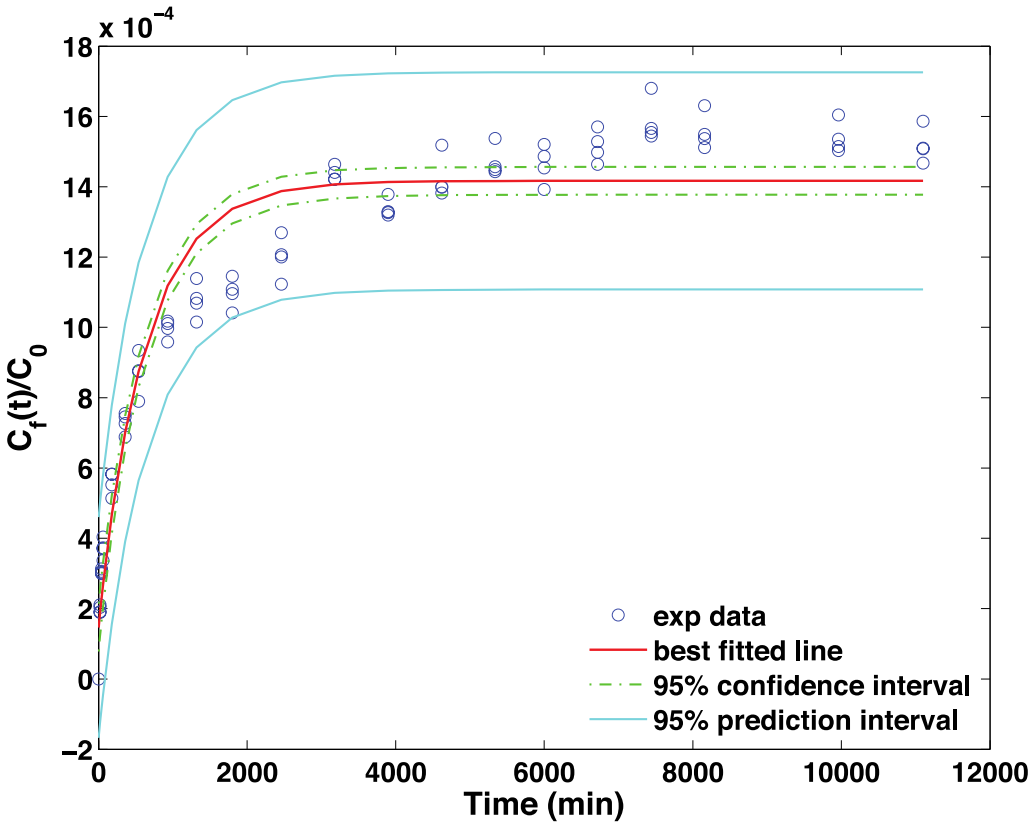

Figure 5A- 4 Migration of 2.6 wt.% α-tocopherol into ethanol at 23 °C.

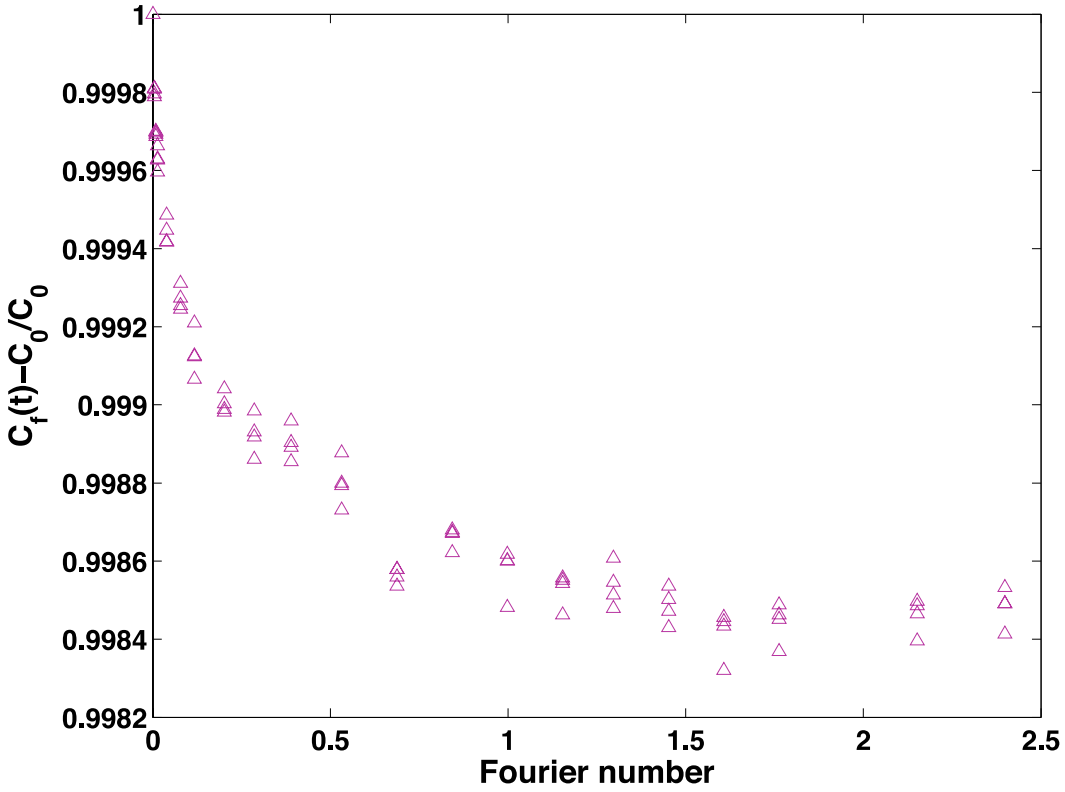

Figure 5A- 5 Desorption kinetics of PLA-2.6 wt.% α-tocopherol at 23 °C in the dimensionless time space (Fourier number=$\frac{Dt}{L^2}$).

Figure 5A-6 demonstrates the residuals plot for the two estimated parameters (*i.e.*, D and $K_{p,f}$). Signature of the residuals can be observed, in particular at the beginning of the experimental duration.

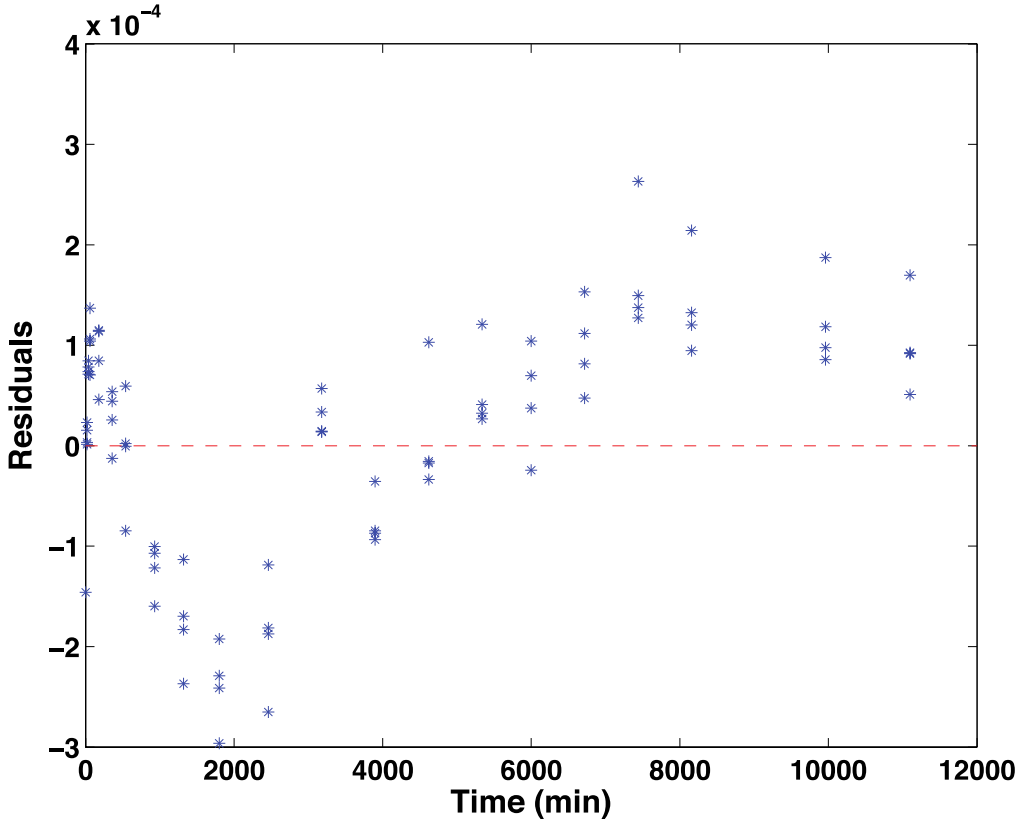

Figure 5A- 6 Residual plot for migration of 2.6 wt.% α-tocopherol into ethanol at 23 °C for two parameters estimation.

OLS results can be found in Table 5A-1 and the comparison between the two estimation approaches (*i.e.,* OLS and sequential) can be observed in Table 5A-2. Figure 5A-7 shows the normalized sequential parameters, which indicated that the parameters had reached their constants state toward the end of experimental duration.

Table 5A- 1 Additional information of OLS estimation for migration of 2.6 wt.% α-tocopherol into ethanol at 23 °C.

Parameters	**Estimates**	**95% Confidence interval**	**Correlation coefficients, ρ**		
			D	***Kp,f*** **(cm^3 PLA/cm^3 ethanol)**	***h***
$D \times 10^{-10}$ (cm^2/min)	64.41 ± 0.075	62.92-65.91			
Kp,f (cm^3 PLA/cm^3 ethanol)	631.54 ± 7.08	617.46-645.63	0.72	Symmetric	
h (cm/min)	NE				

*NE: Not estimated

Table 5A- 2 Comparison between OLS and sequential results.

Parameters	OLS			Sequential		
	Estimates ± Standard error	**Relative errors (%)**	**RMSE × 10^{-5}**	**Estimates ± Standard error**	**Relative errors (%)**	**RMSE × 10^{-5}**
$D \times 10^{-10}$ (cm^2/min)	64.4130±0.753	1.17		64.4323±0.734	1.14	
Kp,f (cm^3 PLA/cm^3 ethanol)	631.54±7.08	1.12	12.29	631.83±7.06	1.12	13.03

Note: RMSE (Root mean square errors) unit= cm^3 ethanol/cm^3 PLA

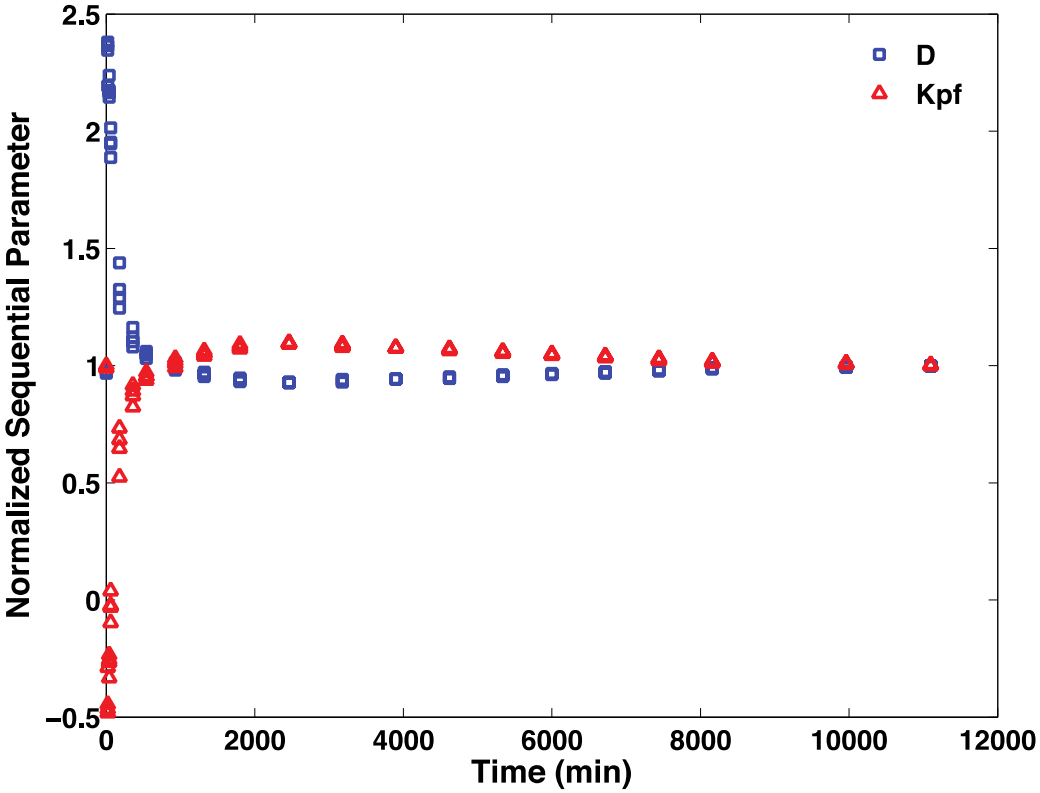

Figure 5A- 7 Normalized sequential parameters as a function of time for migration of 2.6 wt.% of α-tocopherol into ethanol at 23 °C.

Kinetic Phase Diagram (KPD)

Figure 5A-8 (a) shows the KPD for migration of 2.6 wt.% of α-tocopherol into ethanol at 23 °C fitted with the experimental data and Figure 5A-8(b) shows the linear slope that can be used to extrapolate the equilibrium state of α-tocopherol.

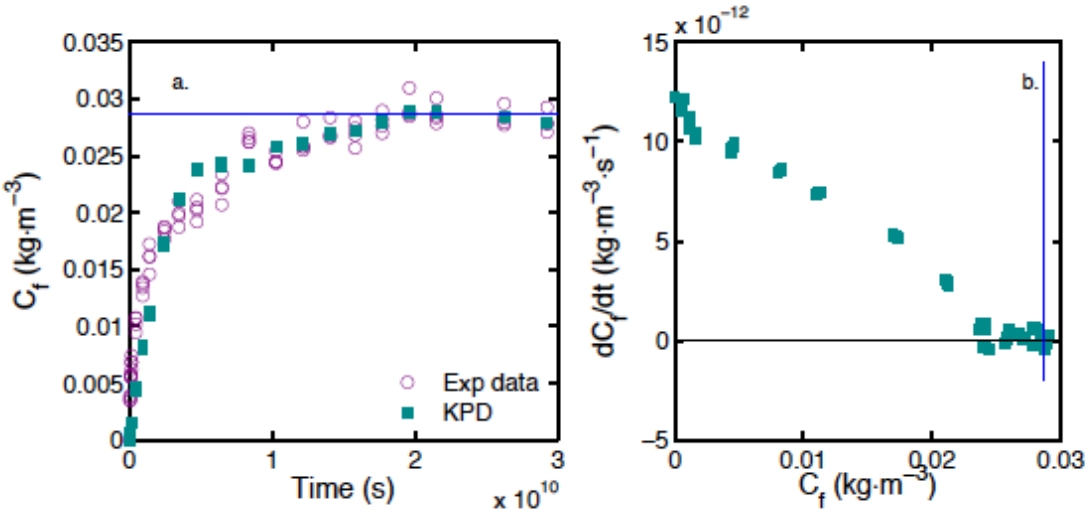

Figure 5A- 8 (a) Sorption kinetic of 2.6 wt.% α-tocopherol into ethanol, and (b) KPD. The blue line indicates the equilibrium state.

Residual Bootstrap

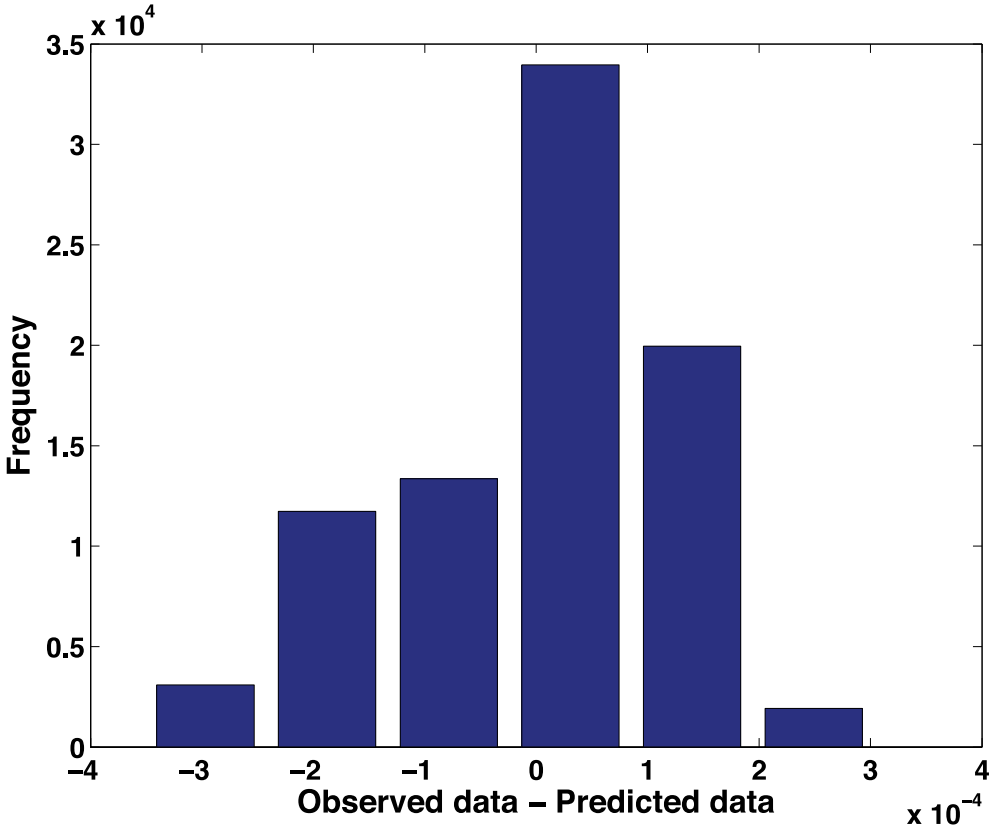

Figure 5A- 9 Histogram of the bootstrap residuals.

The results from residual bootstrapping can be found in Figure 5A-9 and Table 5A-3. Results indicated the improvement of the residual distribution as can be observed in Figure 5A-10.

Table 5A- 3 Comparison between 95% asymptotic and 95% bootstrap confidence intervals of each parameter.

Parameters	95% Asymptotic confidence interval	95% Bootstrap confidence interval
$D\times 10^{-10}$ (cm^2/min)	62.91-65.91	63.49-66.13
Kp,f (cm^3 PLA/cm^3 ethanol)	617.46-645.63	618.26-641.84

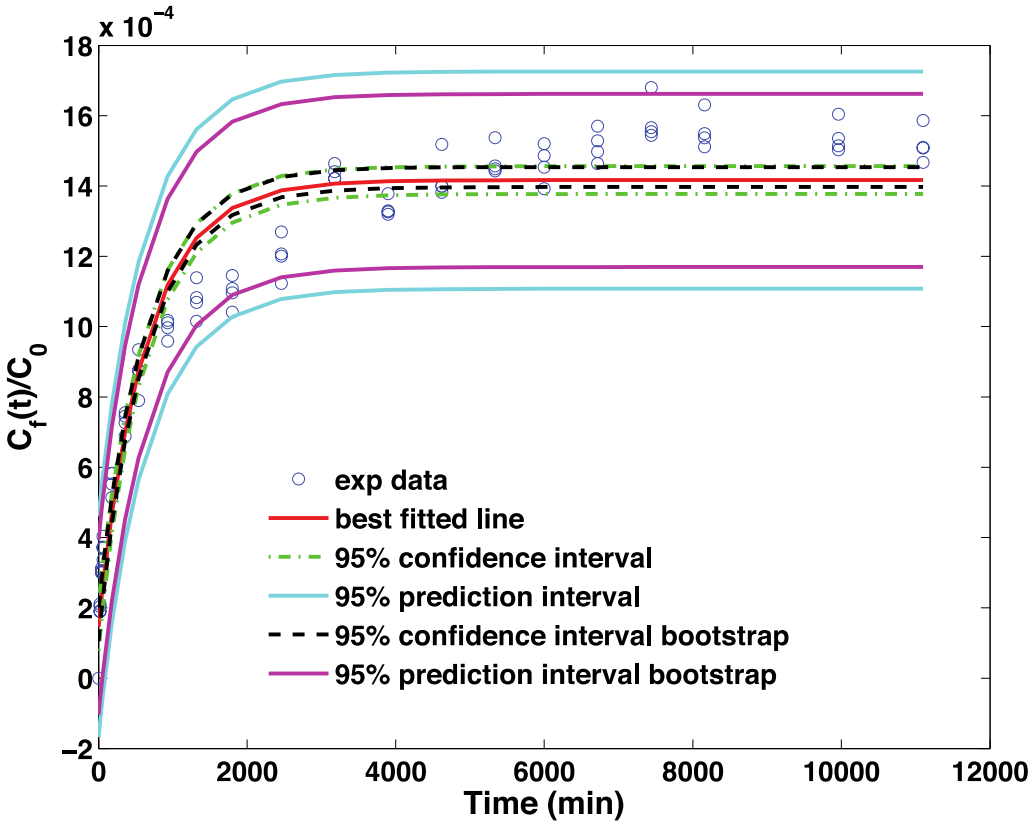

Figure 5A- 10 Migration of 2.6 wt.% α-tocopherol into ethanol at 23 °C with added bootstrap results.

APPENDIX 5B: Migration of poly(lactic acid), PLA incorporated with 1.28 wt.% catechin into 95% ethanol at 40 °C.

Step 1

Figure 5B-1 shows the experimental data fitting of migration of 1.28 wt.% catechin into 95% ethanol at 40 °C from PLA with Eq. 5-19.

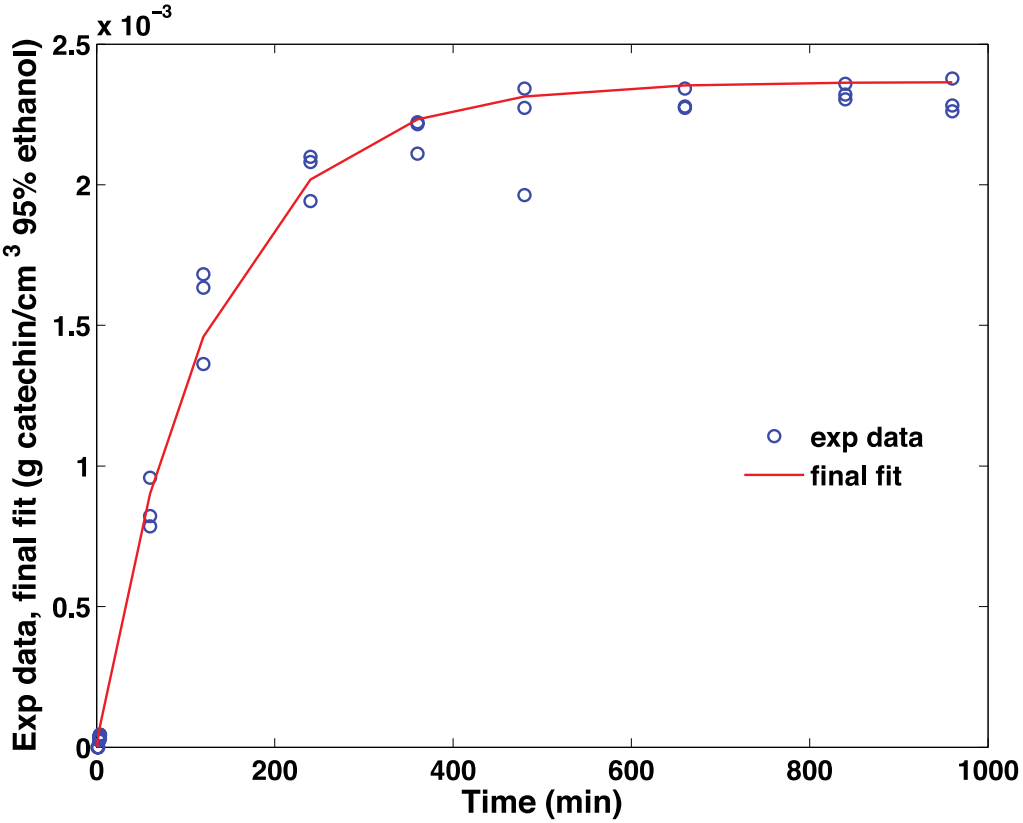

Figure 5B- 1 Experimental data fitting by using a simplified model of step 1. Initial approximation values obtained from this step were: D=1.39 × 10^{-8} cm^2/min, $K_{p,f}$=318.97 cm^3 PLA/cm^3 ethanol, and h=0.0024 cm/min.

Scaled Sensitivity Coefficient, *X'*

Figure 5B-2 indicates that all parameters can be estimated simultaneously for the migration of 1.28 wt.% catechin into 95% ethanol at 40 °C from PLA.

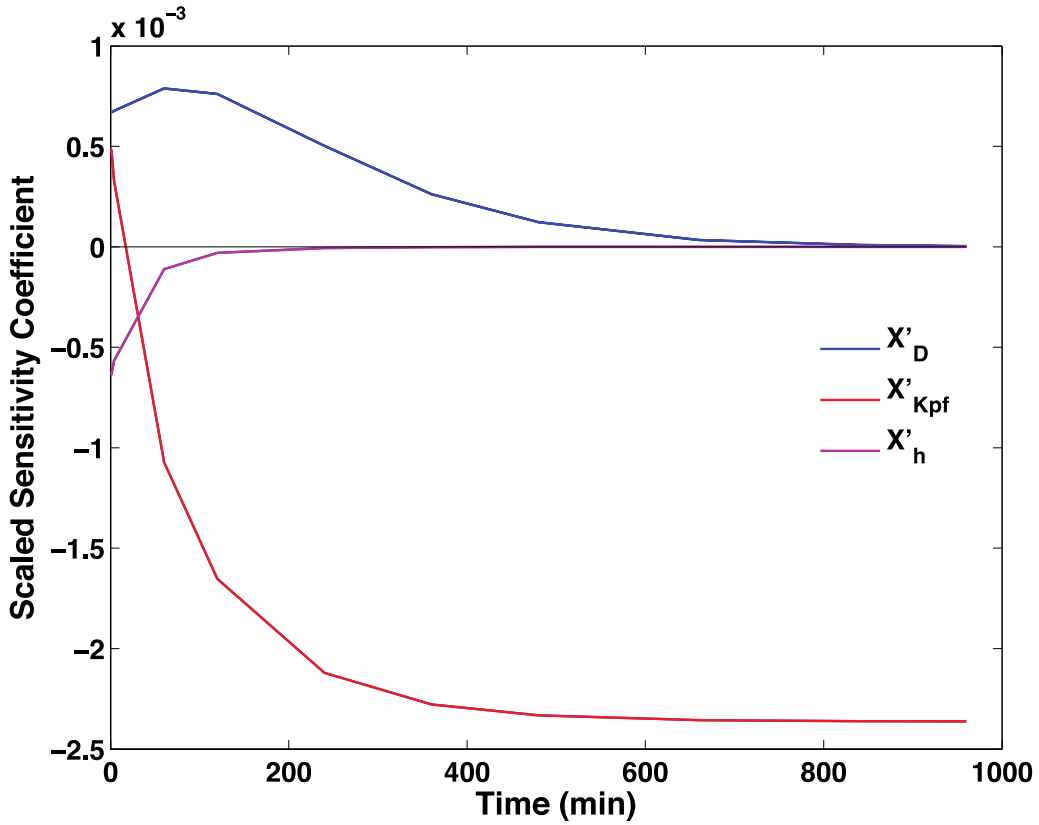

Figure 5B- 2 Scaled sensitivity coefficient of the kinetics migration parameters using initial guesses obtained from step 1. Initial guesses were: D=3.00 × 10^{-8} cm^2/min, $K_{p,f}$=318.97 cm^3 PLA/cm^3 ethanol, and h=0.0040 cm/min.

Step 2

Ordinary Least Square (OLS) Estimation

Figure 5B-3 and Figure 5B-4 show the migration of 1.28 wt.% catechin into 95% ethanol at 40 °C and desorption kinetics of the similar migration study in the dimensionless time space, respectively.

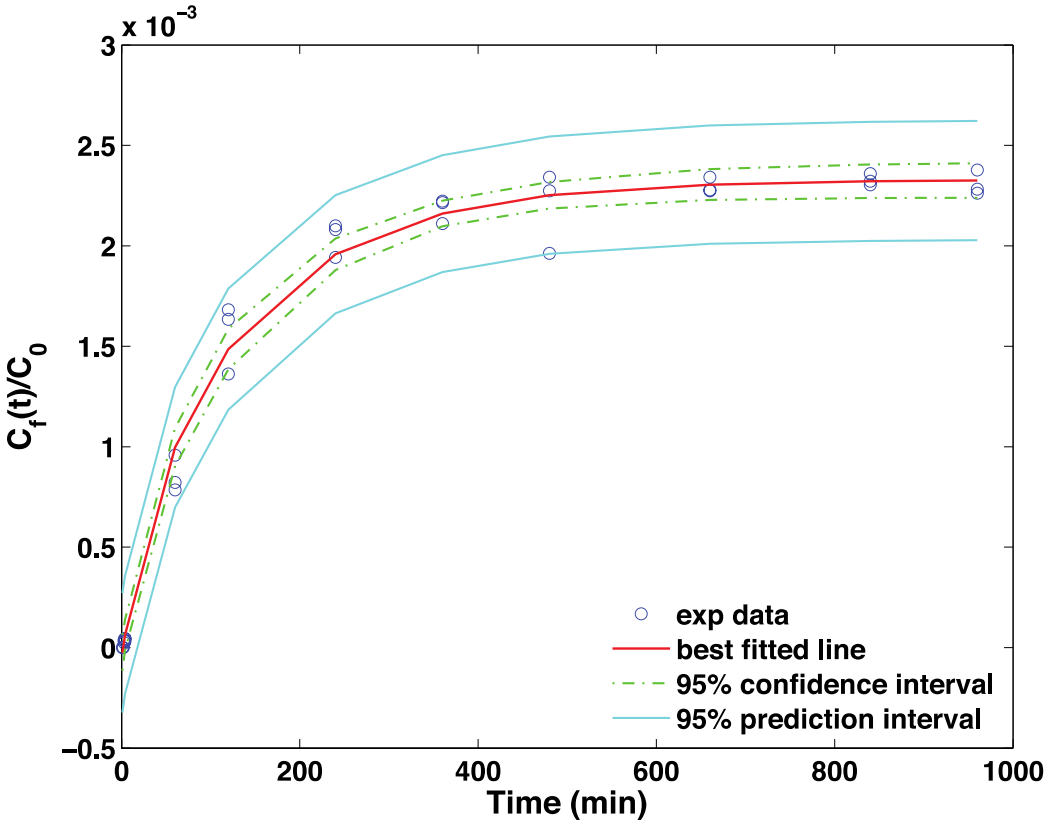

Figure 5B- 3 Migration of 1.28 wt.% catechin into 95% ethanol at 40 °C.

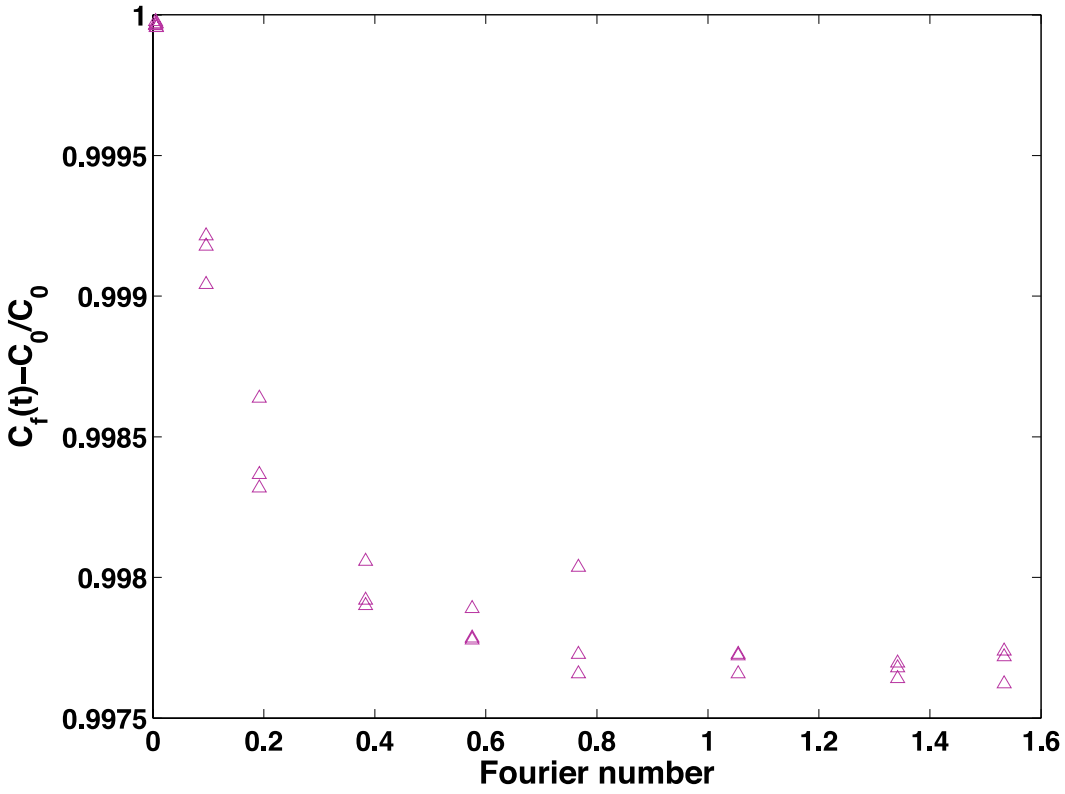

Figure 5B- 4 Desorption kinetics of PLA-1.28 wt.% catechin at 40 °C in the dimensionless time space (Fourier number=$\frac{Dt}{L^2}$).

Residual plot of migration of 1.28 wt.% catechin into 95% ethanol at 40 °C showed better normal residual distribution in comparison with the other two case studies (Figure 5B-5). Comparison between OLS and sequential estimations can be found in Table 5B-2. Additional OLS results are shown in Table 5B-1.

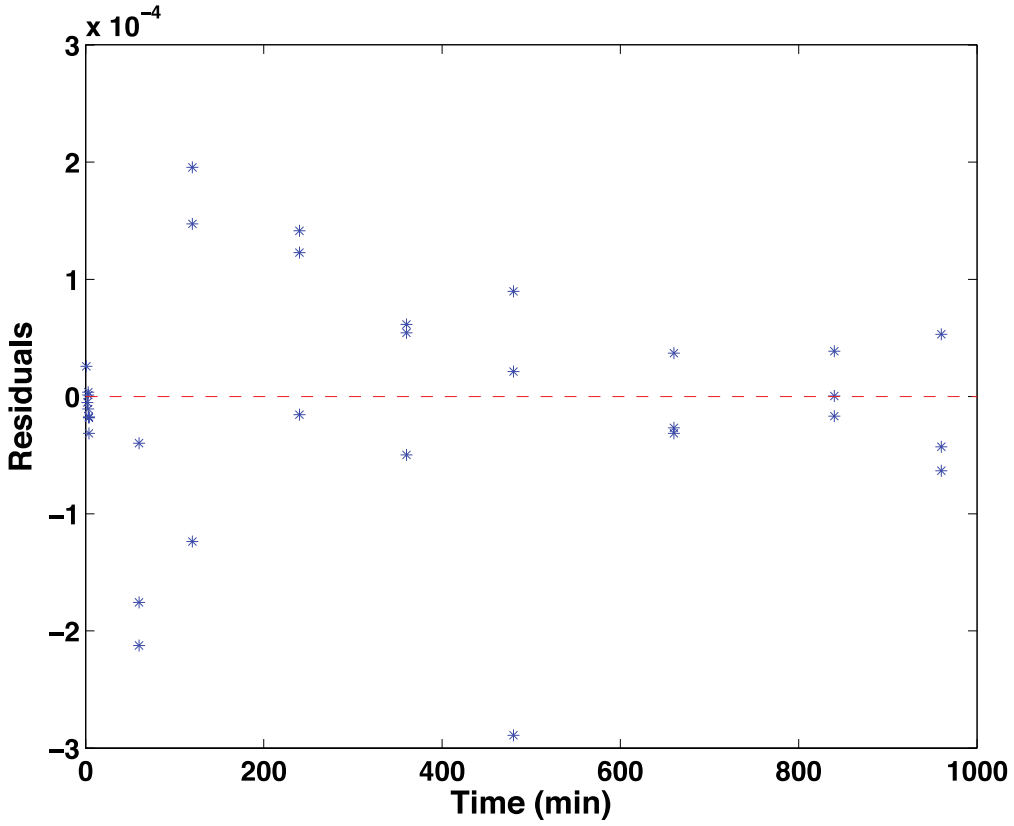

Figure 5B- 5 Residual plot for migration of 1.28 wt.% catechin into 95% ethanol at 40 °C.

Table 5B- 1 Additional information of OLS estimation for migration of 1.28 wt.% catechin into 95% ethanol at 40 °C.

Parameters	**Estimates**	**95% Confidence interval**	**Correlation coefficients, ρ**		
			D **(cm^2/min)**	***Kp,f*** **(cm^3 PLA/cm^3 95% ethanol)**	***h*** **(cm/min)**
$D \times 10^{-10}$ (cm^2/min)	225.86 ± 13.43	198.64-253.08			
Kp,f (cm^3 PLA/cm^3 95% ethanol)	324.04 ± 4.15	315.59-332.49	0.64	Symmetric	
$h \times 10^{-4}$ (cm/min)	44.00 ± 4.26	36.00-53.00	0.60	0.56	

Table 5B- 2 Comparison between OLS and sequential results.

Parameters	OLS			Sequential		
	Estimates ± Standard error	**Relative errors (%)**	**RMSE $\times 10^{-5}$**	**Estimates ± Standard error**	**Relative errors (%)**	**RMSE $\times 10^{-5}$**
$D \times 10^{-10}$ (cm^2/min)	225.86±13.40	5.92		225.84±13.34	5.91	
Kp,f (cm^3 PLA/cm^3 95% ethanol)	324.04±4.15	1.28	9.6412	324.04±4.14	1.28	9.6413
$h \times 10^{-4}$ (cm/min)	44.00±4.26	9.62		44.00±4.25	9.60	

Note: RMSE (Root mean square errors) unit= cm^3 95% ethanol/cm^3 PLA.

Sequential plot of estimated parameters of migration of 1.28 wt.% of catechin into 95% ethanol at 40 °C reached a constant about 8 hrs (500 min) (Figure 5B-6).

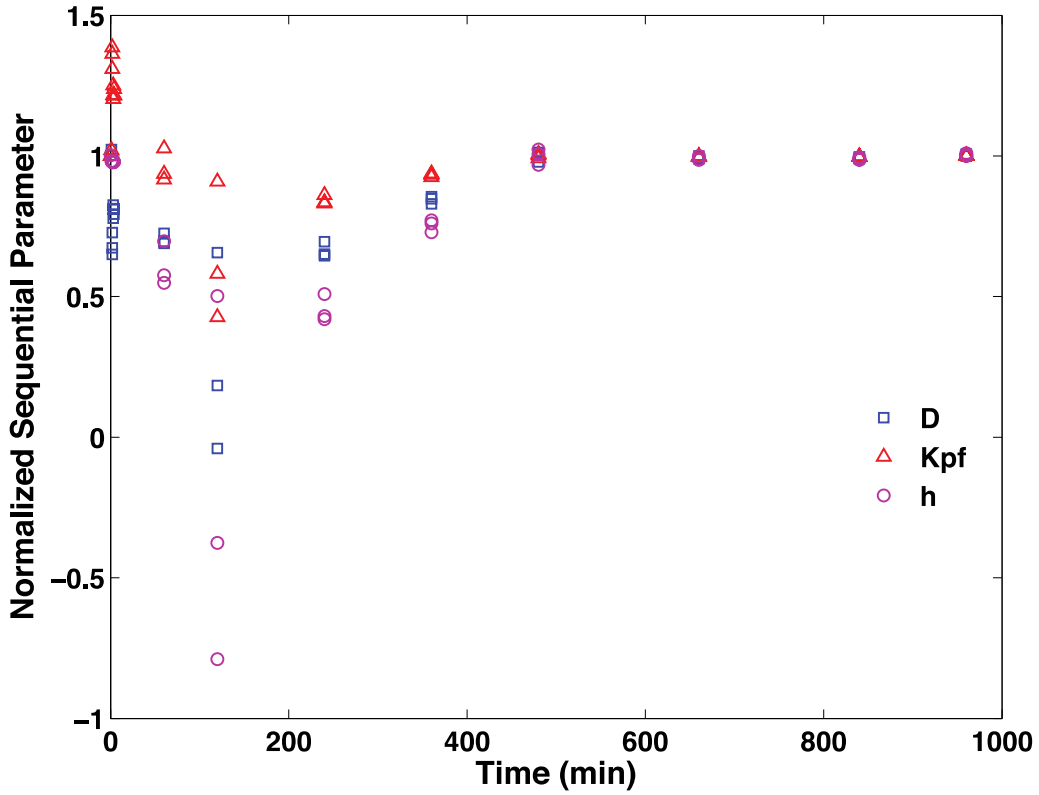

Figure 5B- 6 Normalized sequential parameters as a function of time for migration of 1.28 wt.% of catechin into 95% ethanol at 40 °C.

Kinetic Phase Diagram (KPD)

Figure 5B-7 (a) and (b) indicates the sorption kinetic of 1.28 wt.% catechin into 95% ethanol and its KPD space that corresponding to the theoretical sorption equilibrium.

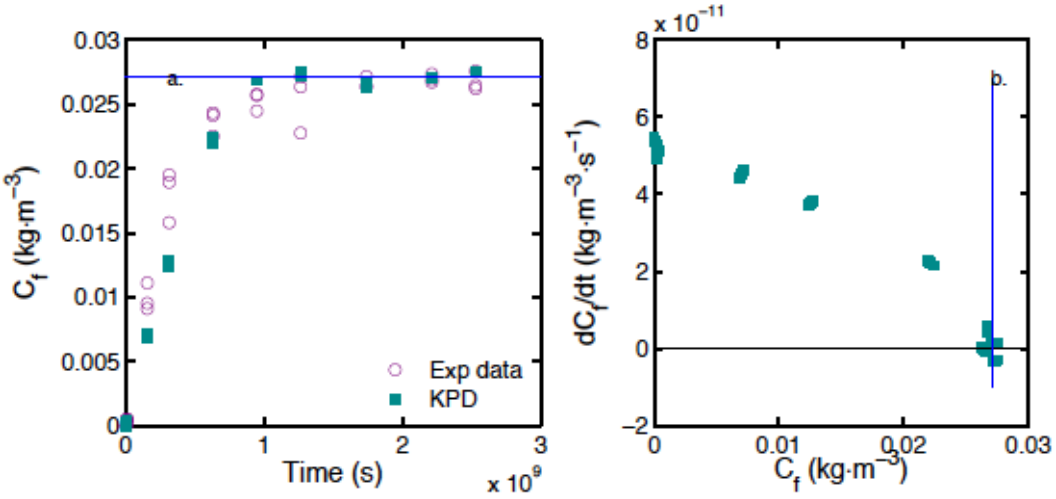

Figure 5B- 7 (a) Sorption kinetic of 1.28 wt.% catechin into 95% ethanol, and (b) KPD. The blue line indicates the equilibrium state.

Residual Bootstrap

The bootstrap residual histogram of migration of 1.28 wt.% catechin into 95% ethanol had a normal Gaussian distribution (Figure 5B-8). The 95% bootstrap confidence interval had a tighter and asymmetrical band compared to 95% asymptotic confidence interval (Table 5B-3), which indicated the flexibility of bootstrap under no assumption of the shape of the residual distribution.

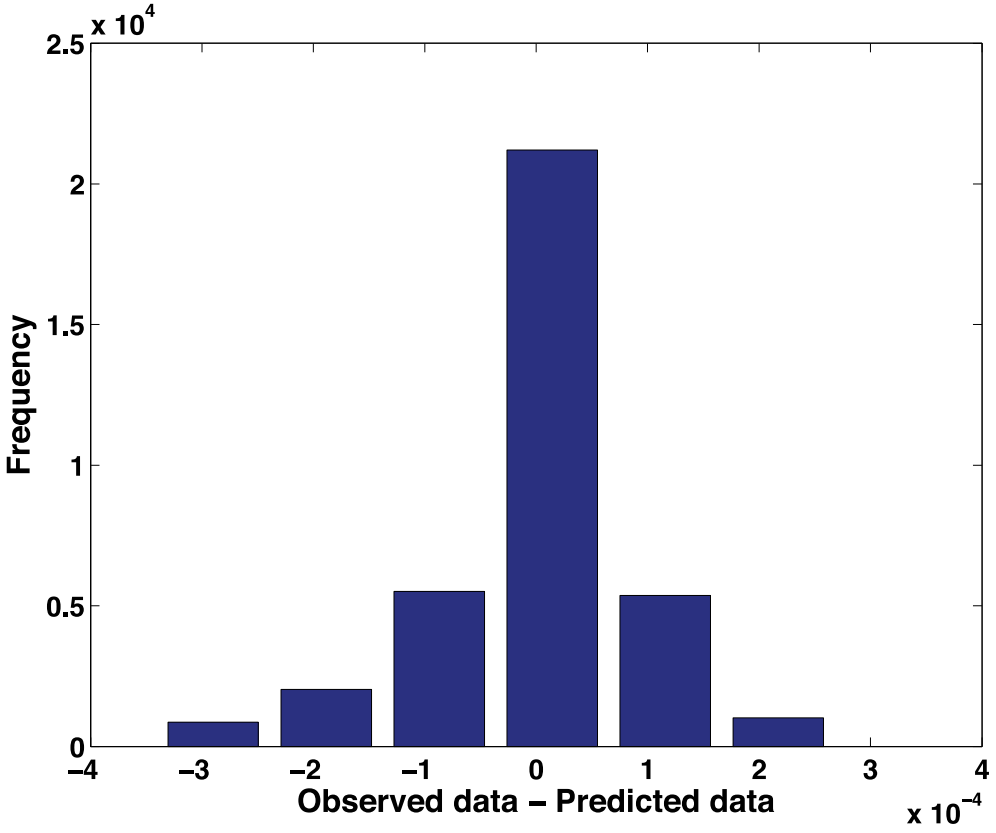

Figure 5B- 8 Histogram of the bootstrap residuals.

Table 5B- 3 Comparison between 95% asymptotic and 95% bootstrap confidence intervals of each parameter.

Parameters	**95% Asymptotic confidence interval**	**95% Bootstrap confidence interval**
$D \times 10^{-10}$ (cm^2/min)	198.64-253.08	203.68-251.37
Kp,f (cm^3 PLA/cm^3 ethanol)	315.59-332.49	318.09-333.00
$h \times 10^{-4}$ (cm/min)	36.00-53.00	39.00-54.00

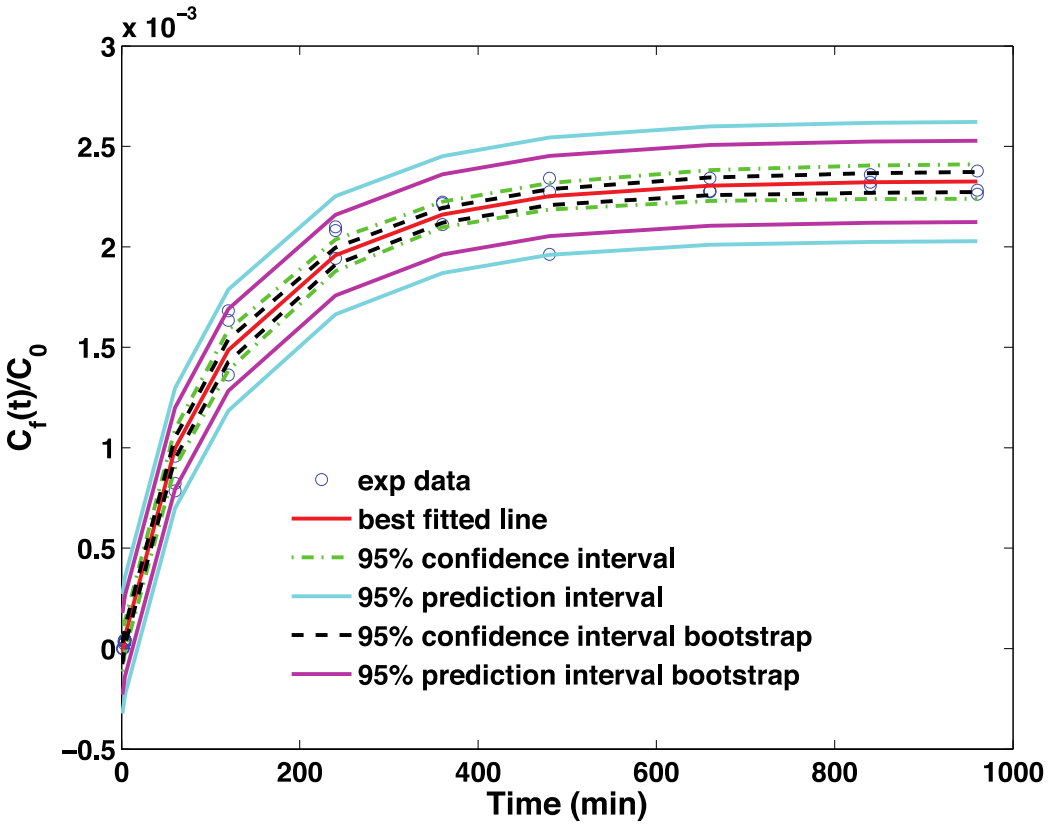

Figure 5B- 9 Migration 1.28 wt.% catechin into ethanol at 40 °C with added bootstrap results.

APPENDIX 5C: Example of MATLAB coding

```
%% CONVECTIVE MASS TRANSFER STUDY
%% HouseKeeping & Data
close all;
clear all;
clc
format long
data =xlsread('PLA_RESV3_9C_REPS');% To read raw data from excel
global L
global alpha
%%
%% File Directory
switch localname
    case '13-138-76.client.wireless.msu.edu'
        local                                                                    =
'/Users/HAYATISAMSUDIN/Documents/MATLAB_EXP/MATLAB_CIADEXP/MODELS
COMPARISON';
        papertype = 'A4';
        paperposition = [0.3397    10.1726    20.3046    9.3322]; %cm
    otherwise
        local = pwd;
        papertype = 'usletter';
```

```
    paperposition = [0.3397   10.1726   20.3046    9.3322]; %update the values to usletter format
    warning('Please set the case for your computer')
end
datafile = 'PLA_RESV3_9C_REPS.xls';
outputfolder = fullfile(local,'Figures_PLARESV3_9C'); if ~exist(outputfolder,'dir'),
mkdir(outputfolder), end
[~,outputfile] = fileparts(datafile);

%% Extracted Info
L=0.00254;%L= half of the thickness, cm
A=3.1416;  %A=area, cm2
Co=0.028115; % Co=Initial concentration, g/cm3
Vf=1.227 % Vf=volume of food,cm3
t=data(:,1);
yobs=data(:,2);
yobs2=data(:,2)./Co;
%% Step 1: Simplified Model
sum1=0;
sum2=0;
R=linspace(0.00000850,0.000009000,100);
N=length(data);
for j=1:length(R)
for i=1:N
   if i == 1
```

```
        fit(i) = 0
    else
     z=1-exp(-R(j)*t(i));
    sum1=sum1+z.*yobs2(i);
    sum2=sum2+z.^2
    P(j)=sum1/sum2
    fit=P(j)*z;
    end
end
fitreverse=fit';
SSE(j)=sumsqr(yobs2-fitreverse)
end
comparison=[P' R' SSE']
Index=0:1:N;
[M,I]=min(SSE);%I is index refers to min value of SSE
showminSSE=[P(I) R(I)] % to display P and R corresponding to I=index of min SSE
figure
[hAx,hLine1,hLine2]=plotyy(SSE,P,SSE,R)
title('Combination of P and R with SSE','FontSize',16,'FontWeight','bold')
xlabel('SSE','FontSize',16,'FontWeight','bold')
ylabel(hAx(1),'P','FontSize',16,'FontWeight','bold') % left y-axis
ylabel(hAx(2),'R','FontSize',16,'FontWeight','bold') % right y-axis
```

```
%%
for i=1:N
   if i == 1
      fit(i) = 0
   else
    z=1-exp(-R(I)*t(i));
   final_fit(i)=P(I)*z;
   end
end
display(final_fit)
predict_obs=final_fit';
Table=[t yobs final_fit' ]
figure
hold on
set(gca, 'fontsize',14,'fontweight','bold');
pl(1)=plot(t, yobs2, 'o','LineWidth',1.01)
pl(2)=plot(t, final_fit,'r','LineWidth',1.01)
xlabel('Time (min)','fontsize',16,'fontweight','bold');
ylabel('Exp data, final fit','fontsize',16,'fontweight','bold');
pll=legend (pl,'exp data','final fit');
set(pll,'box','off','location','Best');
set(gca,'box','on','xticklabelmode','auto','yticklabelmode','auto')
%% Printing
```

```
print_pdf(600,get(gcf,'filename'),outputfolder,'nocheck')

print_png(300,get(gcf,'filename'),outputfolder,[],0,0,0)

%% Initial Guesses Approximations

m0=Vf/(A*L);

m0=P(I)*(Vf/(A*L));

Kpf=(1-m0)/P(I); %P(I)= value contain the lowest SSE from before

m1= (2*(Kpf+(Vf/(A*L))))   %term 1 of R

m2=m1/R(I)

D=1;

h=(2*Kpf)/((m2/(Vf/A))-(L/D))

h1=1

D=L/((m2/(Vf/A))-(2*Kpf/h1)) % R=  %(lowest SSE from before);To obtain the D and h as initial

guesses

D=6.5e-12;       % Initial guess for D (cm2/min)6.5E-12
h=5.9e-6;


 %% Step 2: OLS

%Solving for Eigenvalues


format long

global qn

global Bi

alpha=Vf/(Kpf*A*L);

% qn;
```

```
Bi=(h*L)/D;

Lo=1;

Up=80;

z=@(qn) (Bi-Kpf*alpha*qn^2)*sin(qn)+alpha*Bi*qn*cos(qn);

for i=Lo: Up;

    ev(i)=fzero(z,i); %Newton-Raphson

end;

EV=unique(ev);

EV'

ev=EV(2:end);

qn=ev'

 %% Initial parameter guesses

beta0(1)=6.5; % Initial guess for D (cm2/min) x 10^-12

beta0(2)=6.05; %Kpf x 10^2

beta0(3)=5.9;%h  x 10^-6

beta=beta0; % Set beta to the initial guesses

%% X' = scaled sensitivity coefficients using forward-difference

   % This is a forward problem with known approximate parameters

Xp=SSC_convecdiff(beta,t,@myfunconvecdiff);


%% printing

print_pdf(600,get(gcf,'filename'),outputfolder,'nocheck')

print_png(300,get(gcf,'filename'),outputfolder,[],0,0,0)
```

```
%%
ypredict = myfunconvecdiff(beta,t) % To check and compare with experimental values and to check for matrices dimension
figure
plot(t,yobs2,'o')
hold on
plot(t,ypredict,'-')
%% Nlinfit regression
Nt=length(t);
[beta,resids,J,COVB, MSE] = nlinfit(t,yobs2,@myfunconvecdiff,beta0);
ci=nlparci(beta,resids,J,0.05) %asymptotic 95% confidence interval
[ypredict, delta] = nlpredci('myfunconvecdiff',t,beta,resids,J,0.05,'on','curve'); %CI for mean
[ypredict, deltaobs] = nlpredci('myfunconvecdiff',t,beta,resids,J,0.05,'on','observation');
beta; % parameters estimated
[R, sigma]=corrcov(COVB);
R
sigma % parameter standard errors
relative_error=sigma./beta'% >0.6 the likeliness of CI contains 0 is high (estimate is useless since it is not statistically diff than 0)
MSE
RMSE=MSE^(1/2)
%% Model Discrimination
n = length(ypredict);
```

```
p = length(beta_n);
SS= MSE*(n-p)
K=p +1;
AICC= n*(log(SS/n))+ 2*K+(((2*K)*(K+1))/(n-K-1))
%%
figure
grid on
hold on
plot(t,yobs2,'or')
plot(t,ypredict,'-b')
xlabel('Time (min)','fontsize',16,'fontweight','bold');
ylabel('yobserved, ypredicted','fontsize',16,'fontweight','bold');
 %% Plotting the diffusion of antioxidant into simulant over time and its corresponding residual
plot
 figure
asyCImax1 = ypredict + delta;% Asymtotic confidence interval (CI)
asyCImin1 = ypredict - delta;% Asymtotic confidence interval (CI)
predCImax1 = ypredict + deltaobs;% Prediction interval (PI)
predCImin1 = ypredict - deltaobs;% Prediction interval (PI)
hold on
set(gca, 'fontsize',14,'fontweight','bold');
h1(1) = plot(t,yobs2,'ob'); %Plot y observed over time
h1(2) = plot(t,ypredict,'r', 'LineWidth',1.2); % Plot y predicted over time
```

```
h1(3) = plot(t,asyCImax1,'-.g','LineWidth',1.05); % Plot CI as dotted line
h1(4) = plot(t,predCImax1,'-c','LineWidth',1.05'); % Plot upper PI as solid line
plot(t, asyCImin1,'-.g','LineWidth',1.05);% Plot lower CI as dashed line
plot(t, predCImin1,'-c','LineWidth',1.05);  % Plot lower PI as dashed line
xlabel('Time (min)', 'fontsize', 16, 'fontweight','bold');
ylabel('C_{f}(t)/C','fontsize', 16, 'fontweight','bold');
plf=legend (h1,'exp data','best fitted line','95% confidence interval','95% prediction interval');
set(plf,'box','off','location','Southeast');
set(gca,'box','on','xticklabelmode','auto','yticklabelmode','auto')
%% printing
print_pdf(600,get(gcf,'filename'),outputfolder,'nocheck')
print_png(300,get(gcf,'filename'),outputfolder,[],0,0,0)
%% Residual
figure
hold on
set(gca, 'fontsize',14,'fontweight','bold');
h1(1) = plot(t,resids,'*');% Plot residual over time
xlabel('Time (min)','fontsize', 16, 'fontweight','bold');
ylabel('Residuals','fontsize', 16, 'fontweight','bold');
YLine = [0 0];
XLine = [0 7000];
plot (XLine, YLine,'--r')
set(gca,'box','on','xticklabelmode','auto','yticklabelmode','auto')
```

```
 %% printing
print_pdf(600,get(gcf,'filename'),outputfolder,'nocheck')
print_png(300,get(gcf,'filename'),outputfolder,[],0,0,0)
%% Biot no.
Biot=(beta(3)*L)/beta(1)
 %% Residual Bootstrap
%% simultaneous confidence bands for regression line
CBu=ypredict+delta;
CBl=ypredict-delta;
 %% simultaneous prediction bands for regression line
PBu=ypredict+deltaobs;
PBl=ypredict-deltaobs;
%% bootstrap CI for beta
nboot=1000;
mm=2;%use x1, y1; x2, y2;...method of bootstrapping
%for data bootstraping m=1, use myfunconvecdiff_boot..otherwise
%myfunconvecdiff
%mm=2;%use x1, Ypred1+e1; x2, Ypred2+e2;...residual bootstrapping
nlinfitcheck=statset('nlinfit');
nlinfitcheck.FunValCheck='off';
%options = statset('FunValCheck','on');
for j=1:nboot
    r=round(1 + (n-1).*rand(n,1));%index of random integers from 1 to n
```

```
    for i=1:n
      if mm==1
         tt(i)=t(r(i));% tt(i) each time for bootstrapped datum
         yboot(i)=yobs2(r(i));%yboot(i) is the value for each bootstraped datum
      end
      if mm==2
         tt=t;
         yboot(i)=ypredict(i)+resids(r(i));
         if i==n
           yboot=yboot'
      end
    end
 end
%     yboot'
    %[betab(j,:),rr(j,:),J2,COVB2,mse2]= nlinfit(tt,yboot,'myfunconvecdiff',beta0,options);%betab
are the paramters from the bootstraps
    [betab(j,:),rr(j,:),J2,COVB2,mse2]= nlinfit(tt,yboot,'myfunconvecdiff',beta0);
    ypredb(j,:)=myfunconvecdiff(betab(j,:),t);
    %qq=2;
    clear yboot
end
r2=rr(1,:)';
for j=2:nboot
```

```
    r2=[r2;rr(j,:)'];
end
bsort=sort(betab,1); ysort=sort(ypredb,1); %sorts along columns
K=round(0.05*nboot);
if K==0;  K=1; end; U=round(0.975*nboot);
cib(1,1)=bsort(K,1); cib(1,2)=bsort(U,1);%bootstrap 95% CI for first betaeter
cib(2,1)=bsort(K,2); cib(2,2)=bsort(U,2);%bootstrap 95% CI for second betaeter
cib(3,1)=bsort(K,3); cib(3,2)=bsort(U,3);
for i=1:n
    ybci(i,1)=ysort(K,i); ybci(i,2)=ysort(U,i);%ybci is a n-by-2 matrix with bootstrap CI for y at
each time
end
 %% Compute bootstrap prediction bands
D=RMSE*tinv(.975,n-p);
CIwb(:,1)=ybci(:,1)-ypredict; CIwb(:,2)=ypredict-ybci(:,2) %upper (column 1) and lower (column
2) bootstrap CIwidths
PIwb(:,1)=sqrt(CIwb(:,1).^2+D^2); PIwb(:,2)=sqrt(CIwb(:,2).^2+D^2)%upper and lower widths
of PI
PIb(:,1)=ypredict+PIwb(:,1); PIb(:,2)=ypredict-PIwb(:,2) %PI values
%%
%% Residual histogram for bootstrap residuals
[n1, xout] = hist(r2,6);
figure
```

```
hold on
set(gca, 'fontsize',14,'fontweight','bold');
bar(xout, n1) % plots the histogram
xlabel('Observed data - Predicted data','fontsize',16,'fontweight','bold')
ylabel('Frequency','fontsize',16,'fontweight','bold')
set(gca,'box','on','xticklabelmode','auto','yticklabelmode','auto')
%% printing
print_pdf(600,get(gcf,'filename'),outputfolder,'nocheck')
print_png(300,get(gcf,'filename'),outputfolder,[],0,0,0)
%%
%Monte-Carlo
 %%plot Cobs, Cpred line, confidence band for regression line
figure
hold on
set(gca, 'fontsize',14,'fontweight','bold');
L4 = ['Time (min)'];
xlabel(L4,'fontsize',16,'fontweight','bold');
% ylabel('log{\itS}_a','fontsize',16,'fontweight','bold');
ylabel('C_{f}(t)/C_','fontsize',16,'fontweight','bold');
h1(1)=plot(t,yobs2,'ob');
h1(2) = plot(t,ypredict,'r','LineWidth',2);
h1(3) = plot(t,CBu,'-.g','LineWidth',2);
plot(t,CBl,'-.g','LineWidth',2);
```

```
 %% Plot prediction band for regression line
h1(4) = plot(t,PBu,'c','LineWidth',2);
plot(t,PBl,'c','LineWidth',2);
 %% Plot bootstrap bands
h1(5) = plot(t,ybci(:,1),'--k','LineWidth',2);
plot(t,ybci(:,2),'--k','LineWidth',2);
h1(6) = plot(t,PIb(:,1),'-m','LineWidth',2);
plot(t,PIb(:,2),'-m','LineWidth',2);
pf=legend(h1,'exp data','best fitted line','95% confidence interval','95% prediction interval','95%
confidence interval bootstrap','95% prediction interval bootstrap')
set(pf,'box','off','location','Best');
set(gca,'box','on','xticklabelmode','auto','yticklabelmode','auto')
%% printing
print_pdf(600,get(gcf,'filename'),outputfolder,'nocheck')
print_png(300,get(gcf,'filename'),outputfolder,[],0,0,0)
meanres=mean(resids);
%% Residual scatter plot
figure
hold on
set(gca, 'fontsize',14,'fontweight','bold');
plot(t, resids, 'square', 'Markerfacecolor', 'b')
plot([0,max(t)],[0,0], 'R')
ylabel('Observed Data - Predicted Data','fontsize',16,'fontweight','bold')
```

```
xlabel('time (min)','fontsize',16,'fontweight','bold')
 %% Residual histogram
[n1, xout] = hist(resids,6);
figure
hold on
set(gca, 'fontsize',14,'fontweight','bold');
bar(xout, n1) % plots the histogram
xlabel('Observed Data - Predicted Data','fontsize',16,'fontweight','bold')
ylabel('Frequency','fontsize',16,'fontweight','bold')

beta = beta;
 for i=1:length(beta)
        d=0.001;
        betain = beta;
        betain(i) = beta(i)+beta(i)*d;
        yhat{i} = myfunconvecdiff(betain, t);
        ysens{i}=(yhat{i}-ypredict)/d; %scaled sens coefficient
        X{i} = (yhat{i}-ypredict)/(beta(i)*d);
 end
figure
hold on
set(gca, 'fontsize',14,'fontweight','bold');
L4 = ['Time(min)'];
```

```
xlabel(L4,'fontsize',16,'fontweight','bold');
ylabel('Scaled Sensitivity Coefficient','fontsize',16,'fontweight','bold');
 YLine =[0 0];
XLine = [0 max(t)];
plot (XLine, YLine,'k');
h2(1) = plot(t,ysens{1},'o-b','LineWidth',1);
h2(2) = plot(t,ysens{2},'s-r','LineWidth',1);
h2(3) = plot(t,ysens{3},'^-m','LineWidth',1);
pf=legend(h2,'X"_{D}','X"_{Kpf}','X"_{h}')
set(pf,'box','off','location','Best');
set(gca,'box','on','xticklabelmode','auto','yticklabelmode','auto')
%% printing
print_pdf(600,get(gcf,'filename'),outputfolder,'nocheck')
print_png(300,get(gcf,'filename'),outputfolder,[],0,0,0)
 %% Sequential Estimation
%%
n=length(data); p=3;  %b1=D, b2=Kpf, b3=h
b_old=[6.5 6.05 5.9]';%must use initial guess for b, because of model structure
 sigma=7.9851e-5; sig=sigma*ones(n,1);%close to RMSE value
tol=5e-3; %stopping criterion % start small and increased over time
ratio = 1; %ratio compares new b to old b
d=0.001; %delta for computing sensitivity coefficients
count=1; %counts how many iterations
```

```
 while ratio==1 %run loop while parameter change is greater than tol
Pz=1.0e+5;
b= b_old;
ypred=myfunconvecdiff(b,t);%PUT YOUR FUNCTION IN THIS LINE
e=yobs2-ypred;%this replaces the line for eq. 5.9.8.d in linear sequential
 for i=1:length(b)%loop to compute sensitivity coefficient for each parameter
    bin=b;
    bin(i)=b(i)*(1+d);
    yhat{i}=myfunconvecdiff(bin,t);%PUT YOUR FUNCTION IN THIS LINE
    XX{i}=(yhat{i}-ypred)/(b(i)*d); %sensitivity coefficient
    if i==1
        X=XX{i};
    else
        X=[X XX{:,i}];
    end
end


P=diag((b_old.^2)*10);% squared guesses
 B=b_old';  % B is a row
for ii=1:n;                         %SEQUENTIAL
    A=P*X(ii,:)';                   %eq.(5.9.8a) %SEQUENTIAL
    Delta=sig(ii)^2+X(ii,:)*A;      %eq (5.9.8b) %SEQUENTIAL
    K=A/Delta;                      %eq.(5.9.8c) %SEQUENTIAL
```

```
    b=b+K*(e(ii)-X(ii,:)*(b-b_old));%eq.(7.8.22e) %SEQUENTIAL
    P=P-K*A';                    %eq.(5.9.8f)%SEQUENTIAL
    B=[B;b'];
    if ii==1
       PP=[P(1,1) P(1,2) P(1,3) P(2,2) P(2,3) P(3,3)];% Matrix 3 by 3
    else
       PP=[PP; P(1,1) P(1,2) P(1,3) P(2,2) P(2,3) P(3,3)];
    end
end
b_new=b;%last b is the new b
ratioall=abs((b_new-b_old)./b_old);
for i=1:p
    if ratioall(i)<tol
       ratio=0;
    else
       ratio=1;
    end
end
b_old=b_new;
count=count+1;
end
SSseq=e'*e;
MSE=(SSseq)/(n-p);
```

```
RMSE=sqrt(MSE)
sdrerr=diag(P).^(1/2)
Rel=sdrerr./b_old
%% Plotting


step=0:1:n;
figure
hold on
plot(step,B(:,1),'ob','markerfacecolor','b','markeredgecolor','k')
plot(step,B(:,2),'sr','markerfacecolor','r','markeredgecolor','k')
plot(step,B(:,3),'sm','markerfacecolor','m','markeredgecolor','m')
xlabel('Step index, i','fontsize', 16, 'fontweight','bold')
ylabel('Sequentially estimated parameter','fontsize', 16, 'fontweight','bold')
legend('D','Kpf','h','location','best')
%%
%% sequential normalized plots
BBn=B(:,1)./B(end,1);
BBn(:,2)=B(:,2)./B(end,2);
BBn(:,3)=B(:,3)./B(end,3);
x1=[0;t];% scaling the new axis
figure
hold on
set(gca, 'fontsize',14,'fontweight','bold');
```

```
plot(x1,BBn(:,1),'sb', 'linewidth',1.0)
hold on
plot(x1,BBn(:,2),'^r','linewidth',1.0)
plot(x1,BBn(:,3),'om','linewidth',1.0)
xlabel('Time (min)','fontsize', 16, 'fontweight','bold')
ylabel('Normalized Sequential Parameter','fontsize', 16, 'fontweight','bold')
pf=legend('D','Kpf', 'h')
set(pf,'box','off','location','Best');
set(gca,'box','on','xticklabelmode','auto','yticklabelmode','auto')
%% printing
print_pdf(600,get(gcf,'filename'),outputfolder,'nocheck')
print_png(300,get(gcf,'filename'),outputfolder,[],0,0,0)%%%
%% Desorption plot
MZ=(Co-yobs)/Co;
Fo= (beta(1).*t)/(L^2);% Dimensionless space time
figure
hold on
set(gca, 'fontsize',14,'fontweight','bold');
plot(Fo,MZ,'^m')
xlabel('Fourier number', 'fontsize', 16, 'fontweight','bold');
ylabel('C_{f}(t)-C_/C_','fontsize', 16, 'fontweight','bold');
set(gca,'box','on','xticklabelmode','auto','yticklabelmode','auto')
%% printing
```

```
print_pdf(600,get(gcf,'filename'),outputfolder,'nocheck')

print_png(300,get(gcf,'filename'),outputfolder,[],0,0,0)

%%
```

REFERENCES

REFERENCES

Beck, J. V., & Arnold, K. J. (1977). *Parameter Estimation in Engineering and Science* (Vol. 8): Wiley New York.

Carslaw, H. S., & Jaeger, J. C. (1959). Conduction of heat in solids. *Oxford: Clarendon Press, 1959, 2nd ed., 1*.

Crank, J. (1979). *The Mathematics of Diffusion* (2nd ed.). Bristol: Oxford University Press.

Dhoot, G., Auras, R., Rubino, M., Dolan, K. D., & Soto-Valdez, H. (2009). Determination of eugenol diffusion through LLDPE using FTIR-ATR flow cell and HPLC techniques. *Polymer, 50*(6), 1470-1482.

Dolan, K. D., & Mishra, D. K. (2013). Parameter estimation in food science. *The Annual Review of Food Science and Technology, 4*, 401-422.

Ducruet, V., Vitrac, O., Saillard, P., Guichard, E., Feigenbaum, A., & Fournier, N. (2007). Sorption of aroma compounds in PET and PVC during the storage of a strawberry syrup. *Food additives and contaminants, 24*(11), 1306-1317.

Galotto, M., Torres, A., Guarda, A., Moraga, N., & Romero, J. (2011). Experimental and theoretical study of LDPE versus different concentrations of Irganox 1076 and different thickness. *Food Research International, 44*(2), 566-574.

Gandek, T. P., Hatton, T. A., & Reid, R. C. (1989). Batch extraction with reaction: phenolic antioxidant migration from polyolefins to water. 1. Theory. *Industrial & engineering chemistry research, 28*(7), 1030-1036.

Granda-Restrepo, D. M., Soto-Valdez, H., Peralta, E., Troncoso-Rojas, R., Vallejo-Córdoba, B., Gámez-Meza, N., & Graciano-Verdugo, A. Z. (2009). Migration of α-tocopherol from an active multilayer film into whole milk powder. *Food Research International, 42*(10), 1396-1402.

Hwang, S. W., Shim, J. K., Selke, S., Soto-Valdez, H., Matuana, L., Rubino, M., & Auras, R. (2013). Migration of α-Tocopherol and Resveratrol from Poly (L-lactic acid)/Starch Blends Films into Ethanol. *Journal of Food Engineering*.

Iñiguez-Franco, F., Soto-Valdez, H., Peralta, E., Ayala-Zavala, J. F., Auras, R., & Gámez-Meza, N. (2012). Antioxidant Activity and Diffusion of Catechin and Epicatechin from Antioxidant Active Films Made of Poly (l-lactic acid). *Journal of Agricultural and Food Chemistry, 60*(26), 6515-6523.

Manzanarez-López, F., Soto-Valdez, H., Auras, R., & Peralta, E. (2011). Release of α-Tocopherol from Poly (lactic acid) films, and its effect on the oxidative stability of soybean oil. *Journal of Food Engineering, 104*(4), 508-517.

Mascheroni, E., Guillard, V., Nalin, F., Mora, L., & Piergiovanni, L. (2010). Diffusivity of propolis compounds in Polylactic acid polymer for the development of anti-microbial packaging films. *Journal of Food Engineering, 98*(3), 294-301.

Mishra, D. K., Dolan, K. D., & Yang, L. (2011). Bootstrap confidence intervals for the kinetic parameters of degradation of anthocyanins in grape pomace. *Journal of Food Process Engineering, 34*(4), 1220-1233.

Ortiz-Vazquez, H., Shin, J. M., Soto-Valdez, H., & Auras, R. (2011). Release of butylated hydroxytoluene (BHT) from Poly (lactic acid) films. *Polymer Testing, 30*(5), 463-471.

Pocas, M. F., Oliveira, J. C., Brandsch, R., & Hogg, T. (2012). Analysis of mathematical models to describe the migration of additives from packaging plastics to foods. *Journal of Food Process Engineering, 35*(4), 657-676.

Reinas, I., Oliveira, J., Pereira, J., Machado, F., & Poças, M. (2012). Migration of two antioxidants from packaging into a solid food and into Tenax®. *Food Control, 28*(2), 333-337.

Samsudin, H., Valdez, H. S., & Auras, R. (2014). Poly (lactic acid) film incorporated with marigold flower extract (< i> Tagetes erecta</i>) intended for fatty-food application. *Food Control, 46*, 55-66. doi: 10.1016/j.foodcont.2014.04.045

Soto-Valdez , H., Peralta, E., & Auras, R. (2008). *Poly(lactic acid) films added with resveratrol as active packaging with potential application in the food industry.* Paper presented at the 16th IAPRI World Conference on Packaging Bangkok, Thailand.

Vitrac, O., & Hayert, M. (2006). Identification of diffusion transport properties from desorption/sorption kinetics: an analysis based on a new approximation of fick equation during solid-liquid contact. *Industrial & engineering chemistry research, 45*(23), 7941-7956.

Chapter 6

Assessment of Mass Transfer Models used in Migration Experiments to Determine Diffusion, Partition and Convective Mass Transfer Coefficients

6.0 Introduction

Migration studies in food packaging have been extensively investigated mainly due to safety concern and for compliance with food contact regulations. A significant amount of money and time have been invested to perform experimental studies with different polymer-additive-food simulant combinations. Therefore, a considerable amount of effort has been given to understand and assess the kinetics of migration by solving different mathematical models with different boundary conditions to simulate migration experiments and real case scenarios. This modeling approach allows researchers to identify important factor(s) governing the sorption and/or desorption kinetics of migration.

'A mathematical model is neither a hypothesis nor a theory. Unlike scientific hypotheses, a model is not verifiable directly by an experiment. For all models are both true and false. The validation of a model is not that it is 'true' but that it generates good testable hypotheses relevant to important problems.'-R.Levins, American Scientist 54:421-31,1966 (as cited in (Motulsky & Christopoulos, 2004c)). There are many models available to determine migration parameters which have diverse complexity including molecular simulation, short-contact simulation, analytical solution, and numerical approximation, to name a few (Hwang et al., 2013; Iñiguez-Franco et al., 2012; Pocas, Oliveira, Brandsch, & Hogg, 2012; Poças, Oliveira, Oliveira, & Hogg, 2008; Reynier, Dole, & Feigenbaum, 2002a, 2002b; Samsudin, Valdez, & Auras, 2014; Soto-Valdez, Auras, & Peralta, 2010; Vitrac & Hayert, 2006; Vitrac, Mougharbel, & Feigenbaum, 2007). Off all the listed models, analytical solutions have been widely used due to their simplicity

and direct physical interpretation of the migration kinetics. Analytical solutions applied to migration studies are commonly focused on two main kinetic parameters, which are the diffusion (D) and the partition ($K_{p,f}$) coefficients. Another parameter commonly known as the convective mass transfer coefficient (h) is often considered negligible. As evidence, only a limited number of works have investigated or tried to estimate h (Galotto, Torres, Guarda, Moraga, & Romero, 2011; Gandek, Hatton, & Reid, 1989; Mascheroni, Guillard, Nalin, Mora, & Piergiovanni, 2010; Pocas, Oliveira, Brandsch, & Hogg, 2012; Vitrac, Mougharbel, & Feigenbaum, 2007). h is a key factor for understanding the kinetics of migration at the interface of the polymer-food/food simulant. In the case that convection is not present (continuous stirring or a well-mixed food medium), the h becomes larger and approaches infinity; thus its effect is negligible. However, in real case scenarios, most of the liquid food in contact with the packaging system is left still at the market shelves, the storage temperature is fairly low to extend shelf life, the diffusion process is slow and/or the food has considerably high viscosity. For such aforementioned conditions, if the h effect is not considered, not only its effect as a governing kinetic factor is overlooked, the D estimation will also be underestimated since these two parameters are kinetically correlated in the series of migration resistance as indicated by the *Biot* number definition (i.e., the ratio of the diffusion resistance in the liquid to the internal diffusion resistance in the polymer or $\frac{hL}{D}$).

Therefore, all the kinetic migration parameters (*i.e.*, D, h, and $K_{p,f}$) should be taken into consideration to fully quantify the mass transfer process, and to understand how their individual effects and possible interactions with each other could influence the migration kinetics. A two-step solution to simultaneously determine these three parameters (D, h, and $K_{p,f}$) was proposed in Chapter 5. However, can we assure that this model is sufficient for all migration studies? or are previous solutions and available mathematical expressions used for many years to determine one

of these parameters sufficient? The aim of this study was to compare the proposed two-step solutions presented in chapter 5 with two commonly used mathematical expressions using several selected case studies.

6.1 Materials and Methods

6.1.1 Migration Case Studies

Several migration case studies were chosen to evaluate the different model approaches, which were i) poly(lactic acid), PLA film incorporated with 3 wt.% resveratrol in contact with ethanol at 9 °C (Soto-Valdez , Peralta, & Auras, 2008), ii) PLA film incorporated with 2.6 wt.% α-tocopherol in contact with ethanol at 23 °C (Manzanarez-López, Soto-Valdez, Auras, & Peralta, 2011) - presented in Appendix 6A and iii) PLA film incorporated with 1.28 wt.% catechin in contact with 95% ethanol at 40 °C (Iñiguez-Franco, Soto-Valdez, Peralta, Ayala-Zavala, Auras, & Gámez-Meza, 2012) - presented in Appendix 6B.

The data was analyzed using MATLAB® R2011b (MathWorks, Natick, MA, USA) and statistical analysis was performed using an analysis of variance (ANOVA) with Tukey's test and an independent t-test (SPSS Statistics, version 22, 2013, IBM Corporation©, Armonk, NY, USA) for means comparisons.

6.1.2 Mathematical Models

6.1.2.1 Assumptions

Analytical solutions were derived based on the defined boundary conditions, and assumptions were made and hold true to satisfy those boundary conditions. Those assumptions include, but are not limited to:

i) the initial concentration of the migrants is uniformly distributed in the films

ii) the migration happens on the side of the film that is in contact with the food/ simulant

iii) the food/simulant is well mixed

iv) the film interface and the food is always at an equilibrium

v) no interaction exists between the films and the food/simulant, and the edge effect is negligible (Chung, Papadakis, & Yam, 2001, 2002; Crank, 1979; Poças, Oliveira, Oliveira, & Hogg, 2008)

vi) the overall mass transfer is balanced

vii) the D , $K_{p,f}$ and h do not change with the concentration

viii) the mass transfer parameters are temperature dependent.

6.1.2.2 Model 1: A Two-Step Solution (A detailed discussion of the model's development can be found in Chapter 5)

6.1.2.2.1 Step 1

$$\frac{C_4}{C_0} = P(1 - e^{-Rt}) \qquad \text{(Eq. 6-1)}$$

where $C_4 \equiv C_f$ = concentration of antioxidant in food simulant; $P = \frac{\sum \frac{C_{f,i}}{C_0}(1-e^{-Rt,i})}{\sum(1-e^{-Rt,i})^2}$; $R = \frac{2(K_{p,f}+\frac{V_f}{AL})}{\frac{V_f}{A}(\frac{L}{D}+\frac{2K_{p,f}}{h})}$

6.1.2.2.2 Step 2

$$\frac{C_f(t)}{C_0} = \frac{1-\sum_{q_n}^{\infty} f_q e^{\frac{-q_n^2 Dt}{L^2}}}{K_{p,f}(\alpha+1)} \quad \text{(Eq. 6-2)}$$

where $f_q = \frac{2\alpha(\alpha+1)Bi^2}{Bi^2(1+\alpha)+\alpha Bi[K_{p,f}\alpha+\alpha Bi-2K_{p,f}]q_n^2+K_{p,f}^2\alpha^2 q_n^4}$;

Eigenvalue's root solutions= $tan\ q_n = -\frac{\alpha Bi q_n}{Bi-K_{p,f}\alpha q_n^2}$; $\alpha = \frac{V_f}{K_{p,f}AL}$ and $Bi = \frac{hL}{D}$

where C_f = concentration of antioxidant in the food simulant; C_0 = initial concentration of antioxidant in the polymer; α =the ratio of the mass of antioxidant migrated into food simulant to the mass of antioxidant left in the polymer, at equilibrium; V_f=volume of food simulant; *A*=area; *L*=half of the film's thickness; Bi =Biot number; q_n = the non-zero roots.

The number of terms needed for the analytical solution of model 1 to converge to a given accuracy (~98%) can be calculated as shown in Chapter 5.

6.1.2.3 Model 2: Crank's solution with partition coefficient, $K_{p,f}$ and diffusion coefficient (*D*) as the governing factors (Carslaw & Jaeger, 1959; Crank, 1979)

Model 2 is a special case of model 1 for large *Biot* number. *Biot* number could become large as $h \to \infty$ or $L \to \infty$ or $D \to 0$ or any combination thereof. In the case that the food is well mixed (*i.e.*, continuous stirring), convection is fast ($h \to \infty$) and local equilibrium at the interface is obtained (boundary condition at $x = L$; $C_p \to K_{p,f}C_f$). Model 2 can be derived from step 2 of model 1 as follows:

$$\frac{C_f(t)}{C_0} = \frac{1-\sum_{q_n}^{\infty} f_q e^{\frac{-q_n^2 Dt}{L^2}}}{K_{p,f}(\alpha+1)} \quad \text{(Eq. 6-2)}$$

where $f_q = \frac{2\alpha(\alpha+1)Bi^2}{Bi^2(1+\alpha)+\alpha Bi\left[K_{p,f}\alpha+\alpha Bi-2K_{p,f}\right]q_n^2+K_{p,f}^2\alpha^2 q_n^4}$

$$\text{and } tan\ q_n = -\frac{\alpha q_n}{1-\frac{K_{p,f}\alpha q_n^2}{Bi}} \quad \text{(Eq. 6-3)}$$

As $Bi \to \infty$, Eq. 6-2 becomes;

$$\frac{C_f(t)}{C_0} = \frac{1-\sum_{q_n}^{\infty} f_q e^{\frac{-q_n^2 Dt}{L^2}}}{K_{p,f}(\alpha+1)} \quad \text{(Eq. 6-4)}$$

where $f_q = \frac{2\alpha(\alpha+1)}{(1+\alpha)+\alpha^2 q_n^2}$ and the eigenvalues satisfy $tan\ q_n = -\alpha q_n$

The number of terms needed for a given accuracy (~98%) for the analytical solution of model 2 to converge can be calculated as follows:

Let's z= $exp^{\frac{-Dt}{L^2}}$ where $0 < z \leq 1$

The solution converges faster when z decreases, thus the worst-case scenario is when z=1 (slowest convergence).

% Accuracy=$\frac{sum\ of\ finite\ series}{sum\ of\ infinite\ series} \times 100$ where sum of finite series=$\sum_{n=1}^{n=70} f_q\, z^{qn^2}$ and sum of infinite series=$\sum_{n=1}^{n=\infty} f_q\, z^{qn^2}$. The infinite series was estimated with 100,000 terms, which is a good estimation.

6.1.2.4 Model 3: Crank's solution with diffusion coefficient (*D*) as the only governing factor (Crank, 1979)

Model 3 is a special case for model 1 and model 2. It can be solved simply by the separation of variables technique. As $Bi \to \infty$ and $\alpha \to \infty$, the boundary conditions at the interface ($x =$

$L;\ C_f(x,0) = 0$ and $-D\frac{\partial C_p}{\partial x}\Big|_{x=L} = \frac{V_f}{A}\frac{\partial C_f}{\partial t}\Big|_{x=L}$) are satisfied with a partial differential equation (PDE) of $\frac{\partial C_p}{\partial t} = D\frac{\partial^2 C_p}{\partial x^2}$. Thus, model 3 can be derived as follows;

$$C(x,t) = F(x).G(t) \qquad \text{(Eq. 6-5)}$$

Substitute Eq. 6-5 into the PDE $\frac{\partial C_p}{\partial t} = D\frac{\partial^2 C_p}{\partial x^2}$;

$$FG' = DF''G \qquad \text{(Eq. 6-6)}$$

Divide Eq. 6-6 by DFG;

$$\frac{G'}{DG} = \frac{F''}{F} = -\lambda^2 \qquad \text{(Eq. 6-7)}$$

Separate Eq. 6-7 into two equations;

$$G' + \lambda^2 DG = 0 \Rightarrow G = C_1 e^{-\lambda^2 Dt} \qquad \text{(Eq. 6-8)}$$

$$F'' + \lambda^2 F = 0 \Rightarrow F = C_2 sin\lambda x + C_3 cos\lambda x \qquad \text{(Eq. 6-9)}$$

where C_1, C_2, C_3 are constants.

$$\text{At } x = 0\text{: } \frac{\partial C_p}{\partial t} = 0 \Rightarrow F|_{x=0} = 0 = C_2\lambda, \therefore C_2 = 0 \qquad \text{(Eq. 6-10)}$$

$$\text{At } x = L\text{: } C_f(x,0) = 0 \Rightarrow F|_{x=L} = C_3 cos\lambda L = 0 \qquad \text{(Eq. 6-11)}$$

Since C_3 cannot be 0, otherwise a trivial solution will be obtained,

$cos\lambda L = 0 \Rightarrow \lambda L = \frac{\pi}{2}, \frac{3\pi}{2}, \frac{5\pi}{2}, ...= \left(n + \frac{1}{2}\right)\pi, n = 0,1,2,3$; thus $\lambda = \frac{(n+\frac{1}{2})\pi}{L}$

Substitute Eq. 6-10 and Eq. 6-11 into Eq. 6-5;

$$C(x,t) = \sum_{n=0}^{\infty} C_n cos\frac{(n+\frac{1}{2})\pi x}{L} \cdot e^{\frac{-(n+\frac{1}{2})^2\pi^2 Dt}{L^2}} \qquad \text{(Eq. 6-12)}$$

where the Cn are arbitrary constants.

Eq. 6-12 satisfies the boundary conditions and the PDE.

The initial condition (at $t = 0, C = C_0$) requires that;

$$C_0 = \sum_{n=0}^{\infty} C_n cos\,\frac{(n+\frac{1}{2})\pi x}{L} \qquad \text{(Eq. 6-13)}$$

Multiplying by the m[th] cosine function and integrating,

$$\int_0^L C_0 cos\left(m+\frac{1}{2}\right)\frac{\pi x}{L}dx = \sum_{n=0}^{\infty} C_n \underbrace{\int_0^L cos\left(m+\frac{1}{2}\right)\frac{\pi x}{L} + \cos\left(n+\frac{1}{2}\right)\frac{\pi x}{L}dx}_{will\ be\ zero\ if\ m\neq n\ and\ \frac{L}{2}\ if\ m=n} \qquad \text{(Eq. 6-14)}$$

where $\frac{C_0 sin\left(m+\frac{1}{2}\right)\pi}{\left(m+\frac{1}{2}\right)\frac{\pi}{L}} = C_m\frac{L}{2}$, thus $C_m = \frac{2}{\pi}C_0(-1)^m/\left(m+\frac{1}{2}\right)$

$$\Longrightarrow \frac{C(x,t)}{C_0} = \frac{2}{\pi}\sum_{q_n}^{\infty}\frac{(-1)^n cos\left(n+\frac{1}{2}\right)\frac{\pi x}{L}\cdot exp^{\frac{-(n+\frac{1}{2})^2\pi^2 Dt}{L^2}}}{(n+\frac{1}{2})} \qquad \text{(Eq. 6-15)}$$

The mass that remains in the polymer at time *t*, $M_p(t)$ is

$$M(t) = \int_0^L C(x,t)\,A\,dx \qquad \text{(Eq. 6-16)}$$

$$= \frac{2}{\pi}C_0 A\int_0^L \sum_{q_n}^{\infty}\frac{(-1)^n cos\left(n+\frac{1}{2}\right)\frac{\pi x}{L}\cdot exp^{\frac{-(n+\frac{1}{2})^2\pi^2 Dt}{L^2}}}{(n+\frac{1}{2})}dx \qquad \text{(Eq. 6-17)}$$

$$= \frac{2}{\pi}C_0 A\sum_{q_n}^{\infty}\frac{(-1)^n\cdot exp^{\frac{-(n+\frac{1}{2})^2\pi^2 Dt}{L^2}}}{(n+\frac{1}{2})}\underbrace{\int_0^L \cos\left(n+\frac{1}{2}\right)\frac{\pi x}{L}\,dx}_{\frac{sin\left(n+\frac{1}{2}\right)\pi}{\left(n+\frac{1}{2}\right)\frac{\pi}{L}}=\frac{(-1)^n}{\left(n+\frac{1}{2}\right)\frac{\pi}{L}}} \qquad \text{(Eq. 6-18)}$$

$$= \frac{2}{\pi^2}C_0 AL\sum_{q_n}^{\infty}\frac{exp^{\frac{-(n+\frac{1}{2})^2\pi^2 Dt}{L^2}}}{(n+\frac{1}{2})^2} \qquad \text{(Eq. 6-19)}$$

$$M_f(t) = M_o - M_p(t) \qquad \text{(Eq. 6-20)}$$

where $M_f(t)$ =the mass of antioxidant in the food simulant at time t; M_o=C_0AL =the initial mass of antioxidant in the polymer; $M_p(t)$ =the mass of antioxidant remaining in the polymer at time t

$$C_f(t) = \frac{C_0 AL - M_p(t)}{V_f} \qquad \text{(Eq. 6-21)}$$

where $C_f(t)$ =concentration of antioxidant in the food simulant

Thus, Eq. 6-21 becomes;

$$\frac{C_f(t)}{C_0} = \frac{AL}{V_f}\left[1 - \frac{2}{\pi^2}\sum_{q_n}^{\infty} \frac{e^{\frac{-(n+\frac{1}{2})^2\pi^2 Dt}{L^2}}}{(n+\frac{1}{2})^2}\right] \qquad \text{(Eq. 6-22)}$$

The number of terms needed for a given accuracy (~98%) for the analytical solution of model 3 to converge can be calculated as follows:

The term of $(n+\frac{1}{2})$ is expanded to $(2n+1)$. Then, let's z= $e^{\frac{-\pi^2 Dt}{4L^2}}$ where $0 < z \leq 1$.

The solution converges faster when z decreases, thus the worst case scenario is when z=1 (slowest convergence).

% Accuracy=$\frac{sum\ of\ finite\ series}{sum\ of\ infinite\ series} \times 100$ where sum of finite series=$\sum_{n=0}^{n=70} \frac{z^{(2n+1)^2}}{(2n+1)^2}$ and sum of infinite series=$\sum_{n=0}^{n=\infty} \frac{z^{(2n+1)^2}}{(2n+1)^2}$. The infinite series was estimated with 100,000 terms, which is a good estimation.

Table 6-1 Comparison of the number of terms needed to achieve a given accuracy among model 1, 2, and 3.

Number of terms	% Accuracy		
	Model 1	Model 2	Model 3
1	99.99	40.28	81.06
2	100.00	60.84	90.06
3	100.00	71.64	93.31
.	.	.	.
.	.	.	.
70	100.00	98.67	99.71

6.1.3 Kinetic Parameter Estimation

6.1.3.1 Scaled Sensitivity Coefficient, *X'*

Sensitivity coefficient and scaled sensitivity coefficient are as described in Chapter 2 section 2.7.2.

6.1.3.2 Ordinary Least Square (OLS) Estimation

The parameters were estimated using the non-linear regression fitting function (nlinfit) of MATLAB® R2011b (MathWorks, Natick, MA, USA) by minimizing the sums of squared errors (SSE). Additional information such as residuals and relative error were also obtained. Relative error of each parameter was calculated by dividing the standard error of parameter with the parameter's estimate.

6.1.3.3 Corrected Akaike Information Criterion (AICc)

The model selection was based on the corrected Akaike Information Criterion (AICc). AICc is useful to compare models that are different from each other. Commonly, the higher the number of the parameters the more likely the goodness of fit seems to improve and vice versa. Thus, AICc eliminates the biasness that may be caused by different numbers of parameter among models. The smaller the value of AICc is, the more likely the model is correct (Motulsky & Christopoulos, 2004a).

$$AICc = n\ ln\left(\frac{SSE}{n}\right) + 2K + \frac{2K(K+1)}{n-K-1} \quad \text{(Eq. 6-22)}$$

where n=number of data; p=number of parameter; $K=p+1$

Additionally, Akaike's weights (probability) and the relative likelihood (evidence ratio) were also calculated as follows (Motulsky & Christopoulos, 2004a; Wagenmakers & Farrell, 2004);

$$Probability = \frac{exp^{-0.5\Delta}}{\sum_{m=1}^{M} exp^{-0.5\Delta}} \quad \text{(Eq. 6-23)}$$

where m=model 1...M

$$Evidence\ ratio = \frac{Probability\ that\ model\ X\ is\ correct\ (the\ lowest\ AICc)}{Probability\ that\ model\ Y\ is\ correct} = \frac{1}{exp^{-0.5\Delta}} \quad \text{(Eq. 6-24)}$$

where Δ=the absolute difference of AICc between models.

Akaike's weights or probability provide the information of how much more likely the model with the lower AICc is to be correct. Meanwhile, the evidence ratio informs the likelihood of favoring one model over the others.

6.2 Results and Discussions

A case study of migration of PLA-3 wt.% resveratrol into ethanol at 9 °C was used to demonstrate and discuss the use of model 1, 2, and 3. For model 1 (Eq. 6-2), model 2 (Eq. 6-4), and model 3 (Eq. 6-22); three (*i.e., D,* $K_{p,f}$*, h*), two (*i.e., D,* $K_{p,f}$), and one (*i.e., D*) parameter(s), respectively, were estimated for these models, and the solutions were fitted to the experimental data.

6.2.1 Scaled Sensitivity Coefficient, *X'*

For parameters to be estimated simultaneously, the correlation among them is expected to be as low as possible since each individual parameter has its unique physical meaning in the migration experiment. Thus, a high correlation among parameters means the key factor that governs a migration process cannot be identified separately. The scaled sensitivity coefficient, *X',* of model 1 showed that the three kinetic migration parameters can be simultaneously estimated, so did the two parameters of model 2 (Figure 6-1). Since model 1 was only estimating one parameter, its *X'* plot is not shown. It can also be observed that in both models, the parameter $K_{p,f}$ had the largest absolute magnitude of response, which is expected to give the lowest relative error compared to the other estimated parameters.

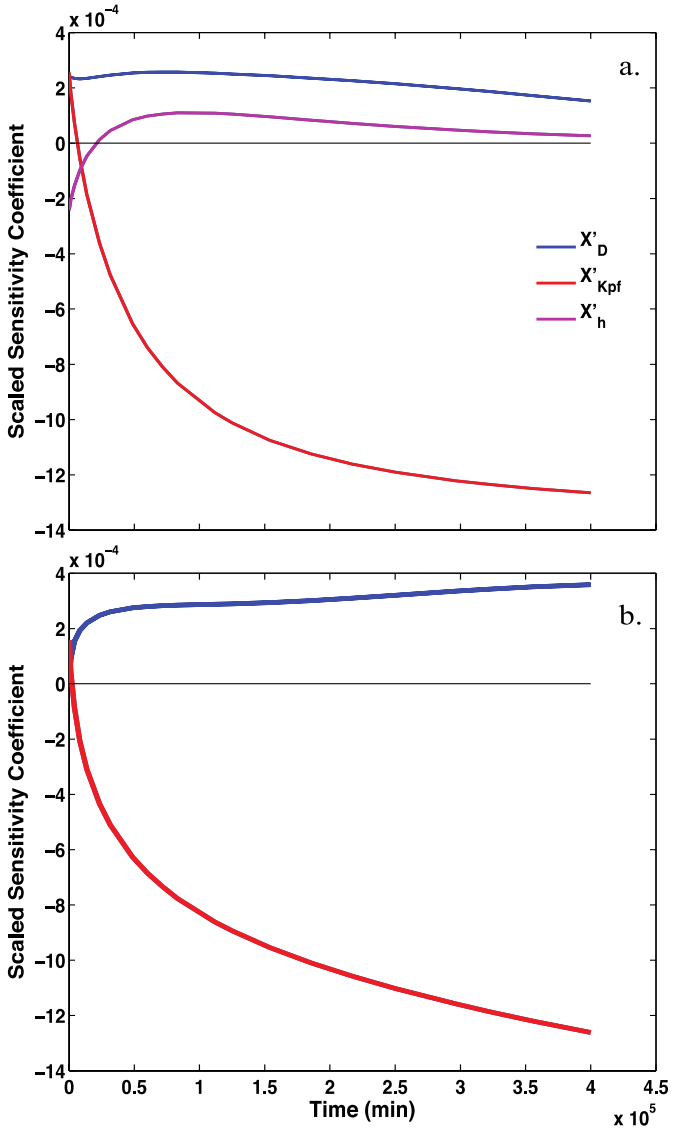

Figure 6-1 Scaled sensitivity coefficient of migration of 3 wt. % resveratrol from PLA film into ethanol at 9 °C of (a) model 1 (initial guesses were: D=6.50 × 10^{-12} cm^2/min, $K_{p,f}$=605.00 cm^3 PLA/cm^3 ethanol, and h=5.9 × 10^{-6} cm/min), and (b) model 2 (initial guesses were: D=5.19 × 10^{-12} cm^2/min and $K_{p,f}$=430.00 cm^3 PLA/cm^3 ethanol).

6.2.2 Ordinary Least Square (OLS) Estimation

The OLS results of all three models can be observed in Table 6-1. The *D* values between model 1 and 2 were significantly different from each other ($p<0.05$). This difference could be attributed to the different counts of estimated parameter in each model. When only one parameter is estimated in a model, only this parameter changes its value within the range to find the estimate that minimized the sums of squared error (SSE). In the case that more parameters are estimated, the combined value of those parameters changes until they end up with the lowest SSE (Motulsky & Christopoulos, 2004b). Similar behavior was also observed in the case of estimated $K_{p,f}$ for both model 1 and 2. The published results of this case study reported a *D* value of 20.9×10^{-12} cm^2/min (Soto-Valdez , Peralta, & Auras, 2008), which was higher than that of the estimated *D* value of model 1, 2, and 3. The difference could be due to the different structure of the models. Meanwhile, the estimated $K_{p,f}$ of model 2 (491.24 cm^3 PLA/cm^3 ethanol) was found to have a closer value to the reported experimental $K_{p,f}$ (506.10 cm^3 PLA/cm^3 ethanol) than that of the estimated $K_{p,f}$ of model 1 (548.87 cm^3 PLA/cm^3 ethanol). No comparison can be made for the estimated *h* value since it is the first time this parameter is being estimated for this particular migration case study. However, higher order of magnitude for *h* has been reported by Vitrac, Mougharbel, & Feigenbaum, 2007 and could be due to the testing temperature and the type of polymer and food simulant. *h* depends on the polymer/simulant selection and the flow environment between the film and the simulants.

Meanwhile, the estimated $K_{p,f}$ for model 1 and 2 was found to have the lowest relative error compared to the other estimated parameters as anticipated from the *X'* plot (Figure 6-1). For model 1, the following parameters were found to be easily and accurately estimated in decreasing order $K_{p,f}$, *D* and *h*. The same order was observed for model 2, except the *h* since it was not estimated.

Model 1 had the lowest root mean square errors (RMSE) followed by model 3 and model 2. In general, the more parameters incorporated into the model, the lower the RMSE would be. However, model 3 with only one parameter resulted in lower RMSE than model 2 with two parameters and this could possibly be due to the ease of fitting less number of parameter to the data set.

The experimental data for the migration of 3 wt.% resveratrol from PLA film into ethanol at 9 °C was fitted using models 1, 2, and 3 (Figure 6-2). The predicted fitting for model 3 (Figure 6-2(c)) was slightly off around 3.7 to 4.0 × 10^5 min compared to those of model 1 and 2 (Figure 6-2 (a),(b)).

Table 6-2 OLS results for the migration study of 3 wt.% resveratrol from PLA film into ethanol at 9 °C for model 1, 2, and 3.

Parameter & Additional Info	**Model**		
	1	**2**	**3**
$D\times10^{-12}$ (cm^2/min)	5.42 ± 0.62[a]	7.50 ± 1.61[b]	0.61 ± 0.015[c]
Relative error (%)	11.38	21.45	2.43
$K_{p,f}$ (cm^3 PLA/cm^3 ethanol)	548.87 ± 21.76[a]	491.24 ± 33.00[b]	N/A
Relative error (%)	3.97	6.72	
$h\times10^{-6}$(cm/min)	2.56 ± 0.38	N/A	N/A
Relative error (%)	14.97		
RMSE×10^{-5} (cm^3 ethanol/cm^3 PLA)	7.91	12.09	9.07

Note: Data represents as mean ± standard error; a,b superscripts represent statistical difference at $p<0.05$ within the same row.

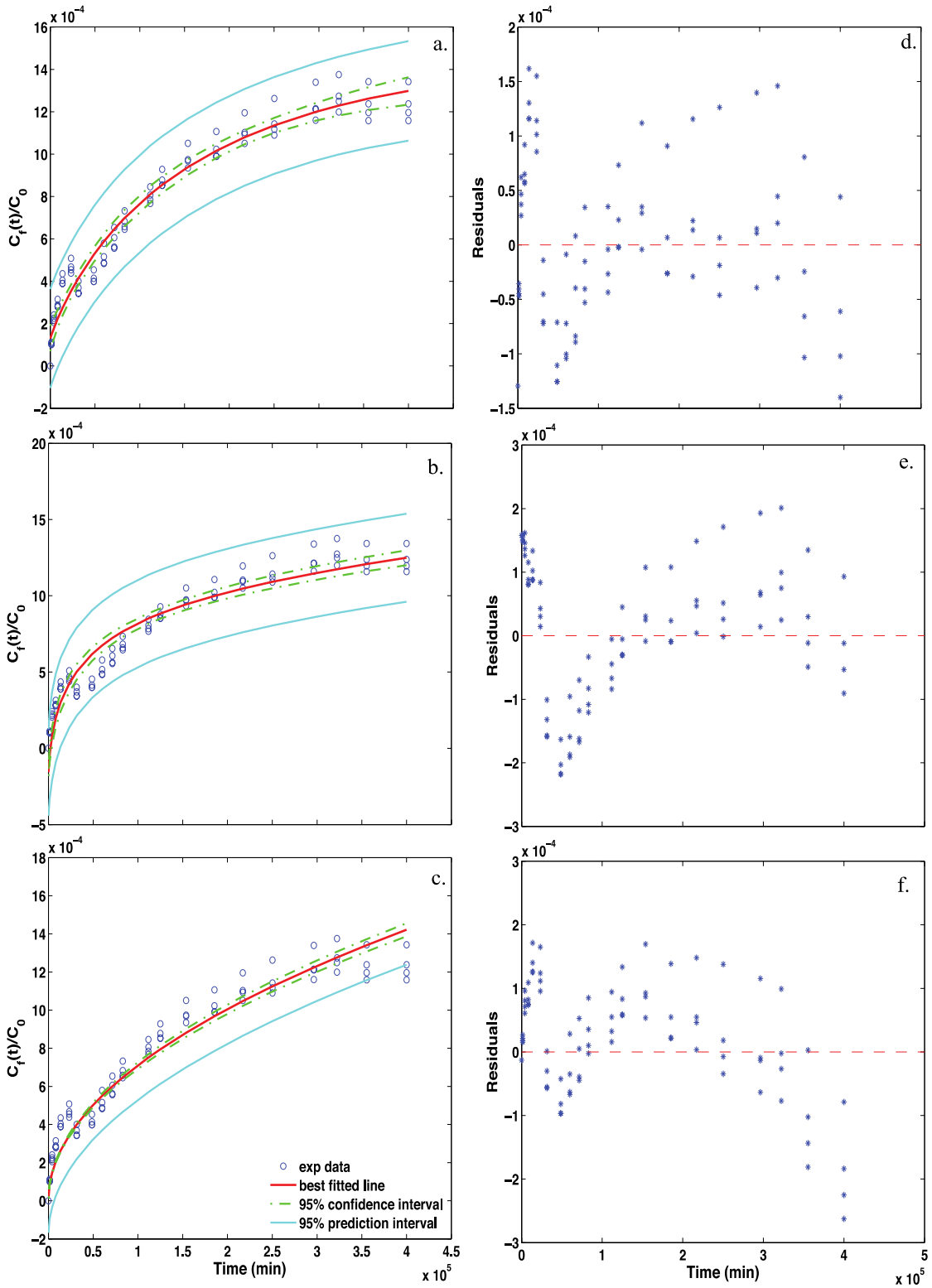

Figure 6-2 Migration of 3 wt. % resveratrol from PLA film into ethanol at 9 °C of (a) model 1, (b) model 2 and (c) model 3 and their corresponding residuals (d), (e), and (f), respectively.

The residual distribution of the three models can be observed in Figure 6-2(d), (e), and (f). Model 1 had a better residuals distribution than model 2 and 3. Model 3 showed a significant signature trend. In general, the plot of residuals is expected to be normally, independently distributed with additive errors, constant variance and zero mean, to name a few, to meet the standard statistical assumptions. However, these conditions seemed to be violated to certain extent particularly for model 3, which shows a clear residual signature; thus further data transformation may be needed for improvement of fitting or the model is not a good fit for this experimental data.

6.2.3 Model Selection Using the Corrected Akaike Information Criterion (AICc)

Since three models were presented in this study, question are raised: which model should be used to represent this particular migration case study?, and what is the criterion needed to provide us enough information for selecting the model? As mentioned earlier, the standard selection criteria can be based on the RMSE and AICc. Often, RMSE introduces bias in the model selection since experimental data is better fitted as an increasing number of parameters is used in a model. The AICc approach can be employed to assist in model selection eliminating bias since it finds a balance between the goodness of fit with the incorporated number of parameters. The AICc is the second order of AIC, which it is applicable when the number of observations (n) is smaller and the number of estimated parameters (p) is larger. As n becomes larger, the correction term ($\frac{2K(K+1)}{n-K-1}$) becomes trivial; thus AICc converges to AIC. Therefore the use of AICc is safe and provides better accuracy when n is small like in migration studies since it penalizes the addition of parameters more than the AIC (Motulsky & Christopoulos, 2004a).

Table 6-2 shows the results based on the AICc approach for selecting the appropriate model for the migration of 3 wt. % resveratrol from PLA film into ethanol at 9 °C. It can be observed that

model 1 resulted in the lowest AICc in comparison with model 2 and 3. The probability that model 1 is a better model than model 2 and 3 was found to be 0.9999 (~99.99%). The evidence ratio of selecting model 1 over model 2 was overwhelming (1.59×10^{15}). In addition, model 1 is 2.20×10^4 times more likely to be the right model over model 3, which is enough evidence for choosing model 1 over model 3. Despite having known which model is likely to be correct, AICc cannot be used to solely reject or accept a particular model. It only gives indications based on how can a certain model best fit a data set and the likelihood of selecting the right model (Motulsky & Christopoulos, 2004a). It is up to researchers to interpret the physical meaning of a constructed experiment in correlation with the parameter of interests within a mathematical model. Therefore, in this particular migration case study, it was found that model 1 is more likely the correct model with D, $K_{p,f}$, and h as the driving factors of the migration. D is the controlling factor inside of the film, while $K_{p,f}$ indicates that the partition effect between the film and food simulant phase is important as not all of the antioxidant (*i.e.*, resveratrol) migrated into the food simulant (*i.e.*, ethanol). The effect of h seemed to be taken place at an early time as indicated in the X' plot, and it is small.

Table 6-3 AICc analysis for selecting the model for the migration of 3 wt. % resveratrol from PLA film into ethanol at 9 °C.

Model	**AICc**	**Probability**	**Evidence Ratio**
1	-1581	0.9999	2.20×10^4
2	-1511	6.30×10^{-16}	1.59×10^{15}
3	-1561	4.54×10^{-5}	

Overall, three different models consisting of different combinations or one particular parameter(s) that govern the kinetics of a migration study have been presented. The comparison among the results based on the OLS estimation was made and model selection was discussed. How can all this information be combined as a well-constructed guideline for researchers to decide which model they should select that best represents their data set obtained from migration experiments? To address this question, Figure 6-4 presents a decision tree analysis as a guideline with extended flexibility to estimate kinetic migration parameters.

The decision tree analysis started with model 1 since it includes all the important kinetic migration parameters. This model also provides the magnitude approximation of initial guesses in the first step to be used in the second step of the non-linear regression estimation. This model allows the estimation of *h*, which is difficult to determine experimentally, hence, the calculation of the *Biot* number. By using the *Biot* number as the key question for the next step, researchers will know if model 1 can appropriately support their experimental data. Otherwise, they may proceed to the next key question for selecting either model 2 or 3. The advantage of assessing model 1 as the initial step is to avoid the assumption that *h* is negligible as presented in the boundary conditions of model 2 and 3. This is particularly important since *h* and *D* are kinetically related in the overall migration resistance series per the *Biot* number definition. For instance, in the absence of convection (*i.e.*, non-stirring food simulant/food), low temperature, and/or viscous food simulant/food etc., the *h* may no longer be assumed negligible. If researchers assume such conditions, not only are they neglecting the possibly important effect of this kinetic parameter, but they also end up underestimating the *D* value. Thus, the estimated *D* value without considering *h* when it is necessary, may be far off from the true *D* value. For such occurrence with respect to

food safety and shelf life estimation, negative consequences are of concern. Additionally, the presented AICc approach can be used to further assist the likelihood of selecting the right model.

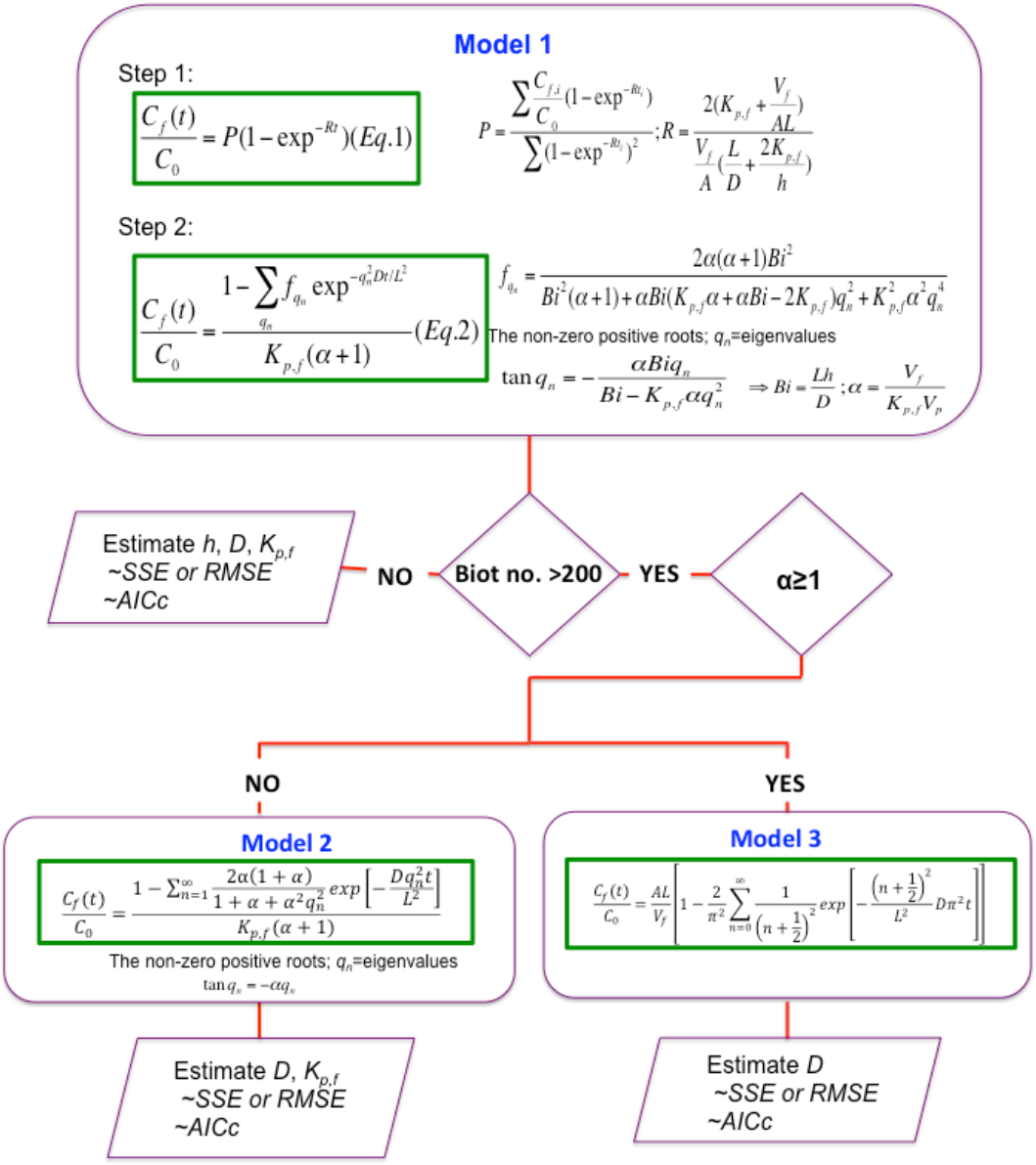

Figure 6-3 Decision tree analysis for determining the kinetic mass transfer parameters (*i.e.*, *D*, $K_{p,f}$, *h*) of a migration study.

6.3 Conclusion

Comparative studies between the two-step solution (model 1) with Crank's mathematical solutions (model 2 and 3) were performed on three different migration case studies. The estimation of the scaled sensitivity coefficient *X'* gave insight into how well each individual parameter in each model can be predicted and the correlation among them. The OLS estimation results were successfully compared among models in each selected migration case study to calculate the *D*, $K_{p,f}$, *h* coefficients. The AICc approach was employed based on its values, probability and likelihood comparisons to assist in the model selection. This approach is not purely statistical since it does not consider hypotheses, but it informs researchers on the data fitting to the model and the likelihood of selecting the correct model. The results obtained from the OLS estimation and AICc were found to be in an agreement with each other. It is worth mentioning that although the AICc can provide information on the likelihood that one model is more likely to be correct than the others, it does not take into consideration the residual distribution. This is because the AICc approach is developed based on the maximum likelihood, information and the entropy of information's theories instead of conventional statistical inference. Having based solely the decision on the AICc approach to choose a model without investigating if all the statistical assumptions have been met could lead to another issue like over fitting, *etc*. Therefore, it is up to the researcher to weigh all the information obtained from both the OLS results and the AICc before choosing a particular model for a data set. In addition, a decision tree analysis was introduced to offer a constructed guideline to select the appropriate model with its respective kinetic migration parameters. Further experimental studies should be conducted to design experiments where *h* is a driving factor during the migration study.

APPENDICES

APPENDIX 6A: Migration of poly(lactic acid), PLA incorporated with 2.6 wt.% α-tocopherol into ethanol at 23 °C.

Scaled Sensitivity Coefficient, *X'*

For both model 1 and 2 of the migration of 2.6 wt.% α-tocopherol from PLA film into ethanol at 23 °C, D and $K_{p,f}$ were not highly correlated to each other (Figure 6A-1), which allows the simultaneous estimation of them. However, for model 1, the h parameter was introduced as a constant parameter since it was highly correlated with the D ($\rho_{D,h} > 0.99$). Besides, the magnitude response of change of this parameter towards pertubation was relatively small.

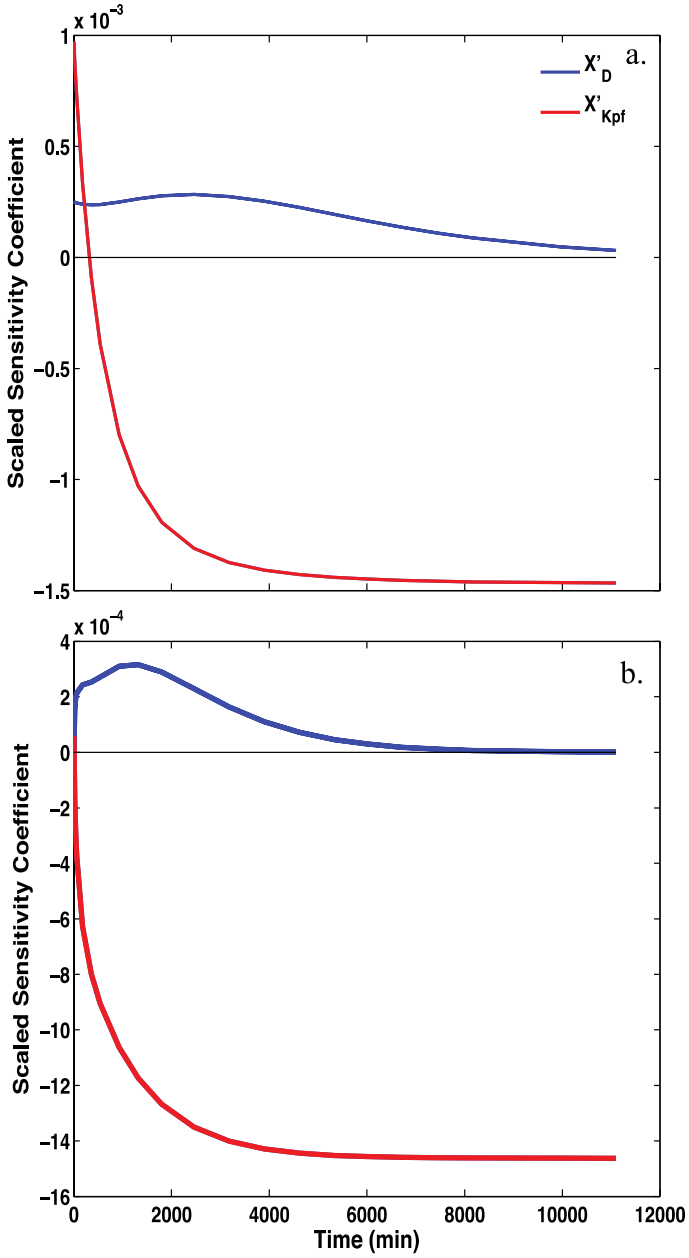

Figure 6A- 1 Scaled sensitivity coefficient of migration of 2.6 wt.% α-tocopherol from PLA film into ethanol at 23 °C of (a) model 1 (initial guesses were: D=2.00 × 10^{-9} cm^2/min, $K_{p,f}$=609 cm^3 PLA/cm^3 ethanol), and (b) model 2 (initial guesses were: D=10.00 × 10^{-9} cm^2/min and $K_{p,f}$=500 cm^3 PLA/cm^3 ethanol). Note: the h was not estimated for model 1 due to high correlation issue with the D.

Ordinary Least Square (OLS) Estimation

The estimated *D* values for both model 1 and 2 were not significantly different ($p>0.05$) from each other (Table 6A-1). However, these estimated *D* values were different than the published result of 1.90×10^{-9} cm^2/min (Manzanarez-López, Soto-Valdez, Auras, & Peralta, 2011). Similarly, the reported $K_{p,f}$ (796.62 cm^3 PLA/cm^3 ethanol) (Manzanarez-López, Soto-Valdez, Auras, & Peralta, 2011) was slightly higher than the estimated $K_{p,f}$ of model 1 and 2. Closer estimation values of *D* and $K_{p,f}$ were anticipated between model 2 and the published result of this migration case study. Lowest relative error of the $K_{p,f}$ in both model 1 and 2 were observed than that of the *D* as expected based on the *X'* plot (Table 6A-1).

The plots of the migration 2.6 wt.% α-tocopherol from PLA film into ethanol at 23 °C (Figure 6A-2(a)) demonstrated that model 2 fits the experimental data better with a normally scattered residual distribution (Figure 6A-2(c)) than that of model 1 since the residual are normally, independently distributed (*NID*). Motulsky & Christopoulos (2004b) discussed that due to the symmetricallity of the asymptotic confidence interval, different ways of expressing a model can result in different output. In addition, the AICc of model 2 turned out to be lower than that of model 1 (Table 6A-2), with overwhelming evidence ratio supporting model 2 as more likely to be the correct model. These outcomes are in agreement with each other.

Table 6A- 1 OLS results for the migration study of 2.6 wt.% α-tocopherol from PLA film into ethanol at 23 °C for model 1 and 2.

Parameter & Additional Info	Model	
	1	**2**
$D \times 10^{-9}$ (cm^2/min)	6.44 ± 0.08[a]	6.74 ± 0.44[a]
Relative error (%)	1.17	6.59
$K_{p,f}$ (cm^3 PLA/cm^3 ethanol)	631.54 ± 7.08[a]	482.71± 5.57[b]
Relative error (%)	1.12	1.15
RMSE$\times 10^{-4}$ (cm^3 ethanol/cm^3 PLA)	1.23	0.84

Note: Data represents as mean ± standard error; a,b superscripts represent statistical difference at $p<0.05$ within the same row.

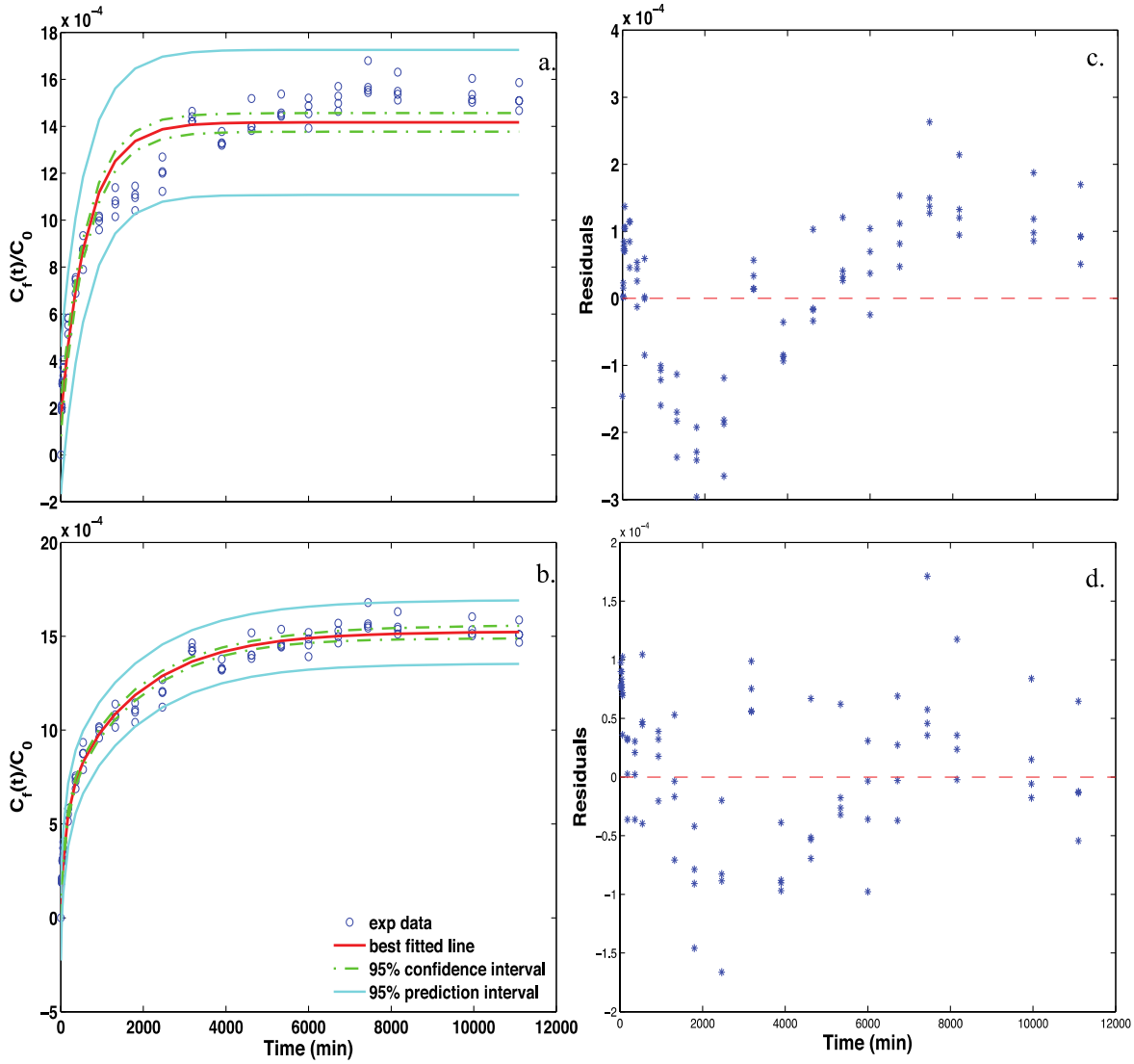

Figure 6A- 2 Migration of 2.6 wt.% α-tocopherol from PLA film into ethanol at 23 °C of (a) model 1 and (b) model 2 and their corresponding residuals (c), and (d), respectively.

Model Selection Using the Corrected Akaike Information Criterion (AICc)

Table 6A- 2 AICc analysis for selecting the model for the migration study of 2.6 wt.% α-tocopherol from PLA film into ethanol at 23 °C.

Model	**AICc**	**Probability**	**Evidence Ratio**
1	-1508	7.68×10^{-15}	1.30×10^{14}
2	-1573	1.00	

APPENDIX 6B: Migration of poly(lactic acid), PLA incorporated with 1.28 wt.% catechin into 95% ethanol at 40 °C.

Scaled Sensitivity Coefficient, *X'*

The *X'* plot of the migration of 1.28 wt.% catechin from PLA film into 95% ethanol at 40 °C indicated no high correlation among the three parameters. Since model 1 was only compared with model 3, the *X'* plot for model 3 is not shown (only one parameter estimated). Model 2 was not considered for the comparison per the decision tree guideline ($\alpha \geq 1$).

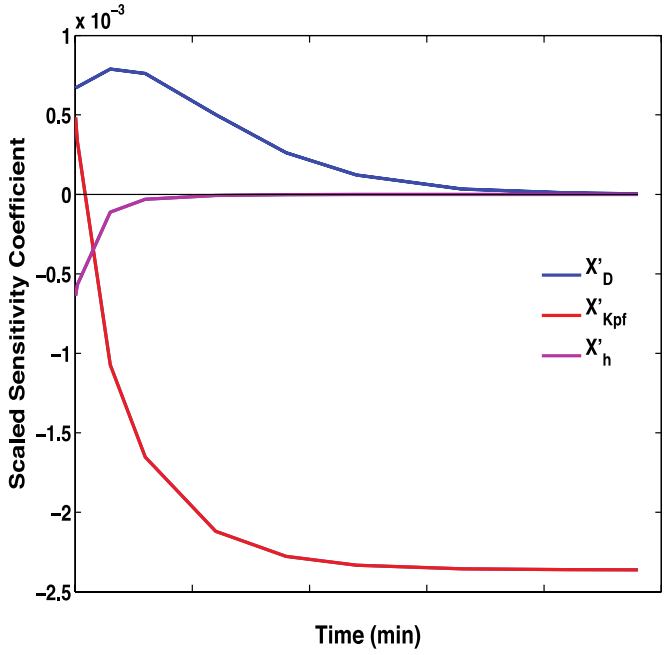

Figure 6B- 1 Scaled sensitivity coefficient of the migration of 1.28 wt.% catechin from PLA film into 95% ethanol at 40 °C of model 1 (initial guesses were: D=3.00 × 10^{-8} cm^2/min, $K_{p,f}$=318.97 cm^3 PLA/cm^3 ethanol).

Ordinary Least Square (OLS) Estimations

The only parameter that can be compared between models 1 and 3 was the *D* and the result was significantly different ($p<0.05$). Interestingly, the estimated *D* value of model 1 was comparable to the reported *D* value (2.87×10^{-8} cm^2/min) of this case study (Iñiguez-Franco, Soto-Valdez, Peralta, Ayala-Zavala, Auras, & Gámez-Meza, 2012). As anticipated, with more parameters estimated in model 1, the resulting RMSE value was lower than that of model 3 (Table 6B-1). The model fitting of the experimental data for models 1 and 3 can be observed in Figure 6B-2. Although model 1 seemed to better fit the experimental data, the residual plot distribution showed the signature in the residuals for both models; therefore, further data transformation may be needed to improve the fitting of both models. The AICc approach results indicated that model 1 had a higher likelihood of being the right model than model 3. This result supported the outcomes from the OLS estimation.

Table 6B- 1 OLS results for the migration of 1.28 wt.% catechin from PLA film into 95% ethanol at 40 °C for model 1 and 3.

Parameter & Additional Info	Model	
	1	**3**
$D\times10^{-8}$ (cm^2/min)	2.26 ± 0.13^a	10.13 ± 0.74^b
Relative error (%)	5.92	7.29
$K_{p,f}$ (cm^3 PLA/cm^3 ethanol)	324.04 ± 4.15	
Relative error (%)	1.28	
$h\times10^{-3}$(cm/min)	4.40 ± 0.43	
Relative error (%)	9.62	
RMSE$\times10^{-4}$ (cm^3 ethanol/cm^3 PLA)	0.96	3.54

Note: Data represents as mean ± standard error; a,b superscripts represent statistical difference at $p<0.05$ within the same row.

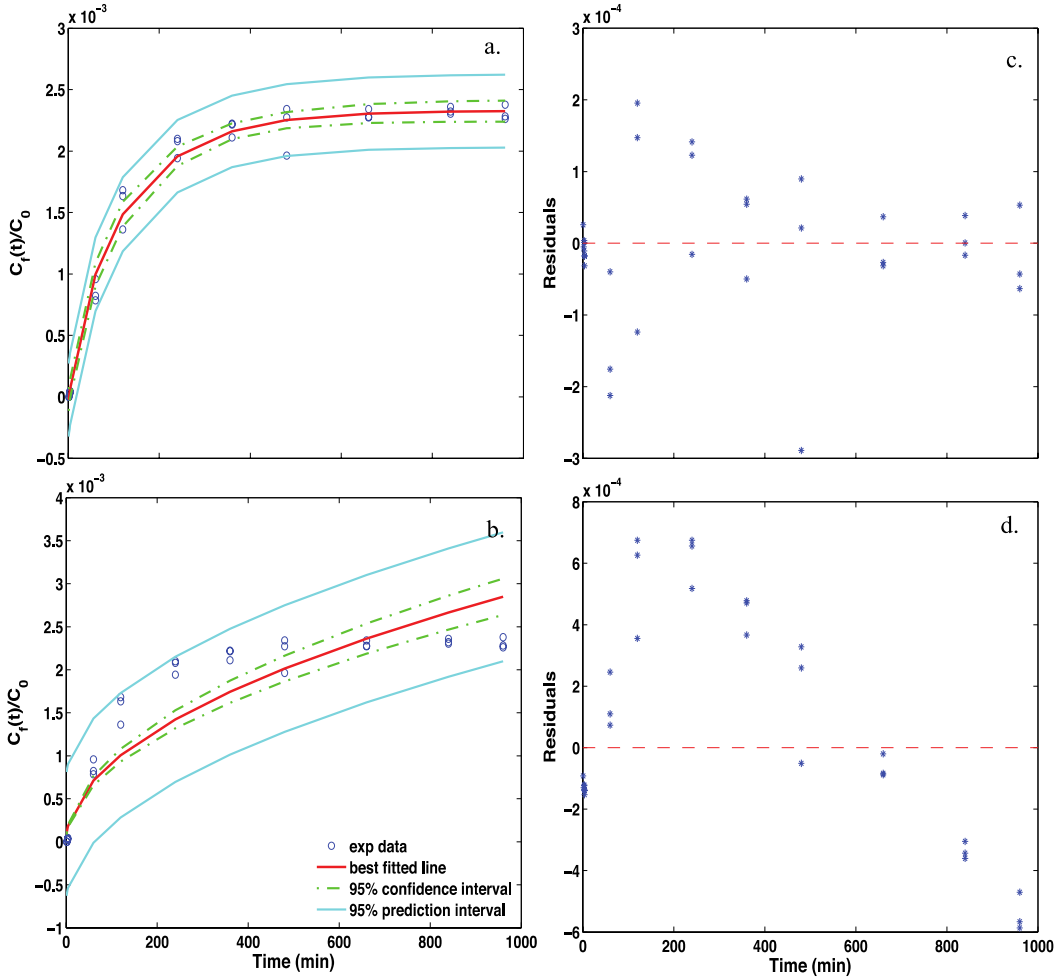

Figure 6B- 2 Migration of 1.28 wt.% catechin from PLA film into 95% ethanol at 40 °C of (a) model 1 and (b) model 3 and their corresponding residuals (c), and (d), respectively.

Model Selection Using the Corrected Akaike Information Criterion (AICc)

Table 6B- 2 AICc analysis for selecting model for the migration of 1.28 wt.% catechin from PLA film into 95% ethanol at 40 °C.

Model	**AICc**	**Probability**	**Evidence Ratio**
1	-659	1.002	3.49×10^{19}
3	-569	$.86\times10^{-20}$	

REFERENCES

REFERENCES

Carslaw, H. S., & Jaeger, J. C. (1959). Conduction of heat in solids. *Oxford: Clarendon Press, 1959, 2nd ed., 1*.

Chung, D., Papadakis, S. E., & Yam, K. L. (2001). Release of propyl paraben from a polymer coating into water and food simulating solvents for antimicrobial packaging applications. *Journal of Food Processing and Preservation, 25*(1), 71-87.

Chung, D., Papadakis, S. E., & Yam, K. L. (2002). Simple models for assessing migration from food-packaging films. *Food Additives and Contaminants, 19*(6), 611-617.

Crank, J. (1979). *The Mathematics of Diffusion* (2nd ed.). Bristol: Oxford University Press.

Dolan, K. D., & Mishra, D. K. (2013). Parameter estimation in food science. *The Annual Review of Food Science and Technology, 4*, 401-422.

Galotto, M., Torres, A., Guarda, A., Moraga, N., & Romero, J. (2011). Experimental and theoretical study of LDPE versus different concentrations of Irganox 1076 and different thickness. *Food Research International, 44*(2), 566-574.

Gandek, T. P., Hatton, T. A., & Reid, R. C. (1989). Batch extraction with reaction: phenolic antioxidant migration from polyolefins to water. 1. Theory. *Industrial & engineering chemistry research, 28*(7), 1030-1036.

Hwang, S. W., Shim, J. K., Selke, S., Soto-Valdez, H., Matuana, L., Rubino, M., & Auras, R. (2013). Migration of α-Tocopherol and Resveratrol from Poly (L-lactic acid)/Starch Blends Films into Ethanol. *Journal of Food Engineering*.

Iñiguez-Franco, F., Soto-Valdez, H., Peralta, E., Ayala-Zavala, J. F., Auras, R., & Gámez-Meza, N. (2012). Antioxidant Activity and Diffusion of Catechin and Epicatechin from Antioxidant Active Films Made of Poly (l-lactic acid). *Journal of Agricultural and Food Chemistry, 60*(26), 6515-6523.

Manzanarez-López, F., Soto-Valdez, H., Auras, R., & Peralta, E. (2011). Release of α-Tocopherol from Poly (lactic acid) films, and its effect on the oxidative stability of soybean oil. *Journal of Food Engineering, 104*(4), 508-517.

Mascheroni, E., Guillard, V., Nalin, F., Mora, L., & Piergiovanni, L. (2010). Diffusivity of propolis compounds in Polylactic acid polymer for the development of anti-microbial packaging films. *Journal of Food Engineering, 98*(3), 294-301.

Motulsky, H., & Christopoulos, A. (2004a). Comparing models using Akaike's Information Criterion (AIC) In: Fitting models to biological data using linear and nonlinear regression: A practical guide to curve fitting: Oxford Univ. Press, New York.

Motulsky, H., & Christopoulos, A. (2004b). How nonlinear regression works In: Fitting models to biological data using linear and nonlinear regression: A practical guide to curve fitting: Oxford Univ. Press, New York.

Motulsky, H., & Christopoulos, A. (2004c). Models In: Fitting models to biological data using linear and nonlinear regression: A practical guide to curve fitting: Oxford Univ. Press, New York.

Pocas, M. F., Oliveira, J. C., Brandsch, R., & Hogg, T. (2012). Analysis of mathematical models to describe the migration of additives from packaging plastics to foods. *Journal of Food Process Engineering, 35*(4), 657-676.

Poças, M. F., Oliveira, J. C., Oliveira, F. A. R., & Hogg, T. (2008). A critical survey of predictive mathematical models for migration from packaging. *Critical Reviews in Food Science and Nutrition, 48*(10), 913-928.

Reynier, A., Dole, P., & Feigenbaum, A. (2002a). Integrated approach of migration prediction using numerical modelling associated to experimental determination of key parameters. *Food Additives & Contaminants, 19*(S1), 42-55.

Reynier, A., Dole, P., & Feigenbaum, A. (2002b). Migration of additives from polymers into food simulants: numerical solution of a mathematical model taking into account food and polymer interactions. *Food Additives & Contaminants, 19*(1), 89-102.

Samsudin, H., Valdez, H. S., & Auras, R. (2014). Poly (lactic acid) film incorporated with marigold flower extract (< i> Tagetes erecta</i>) intended for fatty-food application. *Food Control, 46*, 55-66. doi: 10.1016/j.foodcont.2014.04.045

Soto-Valdez, H., Auras, R., & Peralta, E. (2010). Fabrication of Poly(lactic acid) Films with Resveratrol and the Diffusion of Resveratrol into Ethanol. *Journal of Applied Polymer Science*. doi: 10.1002/app.33687

Soto-Valdez , H., Peralta, E., & Auras, R. (2008). *Poly(lactic acid) films added with resveratrol as active packaging with potential application in the food industry.* Paper presented at the 16th IAPRI World Conference on Packaging Bangkok, Thailand.

Vitrac, O., & Hayert, M. (2006). Identification of diffusion transport properties from desorption/sorption kinetics: an analysis based on a new approximation of fick equation during solid-liquid contact. *Industrial & Engineering Chemistry Research, 45*(23), 7941-7956.

Vitrac, O., Mougharbel, A., & Feigenbaum, A. (2007). Interfacial mass transport properties which control the migration of packaging constituents into foodstuffs. *Journal of Food Engineering, 79*(3), 1048-1064.

Wagenmakers, E.-J., & Farrell, S. (2004). AIC model selection using Akaike weights. *Psychonomic bulletin & review, 11*(1), 192-196.

Chapter 7

Estimation of the Activation Energy in Migration Studies

7.0 Introduction

Migration studies are usually conducted to gain insight on the migration limit and the kinetic behaviors of additives or possible contaminant(s) from a base polymer into a food/food simulant. Kinetic behavior in a migration study provides useful information such as the chemical affinity between a polymer and a food/food simulant (partition coefficient, $K_{p,f}$), the rate of the transfer mechanism (diffusion coefficient, D), and the resistance at the interface (convective mass transfer coefficient, h) as shown in Chapters 4 to 6. Unlike the $K_{p,f}$ that can be measured experimentally at the end of an experiment, the D and h can only be approximated by means of mathematical expressions. Therefore, assessment of these parameters holds its own significance for describing a migration phenomenon. Since migration is a transfer process involving the movement of molecules from high concentration to low concentration following Fick's second law of diffusion, the mass transfer behavior is temperature dependent and can be described using the Arrhenius equation:

$$D = D_0 exp\left(-\frac{E_a}{RT}\right) \quad \text{(Eq. 7-1)}$$

where D = diffusion coefficient; D_0=pre-exponential factor; E_a=activation energy; R=gas constant; T=temperature.

The activation energy (E_a) term embedded in the Arrhenius equation is commonly estimated and can be defined as how the kinetic rate changes with temperatures. Often, the E_a is estimated using its linearized form by taking the natural logarithm (ln) of the equation to eliminate the exponential term (Eq. 7-2). A plot of ln (D) as a function of reciprocal temperature (1/T (°K)) can be constructed and the E_a value can be obtained from the slope × R.

$$\ln(D) = \ln(D_0) - \frac{E_a}{R}\frac{1}{T} \quad \text{(Eq. 7-2)}$$

This practice is commonly considered to simplify the difficulty of estimating the E_a and to avoid the numerical complication of having a high correlation between the two important factors of the Arrhenius equation, which are D_o and E_a. Several authors investigated the fitting of linear versus non-linear approximations of the Arrhenius equation and the outcomes were inconclusive (Brauner & Shacham, 1997; Chen & Aris, 1992; Klicka & Kubácek, 1997; Sundberg, 1998). Despite that, several other authors recommended the reparameterization of the Arrhenius equation (Eq. 7-3) to reduce the correlation tendency between the D_o and E_a by introducing the reference temperature (T_{ref}) that corresponds to the reference D (D_{ref}) (Agarwal & Brisk, 1985a, 1985b; Ahmed, Dolan, & Mishra, 2012; K. D. Dolan, Valdramidis, & Mishra, 2013; Pritchard & Bacon, 1975, 1978; Schwaab, Lemos, & Pinto, 2008; Schwaab & Pinto, 2007; Sulaiman, Dolan, & Mishra, 2013). This concept was introduced by Box, 1960.

$$D = D_{ref}e\left[-\frac{E_a}{R}\left(\frac{1}{T} - \frac{1}{T_{ref}}\right)\right] \quad \text{(Eq. 7-3)}$$

where D_{ref}= the diffusivity rate of the additives at T_{ref}.

The concept of reparameterizing by finding an optimum T_{ref} is crucial to obtain near zero correlation between the rate constant of the reference diffusion, D_{ref} and the E_a since by minimizing the correlation between the two parameters, their respective relative errors will also be minimized. Therefore, the non-linear approximation of the Arrhenius equation is recommended and by using it as a secondary model in an analytical kinetic migration expression, simultaneous estimation of the parameters can be performed.

Moreover, to the author's best knowledge; there is no published work in the food packaging area about the reparameterization of the Arrhenius equation. So, the objectives of this work were; i) to find the optimum T_{ref} that resulted in near zero correlation between the D_{ref} and the E_a by the

insertion of the Arrhenius equation as a secondary model into an analytical kinetic migration equation and ii) to estimate all uncorrelated kinetic migration parameters simultaneously. Additionally, the temperature simulation (T_{sim}) approach was introduced for the first time in the food packaging area to evaluate non-isothermal migration studies based on the work of K. Dolan, 2015.

7.1 Materials and Methods

7.1.1 A Case Study

A case study was selected for this work to demonstrate the estimation of E_a: the migration of 1.28 wt.% catechin from poly(lactic acid), PLA, film into 95% ethanol at 20, 30, 40, and 50 °C (Iñiguez-Franco et al., 2012). All computational data analyses were coded (Appendix 7B) and performed using MATLAB® R2011b (MathWorks, Natick, MA, USA).

7.1.2 Kinetic Parameter Estimation Procedure

The analytical kinetic migration equation describing the movement of additives from polymer films can be represented with model 1 as presented in chapter 5;

$$\frac{C_f(t)}{C_0} = \frac{1-\sum_{qn}^{\infty} f_q e^{\frac{-q_n^2 Dt}{L^2}}}{K_{p,f}(\alpha+1)} \qquad \text{(Eq. 7-4)}$$

where $f_q = \frac{2\alpha(\alpha+1)Bi^2}{Bi^2(1+\alpha)+\alpha Bi\left[K_{p,f}\alpha+\alpha Bi-2K_{p,f}\right]q_n^2+K_{p,f}^2\alpha^2 q_n^4}$;

The eigenvalue's root solutions = $tan\ q_n = -\frac{\alpha Bi q_n}{Bi-K_{p,f}\alpha q_n^2}$; $\alpha = \frac{V_f}{K_{p,f}AL}$ and $Bi = \frac{hL}{D}$

where C_f = concentration of antioxidant in the food simulant; C_0 = initial concentration of antioxidant in the polymer; α = the ratio of the mass of antioxidant migrated into food simulant to

the mass of antioxidant left in the polymer, at equilibrium; V_f = volume of food simulant; A = area; L= half of the film's thickness; Bi = *Biot* number; q_n = the non-zero roots of eigenvalues.

The secondary model (Eq. 7-2 (below)) was inserted into Eq. 7-4, resulted in Eq. 7-5;

$$D = D_{ref} e\left[-\frac{E_a}{R}\left(\frac{1}{\mathrm{T}} - \frac{1}{T_{ref}}\right)\right]$$

$$\frac{C_f(t)}{C_0} = \frac{1-\sum_{q_n}^{\infty} f_q exp\frac{-q_n^2 D_{ref} e\left[-\frac{E_a}{R}\left(\frac{1}{T}-\frac{1}{T_{ref}}\right)\right]t}{L^2}}{K_{p,f}(\alpha+1)} \qquad \text{(Eq. 7-5)}$$

where $f_q = \frac{2\alpha(\alpha+1)Bi^2}{Bi^2(1+\alpha)+\alpha Bi\left[K_{p,f}\alpha+\alpha Bi-2K_{p,f}\right]q_n^2+K_{p,f}^2\alpha^2 q_n^4}$;

7.1.3.1 Step 1:

7.1.3.1.1 Scaled Sensitivity Coefficient, *X'*

Data set of a case study at each temperature was set up for the non-isothermal estimation. The scaled sensitivity coefficient, *X'*, was plotted for the fitting parameters (D_{ref}, $K_{p,f}$, h and E_a). Since this is a forward problem, initial guesses were mostly acquired from published data with some modification. The forward problem provides an explicit solution and the parameters are given; thus it can be run without any data. By using a forward difference approximation, the scaled sensitivity coefficient, *X'*, was computed by taking the first derivatives of the observational data with respect to the parameter and multiplying by the parameter itself. The plot of *X'* as a function of time was plotted to investigate the correlation among the parameters. The magnitude of the change of the response of each parameter to perturbation was observed.

7.1.3.1.2 Temperature Simulation (T_{sim}) Approach

Since temperature is not constant and E_a depends on how D is changing with temperature, the T_{sim} approach was proposed to plot the X' of E_a (K. Dolan, 2015) by inserting an anonymous function in the model's function file as shown below;

$$T_{sim} = @(t)\ T_L + \frac{T_H - T_L}{t_{max}} t \qquad \text{(Eq. 7-6)}$$

where T_L= the lowest temperature (K); T_H= the highest temperature (K); t_{max}=maximum time duration; t= linearly spaced time.

7.1.3.1.3 Non-Linear Regression Estimation

The non-linear regression fitting (nlinfit) function in MATLAB® R2011b (MathWorks, Natick, MA, USA) was used to estimate the parameters. The correlation coefficient matrix obtained was used to confirm any correlation among the parameters as observed in the X' plot. Since there is no available information about the T_{ref} for migration studies, different values were fixed to find a better estimation.

7.1.3.2 Step 2:

The best guess of the T_{ref} was then used as the initial guess to find the correlation between the D_{ref} and the E_a. The plot of the correlation between the D_{ref} and the E_a as a function of the possible range of the T_{ref} was constructed to find the optimum T_{ref}. The optimum T_{ref} value was then used to estimate the parameters (D_{ref}, $K_{p,f}$, h and E_a) for final estimation.

7.2 Results and Discussions

7.2.1 Initial Scaled Sensitivity Coefficient, *X'* and Reference Temperature, T_{ref}

Since there is no available information on the T_{ref} of this particular case study, it is important to start off with the best-considered T_{ref} value to initiate the forward problem estimation process. It has been widely cited that the use of a T_{ref} that approaches large values can cause high correlation between the D_{ref} and the E_a and correspondingly large standard errors. This is because the reparameterized Arrhenius equation converges to its traditional form (Eq.7-1). Most of the researchers recommend the average temperature within the experimental temperature range as the starting point, rather than arbitrarily choosing a particular temperature (Ahmed, Dolan, & Mishra, 2012; K. D. Dolan, 2003; Schwaab & Pinto, 2007). Meanwhile, Datta (1993) and Ahmed, Dolan, & Mishra (2012) suggested the T_{ref} to be closer to the upper range of the experiment temperature range. For this case study, the initial T_{ref} chosen was the average within the migration testing temperature range (*i.e.*, 20 to 50 °C), which was 35 °C. The *X'* plot was then constructed to find any possible correlation among all the parameters of interest. Initial observation from the *X'* plot indicated that the *h* parameter had the smallest magnitude change of response among the rest of the parameters, which is expected to contribute to the largest relative error (Figure 7-1). Therefore, this parameter was kept as constant value since it presence had negligible effect on the overall kinetics of migration and to a certain extent it may introduce more difficulty in estimating the other parameters (as discussed in chapter 5).

Figure 7-2 shows the *X'* plot consisting only of the three parameters (*i.e.*, D_{ref}, $K_{p,f}$, E_a) (Figure 7-2) which has a better improvement in terms of the change in their magnitude of response than Figure 7-1. Both plots were constructed by implementing the T_{sim} approach as explained in section 7.1.3.1.2. The $K_{p,f}$ was identified as the easiest parameter to be estimated; hence, the lowest

relative errors followed by the E_a and D_{ref}. The correlation coefficients among the estimated parameters using the initial T_{ref} can be found in Table 7-1. The correlation coefficient, ρ, between D_{ref} and E_a was fairly high ($\rho = 0.63$) since near zero correlation is desired (Schwaab, Lemos, & Pinto, 2008; Schwaab & Pinto, 2007), thus the iterative search for T_{ref} was continued until ρ showed a possible lower correlation. Additional results for the correlation coefficients between D_{ref} and E_a for different and randomly chosen temperatures are shown in Appendix 7A.

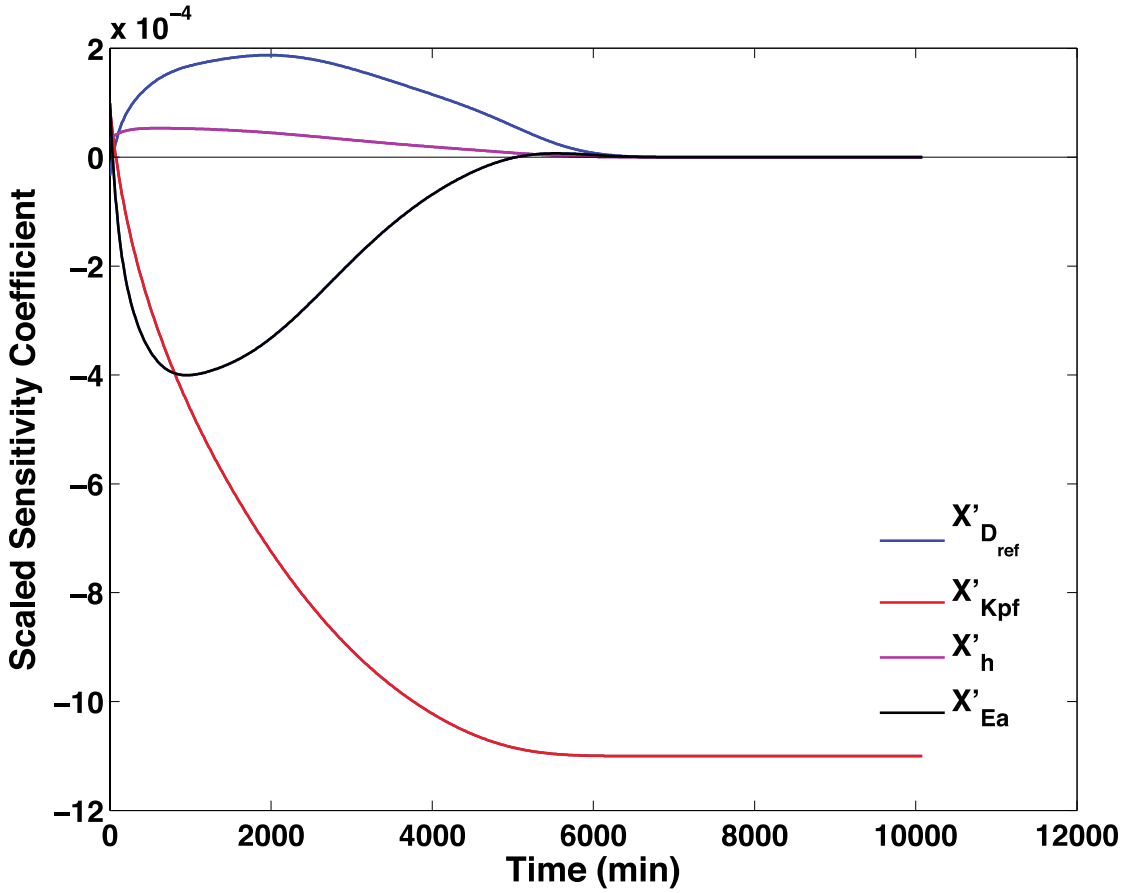

Figure 7-1 Scaled sensitivity coefficient of the activation energy estimation of the migration of 1.28 wt.% catechin from PLA film into 95% ethanol ranging from 20, 30, 40, and 50 °C at T_{ref}=35 °C. Initial guesses were: D_{ref}=1.00 × 10^{-9} cm^2/min, $K_{p,f}$=800 cm^3 PLA/cm^3 ethanol, h=10.00 × 10^{-4} cm/min, and E_a=150000 J/mol).

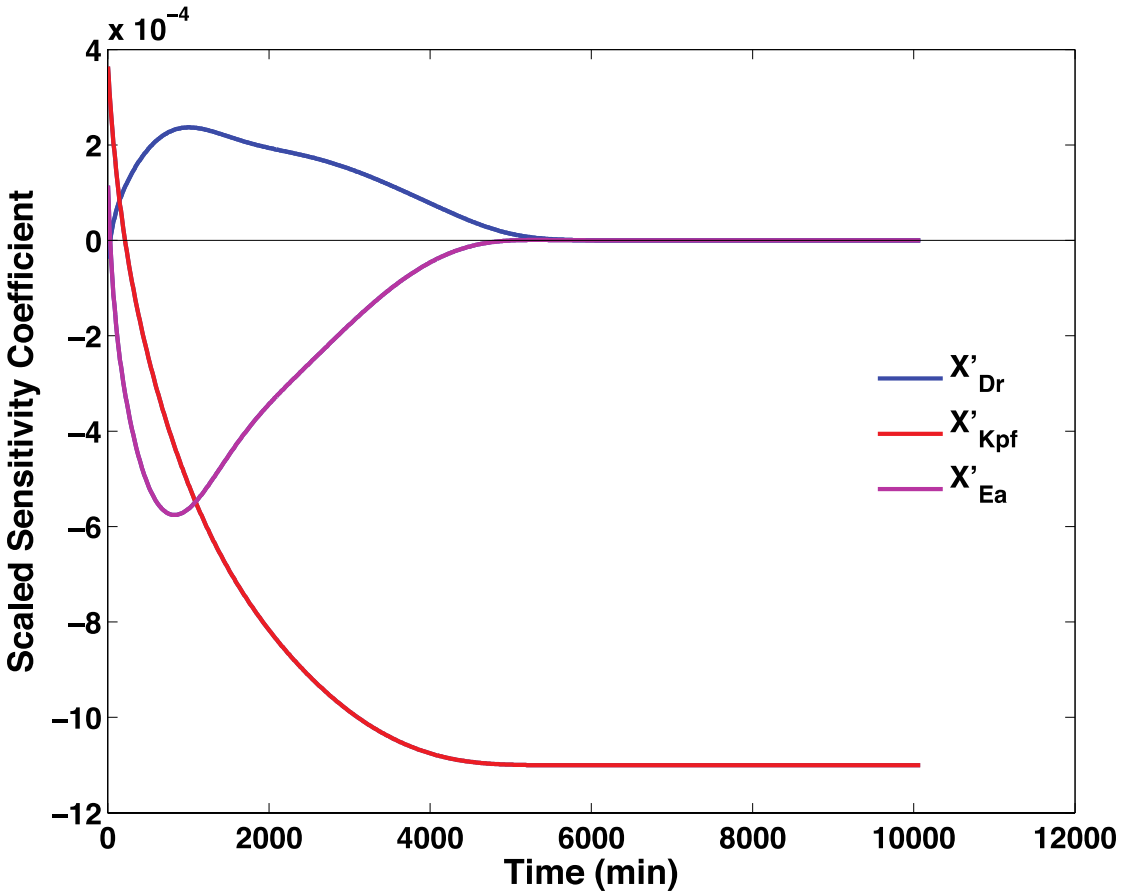

Figure 7-2 Scaled sensitivity coefficient of the activation energy estimation at T_{ref}=35 °C of the migration of 1.28 wt.% catechin from PLA film into 95% ethanol ranging from 20, 30, 40, and 50 °C. Initial guesses were: D_{ref}=2.00× 10^{-9} cm^2/min, $K_{p,f}$=800 cm^3 PLA/cm^3 ethanol, and E_a=150000 J/mol).

Table 7-1 Correlation matrix of the estimated parameters at the average T_{ref}=35 °C.

Parameters	**Correlation coefficients, ρ**			**Relative Error (%)**
	D_{ref}	$K_{p,f}$	E_a	
D_{ref}				11.07
Kp,f	0.11	Symmetric		4.93
E_a	-0.63	-0.29		7.33

After the iterative search was performed, it was found that at T_{ref}=45 °C, the correlation between D_{ref} and E_a was 0.01 with relative errors of 8.34 and 4.21 %, respectively (Table 7-2). Thus, the estimated values obtained at this T_{ref} were then used as the initial guesses to construct the plot of correlation coefficient between the D_{ref} and the E_a as a function of the experimental temperature range (Figure 7-3). From Figure 7-3, the optimum T_{ref} that resulted in near zero correlation between the D_{ref} and the E_a was identified to be 44.94 °C ($\rho = 3.15 \times 10^{-4}$).

Table 7-2 Correlation matrix of the estimated parameters at the T_{ref}=45 °C.

Parameters	**Correlation coefficients, ρ**			**Relative Error (%)**
	D_{ref}	$K_{p,f}$	E_a	
D_{ref}				8.34
$K_{p,f}$	0.33	Symmetric		4.16
E_a	0.01	-0.34		4.21

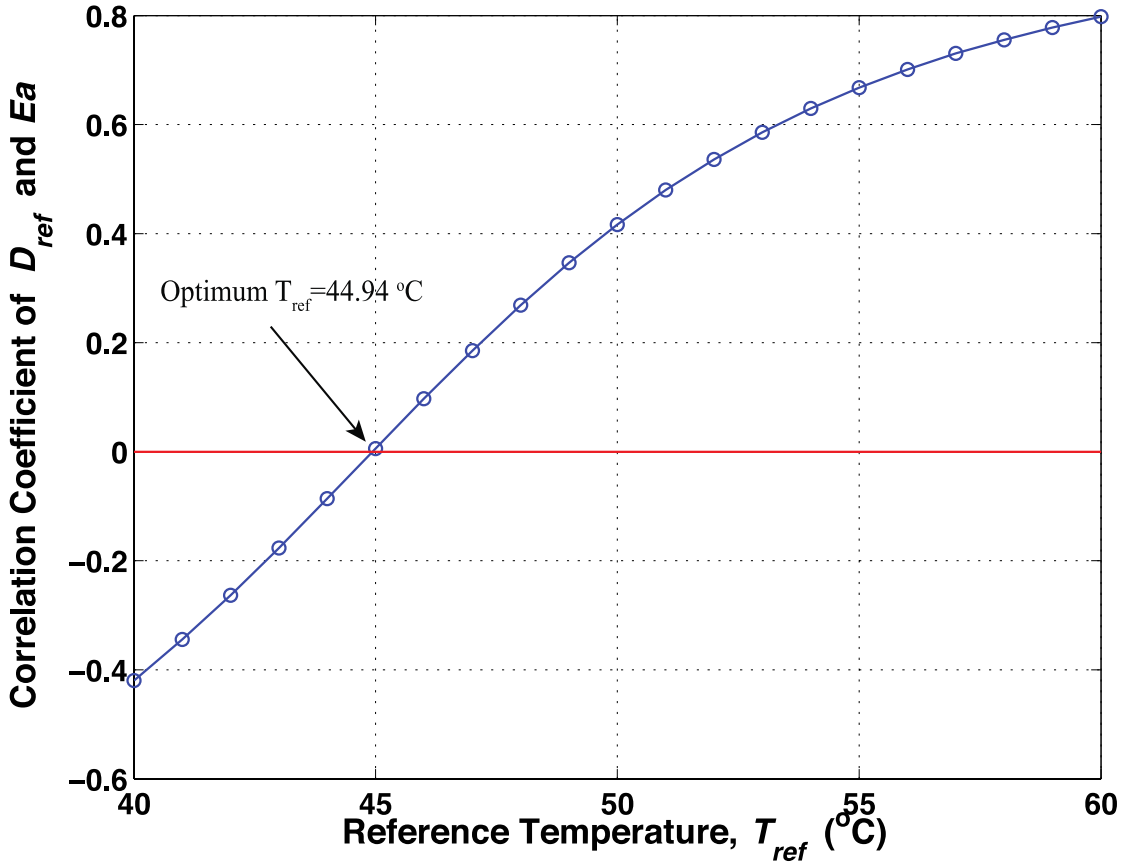

Figure 7-3 Plot of correlation coefficient of the D_{ref} and the E_a as a function of possible T_{ref}

7.2.1 Non-Linear Regression Estimation

The non-linear regression estimation was performed by using the optimum T_{ref} and the results can be found in Table 7-3 and Table 7-4. The lowest correlation between D_{ref} and E_a was found at the identified optimum T_{ref}. As has been widely discussed in several publications (Ahmed, Dolan, & Mishra, 2012; K. D. Dolan, 2003; Schwaab, Lemos, & Pinto, 2008; Schwaab & Pinto, 2007; Sulaiman, Dolan, & Mishra, 2013), the estimation of E_a using the optimum T_{ref} not only is crucial to reduce the correlation issue between the E_a and the D_{ref}, but also is critical to minimize the relative error of D_{ref}. Therefore, the linear estimation of activation energy as shown in Eq. 7-2 should be avoided whenever possible to avoid the risk of over fitting, which means fitting noises

over the actual data. In addition, the re-parameterization approach (Eq. 7-3) helps to minimize the correlation issue as discussed earlier. The estimated D_{ref} and $K_{p,f}$ were found to be 3.70×10^{-9} cm^2/min, and 436.62 cm^3 PLA/cm^3 ethanol, respectively at the optimum T_{ref}=44.94 °C. Meanwhile the estimated E_a in this study was found to be 153.00 kJ/mol, which was significantly higher than that reported by Iñiguez-Franco et al. (2012) of 110.43 kJ/mol. This huge difference could be due to the linearization of the Arrhenius equation. Figure 7-4 shows the final constructed *X'* plot. Significant improvement can be observed in all parameters by taking into consideration their magnitude change of response. The $K_{p,f}$ had the lowest relative error followed by E_a and D_{ref} (Table 7-3) as compared using the initial observation from Figure 7-2.

Table 7-3 Correlation matrix of the estimated parameters at the optimum T_{ref}=44.94 °C.

Parameters	**Correlation coefficients, ρ**			**Relative Error (%)**
	D_{ref}	$K_{p,f}$	E_a	
D_{ref}				8.34
$K_{p,f}$	0.33	Symmetric		4.16
E_a	0.00*	-0.34		4.21

*3.15×10^{-4}

Table 7-4 The parameter estimates at the optimum T_{ref}=44.94 °C.

Parameters	Estimates	RMSE
$D_{ref} \times 10^{-9}$ (cm^2/min)	3.70 ± 0.31	5.06×10^{-4}
$K_{p,f}$ (cm^3 PLA/cm^3 ethanol)	436.62 ± 18.16	
$E_a \times 10^5$ (J/mol)	1.53 ± 0.06	

Note: RMSE (Root mean square errors) unit= cm^3 ethanol/cm^3 PLA.

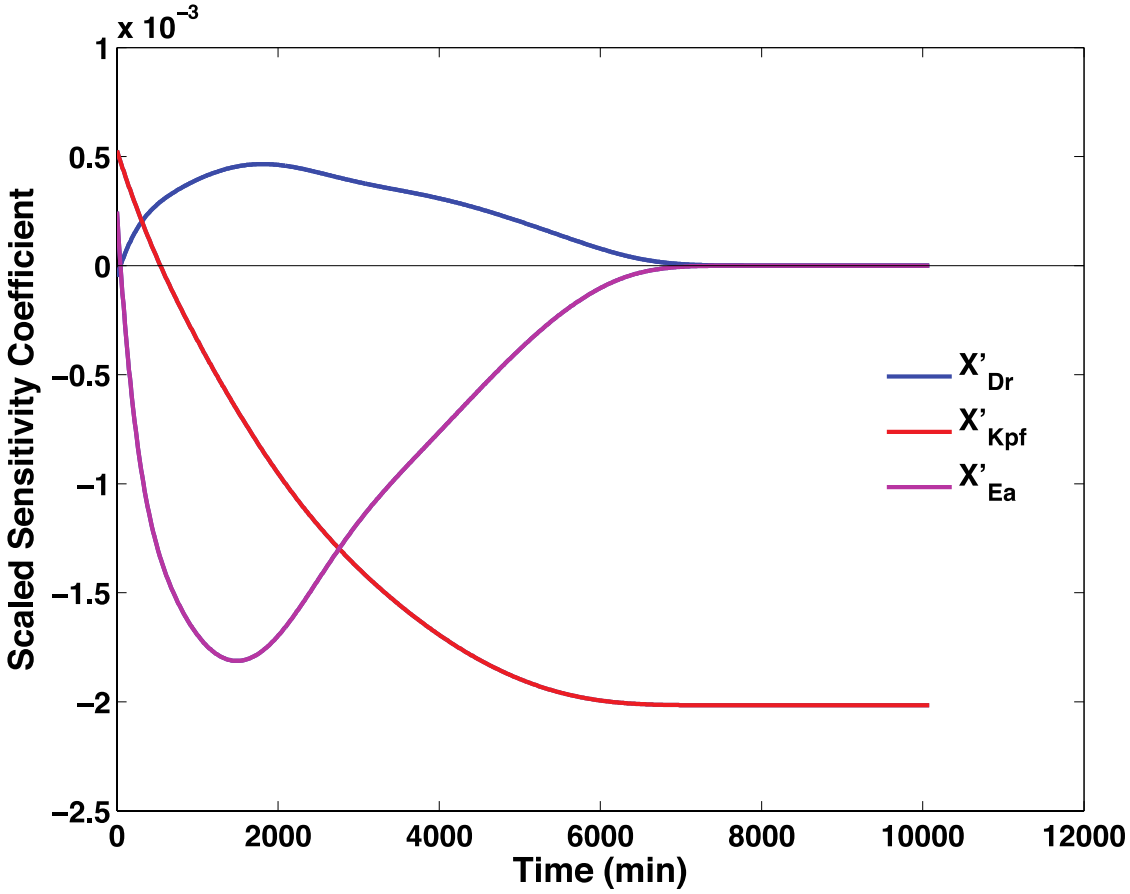

Figure 7-4 Final scaled sensitivity coefficient of the activation energy estimation of the migration of 1.28 wt.% catechin from PLA film into 95% ethanol ranging from 20, 30, 40, and 50 °C. Final estimates were: D_{ref}=3.70× 10^{-9} cm^2/min, $K_{p,f}$=436.62 cm^3 PLA/cm^3 ethanol, and E_a=153000 J/mol).

7.3 Additional Observations

While performing the estimation of the E_a, several difficulties were experienced. Since it is the first time the estimation of the E_a using the reparameterization approach was done for migration studies, finding adequate initial guesses was pretty challenging due to the nature of this non-isothermal experiment. Although there are available published data on these parameters for

other type of experiments such as microbial inactivation, thermal isomerization of compounds, gelatinization of starch, *etc.*, locating appropriate ones that satisfy the overall experimental temperature ranges was difficult. This issue was resolved by using step 1 of model 1 of the two-step solution for mass transfer additives from polymer films developed in Chapter 5. In addition, the fact that the Arrhenius equation was employed as a secondary model increases the complexity of the estimation procedure. Since in this study more than one kinetic constant was estimated, the process of eliminating the correlation issue among parameters cannot be assured. Hence, simultaneous estimation of all parameters may not be possible. Moreover, the T_{ref} may also change accordingly with different mathematical expression. More details on this issue were discussed by Schwaab & Pinto (2008). Two key factors to solve this issue are appropriate initial guesses and the selection of initial T_{ref}, while continuously monitoring the correlation coefficient among the parameters. It was also observed that there was a scaling issue since the initial guesses for D_{ref}, $K_{p,f}$ and E_a were all of different orders of magnitude, which caused a warning in MATLAB ('Rank deficient, rank = 3, tol = 1.768837e-08') indicating that the matrix had an issue with rank deficiency, which means the generated matrix did not having linearly independent rows and columns. The approach to solve this issue is by normalizing the initial guesses of the estimated parameters, so all the parameters are of the same order of magnitude.

7.4 Conclusions

The estimation of E_a for a migration case study was performed for the first time using the reparameterization approach of the Arrhenius equation to reduce the correlation between D_{ref} and E_a, minimizing the relative errors. The optimum T_{ref} at 44.94 °C was successfully obtained by plotting the correlation coefficient of D_{ref} and E_a within the possible reference temperature ranges

(40 to 60 °C). Subsequently, all the parameters (*i.e.*, D_{ref}, $K_{p,f}$ and E_a) were estimated simultaneously with the correlation coefficients ranging between almost 0.00 (3.14×10^{-4} at 44.94 °C) and 0.34. The optimum T_{ref} resulted with the lowest relative errors of parameters was anticipated. The T_{sim} approach allowed the *X'* plotting of E_a, thus the dependency criterion among parameters can be visualized. Further evaluation of different case studies should be performed.

APPENDICES

APPENDIX 7A: Additional results of the randomly chosen T_{ref} within the experimental temperature range.

Table 7A- 1 Correlation matrix of the estimated parameters at the T_{ref}=40 °C.

Parameters	**Correlation coefficients, ρ**			**Relative Error (%)**
	D_{ref}	$K_{p,f}$	E_a	
D_{ref}		Symmetric		9.18
$K_{p,f}$	0.45			4.16
E_a	-0.42	-0.34		4.21

Table 7A- 2 Correlation matrix of the estimated parameters at the T_{ref}=50 °C.

Parameters	**Correlation coefficients, ρ**			**Relative Error (%)**
	D_{ref}	$K_{p,f}$	E_a	
D_{ref}		Symmetric		9.17
$K_{p,f}$	-0.16			4.16
E_a	0.42	-0.34		4.21

APPENDIX 7B: MATLAB coding for the estimation of activation energy

```
%% MIGRATION STUDIES: ESTIMATION OF ACTIVATION ENERGY (REPARAMETERIZATION APPROACH)
%% Notes
% 1. Start Tref with average temperature within the experimental temperature
   % ranges
%2. Use step 1 to find approximation initial guesses
%3. Tsim approach was used to plot Ea.
   %Formula: T_sim=@(t) T_low +(T_high-T_low)/t_max  t ; y=c + mX
 %%
close all;
clear;
clc
format long
global L  % This variable is being shared with all the file that is declared global
global alpha
global qn
global D
global T
global h
%%
data =xlsread('PLACate_95etoh_EA.xls');% To read raw data from excel
%%
switch localname
   case '13-138-76.client.wireless.msu.edu'
      local                                                                    =
'/Users/HAYATISAMSUDIN/Documents/MATLAB_EXP/MATLAB_CIADEXP/ACTIVATIO
N ENERGY/PLA_CATE_EA_TRIAL';
      papertype = 'A4';
```

```
        paperposition = [0.3397   10.1726   20.3046    9.3322]; %cm
    otherwise
        local = pwd;
        papertype = 'usletter';
        paperposition = [0.3397   10.1726   20.3046    9.3322]; %update the values to usletter format
        warning('Please set the case for your computer')
end
datafile = 'PLACate_95etoh_EA.xls';
outputfolder = fullfile(local,'Figures_PLACate_EA'); if ~exist(outputfolder,'dir'), mkdir(outputfolder), end
[~,outputfile] = fileparts(datafile);
%% Additional Info
L=0.003616667;%L= half of the thickness, cm
A=3.1416;  %A=area, cm2
Co=0.011591; % Co=Initial concentration, g/cm3
Vf=1.227 % Vf=volume of food,cm3
%% Data Extraction
t=data(:,1);% time variable (min)
yobs=data(:,2); %Concentration at time t, g/cm3
yobs2=data(:,2)./Co;% Concentration at time t/Concentration at initial time
T=data(:,3); % Temp in Kelvin
t1=linspace(0,max(t),1000)';
sum1=0;
sum2=0;
%% Step 1
R=linspace(0.100,0.000560,200);
%R=linspace(0.00090,0.000400,100);
%%
N=length(data);
for j=1:length(R)
for i=1:N
```

```
    if i == 1
        fit(i) = 0
    else
     z=1-exp(-R(j)*t(i));
    sum1=sum1+z.*yobs2(i);
    sum2=sum2+z.^2
    P(j)=sum1/sum2
    fit=P(j)*z;
    end
end
fitreverse=fit';
SSE(j)=sumsqr(yobs2-fitreverse)
end
comparison=[P' R' SSE'];
Index=0:1:N;
[M,I]=min(SSE);%I is index refers to min value of SSE
showminSSE=[P(I) R(I)] % to display P and R corresponding to I=index of min SSE
 %%
for i=1:N
    if i == 1
        fit(i) = 0
    else
     z=1-exp(-R(I)*t(i));
    final_fit(i)=P(I)*z;
    end
end
display(final_fit)
predict_obs=final_fit';
Table=[t yobs2 final_fit' ]

figure
```

```
hold on
set(gca, 'fontsize',14,'fontweight','bold');
pl(1)=plot(t, yobs2, 'o','LineWidth',1.2)
pl(2)=plot(t, final_fit,'r','LineWidth',1.2)
xlabel('Time (min)','fontsize',16,'fontweight','bold');
ylabel('exp data, final fit','fontsize',16,'fontweight','bold');
pll=legend (pl,'exp data','final fit');
set(pll,'box','off','location','Best');
set(gcf,'Color',[1 1 1]);
%%
m0=Vf/(A*L);
m0=P(I)*(Vf/(A*L));
Kpf=(1-m0)/P(I); %P(I)= value contain the lowest SSE from before

m1= (2*(Kpf+(Vf/(A*L))))   %term 1 of R
m2=m1/R(I)
D=1;
%m3=(Vf/A)*((L/D)+(2*Kpf/h))
h=(2*Kpf)/((m2/(Vf/A))-(L/D))
h1=1
D=L/((m2/(Vf/A))-(2*Kpf/h1))
 %%
%%
Kpf=800;
h=10e-4;
D=2E-9;
%%
global Bi
alpha=Vf/(Kpf*A*L);
% qn;
Bi=(h*L)/D;
```

```
Lo=1;
Up=60;
z=@(qn) (Bi-Kpf*alpha*qn^2)*sin(qn)+alpha*Bi*qn*cos(qn);
for i=Lo: Up;
   ev(i)=fzero(z,i); %Newton-Raphson
end;
EV=unique(ev);
EV';
ev=EV(2:end);
qn=ev'
%% Initial parameter guesses
b1=2;% Initial guess for Dr...fix close to publish data 2 x e-9
b2=8; % Initial guess for Kpf  x 10^2
b3=1.5;% Ea (J/mol)...fix as close to publish data 110 kJ/mol x 10^2
beta0(1)=b1;
beta0(2)=b2;
beta0(3)=b3;

%% X' = scaled sensitivity coefficients using forward-difference
  % This is a forward problem with known approximate parameters
 Xp=SSC_EA3P(beta0,t1,@myfunconvecdiff_EASim3P);
%title('Scaled Sensitivity Coefficients using initial guesses')%%
%printing
print_pdf(600,get(gcf,'filename'),outputfolder,'nocheck')
print_png(300,get(gcf,'filename'),outputfolder,[],0,0,0)
%%
%printing
print_pdf(600,get(gcf,'filename'),outputfolder,'nocheck')
print_png(300,get(gcf,'filename'),outputfolder,[],0,0,0)
%%
ypredict = myfunconvecdiff_EASim3P(beta0,t1);
```

```
%%
[beta,resids,J,COVB, MSE] = nlinfit(t,yobs2,@myfunconvecdiff_EA3P,beta0);
ci=nlparci(beta,resids,J,0.05) %asymptotic confidence interval
[ypredict, delta] = nlpredci('myfunconvecdiff_EA3P',t,beta,resids,J,0.05,'on','curve'); %CI for mean
[ypredict, deltaobs] = nlpredci('myfunconvecdiff_EA3P',t,beta,resids,J,0.05,'on','observation');
[R, sigma]=corrcov(COVB);
R;
sigma; % parameter standard errors
relative_error_n=sigma./beta';% >0.6 the likeliness of CI contains 0 is high (estimate is useless since it is not statiscially diff than 0)
beta; % parameters estimated
MSE;
RMSE=MSE^(1/2);
standard_residuals=resids/RMSE;
[R, sigma]=corrcov(COVB);
n = length(ypredict);
p = length(beta);
SS= MSE*(n-p)
```

Step 2:

```
%%
clc
clear
format long;
%%
switch localname
   case '13-138-76.client.wireless.msu.edu'
      local = '/Users/HAYATISAMSUDIN/Documents/MATLAB_EXP/MATLAB_CIADEXP/ACTIVATION ENERGY/PLA_CATE_EA_TRIAL';
      papertype = 'A4';
```

```
        paperposition = [0.3397   10.1726   20.3046    9.3322]; %cm
    otherwise
        local = pwd;
        papertype = 'usletter';
        paperposition = [0.3397   10.1726   20.3046    9.3322]; %update the values to usletter format
        warning('Please set the case for your computer')
end
datafile = 'PLACate_95etoh_EA.xls';
outputfolder = fullfile(local,'Figures_PLACATE95ETOH_CorrEa_Tref'); if ~exist(outputfolder,'dir'), mkdir(outputfolder), end
[~,outputfile] = fileparts(datafile);
%%
TrV=40:1:60;
TrV=TrV+273.15;
for i = 1:length(TrV)
    Tr = TrV(i)
    corrEA(i) = EaTry(Tr)
end
TrV=TrV-273.15;
figure
hold on
set(gca, 'fontsize',14,'fontweight','bold');
h = plot(TrV,corrEA,'-ob', 'linewidth',1.05);
% xlabel('Reference Temperature \it{T_r}, (^oC_','FontSize',16,'fontweight','bold');
xlabel('Reference Temperature,  \it{T_{ref}}  \rm\bf(^oC)','FontSize',16,'fontweight','bold');
% ylabel('Correlation Coefficient of \itd_r and \itz','FontSize',16,'fontweight','bold');
ylabel('Correlation Coefficient of  \it{D_{ref}} \rm\bf and \itEa','FontSize',16,'fontweight','bold');
% ylabel('Correlation Coefficient of \it{k} and \itE','FontSize',16,'fontweight','bold');
plot([min(TrV),max(TrV)],[0,0], 'R','linewidth',1.05)
set(gca,'box','on','xticklabelmode','auto','yticklabelmode','auto');
grid on
```

```
%%
%printing
print_pdf(600,get(gcf,'filename'),outputfolder,'nocheck')
print_png(300,get(gcf,'filename'),outputfolder,[],0,0,0)
%%
```

REFERENCES

REFERENCES

Agarwal, A. K., & Brisk, M. L. (1985a). Sequential experimental design for precise parameter estimation. 1. Use of reparameterization. *Industrial & Engineering Chemistry Process Design and Development, 24*(1), 203-207.

Agarwal, A. K., & Brisk, M. L. (1985b). Sequential experimental design for precise parameter estimation. 2. Design criteria. *Industrial & Engineering Chemistry Process Design and Development, 24*(1), 207-210.

Ahmed, J., Dolan, K. D., & Mishra, D. K. (2012). Chemical reaction kinetics pertaining to foods. *Handbook of food process design*, 113.

Box, G. E. (1960). Fitting empirical data. *Annals of the New York Academy of Sciences, 86*(3), 792-816.

Brauner, N., & Shacham, M. (1997). Statistical analysis of linear and nonlinear correlation of the Arrhenius equation constants. *Chemical Engineering and Processing: Process Intensification, 36*(3), 243-249.

Chen, N. H., & Aris, R. (1992). Determination of Arrhenius constants by linear and nonlinear fitting. *AIChE journal, 38*(4), 626-628.

Datta, A. K. (1993). Error estimates for approximate kinetic parameters used in food literature. Journal of Food Engineering, 18(2), 181-199.

Dolan, K. (2015, July 9th, 2015). [Simulation Temperature Approach for Non-Isothermal Migration Studies].

Dolan, K. D. (2003). Estimation of kinetic parameters for nonisothermal food processes. *Journal of Food Science, 68*(3), 728-741.

Dolan, K. D., & Mishra, D. K. (2013). Parameter estimation in food science. *The Annual Review of Food Science and Technology, 4*, 401-422.

Dolan, K. D., Valdramidis, V. P., & Mishra, D. K. (2013). Parameter estimation for dynamic microbial inactivation: which model, which precision? *Food Control, 29*(2), 401-408.

Iñiguez-Franco, F., Soto-Valdez, H., Peralta, E., Ayala-Zavala, J. F., Auras, R., & Gámez-Meza, N. (2012). Antioxidant Activity and Diffusion of Catechin and Epicatechin from Antioxidant Active Films Made of Poly (l-lactic acid). *Journal of Agricultural and Food Chemistry, 60*(26), 6515-6523.

Klicka, R., & Kubácek, L. (1997). Statistical properties of linearization of the Arrhenius equation via the logarithmic transformation. *Chemometrics and intelligent laboratory systems, 39*(1), 69-75.

Pritchard, D. J., & Bacon, D. W. (1975). Statistical assessment of chemical kinetic models. *Chemical Engineering Science, 30*(5), 567-574.

Pritchard, D. J., & Bacon, D. W. (1978). Prospects for reducing correlations among parameter estimates in kinetic models. *Chemical Engineering Science, 33*(11), 1539-1543.

Schwaab, M., Lemos, L. P., & Pinto, J. C. (2008). Optimum reference temperature for reparameterization of the Arrhenius equation. Part 2: Problems involving multiple reparameterizations. *Chemical Engineering Science, 63*(11), 2895-2906.

Schwaab, M., & Pinto, J. C. (2007). Optimum reference temperature for reparameterization of the Arrhenius equation. Part 1: Problems involving one kinetic constant. *Chemical Engineering Science, 62*(10), 2750-2764.

Sulaiman, R., Dolan, K. D., & Mishra, D. K. (2013). Simultaneous and sequential estimation of kinetic parameters in a starch viscosity model. *Journal of Food Engineering, 114*(3), 313-322.

Sundberg, R. (1998). Statistical aspects on fitting the Arrhenius equation. *Chemometrics and intelligent laboratory systems, 41*(2), 249-252.

Chapter 8

Overall Conclusion and Recommended Future Work

8.0 Overall Conclusion

Migration of additives from a polymer film into food products has been continuously studied since the early 1960s due to its importance in food safety, quality assurance and shelf life of foods. Earlier on a large amount of research was conducted to determine if the polymer films were safe to be in contact with food products. Lately, a large amount of research was directed into finding natural occurring additives to be incorporated into polymer films and in investigating the effectiveness of these additives to prolong the shelf life of the intended product while monitoring its threshold limit (Barbosa-Pereira et al., 2013; Chen, Lee, Zhu, & Yam, 2012; Colín-Chávez, Soto-Valdez, Peralta, Lizardi-Mendoza, & Balandrán-Quintana, 2013; Contini et al., 2013; Granda-Restrepo et al., 2009; Hwang et al., 2012; Iñiguez-Franco et al., 2012; Lopez de Dicastillo et al., 2011; Lopez-de-Dicastillo, Alonso, Catala, Gavara, & Hernandez-Munoz, 2010; López-de-Dicastillo, Alonso, Catalá, Gavara, & Hernández-Muñoz, 2010; Peltzer, Wagner, & Jiménez, 2009; Pereira de Abreu, Losada, Maroto, & Cruz, 2010; Sanches-Silva et al., 2014; Sonkaew, Sane, & Suppakul, 2012; Zhu, Schaich, Chen, & Yam, 2013). Meanwhile, a small number of studies have been performed to assess the kinetics of migration using mathematical modeling or centered on determining the migration parameters. Most of the work published in this area used previously developed mathematical modeling and solutions to identify the rate at which the diffusion of additives takes place known as the diffusion coefficient, D. To a certain extent, the chemical affinity between a polymer and a food/food simulant known as the partition coefficient, $K_{p,f}$ is determined experimentally at the end of the experimental duration (Baner, 2000; Baner, Franz, & Piringer, 1994, 2011; Crank, 1979; Dole et al., 2006; Piringer & Beu, 2000; Pospíšil &

Nešpùrek, 2000; Vitrac & Hayert, 2006; Vitrac, Mougharbel, & Feigenbaum, 2007). The measurement of these parameters often takes time and is costly. Therefore, this dissertation aimed at understanding the kinetics of migration of additives, especially antioxidants, from polymer films. Migration of these additives from a biodegradable polymer, poly(lactic acid), PLA into regulated food simulants by using parameter estimation approach was conducted and the method to calculate these parameters is presented. Parameter estimation is defined as "a discipline that provides tools for the efficient use of data in the estimation of constants appearing in mathematical models and for aiding in modeling of phenomena" (Beck & Arnold, 1977).

The first initiative taken to perform the parameter estimation approach was to produce a bilayer PLA film incorporated with marigold flower extract via a blown extrusion process (Chapter 3). This produced film was subjected to three different parts; *i*) migration study of astaxanthin (the dominant antioxidant presence in the Marigold flower extract) into 95% ethanol at 30 and 40 °C, *ii*) characterization of the produced film by thermal, barrier, physical and morphological analyses, and *iii*) the oxidative stability assessment of the antioxidant toward a real fatty food product (*i.e.*, soybean oil). This study found that the addition of the marigold flower extract did not affect the polymer properties except for molecular weight, water vapor permeability and polymer infrared (IR) spectra. The migration of astaxanthin to 95% ethanol was estimated using the general Crank mathematical solution and followed Fick's second law of diffusion. However, the diffusion of astaxanthin into soybean oil was too slow to be able to retain the freshness of the product within the limit of Codex Alimentarius, which may be attributed to the lower chemical affinity between the astaxanthin and soybean oil. In this work, parameter estimation was done using ordinary least square (OLS) estimation. Instead of estimating only *D*, the concentration of the migrant migrating

into the food simulant at equilibrium, M_∞ was also estimated to understand the migration kinetics in the food simulant.

From chapter 3, it was observed that the assessment of an additional parameter did provide additional information on the kinetics of a migration phenomenon. Therefore, effort was allocated to further understand the mass transfer process in polymer films from the parameter estimation point of view, presented in chapter 4. The impact of estimating one (1P), two (2P) and three (3P) parameters by analyzing the scaled sensitivity coefficient, X' before performing the OLS estimation and the optimal experimental design was examined. By assessing a different number of parameters inside a mathematical expression, the physical meaning behind a migration experiment was better understood. Also, by conducting this assessment the issue of under parameterized or over parameterized migration experiments was explored. Assessment of only one parameter estimate could cause an under parameterized issue when there is a possibility of obtaining additional insight from other parameters. Meanwhile, assessment of more parameters could have induced the complexity of the estimation process by introducing more uncertainty and reduction of estimation accuracy. Therefore, the X' plot was introduced and constructed to foresee the possibility of estimating all parameters at once and to study each parameter's sensitivity towards perturbation. The desirable parameters to be estimated would be the ones with larger magnitude change of response that are uncorrelated with the other parameters. Optimal experimental design was employed to identify the time needed for a migration experiment to be able to accurately estimate the parameters of interest. The AICc approach in addition to RMSE value was used as a tool for model selection. Several selected migration case studies (based on PLA) were chosen to demonstrate the parameter estimation approach introduced chapter 4. Interesting results included; *i)* the assessment of the third migration parameter known as α (ratio of the mass of migrant

migrated into food/simulant to the mass of migrant left in the polymer, at equilibrium) was observed to be better estimated at the initial experimental time instead of at equilibrium, which goes against the general assumption that it should be determined at the end of the migration experiment, *ii)* both the *X'* and the optimal experimental design plots indicated that most of the migration studies were performed beyond the necessary time. Therefore, with adequate initial guesses for the polymer-additive system, one can predict the optimal time needed to conduct a migration experiment while being able to accurately estimate the parameters via maximization of the determinant. The overall highlight from this chapter was that the kinetic migration parameter α that is directly related to $K_{p,f}$ should be investigated at an early time in the experiment. Additionally, another kinetic parameter known as the convective mass transfer coefficient, *h*, is presented at the early time of experiment, which holds large importance in migration experiments when the simulant is not stirred or viscous simulants. Consequently, these highlights led to the development of a two-step solution in chapter 5 to estimate *h* in addition to the other two kinetic migration parameters (*i.e.*, D and $K_{p,f}$).

In chapter 4, Crank's general mathematical solutions based on Fick's second law of diffusion was used to estimate *D*, M_∞, and α to understand the kinetics of migration (Crank, 1979). Based on our finding from chapters 3 and 4, we identified that *D* and α did have significant impact on the overall kinetics of migration. Hence, in chapter 5, three driving factors that govern the sorption and/or desorption kinetics of migration from polymer films were estimated; *D*, $K_{p,f}$ and *h*. These three parameters are beneficial for providing in-depth insight on the physical meaning behind a migration phenomenon. Therefore, a two-step solution based on the boundary conditions of Crank's solutions was developed. The first step of this two-step solution was used to find the combination of *D*, $K_{p,f}$ and *h* that minimized the sums of squared errors (SSE). Unlike the linear

equation that contains a unique local minimum, a non-linear equation contains many local minima, thus the use of step 1 served to find the right local minima region to start the estimation of the migration parameters and can provide the true solution of the parameters. From the initial guesses from step 1, OLS estimation could be used in step 2. The OLS estimation was performed by using the proposed analytical solution containing the D, $K_{p,f}$ and h. A migration case study of PLA incorporated with 3 wt.% resveratrol in contact with ethanol at 9 °C was used to demonstrate the use of this two-step solution, which was later named as model 1 in chapter 6. Additional parameter estimation approaches such as the sequential, bootstrap and the kinetic phase diagram were also performed to acquire a better knowledge about the kinetics of migration.

Chapter 6 is presented as the continuation of chapter 5, where the two-step solution (model 1) was compared with Crank's general mathematical solutions containing D and $K_{p,f}$ (model 2) and containing only D (model 3) by using three different migration case studies. The OLS estimation and the model selection were based on the corrected Akaike information criterion (AICc) approaches. Consequently, a decision tree analysis containing all three models was proposed as a tool for selecting the appropriate model to analyze migration studies of additives from polymer films.

After an extensive focus on the kinetics of migration at one particular temperature (isothermal), a quest for the kinetics of migration involving several temperatures (non-isothermal) was pursued in chapter 7. The Arrhenius equation was employed as the secondary model to model 1 presented in chapter 5. The reparameterization approach was applied to find the optimum reference temperature, T_{ref} corresponding to reference D, D_{ref}, to solve the correlation issue associated with D_{ref} and the activation energy, E_a while minimizing the parameters' relative errors. The simulation temperature, T_{sim} approach was introduced in this chapter for the purpose of

constructing E_a of the X' plot. The reparameterization approach improved the estimation of E_a as indicated by the observed relative errors of parameters. Hence, it was proven that with the T_{ref} (optimum) that gave the near zero correlation between D_{ref} and E_a, the lowest relative error of D_{ref} was achieved. This finding highlights the importance of having the optimum T_{ref} instead of arbitrarily choosing any temperature within the experimental range to obtain better accuracy of the parameters estimation.

All things considered, the work performed in this dissertation is just the beginning of introducing a prediction technique to determine the kinetic migration parameters and to reduce their uncertainty. Additional and more comprehensive and extensive works should be theoretically and experimentally executed to further gain understanding of the kinetics of migration of additives from polymer films.

8.1 Recommended Future Work

All the migration case studies selected for demonstrating the use of different models were performed in the presence of continuous stirring (presence of turbulent flow), thus the effect of h on the overall migration kinetics may have not been observed much. Figure 8-1 demonstrated two different cases (a) small h, thus Biot number < 200 (Bi=146), and (b) larger h, thus Biot number >200 (Bi= 2920). Future work should focus on conducting and getting experimental data for a migration experiment that could be reflected by Figure 8-1(a), which means the resistance at the interface between the polymer and the food simulant is larger. Several scenarios such as the absence of convection, the use of viscous food simulants such as oil, Miglyol®, emulsion *etc.* and the effect of various polymer thickness should be designed and investigated in a migration experiment to assess the kinetics parameters using the two-step solution (model 1) proposed in

chapter 5. Comparative modeling should also be performed with other available mathematical models provided by other authors (Carslaw & Jaeger, 1959; Crank, 1979; Gandek, Hatton, & Reid, 1989; Piringer & Beu, 2000; Vitrac & Hayert, 2006; Vitrac, Mougharbel, & Feigenbaum, 2007).

While model 1 can provide an exact solution to a migration study and direct physical interpretation on the kinetics of migration, it does not assess additional cases when the polymer film may degrade or the diffusion coefficient changes with the concentration. So, parameter estimation through numerical approximation considering all three kinetic migration parameters should also be explored to obtain migration kinetic parameters and to complement the analytical solution approach when D, $K_{p,f}$ and h change as a function of time.

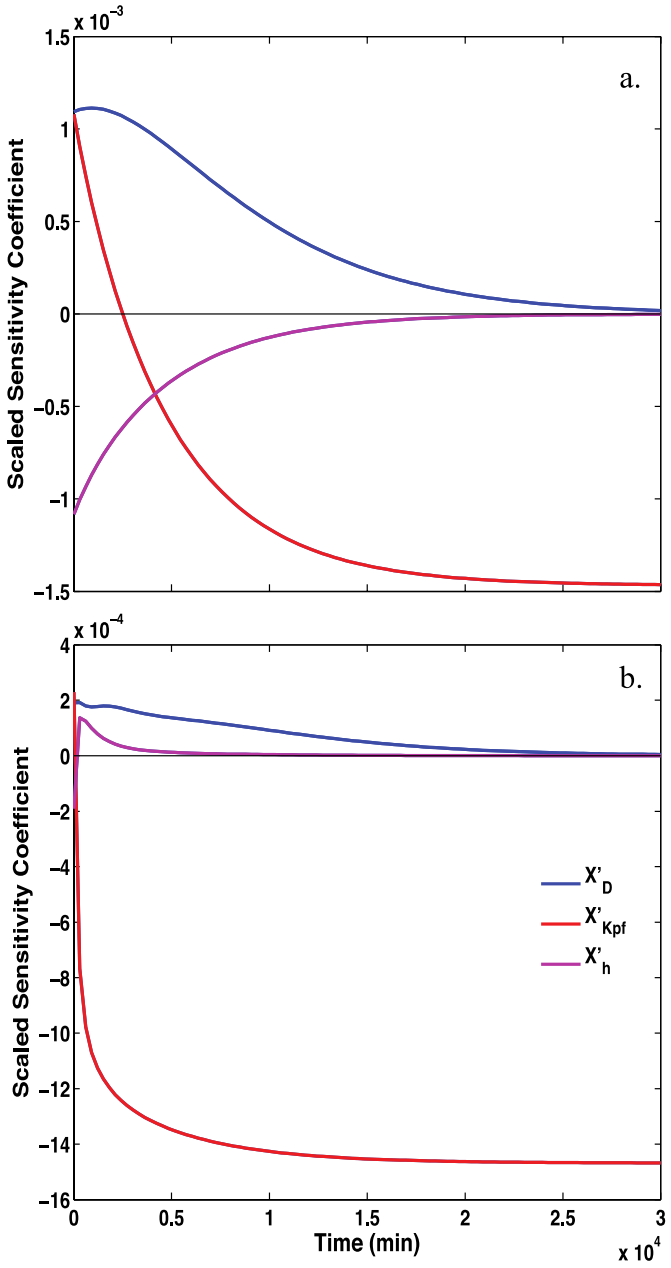

Figure 8-1 Scaled sensitivity coefficient of (a) the case with *Biot* number < 200 (Initial guesses were: D_{ref}=3.00 × 10^{-9} cm^2/min, $K_{p,f}$=608 cm^3 PLA/cm^3 ethanol, and h=8 × 10^{-5} cm/min), (b) the case with *Biot* number > 200 (Initial guesses were: D_{ref}=3.00 × 10^{-9} cm^2/min, $K_{p,f}$=608 cm^3 PLA/cm^3 ethanol, and h=1.60 × 10^{-3} cm/min).

APPENDIX

APPENDIX: List of Conference Presentations and Publications Generated from this Dissertation

Peer Reviewed Journal Article

Samsudin, H., Soto-Valdez, H. & Auras, R. (2014). Poly(lactic acid) membrane incorporated with marigold flower extract (*Tagetes erecta*) intended for fatty-food application. Food Control, Volume 46, pages 55-66.

Book Chapter

Samsudin, H. & Auras, R. Food Packaging Interaction in Introduction to Food Packaging. Submitted to John Wiley & Sons and Institute of Food Technologists (IFT) Press, February 2015. (Submitted and under review)

Grant Application

Samsudin, H., Auras, R., Soto-Valdez, H. The NineSigma RFP (2013)- Using Nature's Best Anti-Oxidants to Improve Oxidation Stability of Synthetic Polymers (RFP# 69117)

Conferences

1. Hayati Samsudin, Rafael Auras, Gary Burgess, and Herlinda Soto-Valdez. A Decision Tree Analysis for Determining Mass Transfer Parameters for Migration Studies. 3rd International Meeting of Material/Bioproduct Interaction (MATBIM) 2015, Spain

2. Javiera Rubilar, Rafael Auras, Hayati Samsudin, and Franco Pedreschi. Release of Citral, Carvacrol and Eugenol from Poly(lactic acid) Nanocomposite Films. 3rd International Meeting of Material/Bioproduct Interaction (MATBIM) 2015, Spain

3. Hayati Samsudin, Rafael Auras, Kirk Dolan, Dharmendra Mishra, and Herlinda Soto-Valdez. Assessing The Kinetics of A Migration Study by Estimating A Two or Three-Parameter Models. Inverse Problems Symposium (IPS) 2015, East Lansing (Poster)
4. Hayati Samsudin, Rafael Auras, Kirk Dolan, Dharmendra Mishra, and Herlinda Soto-Valdez. Application of Parameter Estimation to Predict Migration of Antioxidant Films. The Shelf Life International Meeting (SLIM) 2014, New Jersey (Poster). 3rd place in the poster competition sponsored by the Elsevier©.

Seminar:

Hayati Samsudin and Herlinda Soto-Valdez. Migración de Astaxantina de una Película de Ácido Poliláctico (Migration of Astaxanthin from a Poly(lactic acid) Film), Center for Food and Research Development (CIAD), September, 2011, Sonora, Mexico.

REFERENCES

REFERENCES

Baner, A. L. (2000). Partition coefficient. In A. L. Baner & O.-G. Piringer (Eds.), *Plastic Packaging Materials for Food, Barrier Function,Mass Transport, Quality Assurance and Legislation* (pp. 79-123). Weinheim: Wiley-VCH.

Baner, A. L., Franz, R., & Piringer, O. (1994). Alternative fatty food simulants for polymer migration testing. In M. Mathlouthi (Ed.), *Food Packaging and Preservation* (pp. 24-31). Glasgow: Blackie Academic and Professional.

Baner, A. L., Franz, R., & Piringer, O. (2011). Alternative fatty food simulants for polymer migration testing: experimental confirmation. *Journal of Polymer Engineering, 15*(1-2), 161-180.

Barbosa-Pereira, L., Cruz, J. M., Sendón, R., Rodríguez Bernaldo de Quirós, A., Ares, A., Castro-López, M., . . . Paseiro-Losada, P. (2013). Development of antioxidant active films containing tocopherols to extend the shelf life of fish. *Food Control, 31*(1), 236-243.

Beck, J. V., & Arnold, K. J. (1977). *Parameter Estimation in Engineering and Science* (Vol. 8): Wiley New York.

Carslaw, H. S., & Jaeger, J. C. (1959). Conduction of heat in solids. *Oxford: Clarendon Press, 1959, 2nd ed., 1*.

Chen, X., Lee, D. S., Zhu, X., & Yam, K. L. (2012). Release kinetics of tocopherol and quercetin from binary antioxidant controlled-release packaging films. *Journal of Agricultural and Food Chemistry, 60*(13), 3492-3497.

Colín-Chávez, C., Soto-Valdez, H., Peralta, E., Lizardi-Mendoza, J., & Balandrán-Quintana, R. R. (2013). Fabrication and Properties of Antioxidant Polyethylene-based Films Containing Marigold (Tagetes erecta) Extract and Application on Soybean Oil Stability. *Packaging Technology and Science, 26*(5), 267-280. doi: 10.1002/pts.1982

Contini, C., Valzacchi, S., O'Sullivan, M., Simoneau, C., Dowling, D. P., & Monahan, F. J. (2013). Overall Migration and Kinetics of Release of Antioxidant Compounds from Citrus Extract-Based Active Packaging. *Journal of Agricultural & Food Chemistry, 61*(49), 12155-12163.

Crank, J. (1979). *The Mathematics of Diffusion* (2nd ed.). Bristol: Oxford University Press.

Dole, P., Voulzatis, Y., Vitrac, O., Reynier, A., Hankemeier, T., Aucejo, S., & Feigenbaum, A. (2006). Modelling of migration from multi-layers and functional barriers: Estimation of parameters. *Food Additives & Contaminants, 23*(10), 1038-1052.

Gandek, T. P., Hatton, T. A., & Reid, R. C. (1989). Batch extraction with reaction: phenolic antioxidant migration from polyolefins to water. 1. Theory. *Industrial & engineering chemistry research, 28*(7), 1030-1036.

Granda-Restrepo, D. M., Soto-Valdez, H., Peralta, E., Troncoso-Rojas, R., Vallejo-Córdoba, B., Gámez-Meza, N., & Graciano-Verdugo, A. Z. (2009). Migration of α-tocopherol from an active multilayer film into whole milk powder. [doi: 10.1016/j.foodres.2009.07.007]. *Food Research International, 42*(10), 1396-1402.

Hwang, S. W., Shim, J. K., Selke, S. E. M., Soto‐Valdez, H., Matuana, L., Rubino, M., & Auras, R. (2012). Poly (L‐lactic acid) with added α‐tocopherol and resveratrol: optical, physical, thermal and mechanical properties. *Polymer International, 61*(3), 418-425.

Iñiguez-Franco, F., Soto-Valdez, H., Peralta, E., Ayala-Zavala, J. F., Auras, R., & Gámez-Meza, N. (2012). Antioxidant Activity and Diffusion of Catechin and Epicatechin from Antioxidant Active Films Made of Poly (l-lactic acid). *Journal of Agricultural and Food Chemistry, 60*(26), 6515-6523.

Lopez de Dicastillo, C., Nerin, C., Alfaro, P., Catalá, R., Gavara, R., & Hernandez-Muñoz, P. (2011). Development of new antioxidant active packaging films based on ethylene vinyl alcohol copolymer (EVOH) and green tea extract. *Journal of Agricultural and Food Chemistry, 59*(14), 7832-7840.

Lopez-de-Dicastillo, C., Alonso, J. M., Catala, R., Gavara, R., & Hernandez-Munoz, P. (2010). Improving the Antioxidant Protection of Packaged Food by Incorporating Natural Flavonoids into Ethylene− Vinyl Alcohol Copolymer (EVOH) Films. *Journal of agricultural and food chemistry, 58*(20), 10958-10964.

López-de-Dicastillo, C., Alonso, J. M., Catalá, R. n., Gavara, R., & Hernández-Muñoz, P. (2010). Improving the Antioxidant Protection of Packaged Food by Incorporating Natural Flavonoids into Ethylene− Vinyl Alcohol Copolymer (EVOH) Films. *Journal of Agricultural and Food Chemistry, 58*(20), 10958-10964.

Peltzer, M. A., Wagner, J., & Jiménez, A. (2009). Migration study of carvacrol as a natural antioxidant in high-density polyethylene for active packaging. *Food Additives and Contaminants, 26*(6), 938-946.

Pereira de Abreu, D. A., Losada, P. P., Maroto, J., & Cruz, J. M. (2010). Evaluation of the effectiveness of a new active packaging film containing natural antioxidants (from barley husks) that retard lipid damage in frozen Atlantic salmon (Salmo salar). *Food Research International, 43*(5), 1277-1282.

Piringer, O. G., & Beu, T. (2000). Transport equations and their solutions. In A. L. Baner & O.-G. Piringer (Eds.), *Plastic Packaging Materials for Food, Barrier Function,Mass Transport, Quality Assurance and Legislation* (pp. 195-246). Weinheim: Wiley-VCH.

Pospíšil, J., & Nešpùrek, S. (2000). Additives for Plastics and Their Transformation Products. In O.-G. Piringer & A. L. Baner (Eds.), *Plastic Packaging Materials for Food, Barrier Function,Mass Transport, Quality Assurance and Legislation* (pp. 53-77). Weinheim: Wiley-VCH.

Sanches-Silva, A., Costa, D., Albuquerque, T. G., Buonocore, G., Ramos, F., Castilho, M. C., . . . Costa, H. S. (2014). Trends in the use of natural antioxidants in active food packaging: a review. *Food Additives & Contaminants: Part A*(just-accepted).

Sonkaew, P., Sane, A., & Suppakul, P. (2012). Antioxidant activities of curcumin and ascorbyl dipalmitate nanoparticles and their activities after incorporation into cellulose-based packaging films. *Journal of Agricultural and Food Chemistry, 60*(21), 5388-5399.

Vitrac, O., & Hayert, M. (2006). Identification of diffusion transport properties from desorption/sorption kinetics: an analysis based on a new approximation of fick equation during solid-liquid contact. *Industrial & Engineering Chemistry Research, 45*(23), 7941-7956.

Vitrac, O., Mougharbel, A., & Feigenbaum, A. (2007). Interfacial mass transport properties which control the migration of packaging constituents into foodstuffs. *Journal of Food Engineering, 79*(3), 1048-1064.

Zhu, X., Schaich, K. M., Chen, X., & Yam, K. L. (2013). Antioxidant Effects of Sesamol Released from Polymeric Films on Lipid Oxidation in Linoleic Acid and Oat Cereal. *Packaging Technology and Science, 26*(1), 31-38. doi: 10.1002/pts.1964